

Sheffield Hallam University

ATR-FTIR spectroscopy and Raman microscopy studies of organosilane diffusion and hydrolysis in PVC films.

EATON, Peter Jonathan.

Available from the Sheffield Hallam University Research Archive (SHURA) at:

<http://shura.shu.ac.uk/19594/>

A Sheffield Hallam University thesis

This thesis is protected by copyright which belongs to the author.

The content must not be changed in any way or sold commercially in any format or medium without the formal permission of the author.

When referring to this work, full bibliographic details including the author, title, awarding institution and date of the thesis must be given.

Please visit <http://shura.shu.ac.uk/19594/> and <http://shura.shu.ac.uk/information.html> for further details about copyright and re-use permissions.

LEARNING CENTRE
CITY CAMPUS, POND STREET,
SHEFFIELD, S1 1WB.

101 651 887 0



REFERENCE

ProQuest Number: 10694475

All rights reserved

INFORMATION TO ALL USERS

The quality of this reproduction is dependent upon the quality of the copy submitted.

In the unlikely event that the author did not send a complete manuscript and there are missing pages, these will be noted. Also, if material had to be removed, a note will indicate the deletion.



ProQuest 10694475

Published by ProQuest LLC (2017). Copyright of the Dissertation is held by the Author.

All rights reserved.

This work is protected against unauthorized copying under Title 17, United States Code
Microform Edition © ProQuest LLC.

ProQuest LLC.
789 East Eisenhower Parkway
P.O. Box 1346
Ann Arbor, MI 48106 – 1346

**ATR-FTIR Spectroscopy and Raman Microscopy Studies of
Organosilane Diffusion and Hydrolysis in PVC Films**

Peter Jonathan Eaton

A thesis submitted in part fulfilment of the requirements of Sheffield
Hallam University for the degree of Doctor of Philosophy

September 1998

Collaborating Organisation: Pilkington plc

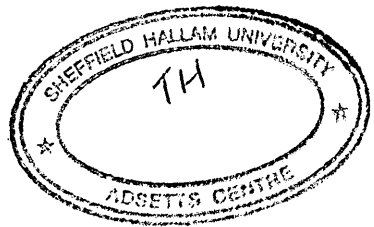
1. The first part of the document is a list of names of people who have been involved in the project. The names are listed in alphabetical order and include the following: [illegible]

[illegible]

2. The second part of the document is a list of names of people who have been involved in the project. The names are listed in alphabetical order and include the following: [illegible]

[illegible]

3. The third part of the document is a list of names of people who have been involved in the project. The names are listed in alphabetical order and include the following: [illegible]



Declaration

The work described in this thesis was carried out by the author in the Materials Research Institute, Sheffield Hallam University, between October 1995 and September 1998. The author declares that this work has not been submitted for any other degree. The work is original except where acknowledged by reference.

Author :

(Peter Jonathan Eaton)

Supervisor :

✓
(Professor Jack Yarwood)

Acknowledgements

I'd first of all like to thank my supervisors Prof. Jack Yarwood at Sheffield Hallam University and Dr. Paul Holmes at Pilkington plc., for their support and advice throughout this project. Thanks are also due to the other staff at Pilkington who have helped me throughout this work, especially Stuart Jamieson who carried out the DSC analysis.

Secondly, I'd like to thank my colleagues and friends at Sheffield for making the three years fun, and even for occasional advice! Thanks to Chris, Franny, Jason, Sohail, Carine, Delphine, Jeff, Obelix, Asterix, Chris Constable, Terry M., and Claudia. Last, but not least, extra special thanks must go to Jane and Pierre, for help and support above and beyond the call of duty. It is very much appreciated.

My biggest thanks go to all my family, but especially to my parents for support throughout my academic career. I couldn't have done it without you.

Abstract

Organosilanes are widely used to bond organic materials such as polymers to inorganic materials in polymer composites. However, the mechanism of adhesion is poorly understood. One postulated mechanism is the interdiffusion of the silane and polymer, along with condensation of the silane to form an interpenetrating polymer network (IPN).

The techniques of attenuated total reflectance Fourier transform infrared spectroscopy (ATR-FTIR) and Raman confocal microscopy have been used to study the diffusion, hydrolysis and condensation of three organosilanes in silicon / PVC / silane laminates. These processes are thought to contribute to the formation of the IPN, and hence to be vital for adhesion. The organosilanes studied were [3-(amino)propyl]trimethoxysilane, also known as A1110, [3-(phenylamino)propyl]trimethoxysilane, known as Y9669, and [3-(mercapto)propyl]triethoxysilane, known as A1891.

ATR-FTIR was shown to be an excellent technique for studying the kinetics of silane diffusion through PVC films. It was shown that at room temperature, no diffusion through unplasticised PVC films occurred. At 70 °C, however, diffusion occurred readily for Y9669 and A1891. In plasticised PVC films, diffusion was observed for all three silanes at room temperature. It was shown that the diffusion occurred more quickly with higher plasticiser concentrations, and hence lower glass transition temperatures. The kinetics of diffusion was found to fit a dual mode sorption model. Hydrolysis of the silanes was also followed by infrared spectroscopy, and the kinetics of hydrolysis and condensation were shown to be highly dependent upon silane type, the concentration of water, and the presence of an acid catalyst. The hydrolysis of the silanes was found to slow their diffusion through both plasticised and unplasticised PVC films. It was shown that the presence of water in the films caused the hydrolysis of the silanes *in situ*.

Raman depth profiles were measured of the films before, during and after diffusion. The spatial resolution was shown to be adversely affected by refraction at the air / PVC interface. It was shown that it is possible to deconvolve the confocal response of the microscope from the depth profiles, resulting in greater spatial resolution. Hydrolysis of the silanes was followed in solution by Raman spectroscopy, and it was found that each of the three silanes showed different rates of hydrolysis and condensation. It was shown that it was also possible to follow the kinetics of diffusion by Raman microscopy, and the results agreed well with those shown by ATR-FTIR spectroscopy.

Contents

Chapter 1 : Introduction	1
1.1 : Objectives	1
1.2 : The applications of organosilanes	2
1.3 : The reactions of organosilanes	6
1.4 : The diffusion of organosilanes	26
References	33
Chapter 2 : Spectroscopic Techniques	39
2.1 : Infrared Spectroscopy	39
2.1.1 : Introduction	39
2.1.1.1 : Interaction of infrared light with molecules	39
2.1.1.2 : Dispersive infrared spectrometers	41
2.1.2 : Fourier transform infrared spectroscopy	42
2.1.2.1 : The Michelson Interferometer	42
2.1.2.2 : The advantages of FTIR spectroscopy	46
2.1.2.3 : The disadvantages of FTIR spectroscopy	49
2.1.3 : Attenuated Total Reflection (ATR)	51
2.1.3.1 : The advantages of ATR	56
2.1.3.2 : The disadvantages of ATR	57
2.1.4 : Diffusion measurements with ATR - FTIR	57
2.1.4.1 : Models of diffusion	58
2.2 : Raman Spectroscopy	58

2.2.1 : Introduction	62
2.2.2 : The Raman effect	63
2.2.3 : Raman microscopy	67
2.2.4 : The Renishaw Ramascope	68
2.2.5 : Confocal Raman microscopy	71
2.2.6 : Advantages of confocal Raman microscopy	80
2.2.7 : Disadvantages of confocal Raman microscopy	81
References	82
Chapter 3 : Infrared diffusion results	85
3.1 : Experimental	85
3.1.1 : Materials	90
3.1.2 : Spectroscopic measurements	91
3.1.3 : Spectra of materials	92
3.2 : Silane underlayer experiments	95
3.3. : Silane overlayer experiments	98
3.3.1 : Silane overlayer experiments : heat - induced diffusion	98
3.3.2 : Silane overlayers - plasticised PVC	108
3.3.3 : Silane overlayer experiments : kinetic analysis of data	115
3.3.4 : Silane overlayers - PVC plasticised with polymeric plasticiser	129
3.4 : DSC analysis of plasticised PVC films	135
3.5 : Silane overlayers - hydrolysed silanes	141
References	152

Chapter 4 : Raman depth profile studies of organosilane diffusion	155
4.1 : Experimental	155
4.1.1 : Materials	156
4.1.2 : Spectroscopic measurements	157
4.1.3 : Spectra of materials	158
4.2 : Silane underlayer experiments	163
4.3 : Silane overlayer experiments	171
4.4 : Fourier Deconvolution of Depth Profiles	179
References	197
Chapter 5 : Raman studies of organosilane hydrolysis	200
5.1 : Experimental	200
5.1.1 : Materials	201
5.1.2 : Spectroscopic Measurements	201
5.1.3 : Spectra of Materials	201
5.2 : Y9669 Hydrolysis Results	204
5.3 : A1110 Hydrolysis Results	209
5.4 : A1891 Hydrolysis Results	211
References	221
Chapter 6 : Studies of organosilane diffusion in humidity - controlled films	222
6.1 : Experimental	222
6.1.1 : Materials	222
6.1.2 : Spectroscopic measurements	223

6.2 : Raman analysis of Y9669 diffusion in PVC exposed to atmospheric conditions	224
6.2.1 : Infrared analysis of Y9669 diffusion in PVC exposed to atmospheric conditions	227
6.3 : Raman analysis of Y9669 diffusion in PVC exposed to K₂CO₃(aq) vapour	229
6.3.1 : Infrared analysis of Y9669 diffusion in PVC exposed to K₂CO₃(aq) vapour	230
6.4 : Raman analysis of Y9669 diffusion in PVC exposed to NH₄Cl(aq) vapour	231
6.4.1 : Infrared analysis of Y9669 diffusion in PVC exposed to NH₄Cl(aq) vapour	236
References	241
Chapter 7 : Conclusions	242
7.1 : ATR-FTIR analysis of the kinetics of diffusion	242
7.2 : Raman depth profile analysis of diffusion	244
7.3 : Raman hydrolysis measurements	245
7.4 : Diffusion in humidity- controlled films	246
7.5 : The interrelation of the results	247
7.6 : Overall conclusions	254
7.7 : Future Work	256
References	258
Conferences Attendeed	259

Chapter 1 : Introduction

1.1 Objectives

Organosilanes may be used in a laminate containing poly(vinylchloride) (PVC) and glass, to increase the adhesion between the two materials. The main objective of this project is to measure the factors that affect adhesion in the glass / PVC / organosilane laminate system. More specifically, the factors which affect diffusion and hydrolysis of the organosilanes in the laminates are to be determined. It is believed that hydrolysis of the organosilanes and their diffusion through the PVC film in a laminate are both very important factors which determine the ultimate adhesion achieved in the laminate.

In order to do this, the primary techniques used are infrared and Raman spectroscopy; collectively vibrational spectroscopy. These techniques are ideal for the study because they can give distribution information on the required micrometer scale, as well as structural and chemical information. This is important because the factors that may be expected to affect adhesion include the distribution of the organosilanes, and the chemical structures and reactions of these materials. This project was sponsored by Pilkington plc, and therefore the materials and methods used are those of interest to Pilkington. However, as will be shown, the adhesion of minerals such as glass to polymers with organosilanes is of wide interest, and the results are therefore widely relevant. This

chapter discusses the literature on organosilanes, including their uses, reactions, and distribution in polymer films.

1.2 The uses of organosilanes

Organosilanes, also known simply as silanes, are used in a wide variety of scientific and commercial applications. These include uses as adhesion promoters (or coupling agents)¹⁻³, lubricants⁴, chromatography substrates^{5,6}, and chemical reagents⁷. However, this project centres on their use as coupling agents, so only literature relevant to this application will be reviewed. Silanes may be used to improve adhesion in systems where limited adhesion already exists⁸, to allow adhesion of materials which normally have no adhesion,^{9,10} or as a primer to provide a better substrate for another adhesive, such as an epoxy resin¹¹. The most common use of silane coupling agents is in adhering inorganic materials such as glass to organic materials such as polymers.

Organosilanes are so called because they consist of a functional organic group and an alkoxysilane group, usually joined by a short aliphatic chain. The structures of the silanes used in this project are shown in figure 1.1. The materials shown are [3-(amino)propyl]trimethoxysilane, henceforth known as A1110, [3-(phenylamino)propyl]trimethoxysilane, known as Y9669, and [3-(mercapto)propyl]triethoxysilane, known as A1891. Another silane widely studied is 3-

(amino)propyl]triethoxysilane (A1100) which is identical to A1110, but with the methoxy groups replaced by ethoxy groups.

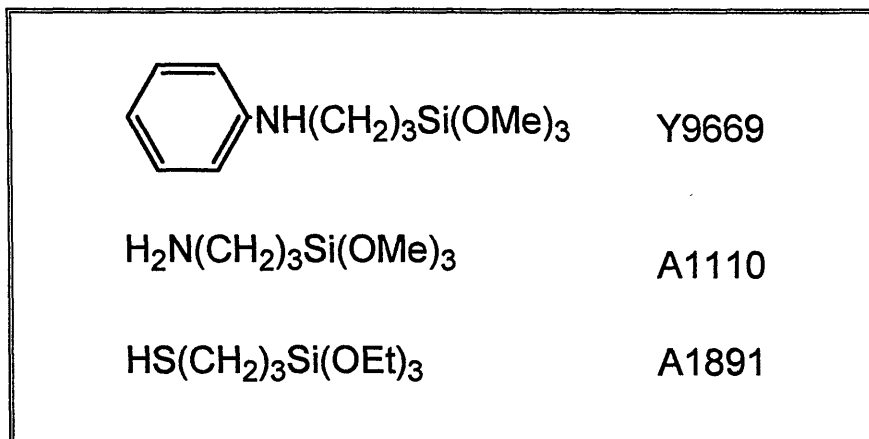


Figure 1.1 : The chemical structures of the organosilanes

It is known that the silane functional groups of these molecules are capable of reacting with hydroxyl groups on mineral surfaces to form covalent bonds¹²⁻¹³, and that some organic functional groups may react with functional groups on polymers^{16,17}. This leads to the 'chemical bonding' model of the action of coupling agents, which was proposed over thirty years ago¹⁸⁻²⁰. In this model, covalent chemical bonds would be formed between the silane and inorganic surface, and between the silane and organic surface. The silane is therefore acting as a bridge, and bonding the dissimilar materials together. This is illustrated schematically in figure 1.2.

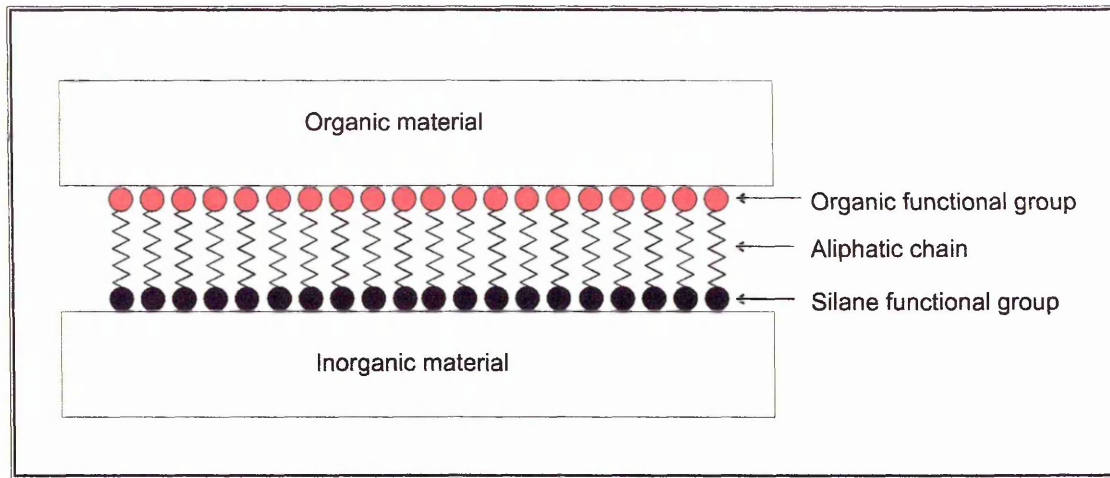


Figure 1.2 : Schematic diagram of the chemical bonding model of silane adhesion

There are, however, several pieces of evidence which this chemical bonding model does not explain. Firstly, it has been noted that in the production of laminated safety glass, optimum adhesion can be achieved by application of silanes such as A1891 to the glass prior to laminating^{21,22}. Laminated safety glass consists of a sandwich of a flexible polymer such as plasticised poly(vinyl chloride) (PVC) between glass sheets, as shown in figure 1.3. However, if the adhesion were explained wholly by the chemical bonding model, a monolayer applied to the glass (as shown in figure 1.2) would be the optimal loading, and this is found not to be the case¹⁸. Instead, it is found that in practice that an amount equivalent to several hundred monolayers is required for adequate adhesion^{23,24}. Therefore this chemical bonding theory does not describe optimum adhesion.

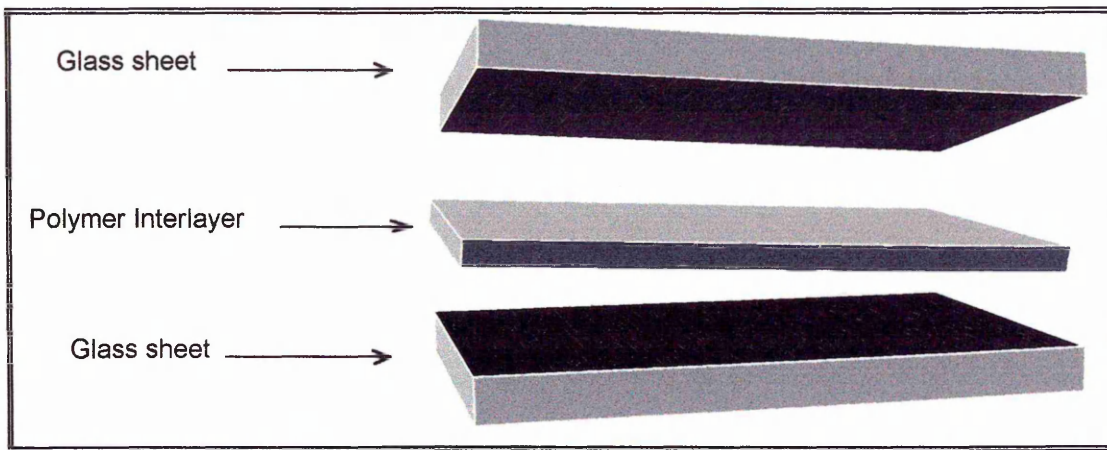


Figure 1.3 : Construction of laminated safety glass

Edwin Plueddemann also studied several systems where covalent bonds between silane and polymer would not be expected, and found good adhesion²⁵. The systems studied were thermosetting plastics, and it was assumed that an interpenetrating polymer network (IPN) was formed between the silane and the polymer. This occurs when crosslinked polymers are interdiffused, so that the strength of the joint is the strength of the bulk materials. The structure of an IPN is compared to interdiffused polymer in Figure 1.4.

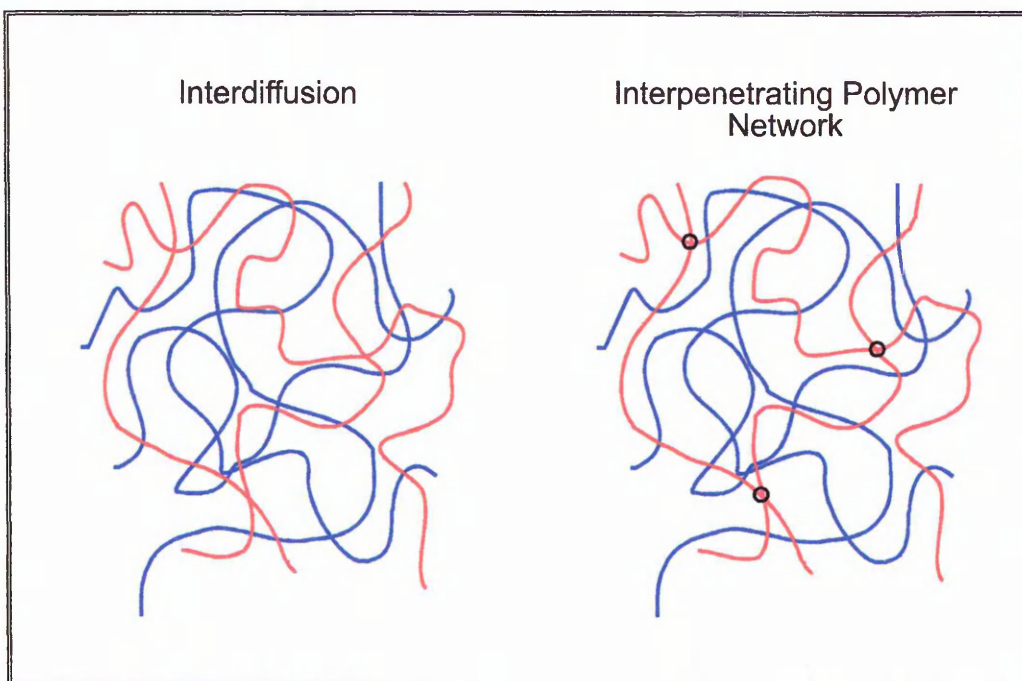


Figure 1.4 : Schematic representations of interdiffused polymers and an interpenetrating polymer network (IPN). Black circles represent crosslinks

In some cases it was assumed that the silane primer acted as a solvent for the unset polymer, thus leading to interdiffusion to form the IPN, however in some cases this was thought not to occur due to the low solubility. It should be noted that the occurrence of interdiffusion, or formation of an IPN is merely a hypothesis, and that no evidence was presented in this work. Evidence of interdiffusion and IPN formation is discussed in section 1.2.3.

1.3 : The reactions of organosilanes

The reactions of organosilanes have been widely studied in order to help elucidate their mechanism of adhesion. One of the most widely studied reactions was the hydrolysis

of the alkoxy silanes to the hydroxy derivative. This involved reaction of the silane with water to give the silanol form of the silane, producing an alcohol. The general mechanism for this is shown in Figure 1.5.

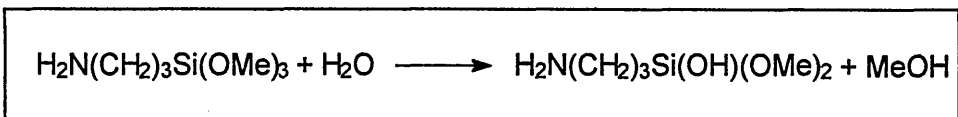


Figure 1.5 : Hydrolysis of silane coupling agents

Further reaction can occur to the bi-silanol or tri-silanol form. The hydrolysed silanes are reactive and condensation is known to occur with other silanol groups to form a siloxane linkage. Therefore a silane which has been exposed to water may contain a mixture of unhydrolysed silanes, silanes with one, two or three hydrolysed alkoxy groups, and condensed silanes that have condensed, and formed siloxane oligomers or polymers²⁶. The overall reaction of condensation is shown below :

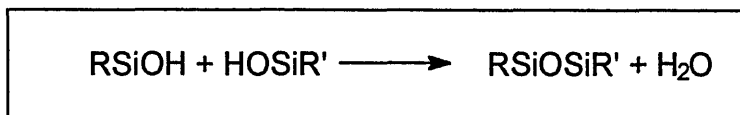


Figure 1.6 : Condensation of silanols

Condensation may also occur at a silicate surface, with surface silanols as shown in Figure 1.7.

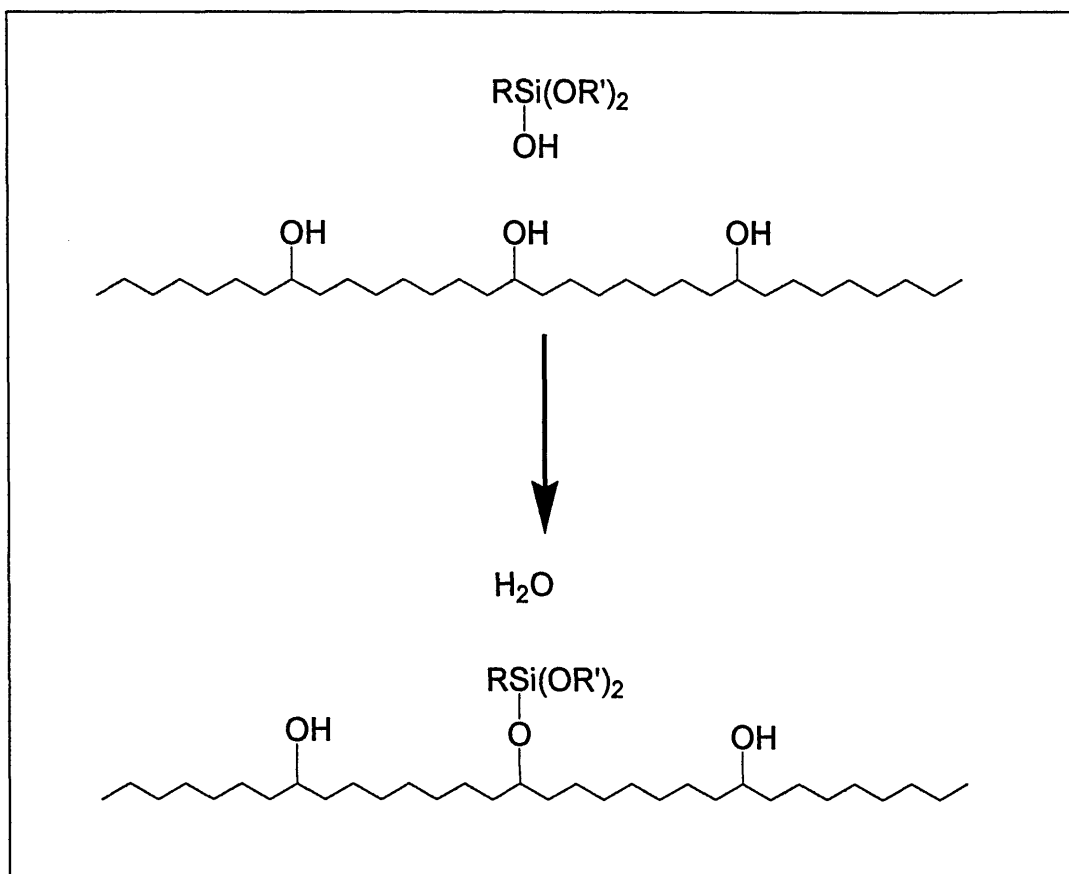


Figure 1.7 : Schematic drawing of silane grafting at a hydrolyslated silicate surface

The silanols undergoing condensation could be from two organosilanes, or from an organosilane and a mineral surface. Thus, a siloxane polymer, or a silane - grafted surface would be formed respectively.

Shih and Koenig²⁷ studied the hydrolysis of silanes in 50 and 2 % aqueous solutions. The hydrolysis was monitored in solution using Raman spectroscopy. The silanes studied were vinylsilane and methacrylsilane. For vinylsilane, a band at 1410 cm^{-1} was thought to be indicative of hydrolysed silanes, and a band at 672 cm^{-1} was assigned to triply hydrolysed silanes. The 1410 cm^{-1} band increases in intensity rapidly at first, and

much more slowly after about 50 minutes. This shows that after this time, there was very little unhydrolysed silane remaining. The 672 cm^{-1} band, on the other hand, increased up to about 50 minutes, but then started to decrease in intensity. This indicated that hydrolysis continued after the first silanol group was formed, and implies that all three alkoxy groups would have been hydrolysed eventually. A very similar result was found with the methacrylsilane, except that the hydrolysis was quicker, the equilibrium point of the 1410 cm^{-1} band being reached after 30 minutes, and the 710 cm^{-1} band (equivalent to the 672 cm^{-1} band in vinylsilane) started to decrease after this time.

Blum *et. al.*²⁸ studied the hydrolysis of a number of coupling agents, including A1110 and A1891. Hydrolysis was followed by measurement of methanol protons by ^1H NMR. The hydrolysis was followed in acetone - water solutions. For A1110, depending on the amount of water and silane present, hydrolysis took between 5 and 200 minutes to reach completion. In some cases, such the hydrolysis of glycidoxypropyltrimethoxysilane, complete hydrolysis was not observed even after several hours. Although the hydrolysis was complex, due to the competing reactions between silanes with different degrees of hydrolysis, the production of methanol was found to fit a first order rate law, so rate constants could be obtained. It was generally found that the aminosilanes hydrolysed much faster than those without amino moieties, although similar rates could be achieved with the non-aminosilanes by adding hydrochloric acid, which acts as a catalyst. The large difference in hydrolysis rates was probably due to the ability of aminosilanes to self - catalyse their hydrolysis²⁹. The behaviour of A1891 was only studied at high pH, but even

in this regime, hydrolysis was slower than that of A1110 under all conditions. The adsorption of A1110 onto high surface area silica was also studied. The silane was used in acetone-water solutions, after hydrolysis was thought to be complete. After reaction with the silica, the silica was removed, and the concentration of the silane remaining was measured with FTIR spectroscopy. Adsorption isotherms were obtained in this way. It was found that above concentrations of around 0.2g. silane per 100 ml. solution, monolayer coverage was obtained, with each silanol on the silica having one grafted silane.

Leyden and Atwater²⁶ also followed the kinetics of silane hydrolysis, but found different results. They used ATR-FTIR spectroscopy to follow the hydrolysis of the model compound trimethylmonomethoxysilane (TMMS) in aqueous solutions. This silane was chosen in order to simplify the kinetics, as just a single methoxy group is available for hydrolysis. The intensity of the Si-O-C stretching vibration at 1083 cm^{-1} was used to determine evolution of methanol and hence the degree of hydrolysis. However, a plot of $\ln[\text{TMMS}]$ vs. time did not show a straight line relationship, indicating that first order kinetics were not obeyed as reported by Blum *et. al.* and previously by other authors^{28,30,31}. The hydrolysis was in fact found to be second order overall : first order in TMMS and first order in water. The rate of condensation was also determined, by measuring the decrease in the intensity of the Si-OH stretching band at 896 cm^{-1} . The rate of condensation was found to be orders of magnitude slower than that of hydrolysis, and also second order overall. Both reactions were also found to be acid - catalysed.

Trens *et. al.*³² also studied adsorption of an aminosilane on silica, although the silane was A1100 it could be expected that the behaviour would be very similar to that of A1110. MPS ([3-(methacryloxy)propyl]trimethoxysilane) was also studied. A1100 was found to adsorb much quicker than MPS. This could be due to the faster hydrolysis of A1100 compared to. MPS. However, the adsorption of A1100 was also compared to that of propylamine. Propylamine and A1100 had similar adsorption enthalpies, which is indicative of a similar bonding mechanism. The removal of adsorbed species by flow of solvent was also studied. It was found that only 40 % of the A1100 was irreversibly bound, although none of the propylamine was. It was presumed that two types of adsorption occur in A1100, adsorption by a mechanism in common with that of propylamine, i.e. involving the amine group, and irreversible adsorption, presumably involving the silanol groups. It was also suggested that it may be possible for molecules to adsorb in both ways simultaneously. The bond via the amino group was likely to be a hydrogen bond with a surface silanol, whereas the irreversible bond was probably a siloxane condensation. This is concordant with work by Johansson *et. al.*³³ who also proposed adsorption of A1100 by both amino and silanol groups.

Piers and Rochester studied the adsorption of unhydrolysed A1110 and A1100 onto silica in carbontetrachloride solutions¹³. Solutions of the silanes with a range of concentrations were allowed to come into equilibrium with silica in solution, and then the transmission infrared spectra measured. It was found that in the more concentrated silane solutions, intermolecular hydrogen bonding between silanes on the silica surface occurred

much more. This occurred in solutions of both silanes. It appeared that bonding to the silica via both the silanol and amino moieties was observed. At higher concentrations, more amino bonding seemed to occur than bonding via the silanol group.

Azzopardi and Arribart³⁴ studied the formation of silane layers at the surface of an ATR (Attenuated Total Reflectance) crystal. ATR is a highly surface sensitive infrared technique, which is explained in more detail in chapter 2. Because the crystal material was silicon, with silica at the interface, the in-situ monitoring of mono- or multi-layer formation was possible. The silanes used were mono- and di-hydrolysable ethyl silanes. These silanes were able to interact with the silica surface only through their silanol groups. With the monohydrolysable silane, a simple monolayer was formed. With the dihydrolysable silane, chains of siloxane were formed at the surface. These were determined to average 10 silane units in length.

Plueddemann used proton NMR to study hydrolysis of silanes in solution³⁵. The methyl protons of silanols were measured to give an indication of level of hydrolysis. A wide range of silanes were studied, including aminosilanes substituted at the 3 position (like A1110) and aminosilanes substituted in the 1 and 4 positions. It was found the 3-aminosilanes exhibited unique behaviour. Unlike other silanes which hydrolyse slowly, and then condense into siloxane dimers and longer siloxane oligomers, 3-aminosilanes hydrolyse very quickly, but then form stable solutions, which were not observed to condense. The structure of 3-aminosilanes in water could not be determined, but based on

the importance of a 3-substituted amino group, one possible structure was proposed by Plueddemann. This is shown in Figure 1.8.

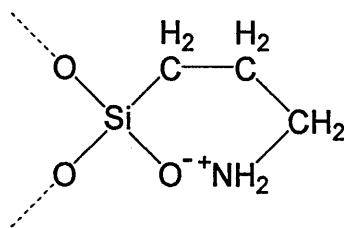


Figure 1.8 : Ring structure of 3-amino silanes proposed by Plueddemann

The ring structure of this structure would explain the stability in water to hydrolysis.

Morrall and Leyden followed the hydrolysis of 3-(amino)propyl]diethoxymethylsilane (APDMS)³⁶. This silane is similar to A1100, but with only two hydrolysable groups. Firstly, hydrolysis upon contact with atmospheric water followed by sealing the sample tube was followed. Infrared spectroscopy was used, monitoring the O-H stretching band area at 3080 to 3500 cm^{-1} in neat silane exposed to air. This was found to increase rapidly, until about 2.5 hours, then decrease to an equilibrium level. The area of the ethoxy mode at 950 cm^{-1} decreased on the same timescale, although it never reached zero. A shoulder at 1050 cm^{-1} also appeared, indicative of Si-O-Si linkages between hydrolysed silane molecules. Clearly, partial hydrolysis as well as some condensation to siloxane oligomers had occurred. Hydrolysis after treatment of an APDMS solution in dry toluene with water was also followed. In this case, the rate of formation of silanol slowed, but did not halt on the time-scale of the experiment (24 hours). A solution of A1100 was studied

in the same way and gave similar results. Although condensation occurred in neat APDMS, no siloxane bands were observed in the solution studies for either silane. The authors also studied the reaction with glass surfaces of silanes deposited from dry toluene solution. The silanes studied were [3-(cyano)propyl]triethoxysilane (CNPTS), A1891, A1100 and (octyl)triethoxysilane (C8TS). The degree of hydrolysis was determined by solution measurement of ethanol, and the interaction with the substrate measured by the capacity factor of the resulting material. Because of the dry solvent, any hydrolysis of the materials is likely to take place after adsorption, by interaction with water adsorbed at the glass surface. The A1100 was by far the fastest silane to adsorb onto the glass surface. It was believed this was because of hydrogen bonding between the silane N-H group and surface Si-OH groups. This led to the A1100 also undergoing the fastest hydrolysis. It was also found that a dried glass greatly slowed the production of ethanol, showing that hydrolysis was indeed occurring at the glass surface. Even taking into account the increased adsorption onto the surface by A1100, hydrolysis of this material was quicker, again showing the catalytic role of the amine group in hydrolysis. In order to determine the limiting step of hydrolysis in dry solution, an alkyl amine was added to the solution with the non amine silanes. This would be expected to perform the same catalytic role as the amine group in A1100. This did not increase the rate of hydrolysis. Therefore in this system, the rate limiting step was adsorption onto the surface, rather than hydrolysis once there.

Gauthier *et. al.*³⁷ studied the hydrolysis of a silane similar to A1891, [mercaptopomethyl]dimethylethoxysilane by FTIR. The reaction was followed in aqueous solution, with HCl present as a catalyst. This did not allow for observation of the $\nu(\text{Si-OH})$ stretching mode of the silanols produced due to interference from water in this spectral region. A band due to the ethoxy group decreased, when compared to the Si-CH₃ band at 833 cm⁻¹. A band also appeared at 886 cm⁻¹ which was assigned to OH stretching of hydrolysed material. No bands appeared in the region where siloxane bands may occur, indicating no condensation. This was in contrast to results seen previously which would lead one to expect the mercaptosilane, once hydrolysed, to continue to react and form siloxane oligomers. The hydrolysis of both this material and the triethoxy equivalent was studied by ¹H NMR. The protons of the ethoxy group and of the evolved ethanol were both observed. In the case of the monoethoxysilane, the solutions were completely hydrolysed when the first measurement was made. The triethoxy silane took longer to hydrolyse, on the time-scale of a few minutes for complete hydrolysis. Hydrolysis was faster with a higher concentration of HCl in solution. ²⁹Si NMR showed very similar results, but it was observed that after a few hours, condensation started to occur.

Ishida and Koenig³⁸ studied E-glass fibres coated with condensed silanes. The treated fibre was exposed to water, and the FTIR spectrum monitored. The authors noted the appearance of a band in the infrared due to Si-O stretching of Si-OH groups, occurring at 870 cm⁻¹. The effect of this hydrolysis of silanes is to break the siloxane bonds of the condensed layer. This showed that the condensation of silanes to oligomers is a reversible

process. This is technologically an important fact, as it means that upon exposure to water, composites involving condensed layers of silane will tend to undergo hydrolysis. This means the siloxane layer is depolymerised, weakening the composite. It was found that the silane layer was considerably more stable to attack by water when polymerised. The most stable was vinylsilane, which could be polymerised via the organofunctional group. It was also found that insolubility in water increased resistance.

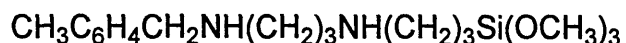
In order to elucidate the effects of moisture on a glass fibre / A1100 / epoxy resin composite, Arvanitopoulos and Koenig³⁹ studied model composites. These consisted of a single fibre mounted in epoxy resin. This fibre was used both with and without application of pre-hydrolysed A1100. The model composites were exposed to water in a humidity cabinet. The composites were studied by FTIR mapping, by automatically moving the sample stage in 8 μ m. steps in a raster pattern, and taking a transmission spectrum at each point. Because the FTIR spectrometer takes a full range spectrum at each point, the data can be analysed later to create maps of the intensity of any band in the spectrum. The $\nu(\text{OH})$ band of water was used to create maps of relative water concentration. The silane treated fibres were found to have the least water near the fibre surface. It was thought that the silane protects the composite against water attack in the interfacial region, thus prolonging the life of composites where it is applied⁴⁰. This may be by inducing hydrophobic character in the glass surface⁴¹. It was also found that the epoxy intensity was maximised at the fibre surface, in the case where silane was not applied. This was thought to be due to the increased amount of water present, as water may catalyse the curing of the

epoxy resin. Composites that had not been exposed to humidity were also analysed. It was found that the aliphatic polyamine curing agent occurred much less at the fibre surface in the case of the silane-treated fibres, and also the spectrum of the epoxy resin near the fibre surface was different when the fibre was silane treated. This was thought to indicate that the epoxy adopts a different conformation when in contact with silane. It is possible that the low level of cure of the epoxy resin near the silane-treated fibres explains the strength increase in composites which use silane. A composite with a low level of cure will be less rigid, and thus fracture at the fibre interface is less likely. A very similar system was investigated with NMR imaging⁴². However, the information available from this technique is somewhat limited compared to FTIR, and few conclusions could be made. It was observed, however that the silane-treated fibres caused no change in the level of cure of the epoxy resin. This is not in agreement with the results from FTIR mapping, as discussed above³⁹, so the effect of silane on epoxy resin cure level is still unclear.

Johansson *et. al.* studied adsorption of vinyl silanes onto glass fibres, followed by deposition of an epoxy resin layer⁴³. It was found that after rinsing of the resulting material with tetrahydrofuran (THF), substantial amounts of polymer remained on the fibres, but that the resin on pure glass fibres showed hardly any polymer retention. This was assumed to occur because copolymerisation occurred between the coupling agent and epoxy resin.

McKnight *et. al.*⁴⁴ cast prehydrolysed silane onto germanium or silicon ATR crystals, and pressed polypropylene films onto these to form model silica / silane /

polypropylene laminates. The chemical formula of the silane used, known as CSS, is shown below.



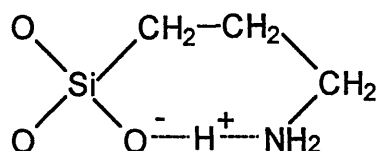
After deposition, a band at 905 cm^{-1} assigned to Si-OH stretching showed partial hydrolysis of the silane. A peak at 115 cm^{-1} with a shoulder at 1038 cm^{-1} showed that some condensation of the silane had occurred. These peaks were present in both the silicon and germanium experiments, indicating that the condensation was oligomerisation of the silane, rather than grafting to the surface. When the silane was heated with polypropylene, no new bands appeared in the spectrum, indicating no chemical interaction. As this system showed good adhesion, this was believed to be evidence for the diffusional mechanism of adhesion enhancement, rather than the chemical bonding theory. The band assigned to Si-OH stretching was monitored as a function of time, after the laminate was exposed to a reservoir of water. The water was observed to diffuse to the ATR crystal / silane interface, and then the SiOH band increased as the silane was hydrolysed *in situ*. This was monitored at room temperature and at $65\text{ }^\circ\text{C}$. At $65\text{ }^\circ\text{C}$ both the water diffusion and the hydrolysis were faster.

Kurth and Bein⁴⁵ formed monolayers of A1100 and A189 (the methoxy derivative of A1891) on oxidised aluminium mirrors. The aim was to form layers with which to compare reaction on surfaces with reaction in solution. The monolayers were deposited by vapour phase adsorption, as adsorption from solution was found to produce thick films, or poor quality monolayers. This was attributed to oligomerisation of silanes in solution. It

was found that A1100 adsorbed giving a thick film. However, the large part could be removed by evacuation, and it was assumed that this part was physisorbed, whereas the remainder was a chemisorbed monolayer. This layer was proved to be a monolayer by ellipsometry and the use of a quartz crystal microbalance. In the case of A189, the entire film could be removed by evacuation, therefore no chemisorbed silane was deposited. However, if the A189 was deposited from aqueous solution, i.e. prehydrolysed, monolayers could be formed reproducibly. The films were measured by reflection-absorption infrared spectroscopy (RAIRS). This technique is very sensitive to thin layers, and can also give some information on the orientation of the layers. The spectra of A189 showed an Si-O-Si mode at 1114 cm^{-1} indicating condensation between the silanes, as well as a shoulder at 1960 cm^{-1} characteristic of $-\text{OCH}_3$ groups. This indicates that there was both partial hydrolysis, and condensation in the monolayer. The RAIRS spectra also indicated that the alkyl chain stands proud of the surface, which was corroborated by the ellipsometric measurements of the layer thickness, which gave a thickness of $9 \pm 1\text{ \AA}$. In the case of A1100, the thickness was $7 \pm 1\text{ \AA}$, again corresponding to a monolayer perpendicular to the surface. The RAIRS spectra also indicated chains perpendicular to the surface, and the products of partial condensation and unhydrolysed silanes were again seen.

Boerio *et. al.*⁴⁶ also used RAIRS to study silanes deposited onto metal mirrors. The silane studied was A1100, and the substrates were polished iron mirrors. Films were deposited from aqueous solution, and air dried. The films were found to be highly hydrolysed. When dipped from the natural pH of the aqueous solutions, bands at 1480 cm^{-1}

and 1550 cm^{-1} were observed, and assigned to the $\delta(\text{NH}_2)$ mode of the amino group. A band at 1105 cm^{-1} from Si-O-Si groups in siloxane oligomers was observed. No ethoxy band at 2970 cm^{-1} was observed, indicating total hydrolysis of the ethoxy groups. The structure proposed for the aminosilanes in the films is shown below:

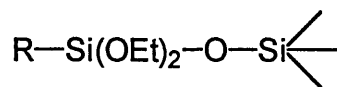


This structure represents a very strongly hydrogen bonded internal chelate form of the silane. This was proposed because it was observed that upon exposure to water and mildly acidic conditions, the band at 1550 cm^{-1} shifts to 1585 cm^{-1} and the band at 1480 cm^{-1} disappears. This was assigned to disruption of the strong hydrogen bonding, and a reversion to a standard hydrogen bonding structure. When deposited from a higher pH (9.5), the $\delta(\text{NH}_2)$ band frequency was as found in free amino groups, at 1600 cm^{-1} , i.e. there was little or no hydrogen bonding. Films formed at pH 12 showed amine bands at 1580 cm^{-1} and 1488 cm^{-1} , which were assigned to NH_3^+ deformation modes, indicating complete proton transfer from silanol to amine. In all cases, oligomerisation had occurred in the films.

Naviroj *et. al.*⁴⁷ also found the structure of adsorbed A1100 on silica to depend critically on the pH of the depositing solution. It was also found that from the same

concentration solution, more silane would be applied from pH 10.6 solutions than from either pH 9 or pH 12 solutions. Two other silanes, namely [3-(methacryloxy)propyl]trimethoxysilane and (vinyl)triethoxysilane were also studied. In the case of these silanes, no pH dependence was shown by the films. Clearly, the pH of the depositing solution can strongly influence the structure of the aminosilane films.

De Haan⁴⁸ *et. al.* studied the adsorption of organosilanes onto silica under dry conditions. The silanes studied were A1100 and MPS ([3-(methacryloxy)propyl]trimethoxysilane). The silica had been dried at 100 °C and the silanes were boiled with the silica under an argon atmosphere. The transmission infrared spectra were then examined to determine the type of bonding present. After the boiling under argon, some unhydrolysed groups remained. Around 40% of the silanes existed as the species shown below :



That is, the silane has one condensed bond to the silica, the other bonds remaining unhydrolysed. 20% of the silanes had two bonds to silica with the remaining bond unhydrolysed, and 35 % had two bonds to silica, with the remaining bond hydrolysed. Other structures, such as silanes polymerised at the surface make up the final 5% of silanes. After the silane-treated silica was heated at 80 °C for 30 minutes, more tri-dentate, and less mono-dentate bonding was present. In another experiment, the same conditions were used,

but some water was included in the boiling mixture. In this case, the silanes reacted more with each other than with the silica.

Vrancken *et. al.*⁴⁹ studied the reaction of silica gel with A1100 in dry toluene solution. Using a combination of ²⁹Si NMR, FTIR photoacoustic spectroscopy (FTIR-PAS) and diffuse reflectance infrared Fourier transform spectroscopy (DRIFTS), it was possible to distinguish between three types of surface silanol on the silica. These are shown schematically in Figure 1.9.

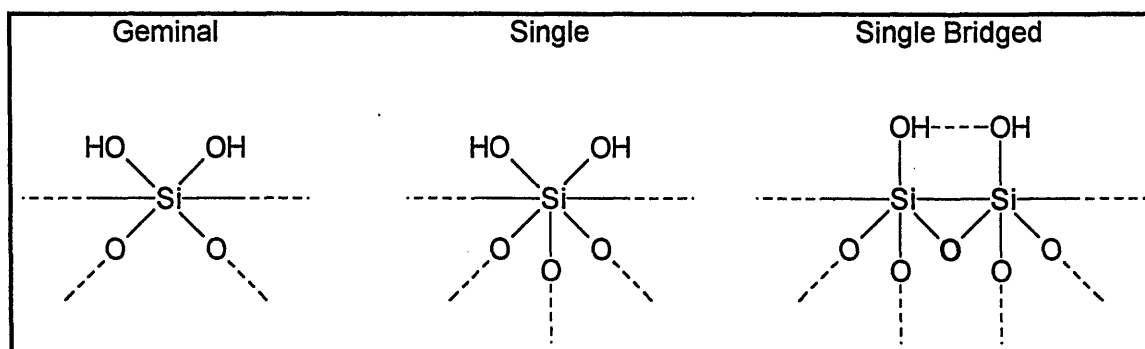


Figure 1.9 : Silica surface silanols observed by Vrancken *et. al.*⁴⁹

The silica was heat-treated at 473, 672 and 973K under vacuum. The high temperature treatments had the effect of reducing the amount of bridged silanols. In the case of either a low concentration of surface silanols, which was achieved by heating at 973K, or low silane solution concentration, the surface had a low density of silane molecules. In these instances the silane silanols could be identified and were stable to condensation. At higher

loadings, however the silanes polymerised on the surface. It was also observed that the high temperature - treated silica showed predominantly monodentate bonding to the silanes, whereas the lower temperature treated materials showed higher co-ordination. This was presumed to be because in the high temperature treated silica, the chance of two adjacent surface silanols is much lower.

Chiang *et. al.* studied the chemical structure of A1110 adsorbed onto glass surfaces from aqueous solutions⁵⁰. The silane was applied by dipping, followed by curing at 80°C. Similarly to Boerio *et. al.*⁴⁶, it was found that the NH₂ deformation mode shifted to 1575 cm⁻¹ upon curing, however it was found that upon further heat treating, the band shifted back to 1600 cm⁻¹. It was shown that this was unlikely to be due to a hydrogen bond with water, as the model compound propylamine did not show the same behaviour. Again, it was suggested that the band was due to an internal hydrogen bond, with partial protonation of the amine group. When deposited on silica surfaces, it was found that total hydrolysis occurred, as no SiOEt groups could be detected. It was suggested that the silanes were bound to the silica surface at both ends of the molecules, and to each other.

Kurth and Bein⁵¹ also studied silane films adsorbed on silicon by infrared spectroscopy. They found that upon continued heating at 75°C, silane films believed to be oligomeric in nature continued to condense, forming what they called a fully polymerised film, with no infrared bands due to hydrolysed silane remaining.

Domingue *et. al.*⁵² studied hydrolysed A1100 applied to silicon wafers, which had had the outer oxide layer removed. Samples for XPS analysis were spin cast, and then extensively washed with deionised water. The films thus produced were found to be approximately 3.5 Å thick, in comparison with the thicker films found by Kurth and Bein⁴⁵.

When examined by XPS, it was found that the silane appeared to have undergone fragmentation and rearrangement, as the peak due to nitrogen was lost upon washing. It was proposed that adsorption of the amino group onto the surface occurred, leading to electron loss and homolytic scission of the N-C bond. This would leave a -C. group to react further, though the products could not be determined. FTIR spectra were also obtained, from similar samples. Before washing, thick films were obtained, which appeared to be similar to the spectra of the neat silane. However after washing, the thin films showed somewhat different spectra, in that no N-H stretching modes could be seen, apparently confirming the XPS results. It may be that these are simply too weak to be seen, however, as the signal to noise ratio from the resulting monolayers is very low. This rearrangement and loss of nitrogen is a result not seen elsewhere, although the conditions used here have not been exactly repeated elsewhere in the literature.

Miller and Ishida⁵³ studied the adsorption of [3-(methacryloxy)propyl]trimethoxysilane onto lead oxide surfaces from aqueous solution.. They used DRIFTS to study the absorption. DRIFTS is a surface sensitive technique used especially for particulate samples, such as the lead oxide powder used here. At monolayer coverage, it was found that some bands due to condensed silane occurred at 1120 cm⁻¹ and

1040 cm^{-1} . The amount of silane condensed was calculated as 5 %, even though it was believed that the silane was completely hydrolysed. A band at 965 cm^{-1} could not be assigned to the silane, nor the substrate, but was assigned to a condensation of the lead oxide with the silanol from the silane, i.e. a vibration of the Pb-O-Si group. This result shows that the silane forms a covalent bond to the lead oxide substrate, which is harder to show in the case of silicon oxide surfaces, due to the similarity between the silane and substrate.

Ishida, Chiang and Koenig⁵⁴ studied the hydrolysis and condensation of A1110 in aqueous methanol solution using Raman spectroscopy. They also studied A1100, [3-(amino)propyl]methyldiethoxysilane and [3-(amino)propyl]dimethylethoxysilane, i.e. A1100 with three, two, and one ethoxy group available for hydrolysis. The Raman spectra of A1110 showed two bands at 615 and 645 cm^{-1} , assigned to stretching of the $\text{Si}(\text{OC})_3$ group. These bands also occurred in the spectra of A1100 at 650 and 619 cm^{-1} . These bands do not occur for the siloxane-condensed dimer in solution, and are therefore indicative of silane monomers. In the case of A1100, at low concentrations, no monomers were detected by this technique, indicating all A1100 existed as oligomers. It was found that low solution concentrations led to smaller oligomers. However, no monomers were seen, except at high concentrations. The model compound [3-(amino)propyl]dimethylethoxysilane was used to simplify the spectrum, because only one condensation product can occur, namely the dimer. Upon condensation, the $\text{Si}(\text{OC})_3$ band at 622 cm^{-1} shifted to 632 cm^{-1} . It was found that upon condensation, a band at 533 cm^{-1}

appeared. This could not be seen upon extraction of the dimer from solution, thus leading the authors to conclude that most molecules existed as monomers.

1.4 : The diffusion of organosilanes

In the paper by Sung et. al⁵⁵, the diffusion of A1100, the ethoxy derivative of A1110, in the sapphire / polyethylene / A1100 laminate system was studied. Chemical reaction between A1100 and polyethylene was said to be unlikely. Therefore the chemical bonding model should not be applicable. Despite this, enhanced adhesion was achieved using A1100. This implies that another mechanism was at work. This is likely to involve some interdiffusion of the silane with the polymer, possibly to form an interpenetrating network (IPN). The location of the silane in the laminate was studied with Scanning Electron Microscopy coupled with Electron dispersive X-ray analysis (SEM-EDX) in order to determine whether diffusion had occurred. It appeared that a change in silicon concentration profile did occur, upon changing the time the A1110 film was allowed to dry. This implied both that diffusion does occur, and that some reaction of the A1100 upon drying influenced the diffusional behaviour. This is likely to be a combination of hydrolysis and condensation, as discussed in section 1.2.2.

In a later paper, Kaul and Sung⁵⁶ studied laminates consisting of sapphire, A1110 and Nylon 6. These showed strong adhesion compared to the polyethylene system. Peel tests were performed to determine bond strength after exposure to water. The strength after

exposure to water (wet strength) is an important factor in polymer laminates, one that is considerably improved by the application of organosilanes^{1,2}. The peel strength without a silane was found to decrease to 14 % of its initial value after exposure to water for 10 days, but application of silane meant only 50 % of peel strength was lost. The silane was applied to the sapphire from aqueous solution, and thus could be expected to be hydrolysed to a large extent. After application, the silane films were dehydrated before laminating with polymer. It was found that increasing dehydration decreased peel strength. It was further found that there was an optimum concentration of silane to apply, implying that there was an optimum thickness of A1110 film required for adhesion. The optimum concentration correlates to a thickness of around 190 nm. This implies that too much silane can impair adhesion. It was thought that the optimum thickness of A1110 may correlate with an 'optimum interdiffusional thickness'. It was thought that the large increase in bonding strength of nylon vs. polyethylene laminates may be due to hydrogen bonding of the nylon with the A1110, which is unlikely in polyethylene.

In the paper by Nordin *et. al.*⁵⁷, the chain length of a silane coupling agent was varied in glass / silane / SBR (silane-butadiene rubber) laminates. The chain length was varied between $n = 4$ and $n = 30$, and the adhesion of the resulting laminate measured by a 180° peel test. It was found that interfacial adhesion energy increased with increasing chain length. If the bridging model was the sole mechanism of adhesion, this would not be the case, therefore there is another mechanism at work. The increase in adhesion with

chain length could be due to interpenetrating of the silane and polymer layers. It was suggested that the silanes diffuse into the matrix, and may also cross link with the polymer.

In the paper by Stein *et. al.*⁵⁸, the system of silica filled and unfilled silicone RTV elastomers, with A1110 as a coupling agent was studied. In order to assess diffusion of the silane through the polymer matrix, Secondary Ion Mass Spectroscopy (SIMS) was used to obtain depth profiles of the materials. The silane was used in both deuterated and undeuterated forms, and was incorporated in the polymer formulation. The depth profiles were obtained over a range of depths of 3 to 60 μm . No change in elemental composition was detected, with deuterated or non deuterated silanes, or filled or unfilled compositions. These results indicate that preferential diffusion to interphase regions does not occur. It also implies that diffusion to the silica filler does not occur, though it may be that the depth resolution of the technique, which involves sputtering the sample away, was not sufficient to determine this.

Chaudhury *et. al.*⁵⁹ studied a laminate consisting of PVC films on silane-primed germanium. The aluminium was treated with a pre-hydrolysed solution of [N-(2-aminoethyl-3-aminopropyl)trimethoxysilane (referred to as AEAPS). The silane films were estimated to be 150 nm. thick, and partly oligomerised. The PVC was then applied as a platisol, and contained 47 % plasticiser (di-isodecyl phthalate) and 1 % stabiliser as applied. It was likely that the film contained considerably less plasticiser when the experiments were carried out, as the film was dried at 175 $^{\circ}\text{C}$. The PVC film was 2 mm.

thick when applied. The drying temperature of the silane film was varied between 25 and 175 °C. The laminate bond strength was measured with a 180° peel test. It was found that there was an optimum drying temperature for maximum bond strength, at about 50 °C. It was hypothesised that formation of an IPN was necessary for optimum adhesion in this system. For this to occur, both interdiffusion of silane and PVC, and polymerisation of the silanes must be maximised. However too much crosslinking before diffusion may reduce the penetration of the silane into the polymer layer. Therefore it was proposed that below 50 °C, sufficient crosslinking of the silane does not occur, but that above 50 °C, the level crosslinking was too high, reducing interdiffusion of the silane and PVC. The laminates were also studied by XPS (X-ray photoelectron spectroscopy) depth profile analysis. This is an elemental surface analysis technique, combined with sputtering of the material to form depth profiles. This technique is somewhat susceptible to errors from sputtering artefacts, meaning that the depth profiling results are often qualitative, rather than quantitative. The laminates studied contained silane layers dried at temperatures of 25 °C and 175 °C. It was found that the film dried at 25 °C diffused further into the PVC than that dried at 175 °C. This was presumably due to a higher level of condensation of the silane when dried at higher temperatures.

Dibenedetto and Scola⁶⁰ investigated S-glass coated with either A1110, epoxy resin, or a mixture of A1110 and epoxy resin. The silanes were deposited pre-hydrolysed, from methylethylketone (MEK) solution. The technique used for analysis was ISS-SIMS (ion scattering spectroscopy - secondary ion mass spectroscopy). This is a surface atomic

analysis technique, but can sputter the surface, and so perform depth profile analysis. The results of the analysis of the silane-coated glass show 3 distinct layers in the silane layer. These consist of the outer 140 Å, which is a hard, highly polymerised silane, a soft oligomeric layer between 160 and 240 Å depth, and finally another hard polymerised layer from 240 Å to the silane-glass interface. A large amount of water was also found at the glass surface. Therefore, it may be that the change in polymerisation level of the silane was due to the availability of water; atmospheric water at the surface, and interfacial water at the glass interface. This was further shown by studying the effect of humidity on the silane layers; upon exposure to 95 % relative humidity for 2 weeks, the entire film was highly polymerised. The depth profiling of the laminates coated with a mixture of silane and epoxy showed very little change in composition with depth, indicating no preferential diffusion of the silane to either the air or the glass interface.

Hoh *et. al.*⁶¹ followed hydrolysis of A1100 with atmospheric water by FTIR spectroscopy. The hydrolysis was followed by monitoring the loss of the Si-O-Et stretching intensity at 960 cm⁻¹. Condensation was also observed as the appearance of the Si-O-Si modes 1120 cm⁻¹ and 1044 cm⁻¹. It was found that hydrolysis was complete after 7 days. In order to study the diffusion of epoxy resin, the silane was pre-hydrolysed, mixed with the un-cured epoxy, and heated in air. The aim was to monitor the extent of cure of the epoxy resin, which is related to the extent of interaction with the silane, as the aminosilane can act as a curing agent for the resin. This was presumed to be a measure of the diffusion of the epoxy resin, because the epoxy must reach the amino groups on the silane in order to be

cured. The cure level of the epoxy was determined by measuring the loss of the epoxy band at 915 cm^{-1} by transmission FTIR spectroscopy. It was found that higher levels of A1100 produced higher levels of cure, as did adding the solvent MEK. The polymer glass transition temperatures (T_g) of mixtures of both hydrolysed and unhydrolysed silane with epoxy resin were measured. It was found that in the case of unhydrolysed silane, increasing levels of silane decreased the polymer T_g . This is not surprising, as the monomeric or oligomeric silane is a much lower molecular weight material than the epoxy resin, and thus acts like a plasticiser for the polymer, reducing its chain stiffness. In all cases, the hydrolysed silane mixtures had higher T_g s than the unhydrolysed mixtures. This was assigned to the ability of the hydrolysed silane to form siloxane polymer networks when interdiffused with the epoxy, i.e. formation of an IPN. The trend in variation in T_g with level of hydrolysed silane in the mixture shows the highest T_g for 40% A1100, with lower polymer T_g s for both more and less silane in the mixture. This may be due to competition between the IPN effect and the plasticising effect of the silane.

Gu *et. al.*⁶² studied the effect of treatment of the silane film on the adhesion of copper / A1100 / epoxy laminates. It was found that there was an optimum concentration of alcoholic A1100 solution for greatest adhesion at 1 % by weight. This formed a film of silane around 1250 \AA thick. At lower thicknesses, adhesion was considerably lower, but only slowly decreased as the thickness was increased above this value. It was noted that at the critical thickness and above, blue patches appeared in the silane layer. Upon inductively coupled plasma analysis (I. C. P.) to determine the elemental composition, it

was discovered that these patches contained relatively large amounts of copper ions. It is possible that the absorption of copper by the silane film is required for good adhesion. Similar results were found when maintaining the solution concentration, and varying the time for which the copper substrates were immersed in the solution. The pH of the treating solution was also found to strongly affect the adhesion obtained. Whilst dry strengths were similar, when the adhesion was tested after boiling the sample in water for 50 hours, the sample treated at pH 7.2 showed greater adhesion than that treated at pH 10.4, and much greater than that treated at pH 5.5. It was suggested that the pH of the treating solution affects the adsorption mechanism of the silane on copper. The effect of variation of the temperature of drying of the silane film was also studied. It was found that increasing the temperature from 25 °C to 110 °C improved the adhesion resistance to water, but that increasing it further to 170 °C decreased the wet adhesion of the laminate. The increase in adhesion at 110 °C was almost certainly linked with increased condensation of the silane layer at this temperature, as this was observed in the infrared spectra. At the higher temperature, the amine band at 1581 cm⁻¹ was replaced by bands at 1605 cm⁻¹ and 1662 cm⁻¹ which were assigned to the C=N stretching mode of an imine formed by oxidation of the amine. This oxidation of amine coupling agents to the imine form at elevated temperatures has been previously reported^{63,64}. Finally, the effects of rinsing the silane layer with alcohol were examined. The rinsed laminates were found to show considerably less wet adhesion than the unrinsed laminates. It was proposed that this may be because the weakly bound material that can be removed by rinsing is required for interdiffusion of the silane with the epoxy.

References

- 1 Plueddemann, E. P., Silane Coupling Agents, 2nd. edition, Plenum Press, New York (1990)

- 2 Pape, P. G. and Plueddemann, E. P., Journal of Adhesion Science and Technology Vol. 5, No. 10, p.831 (1991)
- 3 Pape, P. G., Engineering Plastics Vol. 9, No. 2, p. 109 (1996)
- 4 Owen, M. J. and Williams, D. E., Journal of Adhesion Science and Technology Vol. 5, No. 4, p. 307(1991)
- 5 Kallury, K. M. R., Cheung, M., Ghaemmaghami, V., Krull, U. J. And Thompson, M., Colloids and Surfaces Vol. 63, No. 1-2, p.1 (1992)
- 6 Wikström, P., Mandenius, C. F. and Larsson, P. -O., Journal of Chromatography Vol. 455, p. 105 (1988)
- 7 Hook, D. J., Vargo, T. G., Gardella, J. A., Litwiler, K. S. and Bright, F. V., Langmuir Vol. 7, p.142 (1991)
- 8 Helbert, J. H. and Saha, N., Journal of Adhesion Science and Technology Vol. 5, No. 10, p. 905 (1991)
- 9 Koch, P. E. and D. Jay Schenck, Silanes and other Coupling Agents, p. 541, Ed. K. L. Mittal, VSP (1992)
- 10 Thompson, W. R. and Pemberton, J. E., Chemistry of Materials Vol. 7, p.130 (1995)
- 11 Garton, A. Journal of Polymer Science, Polymer Chemistry Edition Vol. 22, p. 1495 (1984)

- 12 Trens, P. and Denoyal, R. Langmuir Vol. 12, p.2781 (1996)
- 13 Piers, A. S. and Rochester, C. H. Journal of Colloid and Interface Science Vol. 174,
p. 97 (1995)
-
- 14 Plueddemann, E. P., Journal of Adhesion Vol. 2, p.184 (1970)
- 15 De Haan, J. W., Van Den Bogaert, H., Ponjee, J. J. and Van de Ven, L. J. M.,
Journal of Colloid and Interface Science Vol. 110, No. 2, p. 591 (1986)
- 16 Plueddemann, E. P., Journal of Adhesion Vol. 2, p.184 (1970)
- 17 Hearn, M. S., Baird, J. D., Nethsinghe, L. P. and Gilbert, M., Polymer
Communications Vol. 31, p.194 (1990)
- 18 Sterman, S. and Bradley, H. B., SPE Transactions, October 1961 p.224 (1961)
- 19 Plueddemann, E. P., Clark, H. A., Nelson, L. E. and Hoffmann, K. R., Modern
Plastics Vol. 39 (1962)
- 20 Yates, P. W. and Trebilcock, J. W., Proceedings of the 16th. Annual Technical and
Management Conference, Reinforced Plastics Division, S.P.I., Section 8-b (1961)
- 21 Purvis, M. B. et. al., International Patent No. WO 95/19261 (1995)
- 22 Beckmann, R. et. al., United States Patent No. 4,277,538 (1981)
- 23 Schrader, M. E., Lerner, I., D'Oria, F. J, Modern Plastics Vol. 45, p.195 (1967)
- 24 Plueddemann, E. P., Journal of Adhesion Science and Technology Vol. 2, No. 3,
p.179 (1988)
- 25 Plueddemann, E. P., Silane Coupling Agents, Chapter 5, 2nd. edition, Plenum Press,
New York (1990)

- 26 Leyden, D. E. and Atwater, J. B., *Journal of Adhesion Science and Technology* Vol. 5, No. 10, p. 815 (1991)
- 27 Shih, P. T. K. and Koenig, J. L., *Materials Science and Engineering* Vol. 20, p.137 (1975)
- 28 Blum, F. D., Meesiri, W., Kang, H.-J. and Gambogi, J. E. *Journal of Adhesion Science and Technology* Vol. 5, No. 6 (1991)
- 29 Plueddemann, E. P., in *Chemically Modified Surfaces*, Ed. by Leyden, D. E., Gordon and Breach (1986)
- 30 Pohl, E. R and Osterholz, F. D., in *Molecular Characterisation of Composite Interfaces*, Ed. by Ishida, H. and Kumar, G., p. 157, Plenum Press, New York (1985)
- 31 Savard, S., Blanchard, L. P., Leonare, J. and Prud'homme, R. E., *Polymer Composites* Vol. 5, p. 242 (1984)
- 32 Trens, P., Denoyel, R., and Rouquerol, J., *Langmuir* Vol. 11, No. 2, p. 551 (1995)
- 33 Johansson, O. K., Stark, F. O., Vogel, G. E. and Fleischmann, R. M., *Journal of Composite Materials* Vol. 1, p.278 (1967)
- 34 Azzopardi, M.-J. and Arribart, H., *Journal of Adhesion* Vol. 46, p. 103 (1994)
- 35 Plueddemann, E. P., Ed. *Interfaces in Polymer Matrix Composites*, Academic Press, New York, (1974)
- 36 Morrall, S. W. and Leyden, D. E. in *Silanes Surfaces and Interfaces*, Ed. by Leyden, D. E., Gordon and Breach (1985)

- 37 Gauthier, S. ,Aime, J. P., Bouhacina, T., Attais, A. J., and Desbat, B., Langmuir Vol. 12, No. 21 (1996)
- 38 Ishida, H. and Koenig, J. L., Journal of Polymer Science: Polymer Physics Edition, Vol. 18 (1980)
- 39 Arvanitopoulos, C. D. and Koenig, J. L., Applied Spectroscopy Vol. 50, No. 1 (1996)
- 40 Chiang, C. H., and Koenig, J. L., Journal of Polymer Science: Polymer Physics Edition Vol. 20 (1980)
- 41 Shang, S. W., Williams, J. W. And Soderholm, K. J. M., Journal of Materials Science Vol. 29, No. 9, p. 2406 (1994)
- 42 Arvanitopoulos, C. D. and Koenig, J. L., Journal of Adhesion Vol. 53, p. 15 (1995)
- 43 Johansson, O. K., Stark, F. O., Vogel, G. E. and Fleischmann, R. M., Journal of Composite Materials Vol. 1, p.278 (1967)
- 44 McKnight, S H. and Gillespie, J. W., Journal of Applied Polymer Science Vol. 64, part 10, p. 1971 (1997)
- 45 Kurth, D. G. and Bein, T., Langmuir Vol. 9, No. 11 (1993)
- 46 Boerio, F. J., Armogan, L. and Cheng, S. Y., Journal of Colloid and Interface Science Vol. 73, No. 2 (1980)
- 47 Naviroj, S., Culler, S. R., Koenig, J. L. and Ishida, H., Journal of Colloid and Interface Science Vol. 97, No. 2, p.308 (1984)
- 48 De Haan, J. W., Van Den Bogaert, H., Ponjee, J. J. and Van de Ven, L. J. M., Journal of Colloid and Interface Science Vol. 110, No. 2, p. 591 (1986)

- 49 Vrancken, K. C., De Coster, L., Van Der Voort, P., Grobert, P. J. and Vansant, E. F.,
Journal of Colloid and Interface Science Vol. 170, p. 71 (1995)
- 50 Chiang, C.-H., Ishida, H. and Koenig, J. L., Journal of Colloid and Interface Science
Vol. 74, No. 2, p. 396 (1980)
- 51 Kurth, D. G. and Bein, T., Langmuir Vol. 11, No. 2, p. 578 (1995)
- 52 Domingue, A., Piyakis, K., Sacher, E., Di Renzo, M., Dénomée and Ellis, T. H.,
Journal of Adhesion Vol. 40 (1993)
- 53 Miller, J. D. and Ishida, H. in Chemically Modified Surfaces, Ed. by Leyden, D. E.,
Gordon and Breach (1986)
- 54 Ishida, H. , Chiang, C.-H. and Koenig, J. L., Polymer Vol. 23, p. 251 (1982)
- 55 Sung, N. H., Kaul, A., Chin I. and Sung, C. S. P. Polymer Engineering and Science
Vol. 22, no. 10 p.637 (1982)
- 56 Kaul, A. and Sung, N H., Polymer Engineering and Science Vol. 25, No. 18 p. 1171
(1985)
- 57 Nordin, M., Alloun, A. and Schultz, J., C. R. Academie Science Paris, Vol. 315,
Serie II pp. 293-298, (1992)
- 58 Stein, J., Valenty, S. J., Smith, G. A., Brezniak, D. V. and Prutzman, L. C.,
Macromolecules Vol. 19 (1986)
- 59 Chaudhury, M. K., gentle, T. M. and Plueddemann, E. P., Journal of Adhesion
Science and Technology Vol. 1, No. 1, (1987)
- 60 Dibenedetto, A. T. and Scola, D. A., Journal of Colloid and Interface Science Vol.
64, No. 3 (1978)

- 61 Hoh, K.-P., Ishida, H. and Koenig, J. L., Polymer Composites Vol. 9, No. 2 (1988)
- 62 Gu, X. H., Xue, G. and Jiang, B. C. Applied Surface Science Vol. 115 (1997)
- 63 Ondrus, D. J. and Boerio, F. J., ., Journal of Colloid and Interface Science Vol. 124,
No. 1, p.349 (1988)
- 64 Culler, S. R., Ishida, H. and Koenig, J. L., Journal of Colloid and Interface Science
Vol. 109, No. 1, p.1 (1986)

Chapter 2 : Spectroscopic Techniques

2.1 : Infrared Spectroscopy

2.1.1 : Introduction

Infrared spectroscopy has been used for over a century to determine the chemical composition of matter. Infrared light occurs between 0.7 and 500 μm . in the electromagnetic spectrum, between the visible and microwave regions. When infrared light interacts with the oscillating dipole of a molecule, absorption of light can occur. The frequencies absorbed depend upon the fundamental frequencies of the vibrations of the molecules absorbing the light. This is the basis of infrared spectroscopy.

2.1.1.1 : Interaction of infrared light with molecules

The oscillating molecule interacting with an incoming quantum of infrared light can be considered as a quantum mechanical harmonic oscillator. Figure 2.1 shows the allowed vibrational energy levels and transitions for a diatomic simple harmonic oscillator.

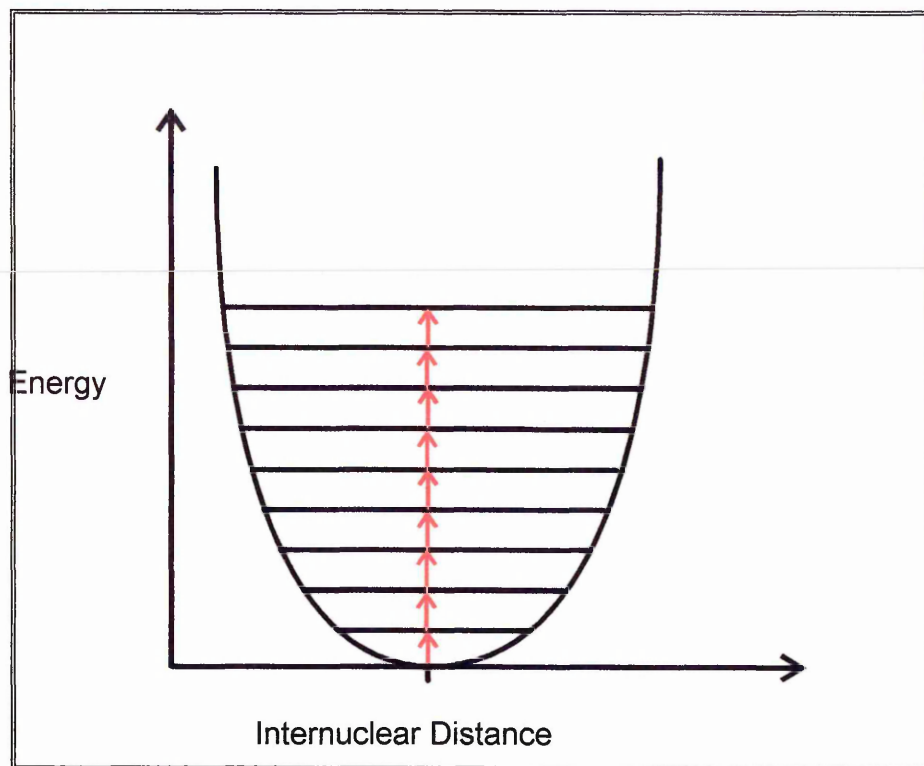


Figure 2.1 : Energy levels and transitions for a simple harmonic oscillator

It can be seen that due to the quantisation of energy, only certain vibrational energies are allowed. This leads to the selection rules for the quantum mechanical harmonic oscillator in infrared.

- i. Infrared absorption only occurs when infrared radiation interacts with a molecule undergoing a change in dipole moment.
- ii. Infrared absorption only occurs when the incoming infrared photon has sufficient energy for the transition to the next allowed vibrational energy state.

$$\text{i.e. } E_{\text{infrared}} = hc\nu_{\text{vibration}}$$

where h = Planck's constant

c = the speed of light

$\nu_{\text{vibration}}$ = frequency of the oscillator

E_{infrared} = energy of the infrared photon

iii. According to the harmonic oscillator selection rule, transitions between non - adjacent energy levels in a system are not allowed.

Spectroscopically, the consequences of these rules are as follows. Rule one means that only those vibrations that give rise to a dipole moment change may absorb infrared. Rule two means that each vibration gives rise to discrete infrared absorption; therefore we can identify a vibration by the frequency of its absorptions. Rule three means that only the fundamental vibrational transition occurs (i.e. $\Delta n = 1$). In reality, molecular vibrations are anharmonic. Therefore the $\Delta n = 2$ and $\Delta n = 3$ etc. transitions can occur, but they are much less likely. In infrared spectroscopy, the $\Delta n = 2$ and $\Delta n = 3$ transitions are known as the first and second order overtones, and occur with much lower intensity than the fundamental vibration.

2.1.1.2 : Dispersive infrared spectrometers

The traditional infrared instrument is a dispersive instrument. It is so called because the light emitted by the infrared source is dispersed into its component frequencies, which are detected one frequency at a time. A schematic of a dispersive

instrument is shown in Figure 2.2. Briefly, it comprises a polychromatic infrared source (such as a Globar rod), optics to direct the light through the sample, some form of dispersive element (usually a grating or prism), and a detector.

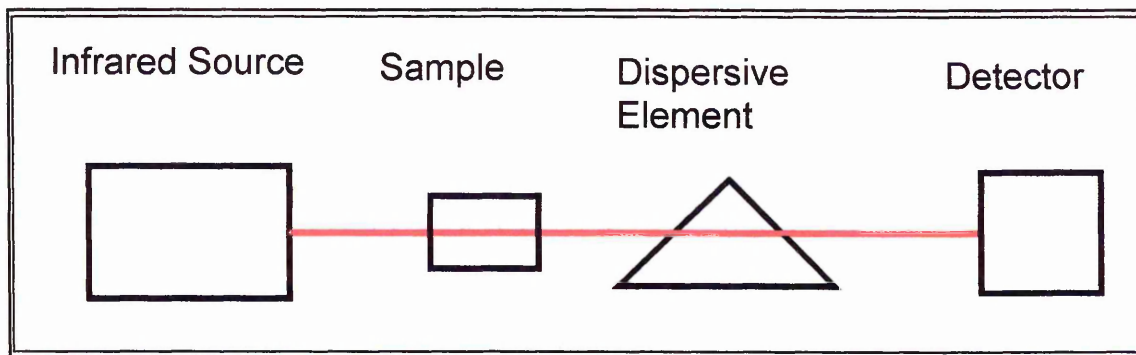


Figure 2.2 : Schematic diagram of dispersive infrared spectrometer

2.1.2 : Fourier transform infrared spectroscopy

Fourier transform infrared spectroscopy (FTIR spectroscopy) is an alternative method of obtaining an infrared spectrum to dispersive spectroscopy. FTIR relies on the use of a Michelson interferometer

2.1.2.1 : The Michelson Interferometer

A schematic of the Michelson interferometer is shown in Figure 2.3. Light from the infrared source passes through the interferometer before it passes through the sample, and is then collected by the detector. At the interferometer, the light strikes a beam splitter which passes 50% of the light to mirror 1 and 50% of the light to mirror 2. Mirror 1 is a

moving mirror, which oscillates back and forth, whereas mirror 2 is stationary. On reflection from these mirrors, the beam splitter recombines the light which is then guided on towards the sample.

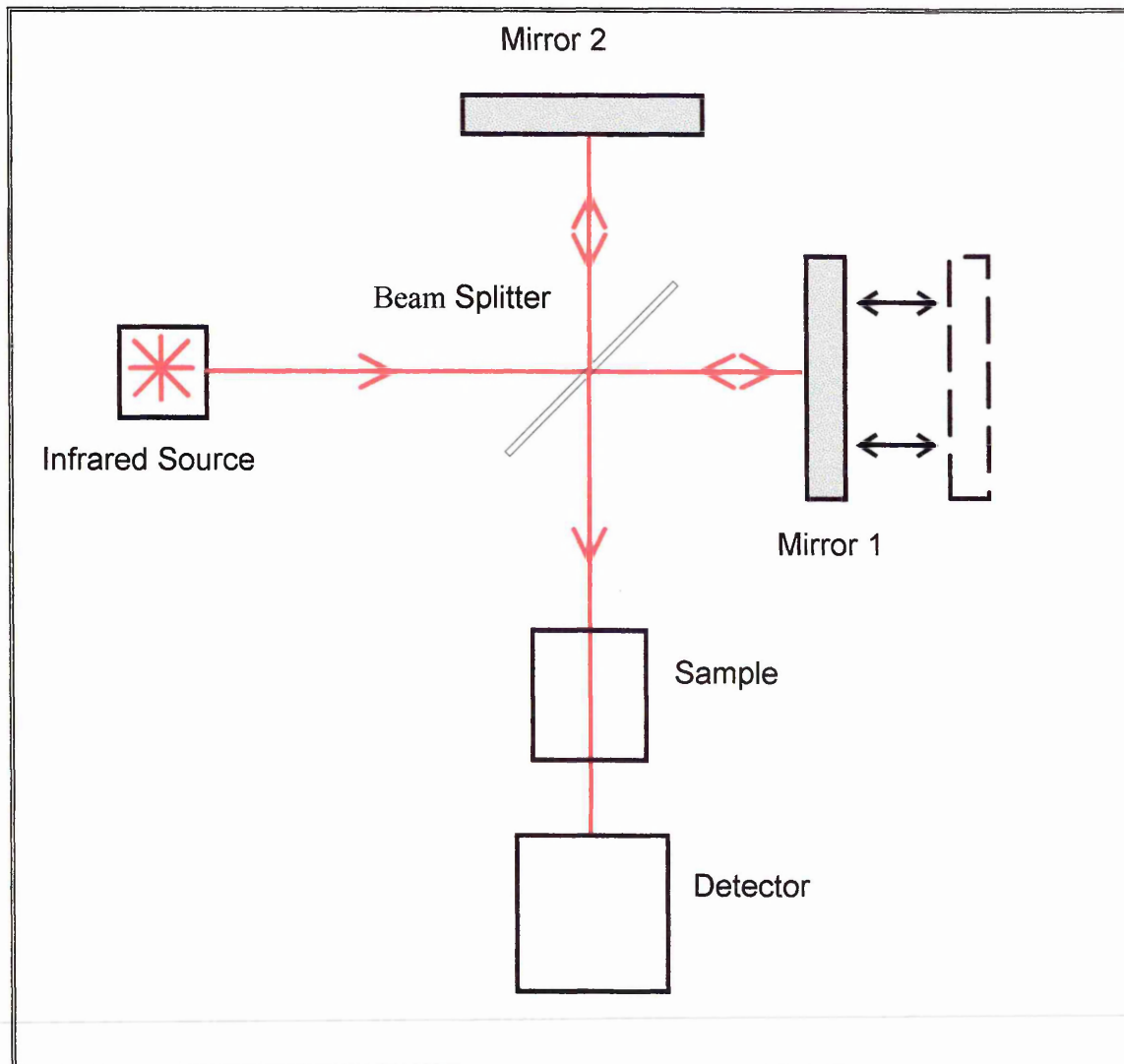


Figure 2.3 : Schematic diagram of the Michelson interferometer in an FTIR spectrometer

When the mirrors are the same distance from the beam splitter, the light will travel the same distance to each mirror, so that constructive interference occurs. This point is known as zero path difference (ZPD). However, if the moving mirror is $1/4 \lambda$ from the ZPD, the

light on the moving mirror optical path will travel $1/2 \lambda$ further than the light reflected from the stationary mirror, and thus destructive interference will occur. The pattern of interference obtained is known as an interferogram. Because the source is polychromatic, the interferogram obtained is the sum of interferograms from all contributing wavelengths.

The detector therefore sees an interferogram as shown in Figure 2.4.

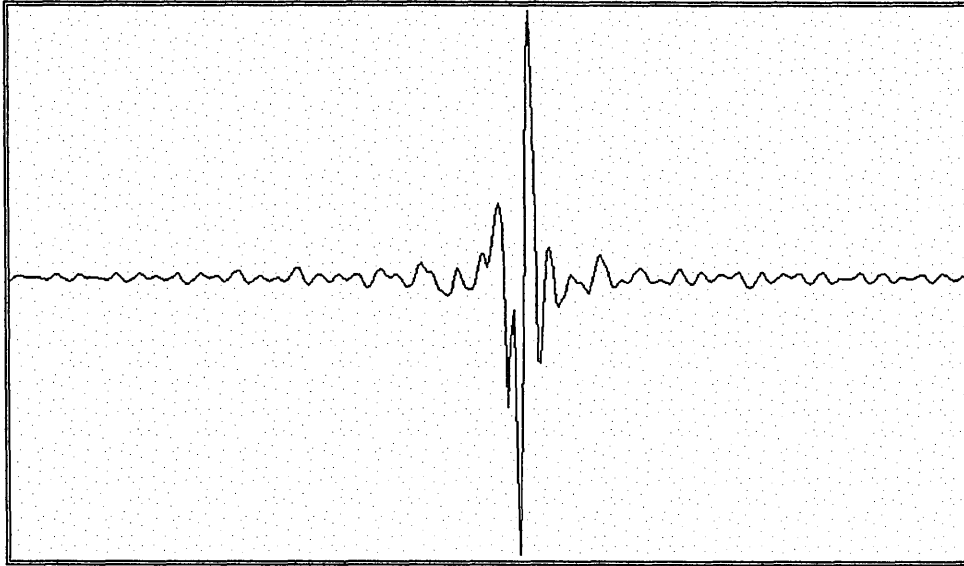


Figure 2.4 : The interferogram as seen by the FTIR detector

To the detector, the appears as a fluctuating intensity in the time domain. In order to convert this signal back to a spectrum (intensity in the *frequency* domain) a Fourier transform is used. The intensity of the infrared radiation at the detector can be written as

$$I(x) = \int_0^{\infty} S(\bar{\nu}) \cos(2\pi\bar{\nu}x) d\bar{\nu} \quad (2.1)$$

where $I(x)$ is the intensity of the signal at the detector

$S(\bar{\nu})$ is the spectral density amplitude

and $\bar{\nu}$ is the frequency (wavenumber)

Because the Fourier Transform must be applied mathematically, the information that the detector collects must be digitised. This is performed by measuring the intensity of the signal at certain set distances of mirror travel, called the sampling interval. The sampling interval is controlled by the frequency of a laser, most commonly a HeNe laser emitting at 632.8 nm. The amplitude of each frequency element in the spectrum is given by :

$$S(\bar{\nu}) = \sum_{x=0}^D I(x) \cos(2\pi\bar{\nu})\Delta x \quad (2.2)$$

where Δx is the sampling interval

The path difference, x is the product of the sampling interval, Δx and the number of samples taken, usually in the range 500 to 10,000. Digitised sampling results in a lower limit on the wavelengths that can be studied. This is given by the following equation :

$$\Delta x \leq \lambda_{\text{minimum}} / 2 \quad 2.3$$

where λ_{minimum} is the minimum frequency that may be studied.

This means that the highest frequency that may be studied, $\bar{\nu}_{\text{maximum}}$ is given by

$$\bar{\nu}_{\text{maximum}} = 1 / 2 \Delta x \quad (2.4)$$

This is called the aliasing frequency. If infrared radiation of a frequency higher than the aliasing frequency is present, then severe distortion of the spectrum occurs. The most common frequency used to control the sampling interval in FTIR spectrometers is a HeNe

laser line at 632.8 nm. Thus, if sampling every two wavelengths, the aliasing frequency is 7960 cm^{-1} . In spectrometers with KBr beam splitters, this does not cause a problem, as the spectral window of KBr limits the infrared light used to much lower frequencies.

2.1.2.2 : The advantages of FTIR spectroscopy

Clearly, FTIR spectrometers are much more complex than dispersive spectrometers, and more complex processing of the data obtained is required. However, FTIR spectroscopy was developed because it shows several advantages over dispersive infrared spectroscopy.

I) The Fellgett Advantage

The Fellgett, or multiplex advantage arises because all of the spectral elements are measured simultaneously. Thus, a spectrum can be obtained very quickly. The number of spectral elements in a digitised spectrum are given by

$$N = \frac{\bar{\nu}_H - \bar{\nu}_L}{\Delta\nu_R} \quad (2.5)$$

where N is the number of spectral elements

$\bar{\nu}_H$ is the highest wavenumber

$\bar{\nu}_L$ is the lowest wavenumber

and $\Delta\bar{\nu}_R$ is the resolution

For thermal detectors, the signal to noise ratio (S / N) of the spectrum obtained is proportional to the square root of the time each element is observed. Therefore in an FTIR system, the signal to noise is given by

$$S / N \propto T^{1/2} \quad (2.6)$$

where T is the total time of the experiment.

Whereas a dispersive system observes each spectral element in turn, therefore

$$S / N \propto T^{1/2} / N^{1/2} \quad (2.7)$$

Therefore, a dispersive system obtains a poorer S / N in the same time, or takes longer to acquire a spectrum with the same S / N. Therefore FTIR has obvious advantages for kinetic analysis, or where there is poor S / N.

II) The Jacquinot Advantage

The Jacquinot, or throughput advantage arises because unlike dispersive spectrometers, FTIR spectrometers have no slits which attenuate the infrared light.

The spectral optical throughput of a grating instrument is given by

$$G_{\nu}^G = \frac{hH}{fv} R_0 \quad (2.8)$$

where G_{ν}^G is the optical throughput per wavenumber

H is the height of the grating

h is the length of the entrance slit

f is the focal length of the collimator

and R_0 is the theoretical resolving power.

In the case of the interferometer, assuming the beam area is equal to the beam area at the grating,

$$G_{\nu}^I = \frac{2\pi H^2}{\nu} \quad (2.9)$$

where G_{ν}^I is the optical throughput of the interferometer. The ratio of the optical throughputs is therefore given by

$$\frac{G_{\nu}^I}{G_{\nu}^G} = \frac{2\pi f}{h} \quad (2.10)$$

For a sensitive grating spectrometer, f / h may be greater than 30. Therefore the FTIR optical throughput would be around 190 times that of the grating spectrometer. This means the signal reaching the detector is much higher, leading to a greater S / N for an FTIR system.

III) The Connes Advantage

The Connes advantage arises because the frequency scale of the spectrum is known very accurately. This is because the time domain of the interferogram is fixed extremely precisely by the wavelength of the laser. Therefore when the Fourier transform is applied, the wavelength domain is very precisely known. This control over the calibration of the wavelength domain means mirror movement averaging is possible. This means the collection of many spectra and their co-addition. The addition of many spectra increases signal to noise ratio, because $S / N \propto T^{1/2}$ (eq. 2.6). An additional advantage of the accurate wavelength calibration is that because the wavelength is known absolutely, techniques such as spectral subtraction can be used without any wavelength calibration.

2.1.2.3 : The disadvantages of FTIR spectroscopy

FTIR instruments do have some disadvantages as compared to dispersive instruments. Firstly, FTIR instruments do not measure spectra; they measure interferograms. Interferograms are difficult to interpret without first performing a Fourier

transform to produce a spectrum. This used to be a major problem, but since the dramatic increase in computing power, performing a Fourier transform is now a quick and easy process. However, the way the interferogram is transformed can affect the results, and so care must be taken.

Secondly, in systems that are source noise-limited, the Fellgett disadvantage applies. This arises because all regions of the spectrum are observed simultaneously. Therefore, if noise occurs in one part of the radiation from the infrared source, it will be spread throughout the spectrum in an FTIR system. In a dispersive system, the noise would be seen only in the region of the spectrum in which it arose. Fortunately, in mid-infrared systems, as used here, the system is detector noise-limited, therefore the Fellgett advantage applies, but not the Fellgett disadvantage,

Most importantly, FTIR instruments have a single beam, whereas dispersive instruments usually have a double beam. Double beam instruments take a background at the same time as the sample, whereas single beam instruments rely on taking a background before the sample is inserted. Assuming there is no change in atmospheric conditions throughout the experiment, this does not cause a problem. However, for highly sensitive work, and experiments which take along time, changes in infrared absorbing gas concentrations can severely affect the results. Therefore, when using an FTIR instrument, it is necessary to purge the instrument of CO₂ and water vapour using an infrared transparent gas such as nitrogen. Otherwise changes in CO₂ or water vapour level between

taking the background and sample spectra will cause absorption from these gases to appear in the spectrum.

2.1.3 : Attenuated Total Reflection (ATR)

The most common sampling technique used in infrared spectroscopy is transmission, as shown in Figure 2.2. This technique simply involves steering the infrared beam through the sample, and into the detector. Transmission has the advantage of simplicity and ease of use, but has several restrictions. Firstly, the technique is limited to weakly absorbing samples, in order that total absorption of the infrared light does not occur. More importantly for this work, transmission provides very limited spatial information, thus limiting its use *in situ*. For example, if a thin polymer film is examined in transmission, the infrared beam samples the film throughout its depth, and therefore diffusion in the film would be impossible to measure.

The technique of ATR on the other hand, is extremely well suited to the sampling of strongly absorbing samples, and is highly surface sensitive, allowing the differentiation between bulk and surface spectra. The detailed theory of ATR has been well reviewed by Mirabella¹ and Harrick², therefore only the relevant points will be discussed here.

A schematic of the ATR experiment is shown in Figure 2.5.

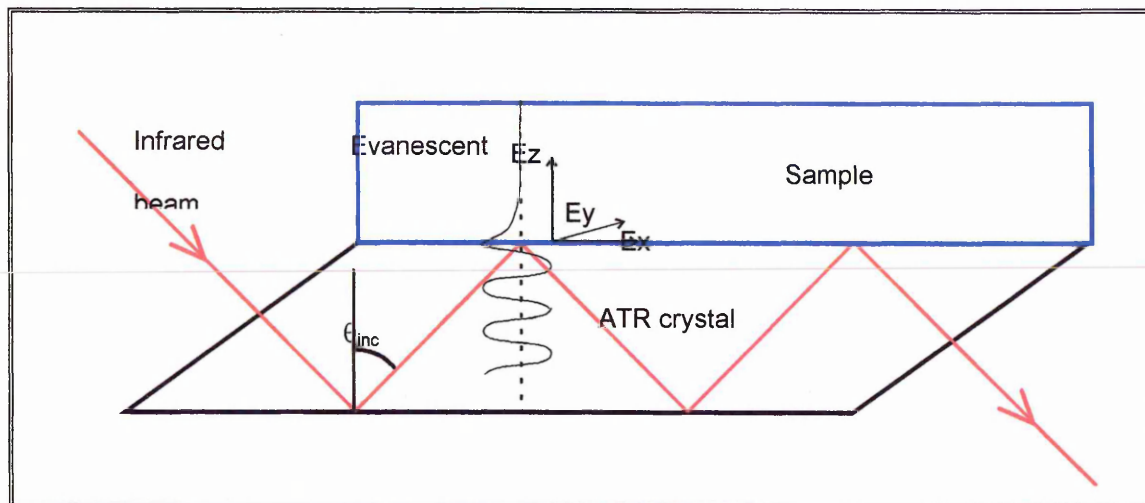


Figure 2.5 : Schematic of the ATR experiment

To perform ATR spectroscopy, the infrared beam is guided into an ATR crystal in optical contact with the sample. The incident angle (θ_{inc}) must be greater than the critical angle θ_c , and the ATR crystal must have a refractive index higher than that of the sample. Under these conditions, the infrared light undergoes total internal reflection at the interface between the optically dense medium (i.e. the ATR crystal) and the optically rare medium (i.e. the sample). At the interface, a decaying evanescent field is created. The evanescent field has components in all spatial directions, and decays exponentially with distance from the crystal surface. This is the basis for the surface sensitivity of the ATR technique. In the case of the geometry shown in Figure 2.5, an evanescent field is present at each interaction of the light with the interface. If an infrared absorbing medium is in contact with the ATR crystal, the reflection will be attenuated, and therefore the material will be sampled at each reflection.

Since the evanescent field samples the material of interest, its properties are extremely important to the spectroscopist. The important points can be summarised as follows :

1. There is no loss of energy at the interface between the optically dense and rare media, and therefore total internal reflection occurs.

2. The evanescent field in the rare medium is not transverse and has components in all directions. Therefore the field can interact with dipoles in the rare medium occurring in all directions.

3. There is a non-zero energy flow parallel to the interface resulting in a displacement of the incident and reflected waves. This is known as the Goos-Hänchen shift.

4. The evanescent field is confined to the surface of the rare medium and decreases with intensity with distance from the interface (i.e. along the z axis).

This last point is extremely important, because the decay of the evanescent field determines how much of the rare medium is sampled. The decay can be written as follows :

$$E = E_0 \exp \left[\frac{-2\pi}{\lambda_1} (\sin^2 \theta_{inc} - n_{21}^2)^{1/2} Z \right] \quad (2.11)$$

where E is the amplitude of the electric field a distance Z into the rare medium

E_0 is the electric field amplitude at the interface

θ_{inc} is the angle of incidence

n_{21} is equal to n_2 / n_1

where

n_2 is the refractive index of the rare medium

and n_1 is the refractive index of the dense medium

and λ_1 is the wavelength of light in the dense medium.

Equation 2.11 can be rewritten by replacing the exponential constant with the electric field amplitude decay coefficient, γ :

$$E = E_0 \exp[-\gamma Z] \quad (2.12)$$

$$\text{where } \gamma = \frac{2\pi(\sin^2 \theta_{\text{inc}} - n_{21}^2)^{1/2}}{\lambda_1} \quad (2.13)$$

The depth at which the electric field E decays to $E_0 \exp[-1]$ is known as the depth of penetration, or d_p . The depth of penetration is defined by

$$Z = d_p = \frac{1}{\gamma} \quad (2.14)$$

The depth of penetration, d_p is sometimes referred to as the sampling depth. However, at d_p , the Electric field has approximately 37% of its value at the surface, so some signal is collected from deeper into the rare medium. Although the evanescent field theoretically continues to infinity, a practical sampling depth, d_s is often considered, beyond which very little sampling occurs. The sampling depth, d_s is three times d_p .

It can be seen from equation 2.13 that the decay coefficient γ , and thus d_p depends upon the incident angle, the wavelength of light used, and n_{21} , the refractive index matching between the ATR crystal and the sample. Because it is usually desirable to have a small d_p , high refractive index materials are usually used as ATR crystals. However, the infrared transmission window of a material must also be taken into account. The properties of some common ATR materials are shown in table 2.1

Material	Infrared window	Refractive Index, n_1
Silicon	1300 - 8300 cm^{-1}	3.4
Germanium	600 - 5500 cm^{-1}	4.0
Zinc Selenide	450 - 20000 cm^{-1}	2.4
KRS5	250 - 20000 cm^{-1}	2.4

Table 2.1 : Optical characteristics of common ATR materials

Assuming a refractive index for the rarer medium of 1.5 (common for polymers), silicon as the ATR medium, an incident angle of 45° and infrared of frequency 1600 cm^{-1} , a value for d_p of $0.5 \mu\text{m}$. is found, giving a value for d_s of $1.5 \mu\text{m}$. In practice, d_p tends to vary between 0.1 and $5 \mu\text{m}$. One important consideration arising from equation 2.13 is that across the spectrum d_p will change, meaning that higher frequency bands will absorb less

than low frequency bands. This effect has been used to perform depth profiling with ATR³, as has the change in d_p when the angle of incidence is changed⁴.

It can be shown that

$$A \propto E^2 \quad (2.15)$$

where A is the absorbance measured in the infrared spectrum. I.e. the actual spectrum measured depends on the square of the electric field. The effect of this is shown in Figure 2.6.

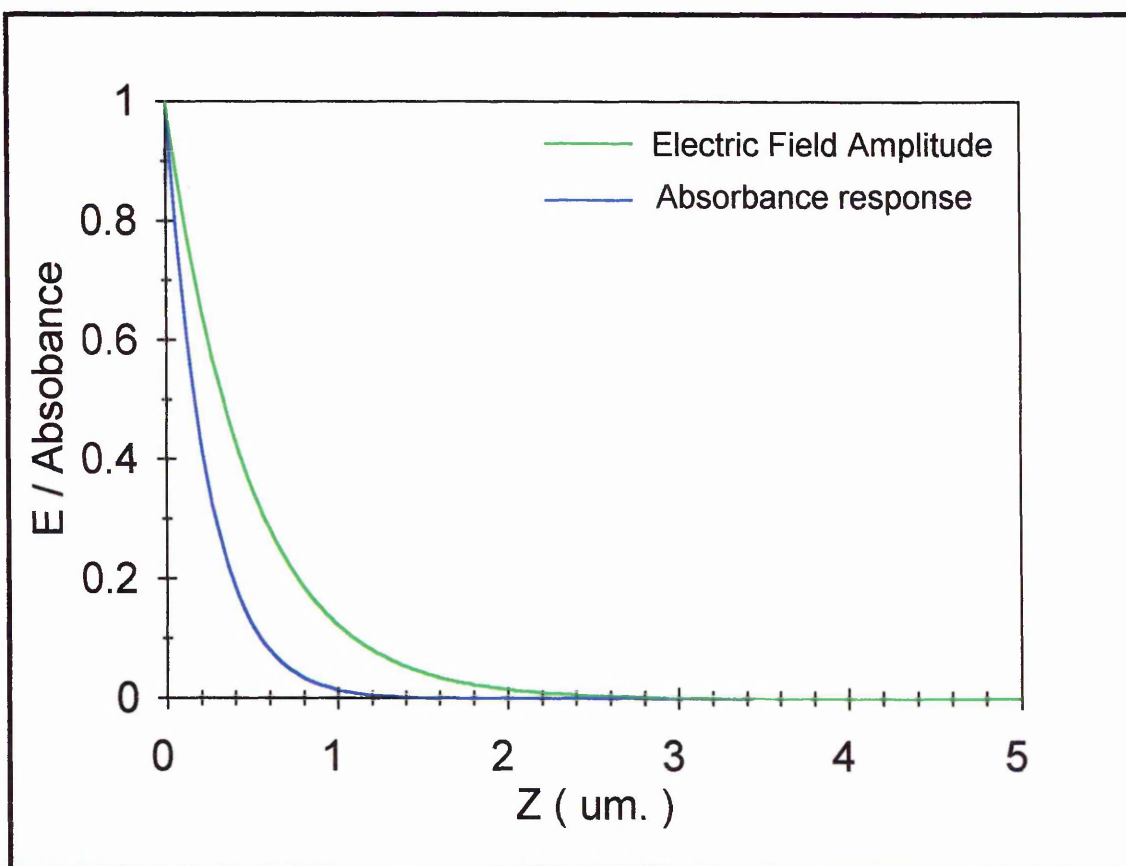


Figure 2.6 : The decay of the electric field amplitude and the absorbance response

2.1.3.1 : The advantages of ATR

1. Many reflections in the ATR crystal lead to large sampling number, thus increasing sensitivity.
2. Thin films can be studied with great sensitivity as most of the signal is obtained from < 1 μm . away from the surface.
3. The interface may be studied selectively, or depth profiling may be performed by manipulation of the evanescent wave.
4. In situ experiments are possible.
5. Interference fringes seen in transmission are not seen in ATR.

2.1.3.2 : The disadvantages of ATR

1. Very good optical contact is required between the sample and ATR crystal.
2. The total internal reflection wave loses energy at each reflection.

2.1.4 : Diffusion measurements with ATR - FTIR

The diffusion of small molecules in polymeric materials has been widely studied, and there is a large body of work on the theoretical background^{5,6}. There are many techniques which have been applied to the study of this diffusion, but most, such as the 'pat and weigh' technique⁷, where a slab of the polymer is immersed in the diffusant, and

removed for weighing, are *ex situ* techniques. In order to obtain kinetic information from measurements, it would be preferable to perform them *in situ*. In order to do this, this work shows the use of ATR -FTIR to monitor diffusion in a PVC film in contact with the ATR crystal, *in situ*. This section will discuss the theoretical basis for these measurements.

2.1.4.1 : Models of diffusion

Ficks' first law states that the rate of transfer of a diffusant through a unit area is proportional to the concentration gradient measured normal to the unit area⁸. This can be written as :

$$F_x = D \left(\frac{\partial C}{\partial x} \right) \quad (2.16)$$

where F_x is the flux of diffusant in the x direction

$\left(\frac{\partial C}{\partial x} \right)$ is the concentration gradient of the diffusant

and D is the diffusion coefficient.

However, Ficks' first law only applies to steady state diffusion, i.e. a fixed concentration of diffusant. For non-steady state conditions, Ficks second law gives the rate of change of penetrant concentration :

$$\left(\frac{\partial C}{\partial t} \right) = D \left(\frac{\partial^2 C}{\partial z^2} \right) \quad (2.17)$$

where C is the concentration of diffusant

t is time

and z is the axis normal to the polymer surface.

The mass of molecules diffused at time t into a polymer sheet may be given by: _____

$$\frac{M_t}{M_\infty} = \frac{4}{L} \left(\frac{Dt}{\pi} \right)^n \quad (2.18)$$

where M_t is the sorbed mass at time t

M_∞ is the sorbed mass at equilibrium

and L is the sheet thickness.

Experimentally, diffusion in polymeric materials can be categorised as follows^{9,10} :

1. Case I Diffusion : This occurs when the rate of diffusion is less than the mechanical relaxation time of the polymer. This is also known as Fickian diffusion. This is believed to be found when the motion of the diffusant follows a 'random walk' with no interactions. In case I diffusion the parameter n in equation 2.18 has a value of 0.5.

2. Case II diffusion : This occurs when the rate of diffusion is fast compared to the mechanical relaxation time of the polymer. This diffusion is characterised by a sharp moving diffusant boundary which progresses into the polymer at constant velocity. In case II diffusion the parameter n has a value of 1.

3. Case III diffusion : This is also known as non-Fickian diffusion. It may occur when the diffusion and relaxation rates are similar, but is also used to describe all other cases where neither case I or II occur. The parameter n may be between 0.5 and 1. Unlike case I or II, more than one parameter may be required to describe the diffusion.

If one assumes Fickian kinetics, it is possible to derive a general solution to the equation for the mass of diffusant in a film of thickness $2L$:

$$\frac{M_t}{M_\infty} = 1 - \sum_{n=0}^{\infty} \frac{8}{(2n+1)^2 \pi^2} \exp\left[\frac{-D(2n+1)^2 \pi^2 t}{4L^2}\right] \quad (2.19)$$

In the ATR experiment, the measured absorbance does not have a linear relationship with M_t , the mass of molecules. Therefore, in order to measure D , the diffusion coefficient, it is necessary to combine equation 2.19 with Harricks' equations for ATR¹¹ (see section 2.1.3). This has been carried out many times before^{12,13,18,20}, and so only the answers will be shown here.

The equation describing Fickian diffusion in terms of ATR absorbance is given below:

$$\frac{A_t}{A_\infty} = 1 - \frac{8\gamma}{\pi[1 - \exp(2L\gamma)]} \sum_{n=0}^{\infty} \left[\frac{\exp\left(\frac{-D(2n+1)^2 \pi^2 t}{4L^2}\right) \left[\frac{(2n+1)\pi}{2L} \exp(-2\gamma 2L) + (-1)^n (2\gamma) \right]}{(2n+1) \left[4\gamma^2 + \left(\frac{(2n+1)\pi}{2L}\right)^2 \right]} \right] \quad (2.20)$$

where A_t is the absorbance at time t

and A_∞ is the absorbance at equilibrium

A model that fits into the category of case III diffusion is the dual-sorption mode.

This model has been shown to be useful in systems where more than one diffusion coefficient is required to describe the diffusion^{14,15,16}. In the model, one species is mobile and able to diffuse freely in to the polymer matrix, while another species is described as partially mobile. This may be due to some species being trapped in voids in the polymer matrix¹⁷. This results in two different but constant diffusion coefficients. The model also requires the parameter x_1 which describes the proportion of molecules in the partially mobile state.

The equation for describing dual mode diffusion in terms of ATR absorption, as shown below, is a summation of equation 4.20 for the two species, convolved with the proportion factor x_1 ^{18,19}.

$$\frac{A_t - A_0}{A_\infty - A_0} = (1 - \sum D_1)x_1 + (1 - \sum D_2)(1 - x_1) \quad (2.21)$$

where

$$\sum D_x = \frac{8\gamma}{\pi[1 - \exp(2L\gamma)]} \sum_{n=0}^{\infty} \left[\frac{\exp\left(\frac{-D_x(2n+1)^2\pi^2t}{4L^2}\right) \left[\frac{(2n+1)\pi}{2L} \exp(-2\gamma 2L) + (-1)^n(2\gamma) \right]}{(2n+1) \left[4\gamma^2 + \left(\frac{(2n+1)\pi}{2L}\right)^2 \right]} \right]$$

where $x = 1$ or $x = 2$.

Using these two equations (equation 2.20 and equation 2.21) it is possible to determine diffusion coefficients from absorbance data^{20,21}, assuming the value L and which model is appropriate are known. This is applied in chapter 3.

2.2 : Raman Spectroscopy

2.2.1 : Introduction

The Raman effect was observed by C. V. Raman in 1928²². Raman obtained spectra using a mercury lamp, but it was only with the advent of intense, monochromatic and collimated light sources (i.e. lasers) that Raman spectroscopy became a practically useful technique. Therefore, compared to infrared spectroscopy, Raman is a relatively new technique, but further technological advances have caused the use of Raman spectroscopy to grow more widespread in recent years. The theory of Raman spectroscopy has been widely discussed in the literature^{23,24,25}, so only the main points will be discussed here.

2.2.2 : The Raman effect

The Raman effect occurs when light is scattered inelastically by matter. When a photon of light interacts with matter, it may be scattered in one of three ways:

i. Elastic scattering, which results in no net energy transfer between the photon and the matter. This is also known as Rayleigh scattering.

ii. Inelastic scattering where the photon is scattered with lower energy than the incoming energy. This is known as Stokes scattering.

iii. Inelastic scattering where the photon is scattered with higher energy than the incoming energy. This is known as anti-Stokes scattering.

Both types of inelastic scattering (ii and iii) give rise to Raman spectra.

Classically, when a molecule is placed in an electric field E , a dipole moment, μ_{ind} , is induced. The size of the induced dipole is dependent on the polarisability of the molecule, i.e. the ease with which the electron cloud of the molecule may be distorted. The induced dipole is given by

$$\mu_{\text{ind}} = \alpha E \quad (2.22)$$

where α is the polarisability tensor of the molecule. If the applied field is alternating, the induced dipole oscillates at the same frequency. The alternating electric field may be expressed as :

$$E = E^0 \cos 2\pi \nu_0 t \quad (2.23)$$

where E^0 is the electric field at time t

and ν_0 is the angular frequency of radiation

The induced dipole emits or scatters radiation of frequency ν_0 which is Rayleigh scattering. Assuming a simple harmonic oscillator, a diatomic molecule vibrating can be described by

$$q_v = q_0 \cos 2\pi\nu_v t \quad (2.24)$$

where q_v is the displacement at time t

and ν_v is the frequency of vibration.

If this vibration leads to a change in polarisability, the polarisability can be written as

$$\alpha = \alpha^0 + \left(\frac{\partial \alpha}{\partial q_v} \right)_0 q_v \quad (2.25)$$

substituting (2.24) into (2.25) gives

$$\alpha = \alpha^0 + \left(\frac{\partial \alpha}{\partial q_v} \right)_0 \cos 2\pi\nu_v t \quad (2.26)$$

If radiation of frequency ν_0 interacts with the molecule then the induced dipole is given by :

$$\mu_{\text{ind}} = \alpha E = \alpha E^0 \cos 2\pi \nu_0 t \quad (2.27)$$

substituting (2.26) into (2.27) gives

$$\mu_{\text{ind}} = \alpha^0 E^0 \cos 2\pi \nu_0 t + \left(\frac{\partial \alpha}{\partial q_v} \right) E^0 q_0 \cos 2\pi \nu_v t \cos 2\pi \nu_0 t \quad (2.28)$$

$$\mu_{\text{ind}} = \alpha^0 E^0 \cos 2\pi \nu_0 t + \left(\frac{\partial \alpha}{\partial q_v} \right) \frac{E^0 q_0}{2} [\cos 2\pi(\nu_0 + \nu_v)t + \cos 2\pi(\nu_0 - \nu_v)t]$$

Therefore for Raman scattering to occur, a change in the polarisability of the molecule must occur during the vibration. i.e.

$$\left(\frac{\partial \alpha}{\partial q_v} \right)_0 \neq 0 \quad (2.29)$$

must be true for a vibration to be Raman active.

From a quantum mechanical point of view, the processes that may occur upon scattering of a photon are shown in Figure 2.7. When light is scattered, almost all of the photons undergo Rayleigh scattering. The low probability of Raman scattering is the reason why high intensity light sources are required for Raman spectroscopy. It can be seen from Figure 2.7 that Anti-Stokes scattering occurs from a vibrationally excited state.

As the majority of molecules occur in the ground state, Stokes scattering is considerably more likely than Anti-Stokes scattering.

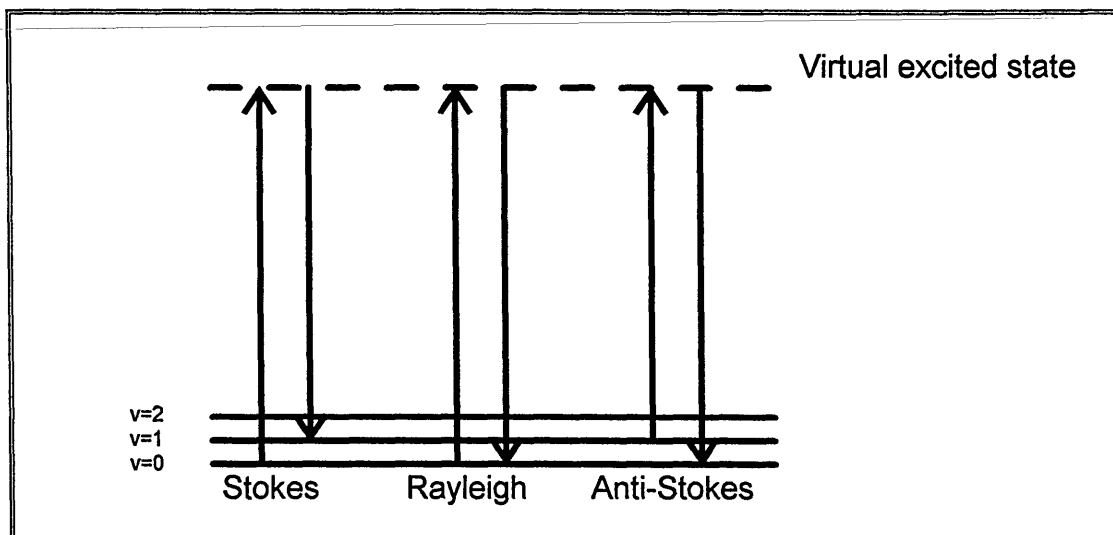


Figure 2.7 : Quantum mechanical scattering processes

It can also be seen from Figure 2.7 that like infrared spectroscopy, Raman spectroscopy probes the vibrational energy levels of a molecule. Because it is often the case that for molecular vibrations, when $\frac{\partial\mu}{\partial Q}$ (the dipole change) is large, $\frac{\partial\alpha}{\partial Q}$ (the polarisability) is small, and vice versa, many vibrations are either strong in the infrared or Raman, but not both. Although strictly incorrect, such vibrations are often said to be either infrared or Raman active. Therefore infrared and Raman give the same kind of information, but often about different molecular vibrations. Infrared and Raman are often said to be complementary techniques.

Practically, Raman spectroscopy is usually carried out on the Stokes part of the spectrum, due to the higher intensity. This is illustrated in Figure 2.8, which shows the Raman spectrum of a silicon surface. The Stokes $\nu(\text{Si-Si})$ vibration of silicon occurs at 520 cm^{-1} relative to the Rayleigh light, and the anti-Stokes vibration at -520 cm^{-1} . It should be noted that the Rayleigh light in this spectrum has been filtered; usually Rayleigh intensities are several orders of magnitude greater than Raman intensities.

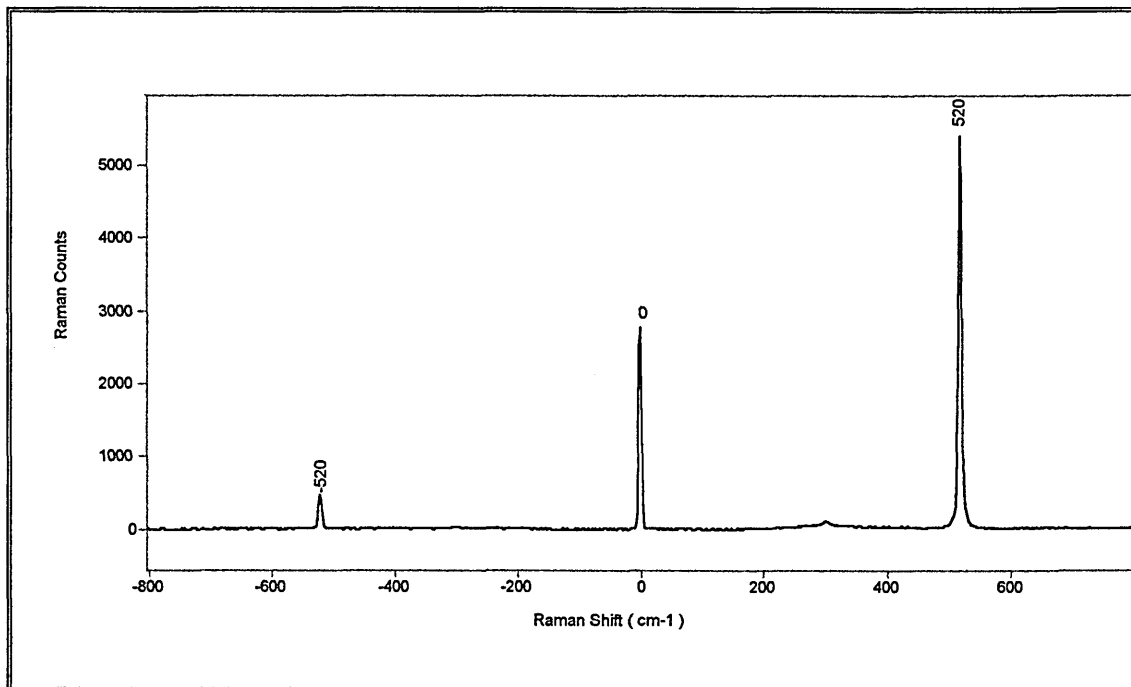


Figure 2.8 : Raman spectrum showing, from left, Anti-Stokes, Rayleigh and Stokes lines

2.2.3 : Raman microscopy

Like infrared spectrometers, traditional Raman spectrometers simply consist of a light source, a dispersive element and a detector. However, Raman light sources need to be monochromatic, in order to facilitate measurement of the Raman shift, which gives the

vibrational information. The most common sources are HeNe, Argon ion, and NdYAG lasers, giving possible excitation wavelengths between 480 and 633 nm. These are visible wavelengths, which makes coupling of a Raman spectrometer to a microscope a relatively simple task, as a standard optical microscope may be used. Unlike infrared spectroscopy, Fourier Transform Raman spectroscopy is still relatively rare, although it is a well developed technique^{26,27}. Most Raman spectrometers use a grating as the dispersive element, such as the Renishaw Ramascope described herein. The use of a monochromator and photomultiplier to reject light and detect the Raman light is common, but the Ramascope, as described below uses a more novel system. As the performance of this spectrometer is of direct relevance to this project, the details of the instrument are discussed in the next section.

2.2.4 : The Renishaw Ramascope

The Raman instrument used in this project was a Renishaw Ramascope system 2000. The system 2000 features an additional optical path used for imaging which is not discussed here. A schematic diagram of the components of the Ramascope is shown in Figure 2.9.

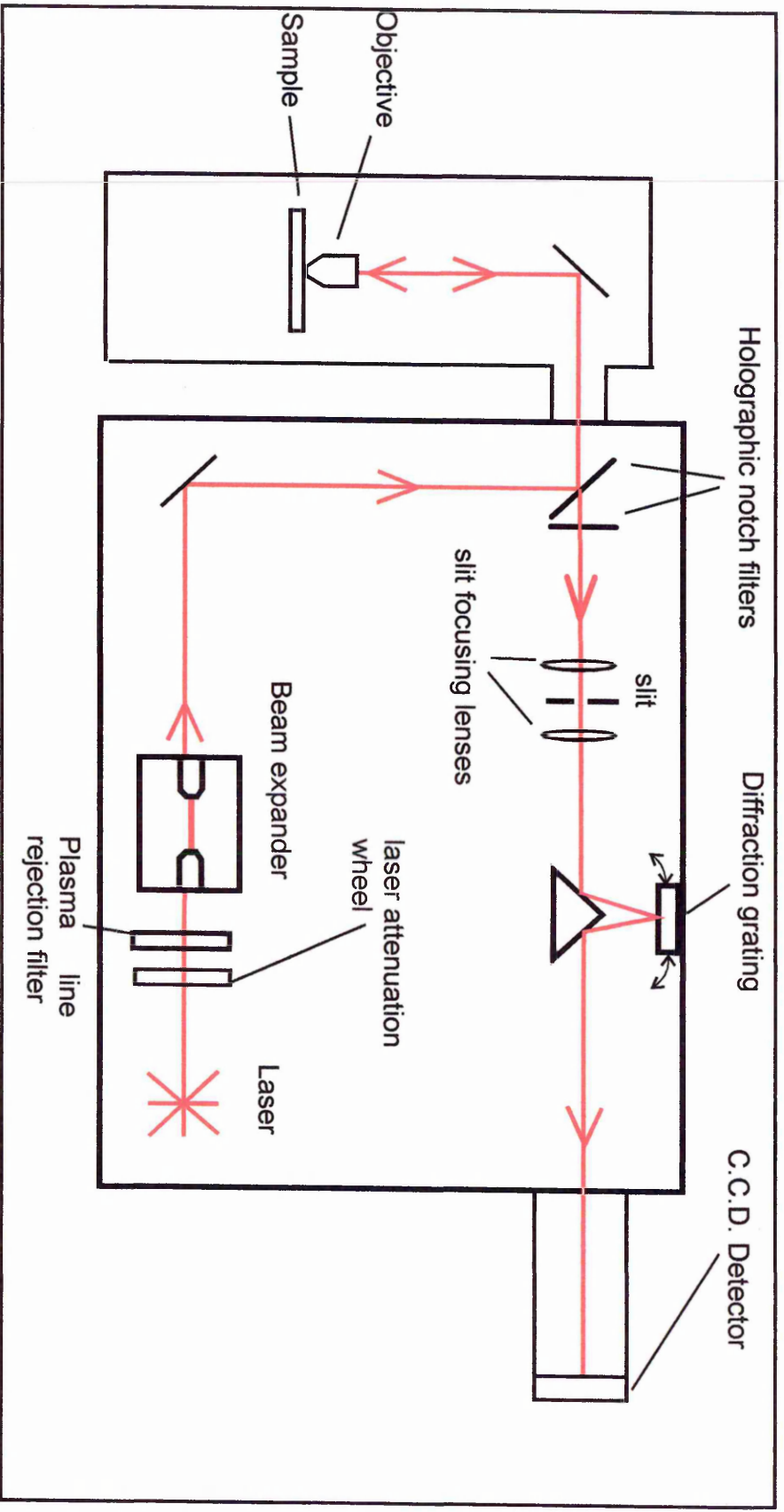


Figure 2.9 : Schematic diagram of the Renishaw Ramascope

The spectrometer functions as follows: The source is a 25 mW. Helium-Neon laser at 632.8 nm. This enters the spectrometer through a laser attenuation wheel. This can be used to reduce the power of the laser. Unless otherwise mentioned, this was used at the full power setting. The laser then passes through a plasma line rejection filter (PLF). The PLF rejects all frequencies except the 632.8 nm. line. The laser is guided into a beam expander, which is simply two objective lenses required to expand the beam to the size used by the microscope objective (approximately 10 mm.). The beam expander may include a pinhole at the focus, to collimate the beam. However, in the system described here, the beam is collimated as it exits the laser, so this is not necessary. The expanded beam is then guided onto the first holographic notch filter (H.N.F.). The H.N.F.s act like monochromators, as they reflect Rayleigh light (i.e. the frequency of the laser), and allow all other frequencies to pass. The first H.N.F. acts as a beam splitter, guiding the laser light into the microscope, whilst allowing the returning Raman light into the spectrometer. The light enters the microscope accessory (an Olympus BH-1 optical microscope), and is directed onto the sample with an ordinary microscope objective. In this work, 100X, 50X and 20X U.L.W.D. (ultra long working distance) objectives have been used.

The light scattered by the sample is collected by the same objective (180° scattering geometry). This light is a mixture of Rayleigh, Stokes and anti-Stokes scattered light. The light is guided into the spectrometer, and passes through the two H.N.F.s. These remove almost all of the Rayleigh light, as can be see in Figure 2.8. Without the H.N.F.s the Rayleigh light swamps the spectrum. The light is next focused through an optical slit. This acts as one part of a spatial filter, and will be explained in the following section,

describing confocal Raman microscopy. The light is then reflected by a triangular mirror onto a diffraction grating. The grating is fixed to a rotating motorised stage, and the angle of the grating determines the wavelengths of Raman light detected. After the grating, the light is focused onto a peltier-cooled C.C.D. (charge-coupled device) detector.

The C.C.D. is a silicon array device which can detect light on any one of it's 600 x 400 pixels. In order to collect a spectrum, the grating disperses light which is focused in a line onto the long axis of the C.C.D. It is therefore possible to detect approximately 600 spectral elements without moving the grating (a 'static' spectrum). In order to collect full range spectra, the grating is rotated. The spectral range of the instrument is approximately 200 to 5000 cm^{-1} . This is somewhat limited at low frequencies compared to monochromator - based spectrometers, which can often detect light at Raman shifts as low as 20 cm^{-1} . However, for organic materials (e.g. polymers) most bands occur between 500 and 3500 cm^{-1} , so it is suited to this work. The advantages of the Renishaw Ramascope are high sensitivity due to the C.C.D. detector, and the ability to perform confocal Raman microscopy, which is discussed in the next section.

2.2.5 : Confocal Raman microscopy

Confocal microscopy is a technique of eliminating light from outside the focal plane. In optical microscopy, this allows images of 'sections' of a transparent material to be obtained. Confocal Raman microscopy allows the collection of a spectrum from a very small volume of material. In the x-y (or focal) plane, it is easy to collect light only from a

small area, by simply focusing the laser to small spot. The area sampled is limited to about $1 \mu\text{m}^2$ by the diffraction limit. In the z (or optical axis) however, it is not as simple to collect a spectrum from a small region only. Confocal microscopy eliminates back scattered light from above or below the focal plane.

The signal intensity that reaches the detector for a given Raman band is given, to a first approximation by

$$SI \approx I_0 \sigma_\lambda \lambda N \theta T_\lambda s_\lambda \quad (2.30)$$

where SI is the signal intensity at wavelength λ

I_0 is the laser irradiance at the sample (in watts / unit area)

σ_λ is the differential cross-section for the analysed Raman band (in $\text{cm}^2 \text{sterad}^{-1}$ molecule $^{-1}$)

N is the number of molecules sampled

θ is the angle of collection of the Raman light

T_λ is the throughput of the instrument

and s_λ is the sensitivity of the detector at the given wavelength.

When in confocal mode, there is clearly a small value for N , as a small volume is sampled. Using a high numerical aperture (NA) objective compensates for this somewhat. The NA of an objective is defined as follows

$$NA = n \sin\left(\frac{\theta}{2}\right) \quad (2.31)$$

where θ is the angle of entrance

and n is the refractive index of the transmitting medium.

The collection geometry is shown in Figure 2.10, which shows both high and low NA objectives. It can be seen from Figure 2.10, that high NA objective can focus the light into a small area, and collect over a wide angle. Raman light is scattered isotropically, so a wide collection angle increases the signal collected per unit volume. In contrast, low NA objectives focus light on a larger volume of material, thus collecting Raman scattering from a large volume. Practically, it is found that for optimum signal, assuming a large sample, an intermediate NA is ideal.

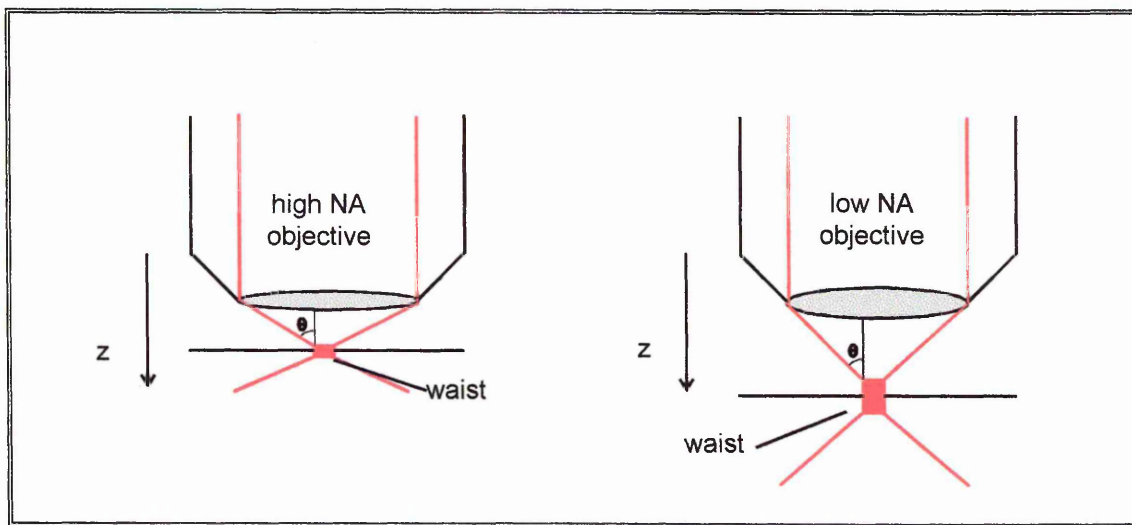


Figure 2.10 : The distribution of laser light near focus for high and low NA objectives

The NA, entrance angle and depth of focus (L) of the objectives used in this work are shown in table 2.2 :

Objective	NA	θ (°)	Depth of focus, L
			($\mu\text{m.}$)
x 100	0.95	71.8	0.1
x 50	0.80	53.13	0.4
x 20 (U.L.W.D.)	0.40	23.58	3.3

Table 2.2 : Optical parameters of objective lenses used

Confocal operation is traditionally obtained by placing a pinhole in the back focal plane of the microscope²⁸. The alignment of this pinhole is critical to the performance of the microscope. Unfortunately, pinhole alignment is a difficult and time consuming task, so the Ramascope uses an alternative method²⁹. This is illustrated in Figure 2.11.

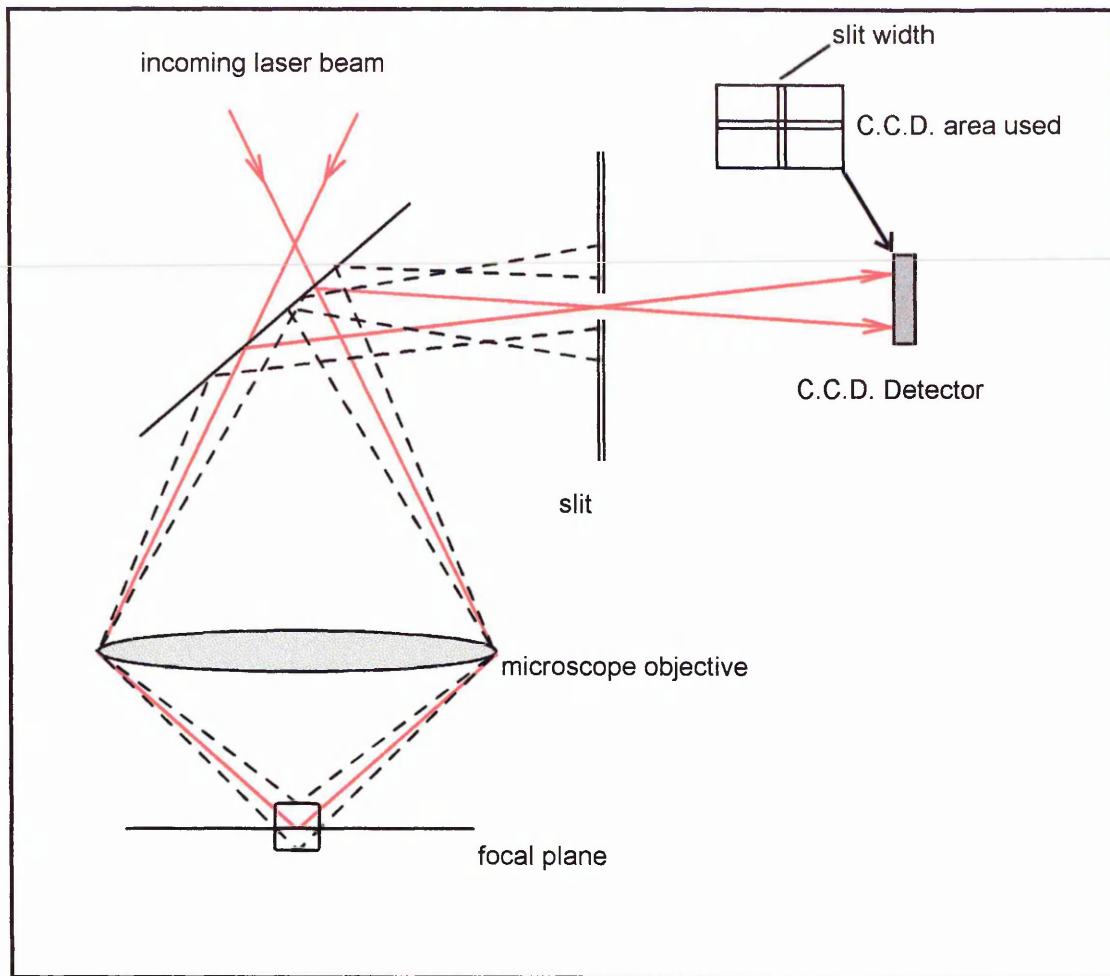


Figure 2.11 : Schematic diagram of the operation of the Ramascope in confocal mode

The Ramascope effectively uses two slits in the back focal plane at right angles to each other to simulate a pinhole. One of these is a mechanical slit, the width of which is micrometer controlled. The other slit is made by selecting a long box of elements on the C.C.D. detector, and binning the data from the other elements.

The geometrical effect of the pinhole is explained here with reference to Figure 2.12, assuming no diffraction occurs at the pinhole. This assumption has been shown to be valid for pinholes greater than $100\mu\text{m}$., as used here³⁰.

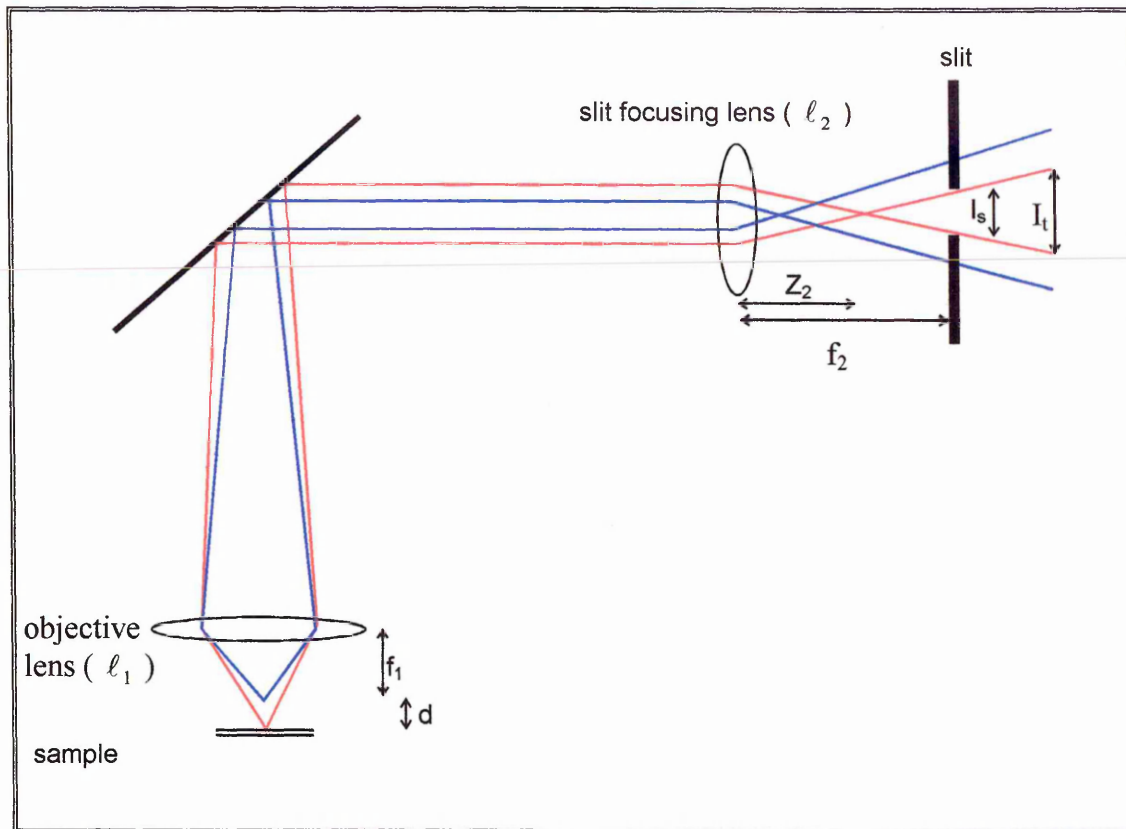


Figure 2.12 : Diagram of confocal microscope showing pinhole operation. For clarity, only the returning (Raman) light is shown, and the light from the focal plane is red, and light from out of focus is blue

The objective lens (l_1) focuses the beam onto the area to be sampled. At this point the beam has it's smallest diameter, but this diameter remains constant within a certain distance from the focal plane³¹. This distance is known as the waist, or the depth of focus (L). L is given by :

$$L = 6.4 \left(\frac{\lambda}{2\pi} \right) \left(\frac{1}{\tan\theta} \right)^2 \quad (2.32)$$

The values of L for the objectives used are given in table 2.2.

The size of the laser spot can be expressed as :

$$s(f_1 \pm d) = s(f_1) \quad \text{for} \quad d < \frac{L}{2} \quad (2.33)$$

$$s(f_1 \pm d) = s(f_1) + 2\left(d - \frac{L}{2}\right)\tan\theta \quad \text{for} \quad d > \frac{L}{2} \quad (2.34)$$

where f_1 is the focal length of the objective lens

and d is the distance from the plane of focus

In Figure 2.12 it can be seen that the light from out of the focal plane is imaged at distance Z_2 from the slit - focusing lens (f_2). This leads to the image at the slit of this light being out of focus. The distance Z_2 is given by

$$Z_2 = \left[\frac{1}{f_2} - \frac{1}{f_2 - \left(\frac{1}{f_1} - \frac{1}{f_1 \pm d} \right)^{-1}} \right]^{-1} \quad (2.35)$$

where f_2 is the focal length of the slit focusing lens. The size of this spot is $s(f_1 \pm d)$. The diameter of this image at the slit (I_1) is given by

$$I_1 = \frac{f_2 M [s(f_1 \pm d)]}{Z_2} \quad (2.36)$$

where M is the magnification power of the objective.

As this image is much larger than the image from the focus point (i.e. the laser spot image), it is possible to eliminate most of the out of focus light by including a pinhole of diameter less than I_t in front of the detector. A high NA objective produces a more divergent beam, from outside the focal plane, making it easier to remove the unwanted light.

The experimental confocal response is determined as follows. The laser is focused on the surface of a silicon crystal, and a spectrum taken. The intensity of the 520 cm^{-1} band of silicon (see Figure 2.8) is measured. The focus is then moved $1\text{ }\mu\text{m}$. away from the surface and another spectrum measured. This is repeated to build up a 'confocal response profile'. The full width at half height (FWHH) of this profile is the parameter used as a measure of confocality. This process generates one half of the profile that would be obtained by measuring a thin film in transparent medium. Therefore the profile may be mirrored to get the true value, or the FWHH doubled. Confocal profiles, using the 100X objective, with and without the instrument set up in confocal mode are shown in Figure 2.13.

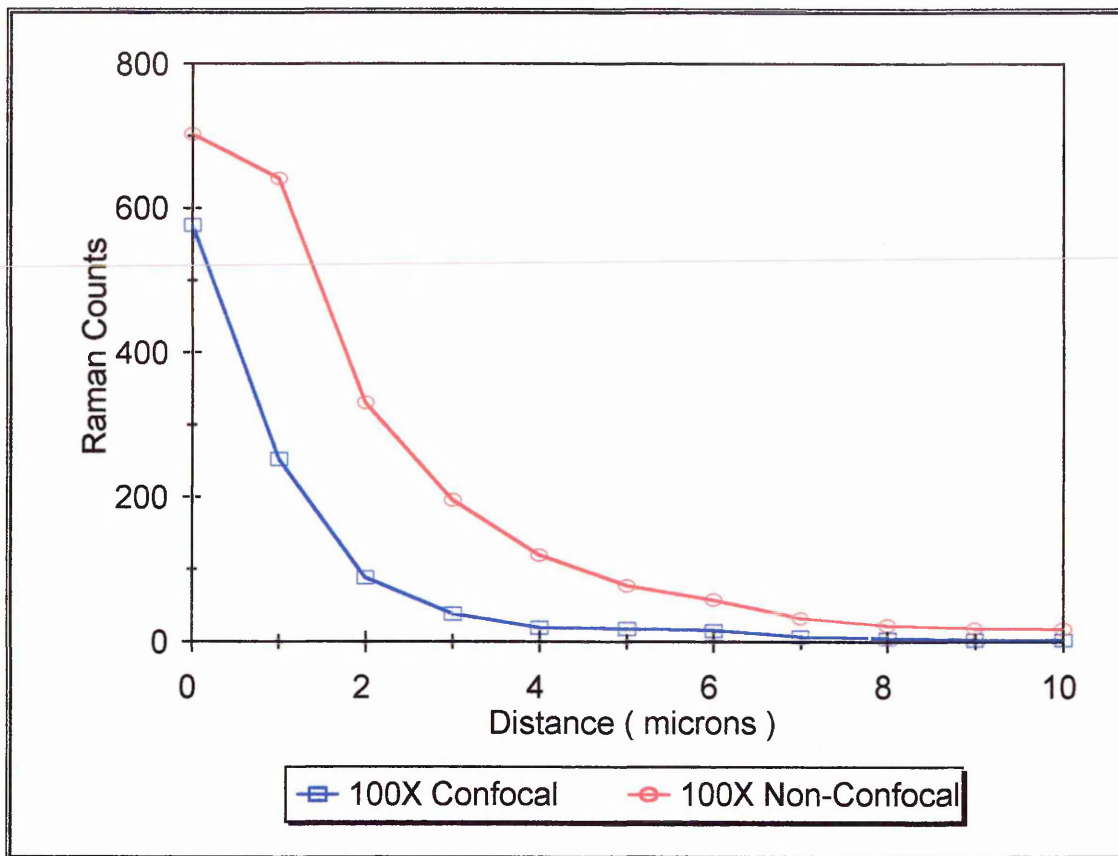


Figure 2.13 : Comparison of confocal and non - confocal modes, using the 100X objective

It can be seen from Figure 2.13 that the spatial FWHH in confocal mode, using the 100X objective is somewhat smaller than $2\mu\text{m}$. As mentioned previously, a high NA objective is required for confocal measurements. To confirm this, confocal profiles were obtained for all three objectives used in this work. These are presented in Figure 2.14.

II. Fluorescence from impurities and the spectrum of the substrate is often eliminated, due to the small volume analysed.

2.2.7 : Disadvantages of confocal Raman microscopy

I. The small volume analysed means signal intensity is always smaller in confocal mode.

II. Due to the concentration of laser power in a small area, the chance of sample burning is increased. Fortunately, in PVC, sample burning is revealed by a highly intense fluorescence spectrum^{32,33}, so it is simple to detect this effect.

Despite these disadvantages, Raman confocal microscopy is an excellent technique for the depth profile analysis of polymer laminates^{29,34}.

References

- 1 Internal Reflection Spectroscopy : Theory and Applications, Ed. by Mirabella, F. M., Marcel - Dekker, New York (1993)

- 2 Internal Reflection Spectroscopy, Ed. by Harrick, N. J., Harrick Scientific Corporation, New York (1987)
- 3 Ishida, H. and Ekgasit, S., Applied Spectroscopy Vol. 51, No. 10, p. 1488 (1997)
- 4 Ishida, H. and Ekgasit, S., Applied Spectroscopy, Vol. 51, No. 4, p.461 (1997)
- 5 The Mathematics of Diffusion, 2nd. Ed., Ed. by Crank, J., Clarendon Press, Oxford (1994)
- 6 Polymer Permeability, Ed. by Windle, A. H. and Comyn, J., Elsevier Applied Science Publishers, London (1986).
- 7 Miglaresi, C., Nicodemo, L., Nicolais, L. and Paserini, L., Polymer Vol. 23, p.687 (1984)
- 8 Diffusion in Polymers, Ed. by Crank, J. and Park, G. S., Academic Press, London (1968)
- 9 Alfrey, T., Gurnee, E. F. and Lloyd, W. G., Journal of Polymer Science, Vol. 12, p. 249 (1966)
- 10 Schlotter, N. E. and Furlan, P. Y., Polymer Vol. 33, No. 16, p. 3323 (1992)
- 11 Harrick, N. J., Journal of the Optical Society of America, Vol. 55, p.851 (1965)
- 12 Van Alsten, J. G., Trends in Polymer Science Vol.3, No.8, p. 272 (1995)
- 13 McKnight, S. H. and Gillespie, J. W., Journal of Polymer Science, Vol. 64, part 10, p.1971 (1997)

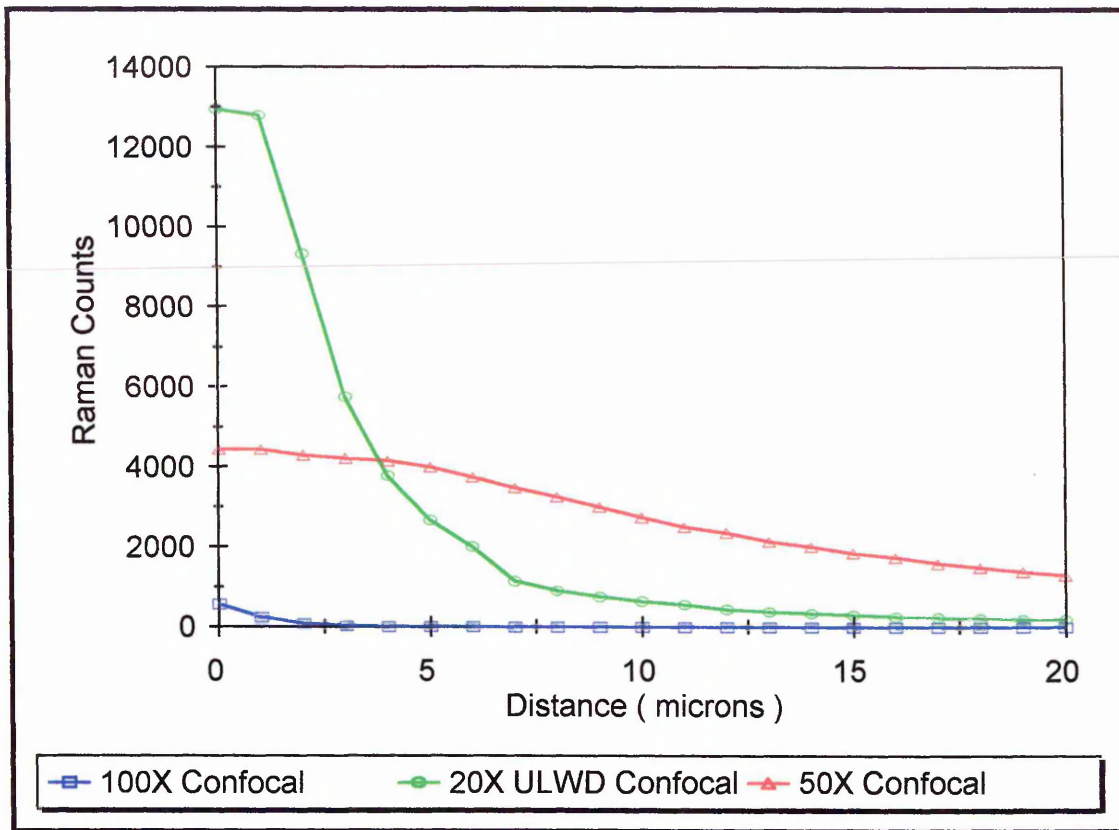


Figure 2.14 : Confocal profiles from the 100X, 50 X and 20X U.L.W.D. objectives

It can be seen from Figure 2.14 that although the optical through put is low, the 100X objective gives by far the best spatial resolution, and therefore only the 100X objective was used for depth profiling work.

2.2.6 : Advantages of confocal Raman microscopy

I. Confocal Raman microscopy allows the collection of *in situ* depth profiles. Without the ability to collect a spectrum from within a transparent polymer film with spatial resolution on the μm . scale, depth profiling would require destructive sample preparation techniques, such as sectioning.

- 14 Vieth, W. R. and Amini, M. A., Papers of the A.C.S. Division of Organic Coatings and Plastics Chemistry Vol. 32, p.442 (1974)
- 15 Petropolous, J. H., Journal of Polymer Science Part A2, Vol. 8, p. 1797 (1980)
- 16 Horwas, J. A. and Nieto, F., Journal of Polymer Science Part B: polymer Physics, Vol. 32, p. 1889 (1994)
- 17 Frisch, H. L., Polymer Journal Vol. 23, No. 5, p. 225
- 18 Hajatdoost, S. and Yarwood, J., Journal of the Chemical Society - Faraday Transactions Vol. 93, No. 8, p.1613 (1997)
- 19 Pereira, M. R. and Yarwood, J., Journal of the Chemical Society - Faraday Transactions Vol.92, No. 15, p.1613 (1997)
- 20 Hong, S. U., Barbari, T. A. and Sloan. J. M, Journal of Polymer Science part B - Polymer Physics, Vol. 36, No. 2, p. 337 (1998)
- 21 Sammon, C., Everall, N. and Yarwood, J., Macromolecular Symposia Vol. 119, p. 189 (1997)
- 22 Ferraro, J. R., Spectroscopy Vol. 11, No. 3, p.18 (1996)
- 23 Clark, R. J. H. and Hester, R. E., Spectroscopy of Surfaces. Advances in Spectroscopy, Vol. 10, Wiley, New York (1988)
- 24 Laser Raman Spectroscopy, Ed. by Gilson, T. R. and Hendra, P. J., Wiley-Interscience, London (1972)
- 25 The Raman Effect, Ed. by Chantry, G. W., Marcel-Dekker, New York (1971)
- 26 Urban, M. W., Abstracts of Papers of the A.C.S., Vol. 215, part 2, p. 11 (1998)

- 27 Hendra, P. J., Wilson, H. M. M., Wallen, P. J., Wesley, I. J., Bentley, P. A., Arruebarrenabaez, M., Haigh, J. A., Evans, P. A., Dyer, C. D., Lehnert, R., and Pellowjarman, M. V., *Analyst* Vol. 120, No. 2, p. 985 (1995)
-
- 28 Puppels, G. L., Otto, C. and Greve, J., *Trends in Analytical Chemistry*, Vol. 10, No. 8, p.249 (1991)
- 29 Williams, K. P. J., Pitt, G. D., Batchelder, D. N., and Kip, B. J., *Applied Spectroscopy* Vol. 48, No.2, p. 232 (1994)
- 30 Dhamelincourt, P., Barbillat, J. and Delhaye, M., *Spectroscopy Europe* Vol. 5, p. 16 (1993)
- 31 Born, M. and Wolf, E., *Principles of Optics*, 6th. Ed., Pergamon Press, Oxford, p.435 (1980)
- 32 Ellahi, S., Hester, R. E. and Williams, K. P. J., *Spectrochimica Acta Part A - Molecular and Biomolecular Spectroscopy* Vol. 51, No. 4, p. 549 (1995)
- 33 Owen, E. D., Shah, M. and Twigg, M. V., *Polymer Degradation and Stability* Vol. 51, No. 2, p. 151 (1996)
- 34 Hajatdoost, S. H., Olsthoorn, M., and Yarwood, J., *Applied Spectroscopy* Vol. 51, No. 12, p. 1784 (1997)

Chapter 3 : ATR-FTIR studies of organosilane diffusion

In order to determine whether interdiffusion of silane and PVC may occur in the glass / silane / PVC system, ATR-FTIR experiments have been carried out. As described in chapter 2, similar experiments have been applied to different systems elsewhere, and have been successful in determining kinetics of diffusion¹⁻⁴. This chapter describes the experiments that have been performed *in situ* to determine the kinetics of diffusion, as well as the factors which affect the kinetics.

3.1 : Experimental

In order to obtain information of relevance to glass / PVC / silane laminates, it was decided to perform experiments on a model laminate. A schematic diagram of the laminates used is presented in Figure 3.1.

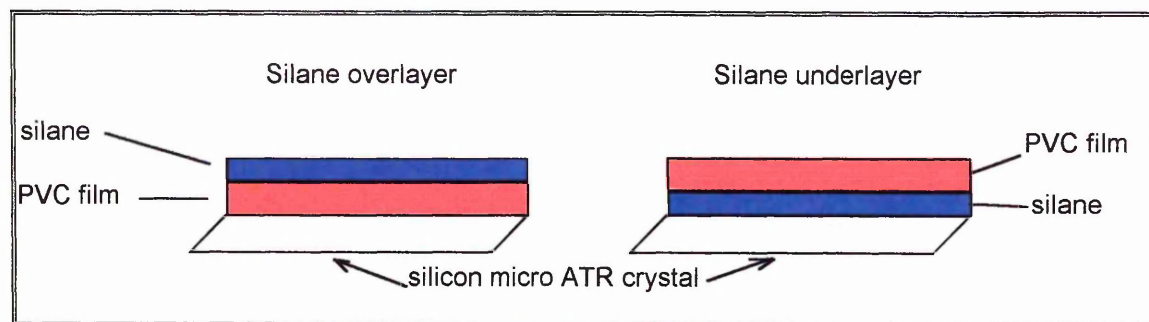


Figure 3.1 : Schematic diagram of model laminates used for ATR-FTIR experiments

The substrate chosen for this laminate was a silicon micro ATR crystal. This serves as a suitable model for glass, as the surface properties of oxidised silicon and glass are similar.

Without pre-treatment to remove the oxide layer of silicon, it would be expected to consist of a hydroxylated surface, i.e. the surface chemistry would be dominated by the presence of -SiOH groups. Unless heat-treated, it would also be expected that a certain amount of surface water would be present⁵. The micro ATR crystal also serves as the optically-dense material in the ATR experiment (see section 2.13). The micro ATR crystal functions in the same way as a normal (or macro) ATR crystal, but is very thin, in this case 0.5 mm. thick. This has the effect of increasing the number of reflections in the ATR experiment, and thus increasing the sensitivity of the experiment. This is illustrated schematically in figure 3.2. The number of reflections (totalled over both sides), N is given by

$$N = \cot\theta \left(\frac{L}{t} \right) \quad (3.1)$$

where θ is the incident angle (see figure 2.5)

L is the length of the crystal

and t is the thickness of the crystal

From equation 3.1, at $\theta = 45^\circ$, a standard macro ATR crystal gave rise to 14 reflections, whereas the micro ATR crystal used (L = 18 mm., t = 0.5 mm.) gave 38 reflections, so that the micro ATR crystal should have been approximately 2.7 times more sensitive. The micro ATR geometry has the disadvantage that focusing the infrared beam onto the face is more difficult, which means that the overall optical throughput is lower. However, in practice the micro ATR crystals were found to be much more sensitive overall, especially for low intensity bands.

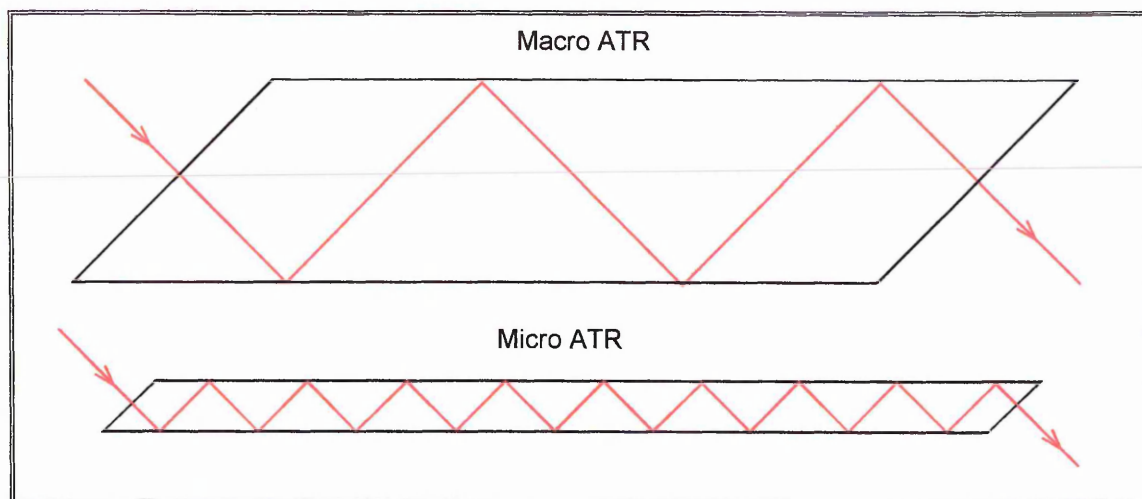


Figure 3.2 : Schematic of the difference between macro ATR and micro ATR

As shown in section 2.1.3, silicon has a somewhat limited mid infrared spectral window, so spectral measurements were made only above 1300 cm^{-1} .

The silicon substrates were cast with 5% PVC solutions from N,N-dimethylformamide. Forming films by casting does not always give films of even thickness over the whole area of the film. The alternative polymer film formation techniques considered were spin coating and dipping. Spin coating was not considered to be a viable alternative, as the films formed were far too thin for this experiment. Dipping was assessed as an alternative technique, but it was found that several coating runs were required for adequate thickness, and that wedge shaped films often resulted. Due to the kinetic analysis of the diffusion results (see section 2.1.4), it is necessary that the films used be as close as possible to an ideal 'slab' of polymer as possible. In order to determine how flat the films were, a Talysurf surface profiler was used. This is a mechanical instrument that measures

the step size between the substrate and film to an accuracy of $\pm 0.02 \mu\text{m}$. The output from a typical Talysurf measurement is shown in figure 3.3.

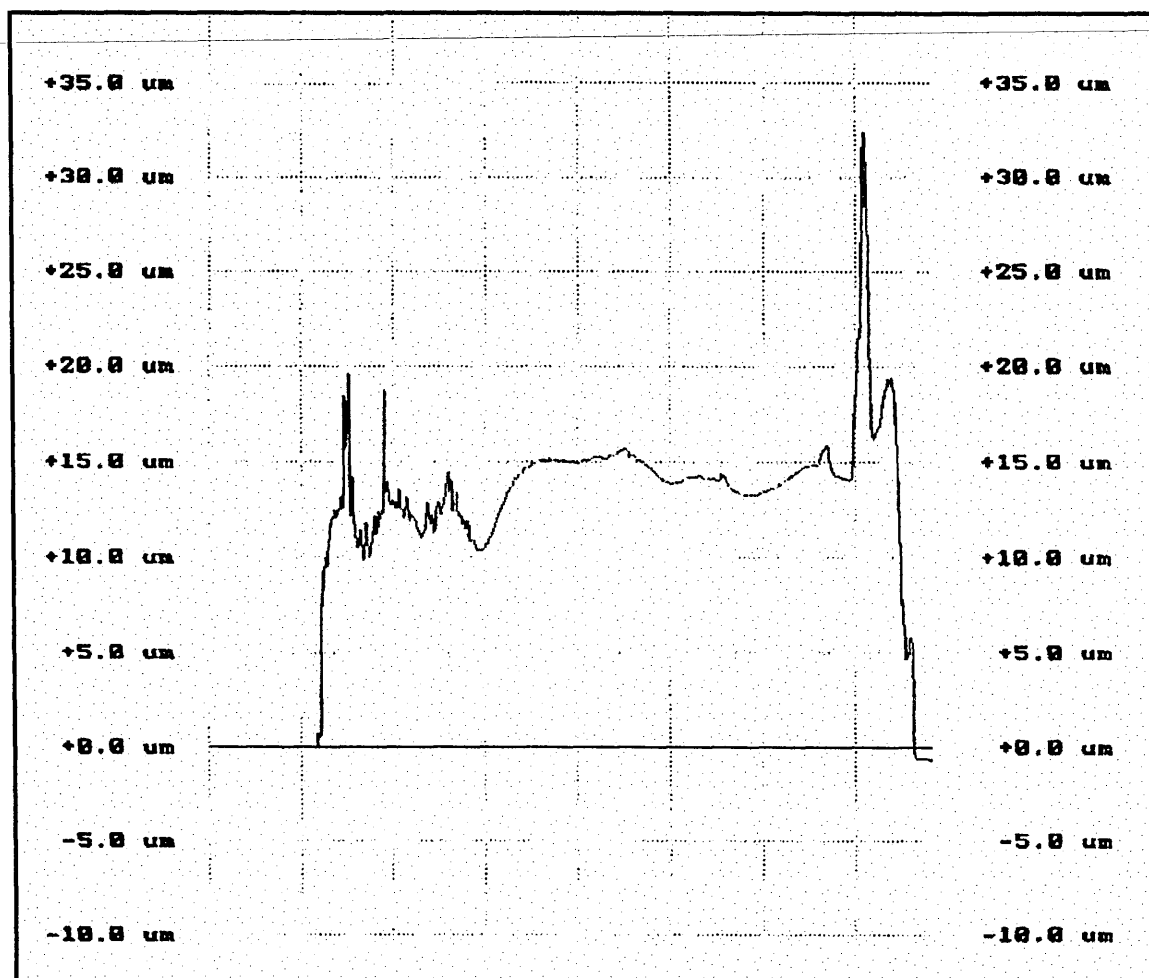


Figure 3.3 : A typical Talysurf surface profile. The horizontal scale is 2mm. per division

It can be seen from figure 3.3 that many samples showed considerable heterogeneity in thickness around the edges. In these cases, diffusion was only measured in the centre of the film (by applying silane only to this area).

In order to know the average thickness, the mean value from the Talysurf profile was taken. The cast films were heated for 14 hours at 65°C to remove the solvent. It was

found that after the heating process, the film was often thicker and more variable in thickness around the edges, but thin and of even thickness in the centre of the crystal. In order that this did not affect the diffusion results, in these cases the silane was only applied to the flat portion of the film. The silane was applied by a number of techniques.

The silane was first applied as a 'silane underlayer'. In this configuration, the silane was pre-hydrolysed and cast from solution. The film was then heated to remove solvent. The solvent used was 9:1 (v/v) IPA / H₂O mixture, with 3% (v/v) added acetic acid as hydrolysis catalyst. This solution has been previously reported to hydrolyse organosilanes rapidly⁶. After drying, PVC was cast onto the silane layer from DMF or MEK solution, and the laminate was heated to remove the DMF. In this configuration any silane diffusion would be seen as a decrease in silane band intensity.

In the 'silane overlayer' configuration the PVC was cast directly onto the ATR crystal, and then the DMF removed by heating. The silane was then applied onto the top of the PVC film, either by spraying or brushing. Spraying was found to be preferable in order to apply a fixed amount of silane. Brushing, however, was more convenient when a large amount was to be applied. When spraying, a template was used to ensure that the silane was only applied to the area required. In all cases, the silane was handled in a dry nitrogen atmosphere to avoid premature hydrolysis.

3.1.1 : Materials

The polymer used was poly(vinylchloride) (PVC), secondary standard, molecular weight 80,000, from Aldrich Chemical Company. The silanes used were [3-(amino)propyl]trimethoxysilane (A1110), 97%, [3-(mercapto)propyl]triethoxysilane (A1891, $\geq 80\%$ and [3-(phenylamino)propyl]trimethoxysilane, $\geq 95\%$ from Fluka Chemicals (see figure 1.1). The plasticisers used were dihexyladipate (DHA) provided by Pilkington plc, and Diolpate 7170 from Hyperlast Ltd. Both these materials are adipic esters. The structure of DHA is shown in figure 3.4, Diolpate 7170 is an oligomeric adipate, and so has a very similar structure. The molecular weight of Diolpate 7170 is 1650 gmol^{-1} whereas the molecular weight of DHA is 258 gmol^{-1} .

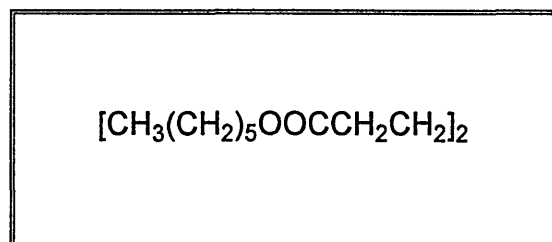


Figure 3.4 : Chemical structure of the plasticiser DHA

Due to the affinity of silanes for hydroxylated surfaces, it was often found that silane grafting to the crystals occurred during experiments. In order to ensure the crystals were free of silane or other contaminants before each experiment, a 3 stage cleaning process was carried out after each experiment. The first stage was washing with hot 2-butanone. This removed PVC from the surface, as well as any physisorbed silane. To remove grafted silane, diamond polishing was carried out with $1 \mu\text{m}$. diamond paste from

Kemet International Ltd. The efficacy of this procedure was verified by examining the infrared spectra of the crystals before the experiment, after the experiment, and after cleaning. No spectrum of silane was visible in the infrared spectra after cleaning. The diamond polishing compound was removed by further rinsing with hot 2-Butanone. The final step was to expose the crystals to hot iso-propyl alcohol (IPA) for 6 hours. This imparted hydrophilic character to the crystal surfaces, leading to more even cast PVC films.

3.1.2 : Spectroscopic measurements

When infrared spectra were taken, the settings were as follows. The spectral range was 400 - 4000 cm^{-1} with a resolution of 4 cm^{-1} . A 90 % open iris and signal gain of 4 were used in order to maximise signal intensity. Purging of the spectrometer was not carried out, as the reduction of water spectral intensity as a function of time would add a systematic error to the results, especially where bands in the water vapour region (i.e. δ (NH) bending at 1600 cm^{-1}) were used. The spectra were ratioed against the background of the film before diffusion was begun. The number of scans co - added to obtain the spectra varied between 76 and 520. Where fast kinetics were observed, fewer scans were used to obtain data quickly, but where slow diffusion occurred, 520 spectra were taken to optimise signal to noise.

3.1.3 : Spectra of materials

All of the results presented in this chapter were obtained by manipulation of the infrared spectra of the materials investigated. This section contains reference spectra of the materials used.

The spectra of the silanes used are presented in Figure 3.5. These were obtained by transmission, by pressing neat liquid silane between two NaCl windows. The peaks integrated for use as markers for diffusion are shown in Table 3.1.

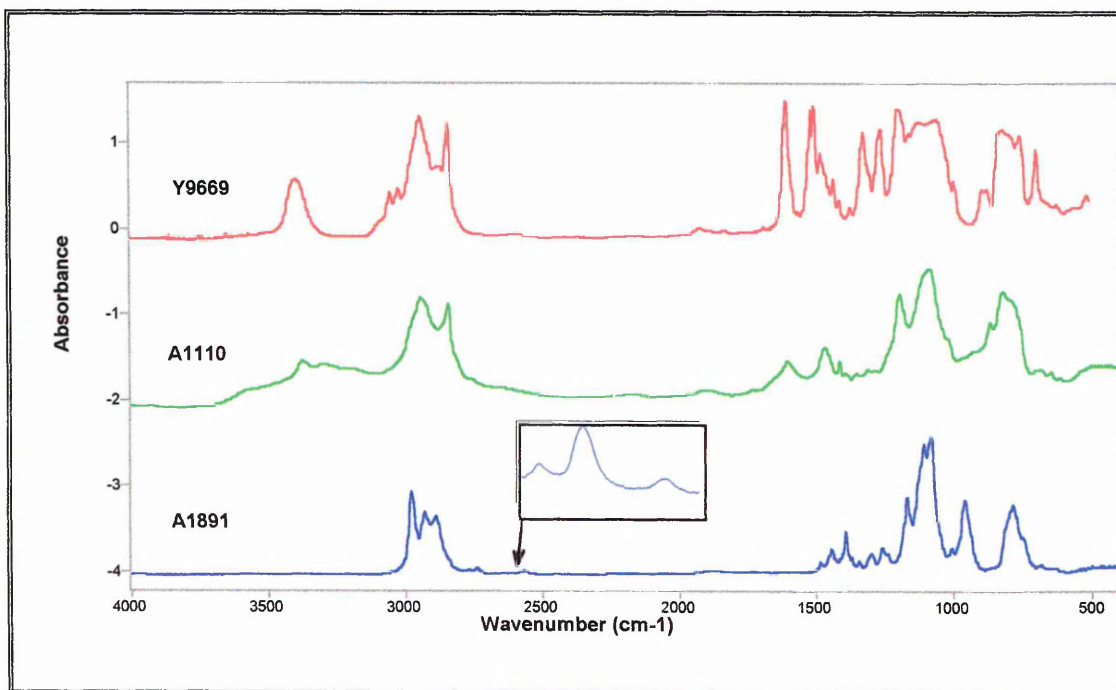


Figure 3.5 : Transmission infrared spectra of the silanes

Silane	Frequency	Assignment
Y9669	1602 cm ⁻¹	C=C ring stretch and N-H bend
Y9669	3408 cm ⁻¹	N-H stretch
A1110	1600 cm ⁻¹	N-H bend
A1891	2565 cm ⁻¹	S-H stretch

Table 3.1 : Infrared bands used for diffusion measurements

The band at 1602 cm⁻¹ in Y9669 is in fact a combination of two bands. The $\delta(\text{NH})$ bend and $\nu(\text{C}=\text{C})$ stretching mode coincide and are impossible to tell apart even using Fourier deconvolution or analysis of the second derivative of the line shape. Henceforth the band is therefore referred to simply as the 1602 cm⁻¹ band of Y9669.

The spectrum of PVC was obtained in the form of a film cast from DMF on an ATR crystal and dried for 14 hours at 65°C. This is shown in Figure 3.6. Also shown is the spectrum of DMF. The lack of the carbonyl stretching band of DMF at 1675 cm⁻¹ clearly demonstrates that the drying method used for the PVC films removes all the solvent. The spectra of the two plasticisers used, DHA and Diolpate 7170 are shown in Figure 3.7.

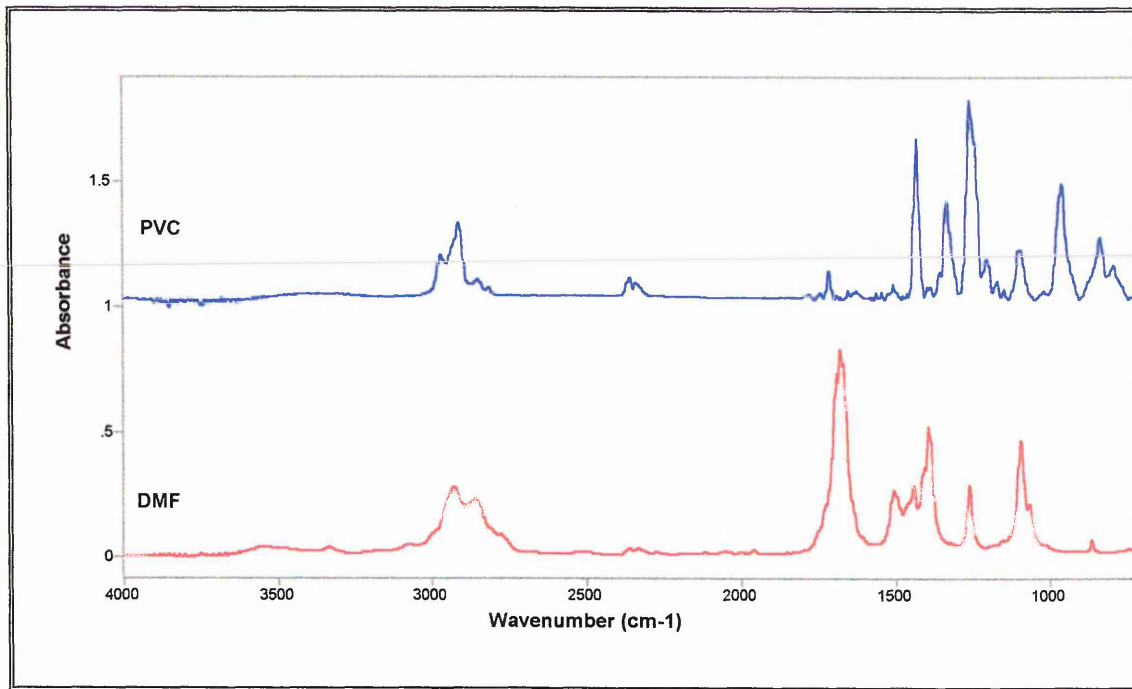


Figure 3.6 : Infrared spectra of a PVC film cast from DMF and of neat DMF

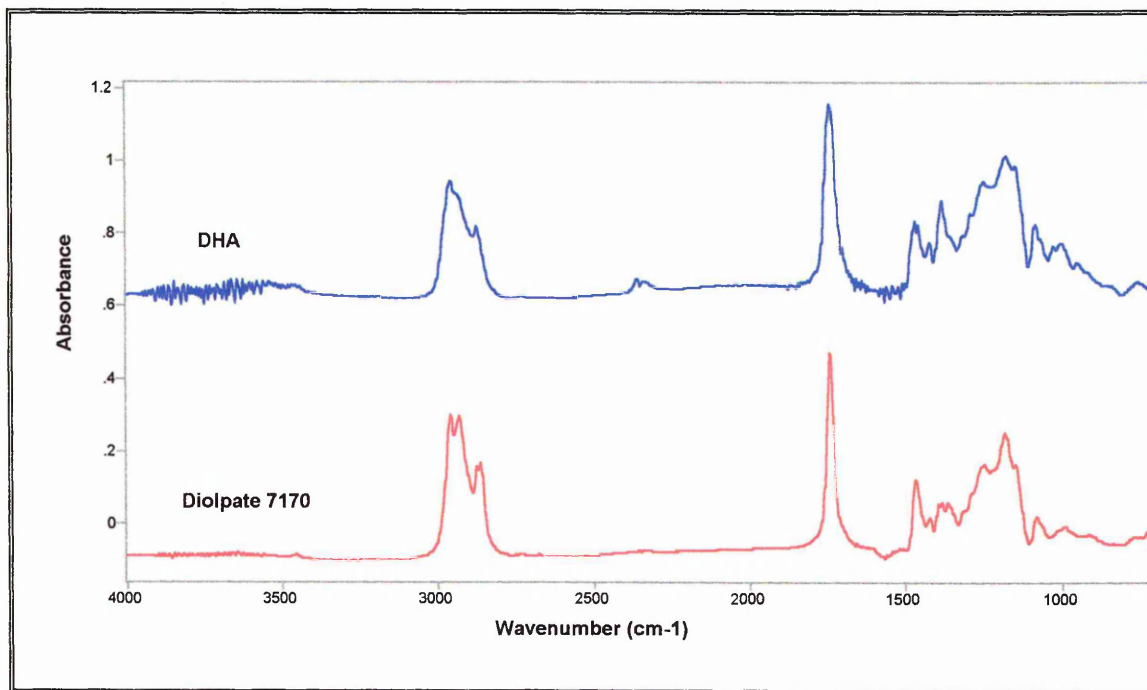


Figure 3.7 : Transmission infrared spectra of dihexyladipate (DHA) and Diolpate 7170

3.2 : Silane underlayer experiments

Silane underlayer experiments were performed with prehydrolysed, dried films.

~~From the literature reviewed in chapter one, these may be expected to consist of~~
polymerised siloxane films.

In the first experiment, the ATR crystal was dipped in a 20% Y9669 solution. PVC was then cast from a 5% MEK solution onto the silane film. The film was then allowed to dry at room temperature in a vacuum desiccator for 30 minutes. A spectrum (128 scans) was taken at this point. This was found to be necessary to avoid blistering of the PVC film, when the laminate was placed in the oven and the highly volatile MEK rapidly boiled. The laminate was then heated at 70°C for an hour and another spectrum taken. It was also examined after 120 minutes, and 150 minutes of heating, also at 70°C. Spectra were also taken every 3 minutes after heating had been completed. The area of the infrared spectra showing the carbonyl stretching mode of the solvent, MEK (at 1700 cm^{-1}) as well as the 1602 cm^{-1} band of the Y9669 is shown in figure 3.8.

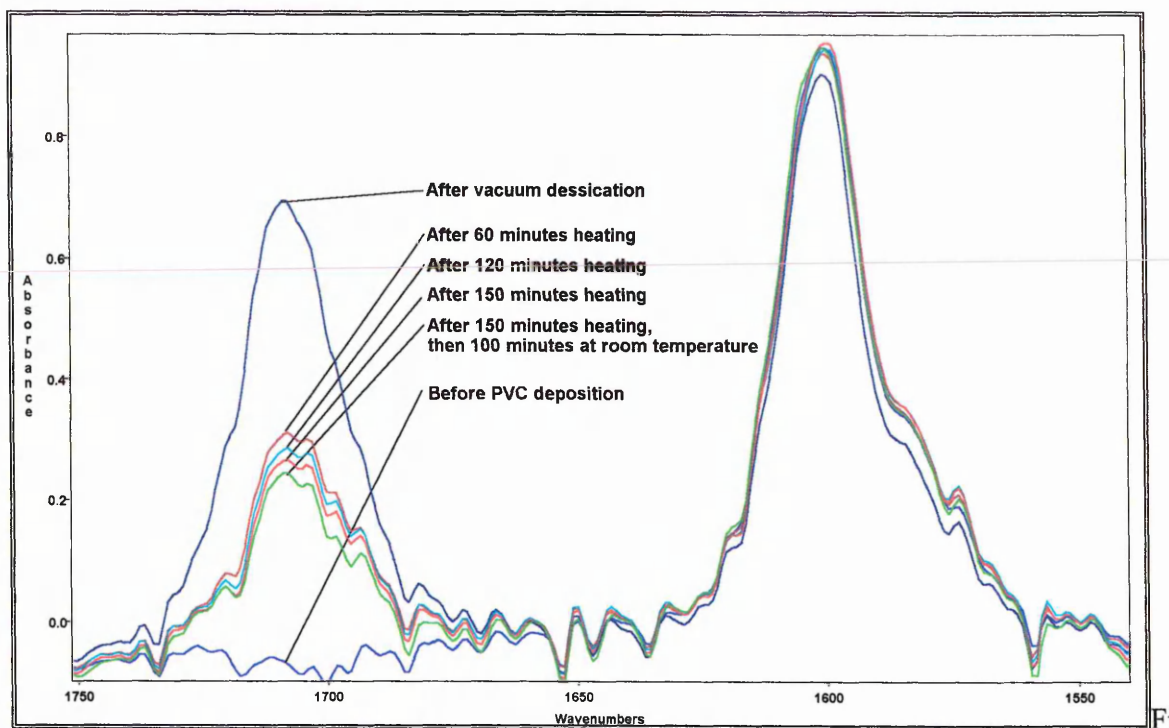


Figure 3.8 : Spectra showing the carbonyl stretching mode of MEK and the 1602 cm^{-1} band of Y9669 in a silane underlayer experiment

Figure 3.8 shows that the intensity of the MEK band increases when the PVC is cast onto the silane. This shows that the evanescent wave extended through the silane film, into the PVC overlayer. Therefore, if diffusion of silane into PVC occurred, the diffusion would have been detected. The MEK band then decreased rapidly when the film was vacuum desiccated, and more slowly after this. This was due to evaporation of solvent from the PVC film. The silane band however did not significantly change in intensity throughout the experiment. This is shown more clearly in Figure 3.9. Figure 3.9 shows the integrated areas of the two bands shown in Figure 3.8, as well as the $\delta(\text{NH})$ stretching band of Y9669 at 3408 cm^{-1} , all plotted against experiment time.

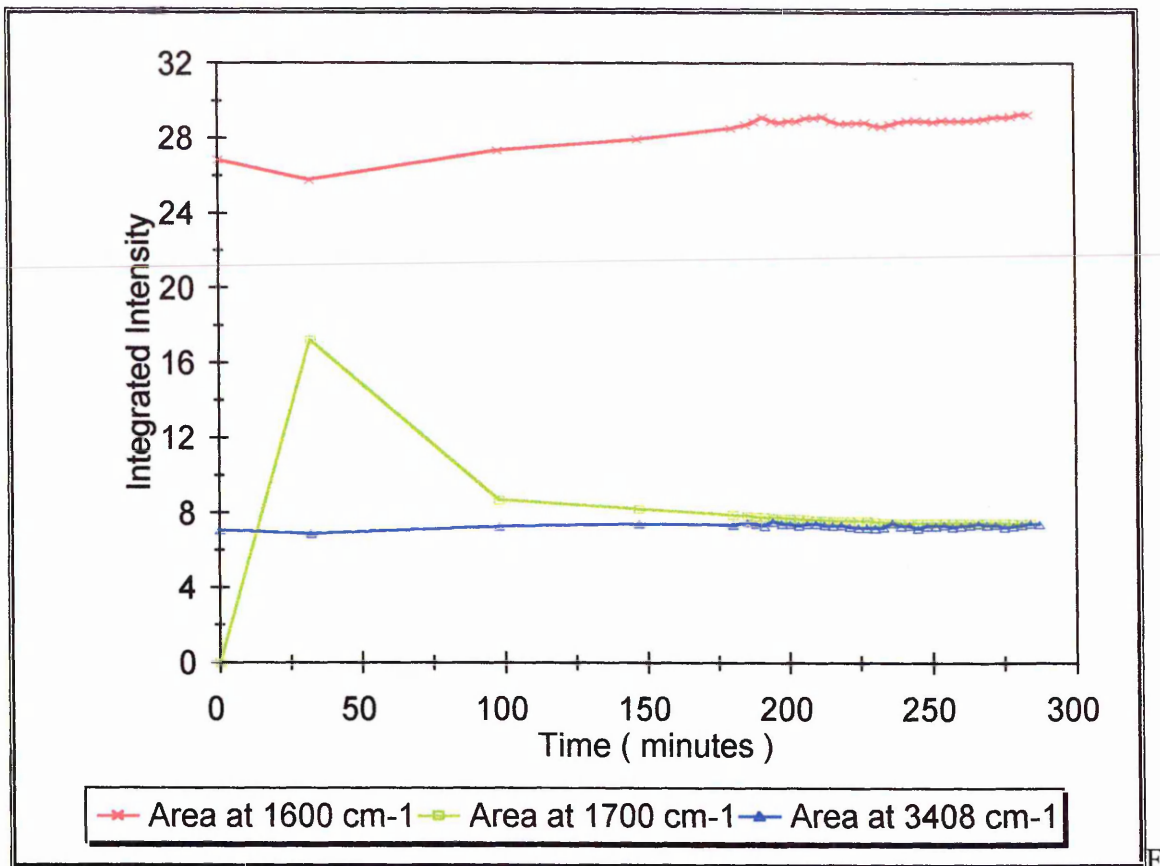


Figure 3.9 : Infrared silane underlayer results, showing area of Y9669 bands at 1602 cm⁻¹ and 3400 cm⁻¹ and solvent band at 1700 cm⁻¹ plotted vs. time

It should be noted firstly that the two silane bands both followed the same trend, showing that any variation was indeed due to concentration change in silane as assumed, and not due to reaction of the bond giving rise to the vibration. It can be seen again that there was little if any change in silane band area, and therefore no silane diffusion. The first part of the experiment was under vacuum conditions at room temperature, then the laminate was exposed to a temperature of 70°C until 170 minutes, and thereafter was left at room temperature. Therefore this experiment shows that the prehydrolysed silane film did not interdiffuse significantly with PVC at room temperature or at 70°C. This experiment was repeated several times, but no indication of interdiffusion was detected.

It seems likely that the reason why no diffusion occurred was condensation of the silane molecules to form a polymerised siloxane film. If the silane film had condensed into a polymerised siloxane upon hydrolysis and heating, then interdiffusion would have been expected to have been considerably slowed, or even stopped compared with un-hydrolysed silane. In order to assess diffusion of un-hydrolysed silane, the silane overlayer geometry was adopted. This is described in the next section.

3.3. : Silane overlayer experiments

3.3.1 : Silane overlayer experiments : heat - induced diffusion

One other reason why interdiffusion could not be seen in the silane underlayer experiments may have been that if diffusion did occur, only a small change in a large value would occur. This is because assuming that most of the silane stayed near the ATR crystal surface, this part would dominate the ATR spectrum. It was therefore decided to investigate the diffusion of silane from the outside of a PVC film towards the ATR crystal. This would take advantage of the sensitivity of the ATR evanescent field, because even a small amount of silane reaching the ATR crystal surface would give rise to a high intensity. The silane could also be investigated in its un-hydrolysed, un-condensed state, which was considered to be more likely to show diffusion.

Another advantage of this configuration was that the PVC film could be prepared more slowly, allowing formation of more even films. To take advantage of this, all the films in the following experiments were cast from 5% DMF solutions which were found to lead to optimal films. This was not used in the silane underlayer experiments, as the low volatility of DMF meant prolonged heating of the films was required to remove solvent, after which any diffusion would presumably already have occurred.

The first PVC film for silane overlayer experiments was dried at 65°C for 14 hours to remove the DMF. A spectrum was taken once the film had dried, which confirmed full removal of solvent. A Talysurf surface profile showed this laminate to be 15µm. thick. Neat Y9669 was then brushed onto the PVC surface, and another spectrum taken. The laminate was then left in the spectrometer at room temperature for three and a half hours, with spectra taken at regular intervals. The sample was then placed in the oven at 70°C for an hour, and another spectrum taken. This was repeated until a total time after deposition of about 600 minutes. The results of experiment 7 are shown in Figure 3.10. All of the experimental measurements were made at room temperature.

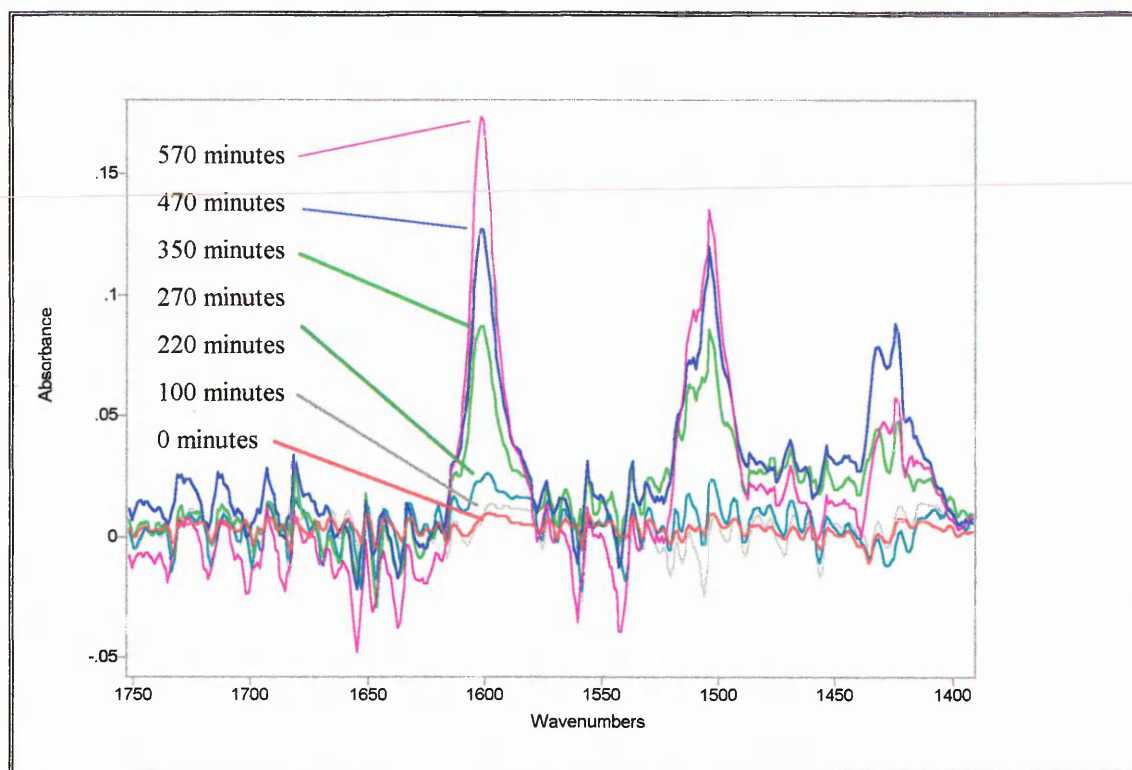


Figure 3.10 : Spectra showing the 1602 cm^{-1} Y9669 after various times at room temperature and after annealing at 70°C

In order to show how the intensity of the silane spectral bands vary with time and temperature, the intensity of the 1602 cm^{-1} band of Y9669 has been plotted versus experiment time. This is shown in Figure 3.11.

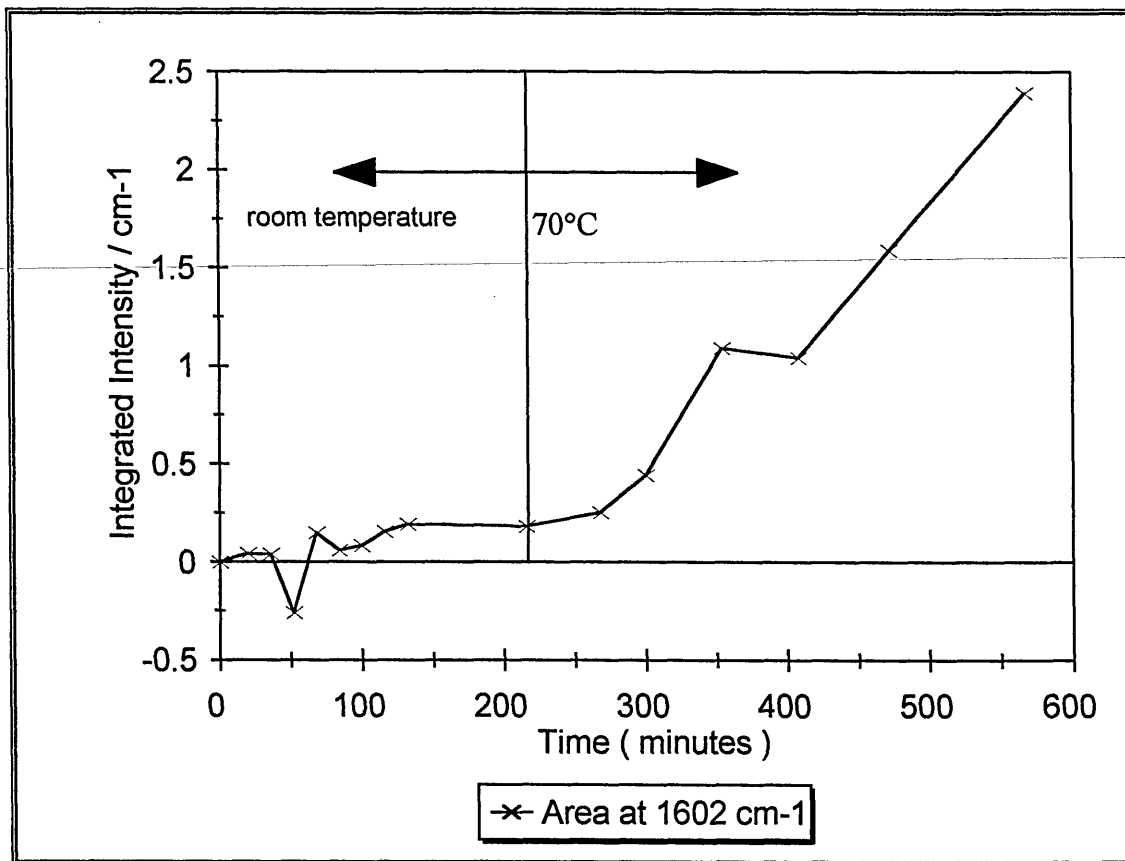


Figure 3.11 : The area of the 1602 cm^{-1} band of Y9669 plotted vs. time for the first silane over layer experiment

When the first spectrum was taken, there was no sign of silane. No silane intensity appeared even after 220 minutes at room temperature. At $70\text{ }^{\circ}\text{C}$ however, silane band intensity increases with time. It appeared that diffusion was still occurring after 350 minutes at $70\text{ }^{\circ}\text{C}$. This implies that diffusion occurs, but only at elevated temperatures. Alternatively, diffusion at room temperature occurs so slowly that on the time-scale used here (*i.e.* up to 4 hours) it is not seen. It was thought that the diffusion at 70°C may have been due to the PVC being near its glass transition temperature (T_g). The T_g of pure PVC is 80°C .

In the second overlayer experiment, similar conditions to those in the first experiment were used, but the laminate was not left at room temperature before heating. The laminate was examined in the spectrometer immediately after silane deposition, and then placed in the oven at 70°C. The sample was then periodically removed from the oven and another spectrum taken. The results of this experiment are shown in

Figure 3.12. This laminate was 13.5 μm thick. It can be seen that after 30 minutes diffusion was almost complete and that after this an equilibrium was reached in the diffusion, little if any further diffusion occurring up to 350 minutes.

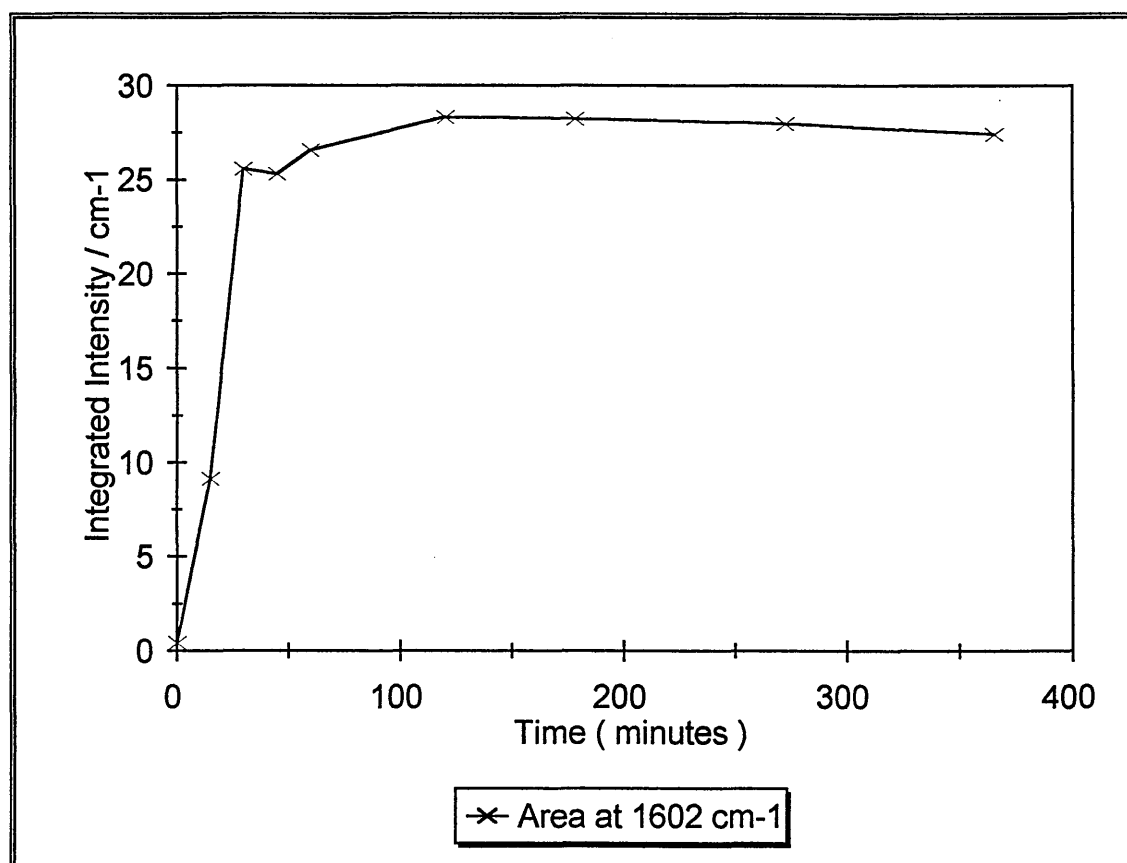


Figure 3.12 : The intensity of the 1602 cm^{-1} band of Y9669 plotted versus annealing time at 70°C for the second silane overlayer experiment (all measurements were made at room temperature)

It is interesting to compare the results of this experiment with those of the previous experiment, which was carried out under the same conditions, but without the 4-hour pause at room temperature at the start. In the first experiment, the heating was stopped after 350 minutes, at which time the diffusion was not complete. In the second experiment however, (and similarly in subsequent experiments) diffusion appears to be almost complete after 30 minutes of heating. The difference in the results must be due to the time spent at room temperature. It has been reported that aminosilanes can hydrolyse over a period of a few hours, after being exposed to small amounts of water⁷ or to atmospheric water^{8,9} (see section 1.2.2). It may be that by the time the heating was carried out, the silane had hydrolysed, leading to a change in diffusion properties. If this is the reason for the change in diffusion rate, this implies that hydrolysed silanes diffuse more slowly. We believe that this is the first time that a definite connection has been made between the hydrolysis of a silane and its ability to diffuse through a polymeric matrix. At first glance, it is not obvious why hydrolysis should reduce a silanes ability to undergo diffusion. However, if the hydrolysis of the silane is considered as merely the first step on the reaction pathway to condensation (see chapter 1), then this result makes more sense. It is well known that larger molecules tend to show much slower diffusion than smaller molecules¹⁰. Therefore it is assumed that the hydrolysis of the silanes slows diffusion by allowing the silanes to condense to form oligomers.

In order to study the diffusion at 70°C for all three silanes, an experiment was carried out under the same conditions for all three silanes. A PVC film was cast from DMF

solution, to give a film 10 μm . thick. The silane was then brushed on top, and the laminate examined in the spectrometer. The laminate was then successively exposed to temperatures of 70 $^{\circ}\text{C}$ for periods of five or ten minutes, and a spectrum taken. The results from the Y9669 experiment are shown in Figure 3.13. These results show the integration of the 1602cm^{-1} band of Y9669 *versus* time.

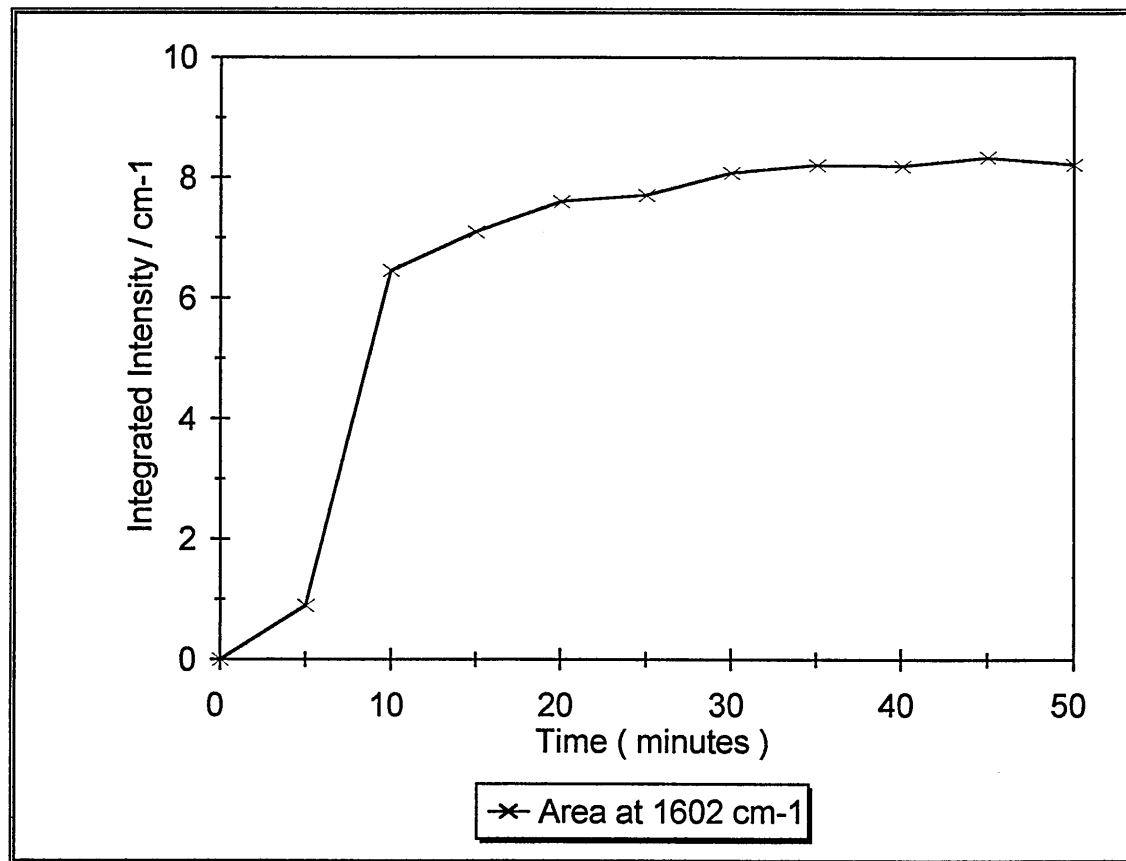


Figure 3.13: The intensity of the 1602cm^{-1} band of Y9669 *vs.* time at 70 $^{\circ}\text{C}$ (all measurements were made at room temperature)

These results, as expected, show much the same as Figure 3.12, i.e. fast diffusion at first, reaching equilibrium after around thirty minutes. This shows the results to be reproducible and also that the kinetics are reasonably independent of the length of time

spent in the oven, as the results shown in Figure 3.12 were obtained with longer heating intervals, but show similar kinetics. The results of the same experiment carried out using A1110 are shown in Figure 3.13. The PVC film was 12 μm . thick.

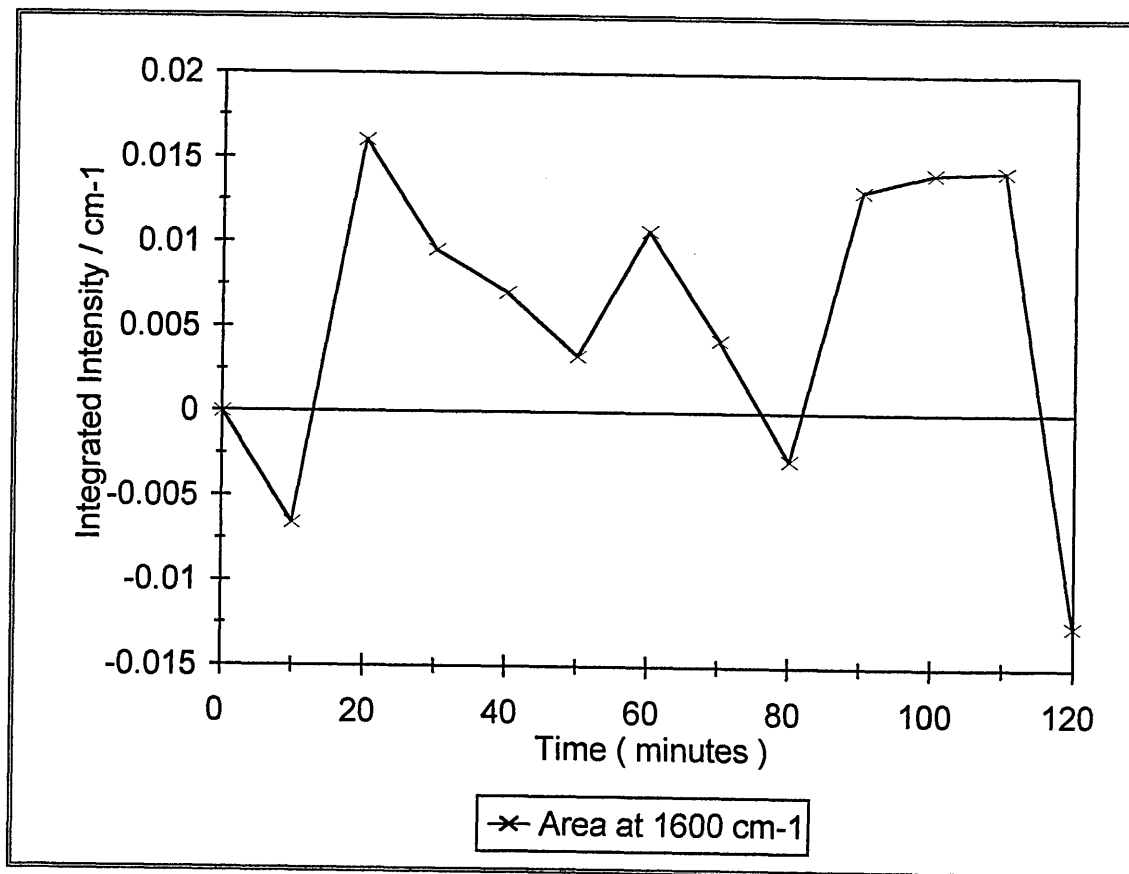


Figure 3.14 : The area of the N-H bending mode of A1110 (1600 cm^{-1}) vs. time at $70 \text{ }^\circ\text{C}$ (all measurements were made at room temperature)

Clearly, in Figure 3.14, no overall trend in the intensity at 1600 cm^{-1} was seen. This indicated either that there was no diffusion, or limited diffusion so that the silane did not reach the evanescent field. The reason for this is not clear. It may be that there was some reaction occurring which prevented the diffusion of the silane. This may be hydrolysis possibly leading to partial condensation of the silane. It might be expected that the heating

process accelerated the hydrolysis and condensation processes. However, if this is the case, it is not clear why this did not occur in the case of Y9669, which also contains an amine group that could catalyse the hydrolysis^{7,8}. The results of a similar experiment using A1891 are shown in Figure 3.15. In this experiment, the PVC film was 11 μm thick.

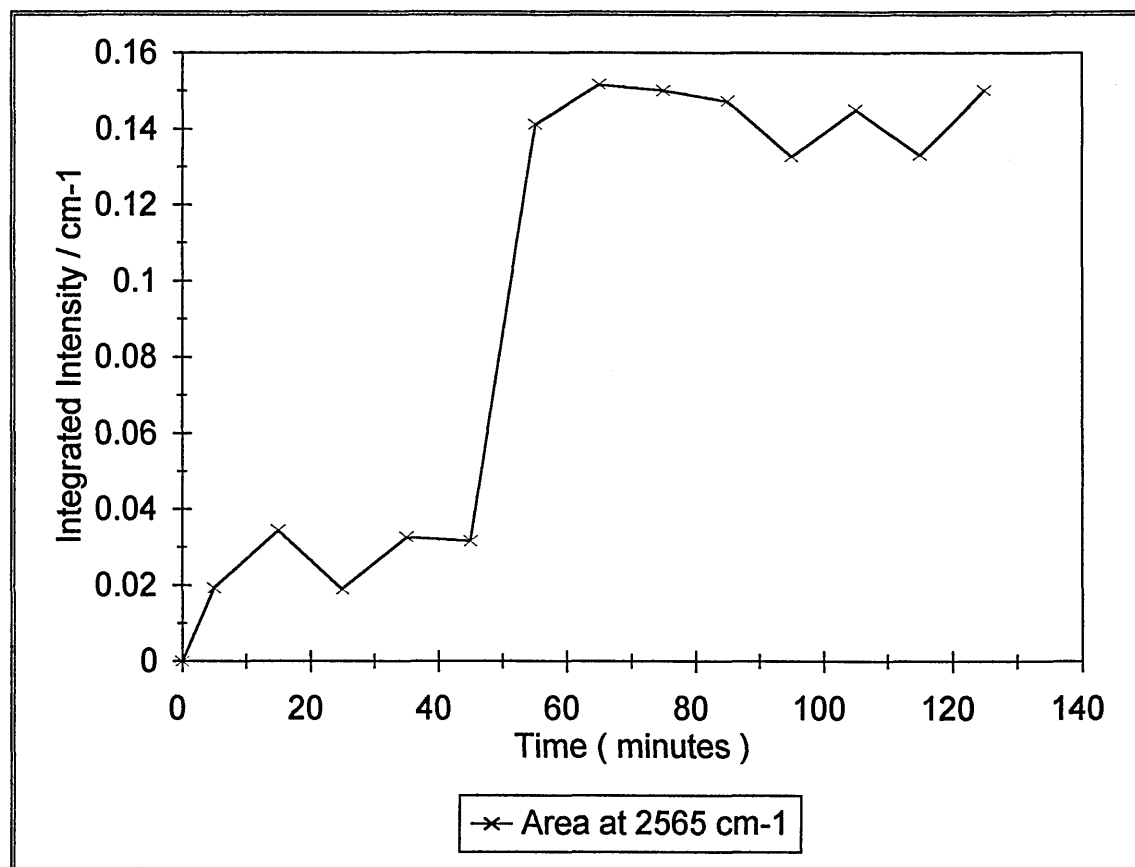


Figure 3.15 : The area of the S-H stretching mode of A1891 (2565 cm^{-1}) vs. time at 70°C (all measurements were made at room temperature)

Figure 3.15 shows that in the case of A1891, diffusion did occur, but the results appear to be rather different to those obtained for Y9669 (i.e. Figure 3.13). Firstly, it can be seen that the area of the band is much smaller throughout the experiment. This is simply due to the lower intensity S-H stretching band used for A1891 as compared to the

very intense C=C ring stretch used for Y9669. The diffusion also appears to be slower, with a period, between zero time and 45 minutes in which little if any diffusion occurs, then a large step at about 50 minutes time, after which equilibrium is attained. One explanation for this is the smaller dp of the A1891 band ($0.3\ \mu\text{m}$. for $2565\ \text{cm}^{-1}$ vs. $0.5\ \mu\text{m}$. for $1602\ \text{cm}^{-1}$, see equation 2.13) compared to the Y9669 band. This means the evanescent field extends less far into the PVC film, so the silane takes longer to interact with it. In fact, as explained in chapter 2, the infrared intensity measured depends upon the square of the evanescent field strength, making the dependence on dp even stronger. This seems unlikely to be the entire explanation however, as the difference between the dp values is quite small compared to the entire distance the polymer diffused (ca. $10\ \mu\text{m}$.). It is known that steric effects can change diffusion rates. Larger molecules tend to diffuse more slowly under the same conditions than small molecules¹⁰. However, this effect would lead one to expect slower diffusion for Y9669, as the phenylamino group is much larger than the mercapto group of A1891. Therefore, steric effects do not explain the change. The film used in the A1891 experiment was somewhat thicker than that used in the Y9669 experiment ($11\ \mu\text{m}$. for Y9669 as opposed to $8\ \mu\text{m}$. for A1891). This seems most likely to explain the differences in the results.

3.3.2 : Silane overlayers - plasticised PVC

In order to test the theory that the PVC being near its glass transition temperature (T_g) allows diffusion, it was decided to plasticise the PVC. Adding a plasticiser to a polymer formula reduces the T_g of the resulting polymer. Different plasticisers are used with different polymers. In the case of PVC, the most common plasticisers are phthalate esters and adipic esters¹¹. The plasticiser used here is the adipic ester DHA (see Figure 3.4). DHA is soluble in DMF, so it was simple to form films with the desired plasticiser content by dissolving both PVC and DHA in DMF prior to casting.

In the first experiment, the plasticised PVC film contained 30% DHA, and was 11 μ m. thick. After removal of the DMF solvent, a background spectrum was taken, and then Y9669 was brushed on top of the PVC film. The laminate was then immediately placed in the spectrometer and one spectrum taken per minute for 2 hours. The film was not heated at all to induce diffusion. The results in the 1600 cm^{-1} region are shown in Figure 3.16.

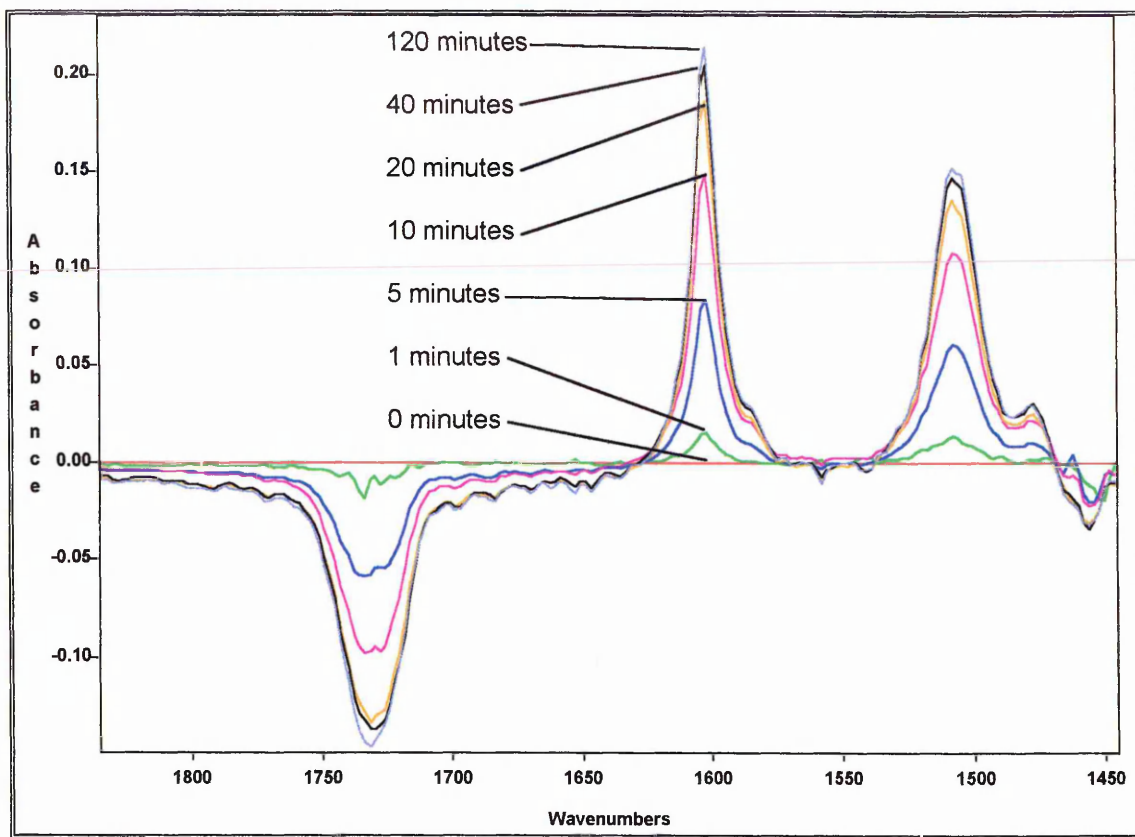


Figure 3.16 : Results of Y9669 diffusion in PVC plasticised by 30% DHA

The intensity of the band at 1602 cm^{-1} in these results is plotted vs. time in Figure 3.17. The time - dependent increase in the 1602 cm^{-1} band and the doublet around 1510 cm^{-1} (assigned to a ring breathing mode of Y9669) in Figure 3.16 shows that diffusion did occur in PVC plasticised by 30% DHA at room temperature. Figure 3.17 shows the kinetics of diffusion more clearly. After only one minute, diffusion had already started, and equilibrium was reached after 30 minutes. By comparing Figure 3.17 with Figure 3.13, it can be seen that diffusion at 70°C in unplasticised PVC showed similar kinetics to diffusion in 30% plasticised PVC at room temperature. The other major feature of Figure 3.16 is the time - dependent decrease in the band at 1735 cm^{-1} . This band is assigned to the carbonyl stretching mode of the plasticiser, DHA. This band appeared to decrease with

very similar kinetics to the kinetics of the increase in the silane bands. This is discussed further later in this section.

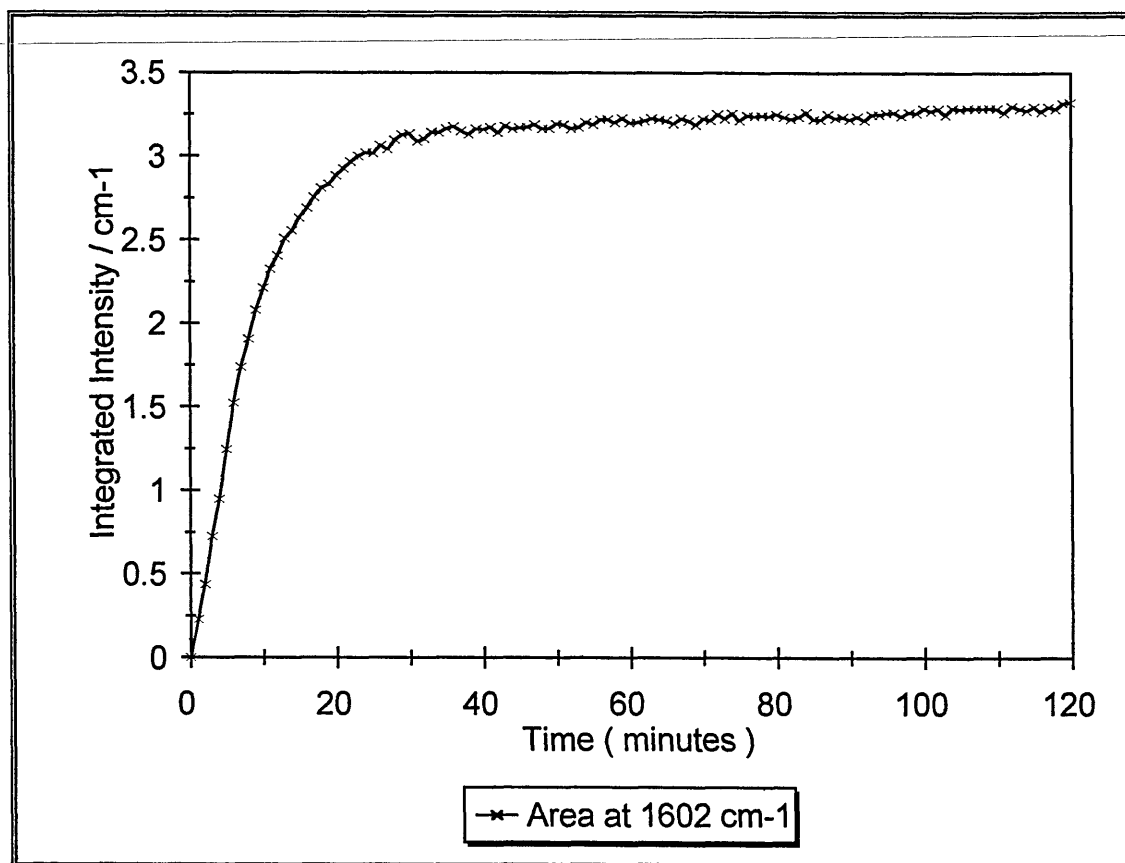


Figure 3.17 : The area of the 1602 cm^{-1} band of Y9669 vs. time for diffusion in PVC plasticised by 30% DHA

In order to determine the effect of silane chemistry on diffusion characteristics, the same experiment was also carried out using A1110 and A1891. Figure 3.18 shows the results of A1110 diffusion in PVC plasticised with 30% DHA. The laminate was $16\text{ }\mu\text{m}$ thick. It can be seen from the increase in NH bending mode intensity at 1600 cm^{-1} that A1110 was observed to have diffused at room temperature in 30% plasticised PVC. It can also be seen that the same decrease in the plasticiser band at 1735 cm^{-1} was observed. The

smaller intensity of the silane band compared to that of Y9669 was not a concentration effect; it can be seen from Figure 3.5 that the band used for A1110 is much smaller than that used for Y9669. Y9669 was chosen for study because although it is not as widely used as A1110 or A1891 industrially^{12,13}, it has very strongly absorbing bands in both infrared and Raman spectroscopy. Throughout the work described here, better signal to noise was found for Y9669 than for A1110 or A1891. The band due to NH bending in A1110 is also broader than the 1602 cm^{-1} band in Y9669, leading to more interference from the water vapour absorptions which occur in this part of the infrared spectrum.

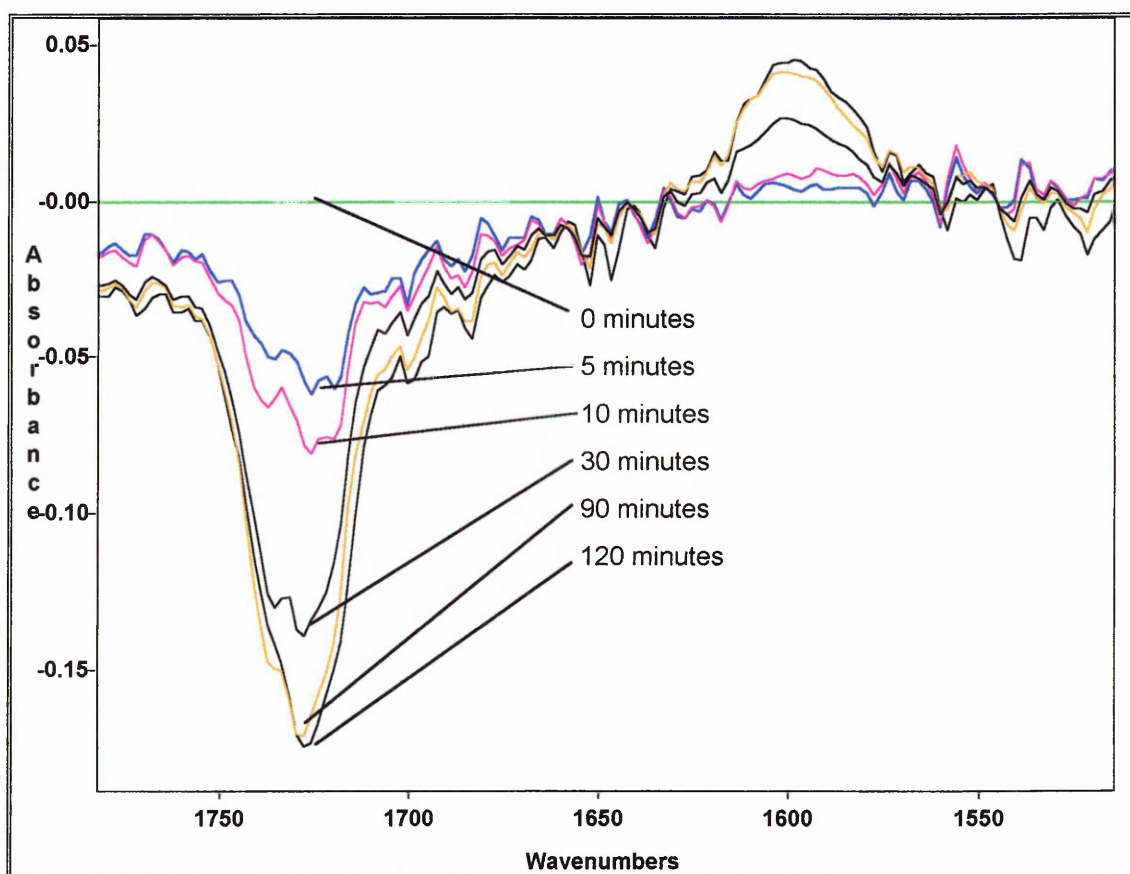


Figure 3.18 : Results of A1110 diffusion in PVC plasticised with 30% DHA

The area of the NH bending band of A1110 vs. time for this experiment is plotted in Figure

3.19.

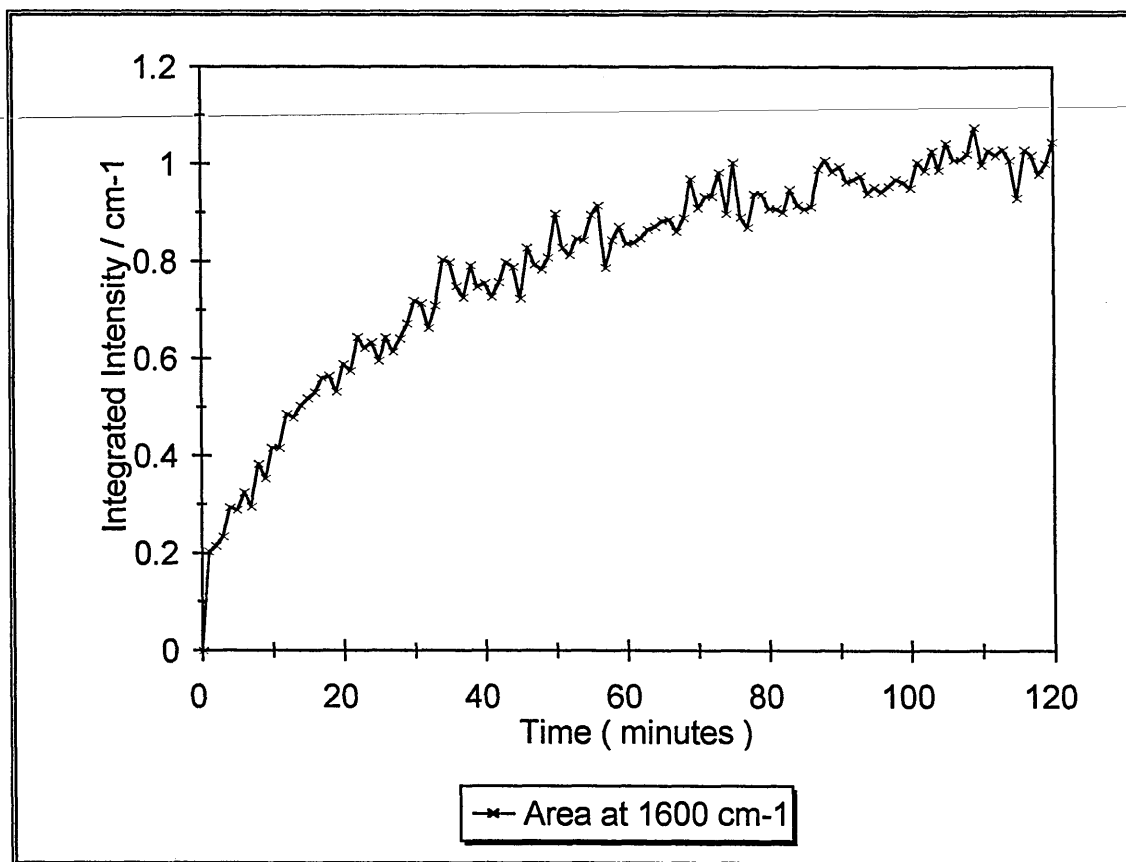


Figure 3.19 : The area of the NH bending mode of A1110 (1600 cm⁻¹) vs. time for A1110 diffusion in 30% DHA plasticised PVC

Figure 3.19 shows that A1110 diffused considerably more slowly than Y9669 in 30% DHA plasticised PVC. Y9669 had reached equilibrium after around 30 minutes, whereas A1110 took about 90 minutes. This might be due in part to the increased thickness of the polymer film.

Figure 3.20 shows the results of A1891 diffusion in 30% DHA plasticised PVC. The laminate was 15 μm . thick. The spectral region shown is that containing the SH

stretching vibration of the A1891. This region does not show any plasticiser bands, but it was observed that the band at 1735 cm^{-1} decreased in intensity with time, as was observed for the other silanes. It can be seen from Figure 3.5 that the intensity of this band (2565 cm^{-1}) is very low, and this explains the low signal to noise ratio seen in Figure 3.20. Fortunately, there is no absorption from water vapour or carbon dioxide in this region, so no interference from these fluctuating bands occurred.

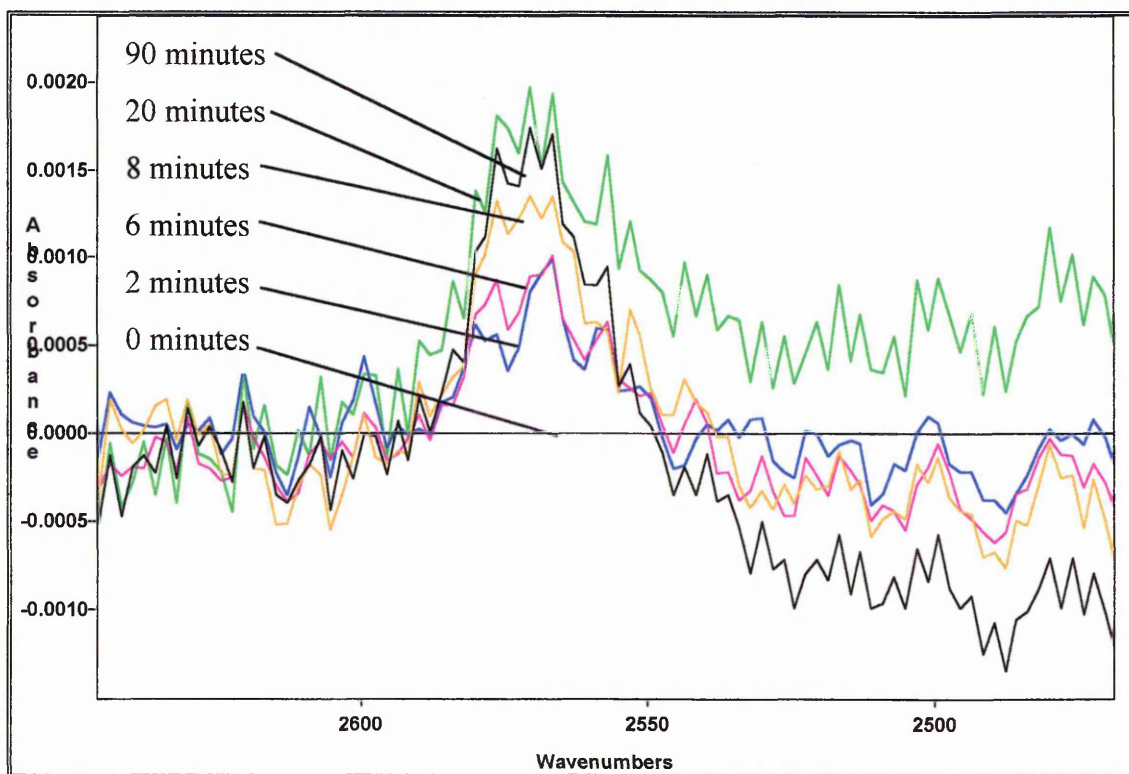


Figure 3.20 : Results of A1891 diffusion in PVC plasticised with 30% DHA

It can be seen from the increase in SH stretching vibration intensity in Figure 3.20 that A1891 also diffused in 30% DHA plasticised PVC at room temperature. The area of the SH stretching vibration of A1891 is plotted vs. time in Figure 3.21 for this experiment.

Figure 3.21 shows a large amount of scatter compared to the results from A1110 and Y9669 diffusion, even though five minute scans were used for the later measurements to increase the signal to noise ratio. This was due to the low signal to noise ratio obtained. It can be seen that the diffusion again took about 90 minutes to reach equilibrium. This may be due to the thickness of the film used being similar to that used for A1110 diffusion.

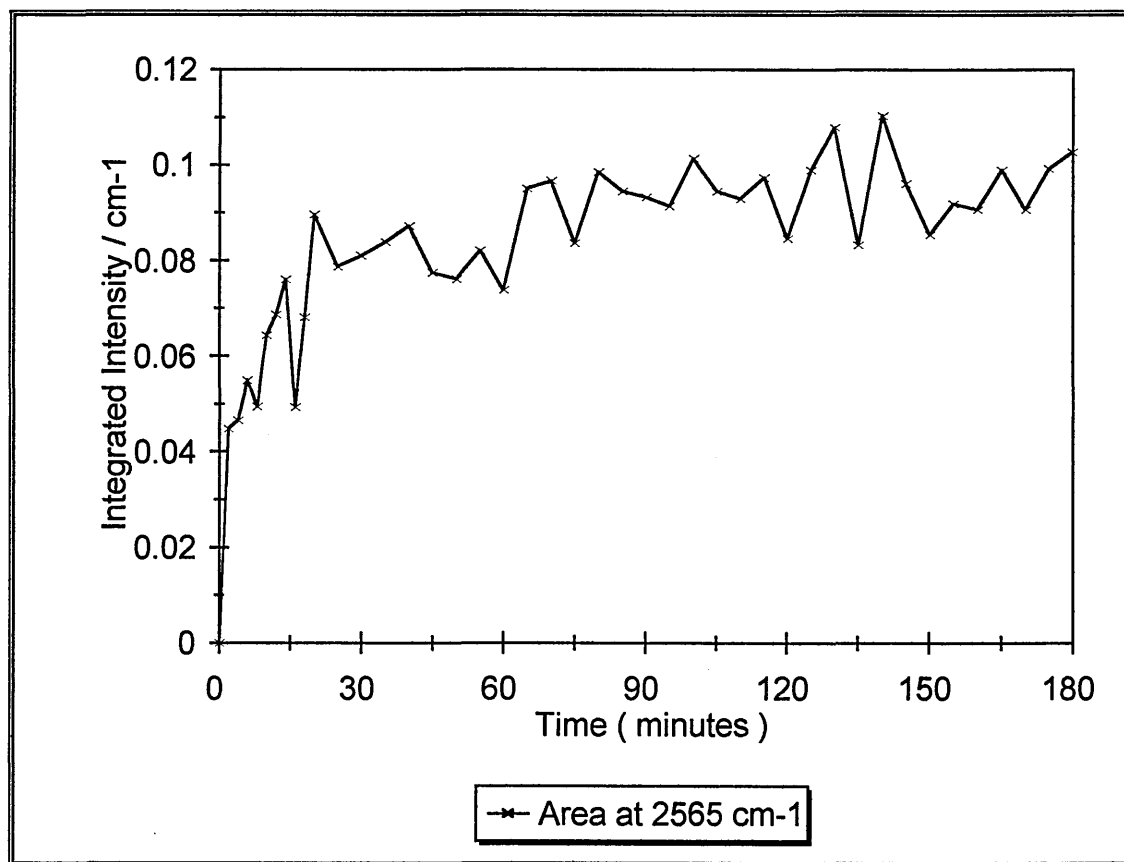


Figure 3.21 : The area of the SH stretching band of A1891 (2565 cm^{-1}) vs. time for A1891 diffusion in 30% DHA plasticised PVC

3.3.3 : Silane overlayer experiments : kinetic analysis of data

It is clear from the results presented above that diffusion of organosilanes in plasticised PVC occurs readily, and that the kinetics of the process may be affected by a number of factors, e.g. film thickness, silane chemistry and plasticiser concentration. In order to quantify the kinetics of diffusion it was decided to attempt the fitting of the data to theoretical models of diffusion (see section 2.1.4.1). The first model investigated was simple Fickian case I diffusion¹⁴. A program written in the Matlab programming and visualisation package was used to perform the fittings. This program has been previously described^{15,16}. The program starts with an estimated value for the Fickian diffusion coefficient, D , and uses the calculated value of dp (obtained from equation 2.14) and measured values of the film thickness, L and the equilibrium value of the absorbance, A_{∞} . The program then uses equation 2.20 to calculate what the diffusion profile would be for the estimated diffusion coefficient. This profile is compared to the input data from the experiment. The χ^2 merit function is used as a measure of the closeness of the fit between the data and the calculated diffusion profile. The diffusion coefficient is then iteratively modified in order to minimise the difference between the calculated and measured diffusion profiles. One disadvantage of this fitting technique is that the program is unable to distinguish between the true 'best fit' and any local minima in the fit error obtained. In order to overcome this problem, several fittings were used for each set of data investigated, using different estimated diffusion coefficients. The result of the fitting performed on the data obtained for Y9669 diffusion in 30% DHA plasticised PVC is shown in Figure 3.22.

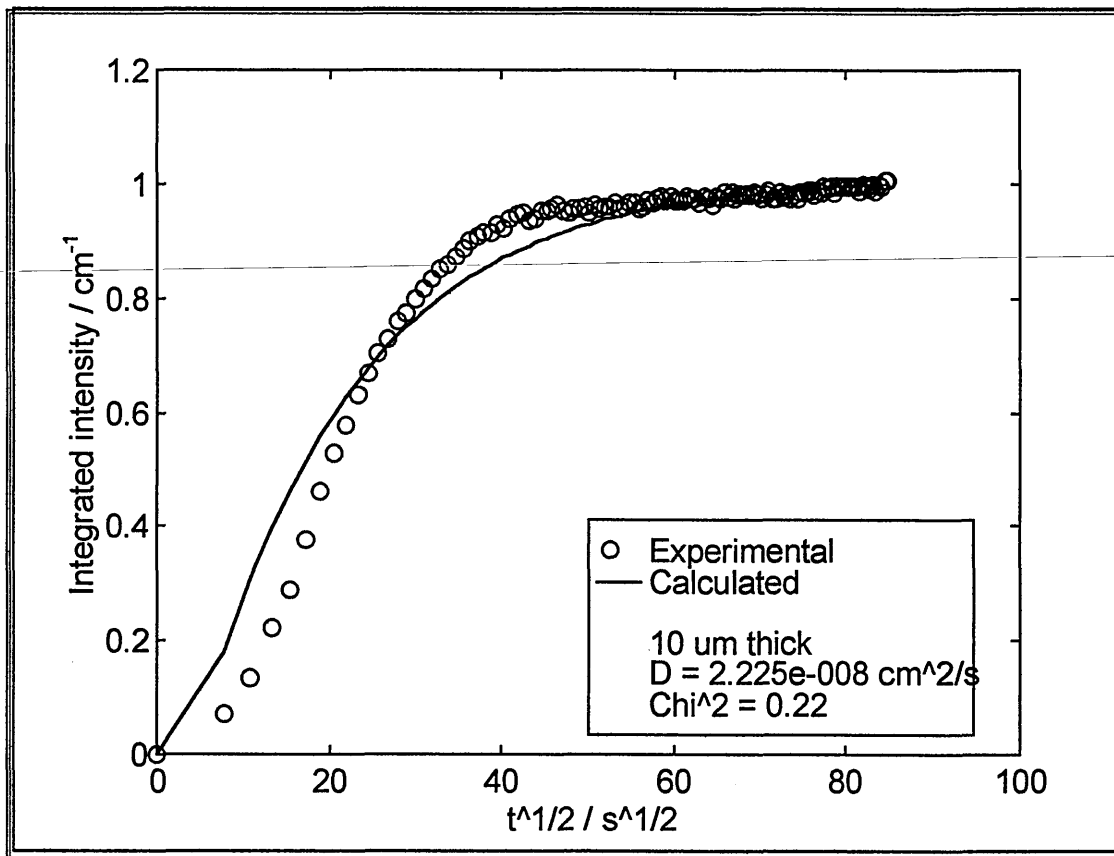


Figure 3.22 : Results of fitting Fickian case I diffusion model to data from Y9669 diffusion in 30% DHA plasticised PVC

Figure 3.22 shows that the data did not fit the Fickian case I diffusion model well at all. This result was found to be typical of the data obtained; in no case did the data fit this model. The second model assessed was the dual mode sorption model (see section 2.1.4.1). The method of fitting was very similar, but because the dual mode sorption model uses two diffusion coefficients, a Pascal program which applies the Levenberg - Marquardt fitting routine to the fitting process was used. This program has been well described previously¹⁷. The Levenberg - Marquardt routine is a method for fitting a set of data with more than one parameter. Like the Fickian case I fitting process, it relies on the minimisation of the χ^2 merit function between the data and the calculated diffusion profile

from estimated parameters. The equation used to generate the calculated curve was equation 2.21. The result obtained from the fitting of the dual mode sorption model to the data obtained for Y9669 diffusion in 30% DHA plasticised PVC is shown in Figure 3.23

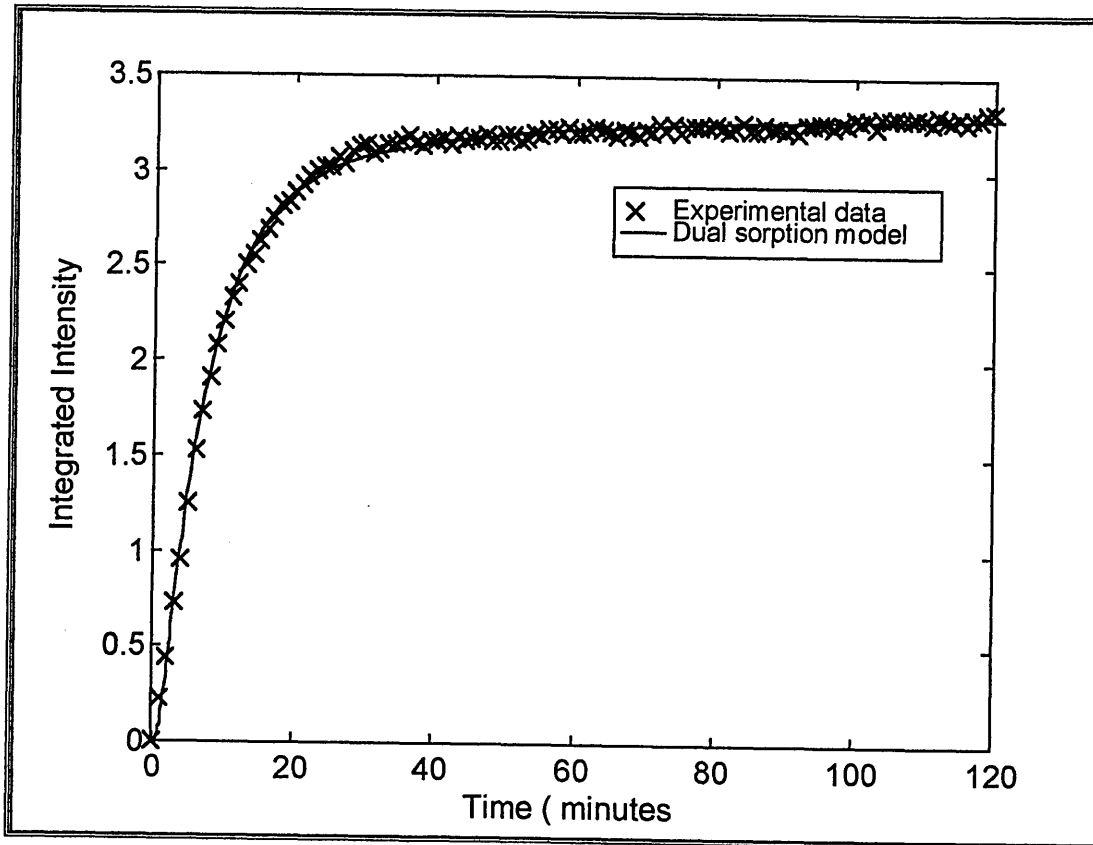


Figure 3.23 : Results of fitting the dual mode sorption model to data from Y9669 diffusion in 30% DHA plasticised PVC

Figure 3.23 clearly shows that the data fit a dual mode sorption model. The parameters obtained for this fitting are shown in Table 3.2.

Parameter	Value
D_1	$6.5 \times 10^{-8} \text{ cm}^2 \text{ s}^{-1}$
D_2	$9.9 \times 10^{-9} \text{ cm}^2 \text{ s}^{-1}$
X_1	0.89

Table 3.2 : Band fitting parameters obtained from dual mode sorption fitting of Y9669 diffusion in 30% plasticised PVC

The dual mode sorption model assumes that two species undergo diffusion into the polymer film. A 'mobile' species diffuses with one diffusion coefficient into the film, and an 'immobile' species diffuses with another diffusion coefficient. It can be seen from Table 3.2 that D_2 is more than an order of magnitude lower than D_1 . The parameter X_1 represents the fraction of material which is 'mobile', i.e. the fraction of diffusion which occurs with diffusion coefficient D_1 . X_1 therefore always has a value between 0 and 1. In the basic theory of dual mode sorption, one species is relatively immobilised at sites in the polymer network, for example voids, whilst the rest of the molecules are free to diffuse through the polymer^{18,19}. However, the two species are in fact both partially mobile. Therefore the two species might not be chemically different molecules, but are often considered to be the same molecule, but in different environments in the polymer matrix.

In order to investigate the effect of different plasticiser concentration on the diffusion, experiments were carried out as described above for PVC films with 15, 20, 25, 30, 35 and 40% DHA for all three silanes. The results are presented in Table 3.3. In several cases, two or three runs were carried out in order to check the validity of the results.

In these cases, mean values of the diffusion coefficients have been presented. It was found that for all the experiments, the dual mode sorption model fitted much better than the case I model. Therefore table 3.3 shows only the diffusion coefficients for the dual mode sorption fitting.

Plasticiser Concentration	Y9669	A1110	A1891
40% DHA	$D_1 = 3.25 \times 10^{-6}$ $D_2 = 5.27 \times 10^{-7}$ $X_1 = 0.88$	$D_1 = 4.35 \times 10^{-6}$ $D_2 = 2.16 \times 10^{-7}$ $X_1 = 0.46$	$D_1 = 1.04 \times 10^{-5}$ $D_2 = 2.76 \times 10^{-7}$ $X_1 = 0.70$
35% DHA	$D_1 = 2.35 \times 10^{-7}$ $D_2 = 1.755 \times 10^{-8}$ $X_1 = 0.95$	$D_1 = 7.49 \times 10^{-6}$ $D_2 = 4.03 \times 10^{-8}$ $X_1 = 0.57$	$D_1 = 6.86 \times 10^{-6}$ $D_2 = 1.36 \times 10^{-7}$ $X_1 = 0.56$
30% DHA	$D_1 = 6.51 \times 10^{-8}$ $D_2 = 8.79 \times 10^{-9}$ $X_1 = 0.81$	$D_1 = 6.02 \times 10^{-7}$ $D_2 = 3.45 \times 10^{-8}$ $X_1 = 0.43$	$D_1 = 7.86 \times 10^{-7}$ $D_2 = 2.89 \times 10^{-8}$ $X_1 = 0.76$
25% DHA	$D_1 = 8.48 \times 10^{-8}$ $D_2 = 3.53 \times 10^{-8}$ $X_1 = 0.62$	$D_1 = 1.84 \times 10^{-7}$ $D_2 = 1.87 \times 10^{-8}$ $X_1 = 0.29$	$D_1 = 9.87 \times 10^{-8}$ $D_2 = 9.51 \times 10^{-8}$ $X_1 = 0.98$
20% DHA	$D_1 = 5.79 \times 10^{-8}$ $D_2 = 7.88 \times 10^{-9}$ $X_1 = 0.37$	$D_1 = 6.02 \times 10^{-8}$ $D_2 = 5.49 \times 10^{-9}$ $X_1 = 0.24$	$D_1 = 6.03 \times 10^{-8}$ $D_2 = 2.43 \times 10^{-9}$ $X_1 = 0.60$
15% DHA	$D_1 = 8.96 \times 10^{-9}$ $D_2 = 8.55 \times 10^{-9}$ $X_1 = 0.69$	$D_1 = 6.16 \times 10^{-8}$ $D_2 = 1.20 \times 10^{-8}$ $X_1 = 0.20$	No result

Table 3.3 : Diffusion coefficients obtained from fitting the data from silane diffusion in DHA plasticised PVC to the dual mode sorption model

It was found that no fitting was possible in the case of A1891 in 15% DHA plasticised PVC. This result is discussed later, with the other A1891 results.

In order to demonstrate graphically the trend in the data in Table 3.3, the log of the diffusion coefficients has been plotted versus the percentage of DHA. The log of the two

diffusion coefficients, D_1 and D_2 for Y9669 diffusion has been plotted versus the percentage of plasticiser used in Figure 3.24.

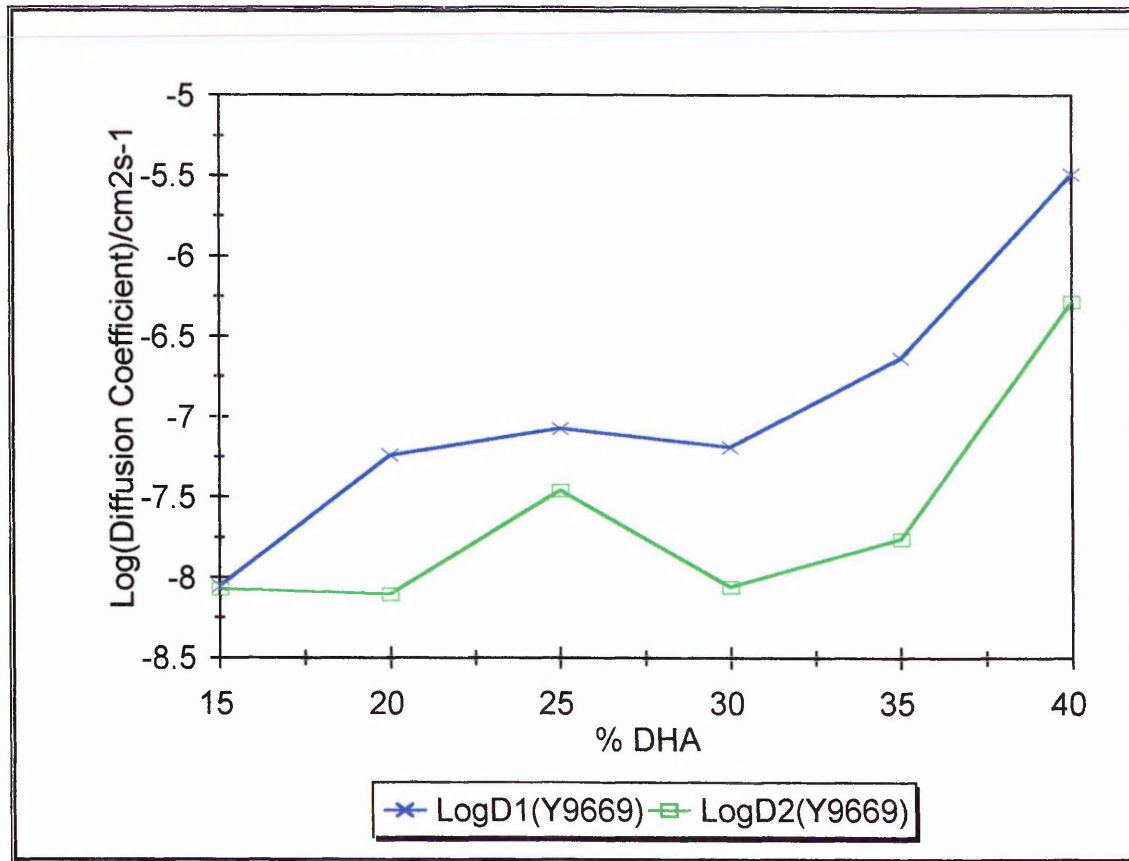


Figure 3.23 : The logarithm of the diffusion coefficients obtained from dual mode sorption fitting of Y9669 diffusion vs. percentage plasticiser in the PVC film

Figure 3.23 : The shows that as the plasticiser concentration of the PVC film was increased, the diffusion coefficients of Y9669 in the film dramatically increased. Over the range 15 to 40% plasticiser, the diffusion coefficients increased by approximately three orders of magnitude. The experiments using 15% plasticiser took 300 minutes to reach equilibrium, whereas in the 40% plasticised PVC, the diffusion came to equilibrium after 5 minutes. As shown in Table 3.3. the diffusion coefficient of the mobile species, D_1 is

generally at least an order of magnitude greater than the diffusion coefficient of the immobile species, D_2 . An exception to this is the data obtained for the 15 % plasticised film. It was thought that this may indicate that this diffusion does not fit the dual mode sorption model properly. The fitting of this data to the dual mode sorption model is shown in Figure 3.24. For comparison, the results of fitting this data to the case I diffusion model are shown in Figure 3.25.

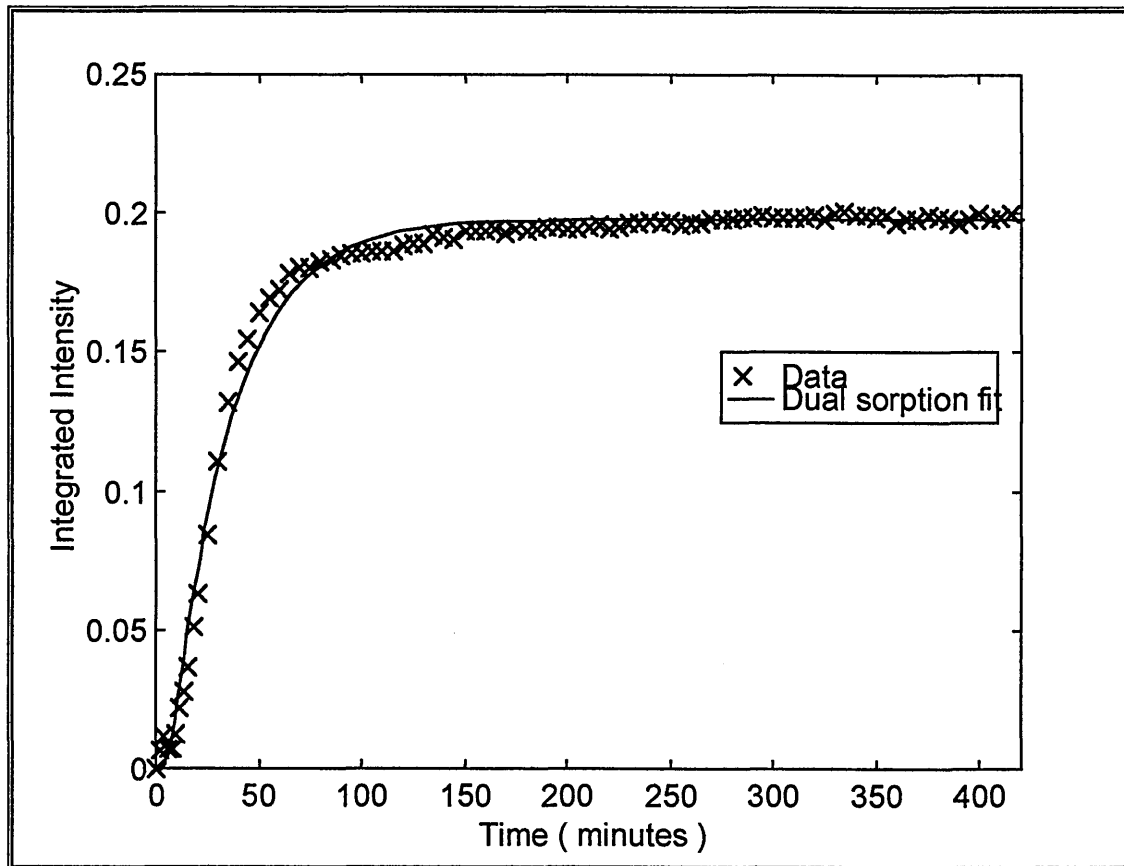


Figure 3.24 : Results of fitting data from Y9669 diffusion in 15% DHA plasticised PVC to the dual mode sorption model

Figure 3.24 shows that although the fit of the data to the dual mode sorption model is not as good as shown by diffusion in 30% DHA plasticised PVC (Figure 3.23), it is still

quite a good fit. Comparison with Figure 3.25 shows that the data fits the case I diffusion model much more poorly. It is not known why the fitting process produced very similar values for D_1 and D_2 in this case.

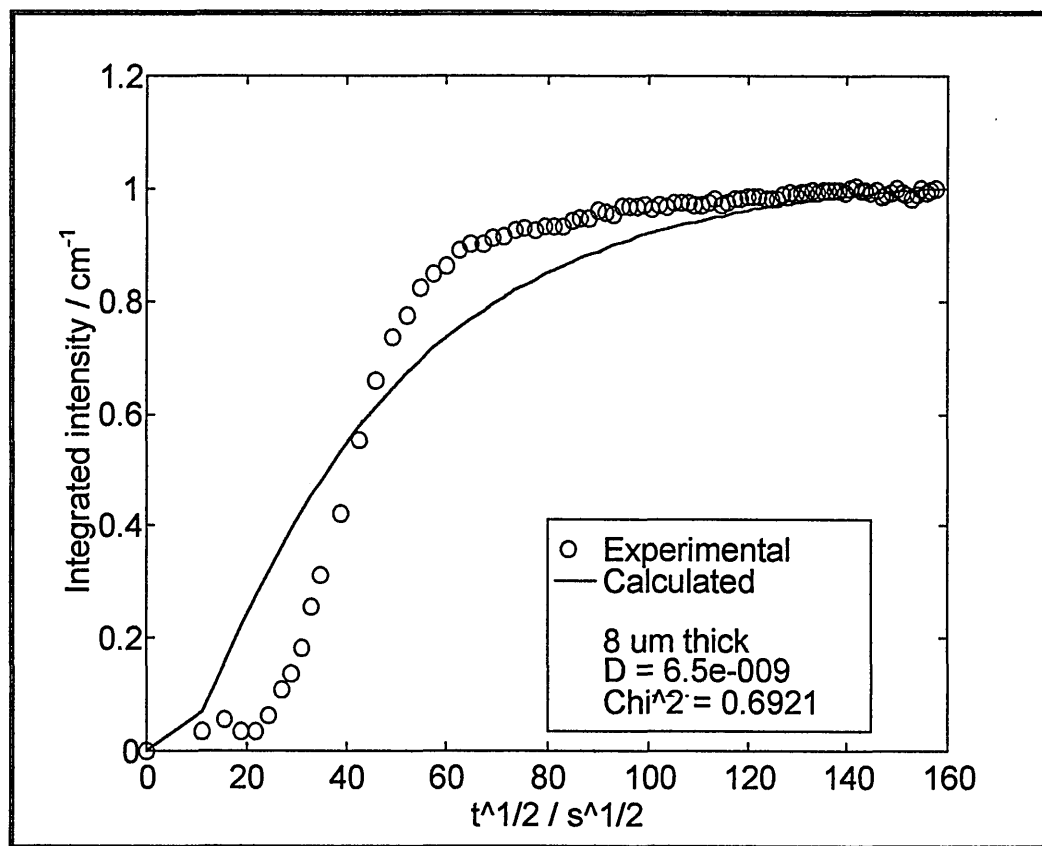


Figure 3.25 : Results of fitting data from Y9669 diffusion in 15% DHA plasticised PVC to the Fickian case I diffusion model

In order to determine the cause of the decrease in plasticiser band intensity (see Figure 3.16), it was decided to attempt to determine the kinetics of the decrease. A plot of the integrated intensity of this band vs. time is shown in Figure 3.26. This data was obtained for Y9669 diffusion in 30% DHA plasticised PVC.

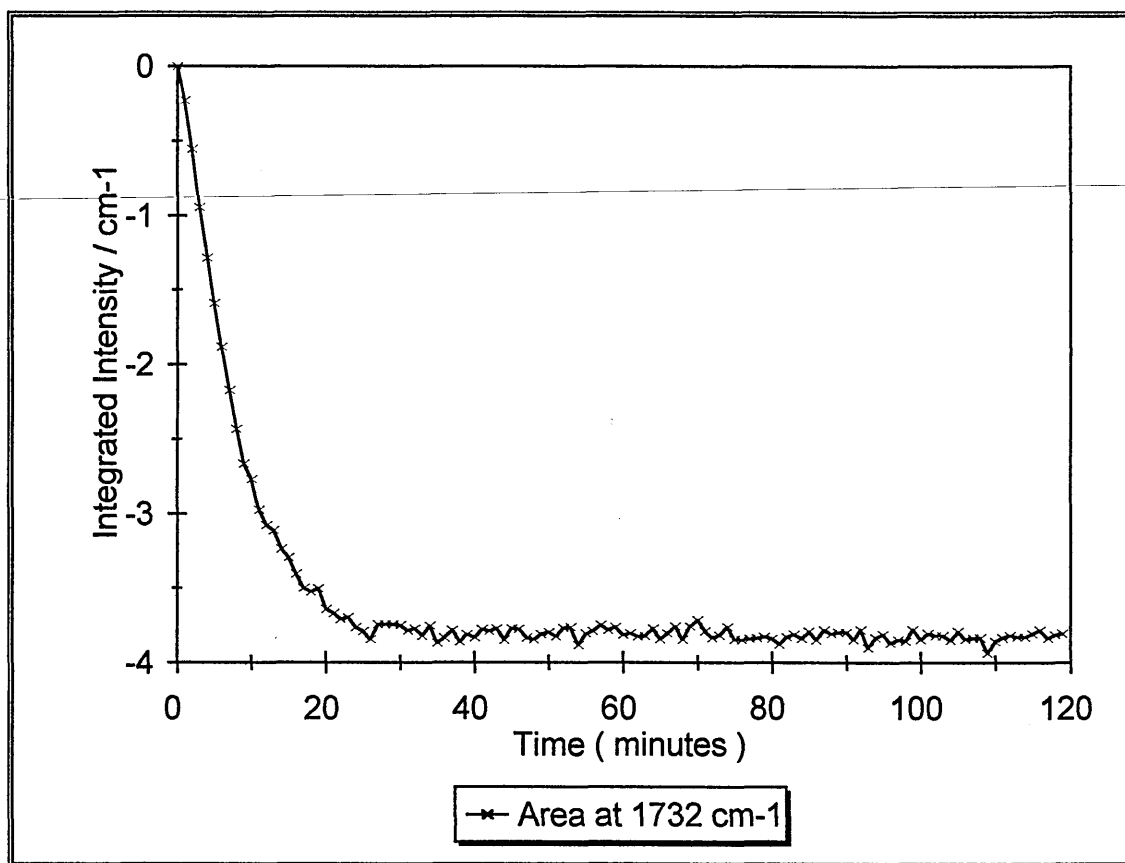


Figure 3.26 : The area of the carbonyl stretching mode of DHA (1732 cm^{-1}) plotted vs. time for Y9669 diffusion in 30% DHA plasticised PVC

Comparison of Figure 3.26 with Figure 3.17 shows that to a first approximation, the decrease in the band intensity of DHA shows the same kinetics as those shown by Y9669. In order to test the match in kinetics more closely, the dual mode sorption fitting program was applied to the data shown in Figure 3.26. The results are shown in Figure 3.27.

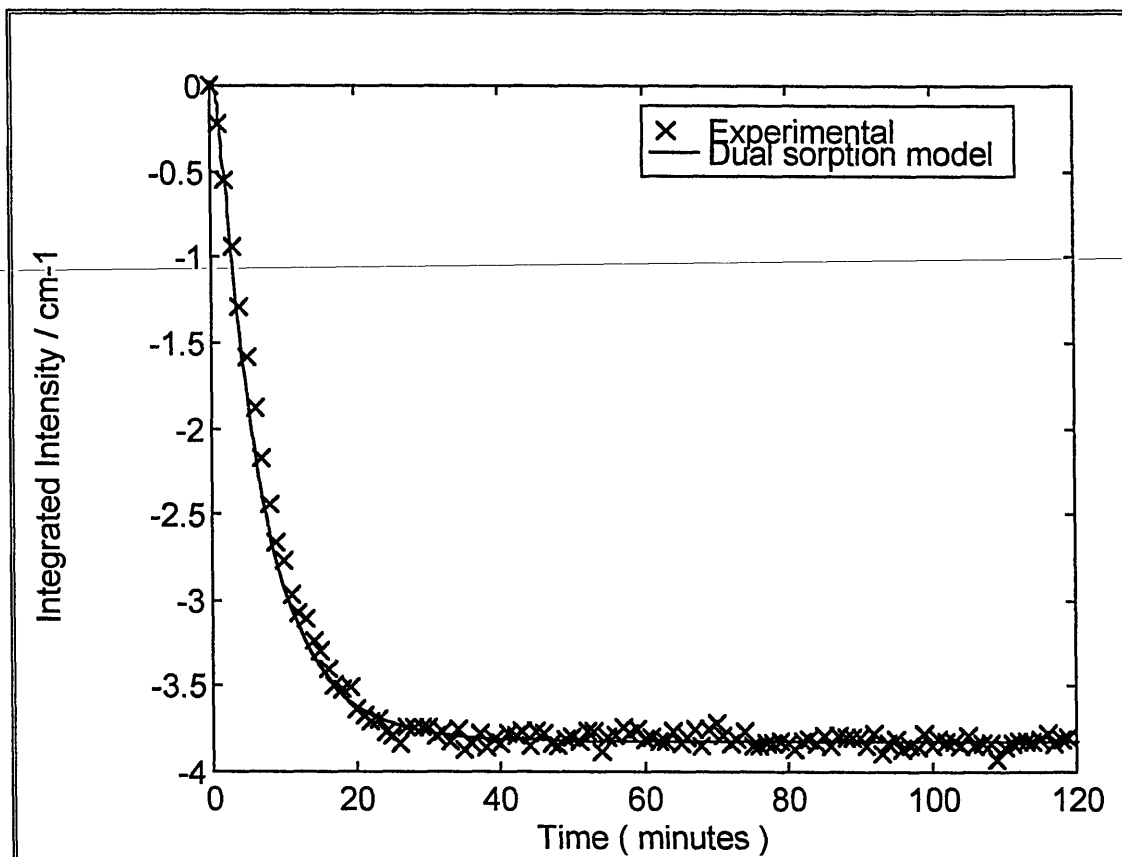


Figure 3.27 : The results of fitting the decrease in DHA band intensity (1732 cm^{-1}) to the dual mode sorption diffusion model

Figure 3.27 shows that the decrease in DHA carbonyl stretching intensity fit very well to the dual mode sorption model. This data was found not to fit well to the case I diffusion model. The diffusion coefficients generated by the fitting procedure are given in Table 3.4.

Parameter	Value
D_1	$8.54 \times 10^{-8} \text{ cm}^2 \text{ s}^{-1}$
D_2	$4.73 \times 10^{-8} \text{ cm}^2 \text{ s}^{-1}$
X_1	0.46

Table 3.4 : Diffusion coefficients obtained from fitting the decrease in DHA band intensity (1732 cm^{-1}) to the dual mode sorption diffusion model

Table 3.4 shows that the mobile diffusion coefficient (D_1) generated for the plasticiser is very similar to that of the silane diffusion. The ‘immobile’ diffusion coefficient (D_2) was somewhat larger however. It is believed that the similarity in the kinetics of the decrease in the plasticiser band and the increase in the silane bands indicates that the silane displaced the plasticiser from the polymer film in the evanescent field, possibly due to swelling of the polymer film, or migration of the plasticiser to the outside of the film. This is discussed in greater detail later.

The log of the two diffusion coefficients, D_1 and D_2 for A1110 diffusion has been plotted versus the percentage of plasticiser used in Figure 3.28.

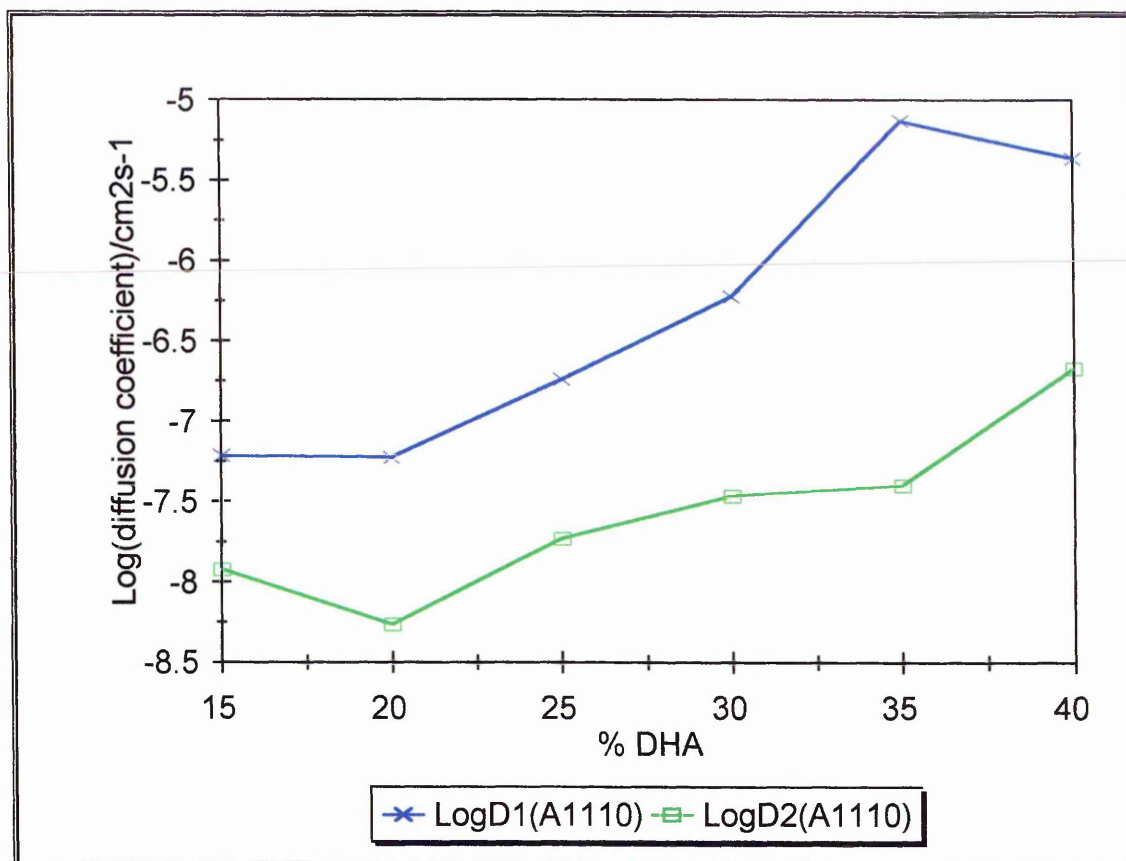


Figure 3.28 : The logarithm of the diffusion coefficients obtained from dual mode sorption fitting of A1110 diffusion vs. percentage plasticiser in the PVC film

Figure 3.28 shows that in the case of A1110 diffusion, much the same trend was seen in the diffusion coefficients as was seen in the case of Y9669 diffusion. Both D_1 and D_2 increased overall with increasing plasticiser concentration. The greatest increase in the size of the diffusion coefficients occurred between 30 and 35 % DHA. Unlike the Y9669 data, at 15% plasticiser, the value of D_2 was approximately an order of magnitude less than that of D_1 , as in all the plasticiser loadings. All the data fitted well to the dual mode sorption model.

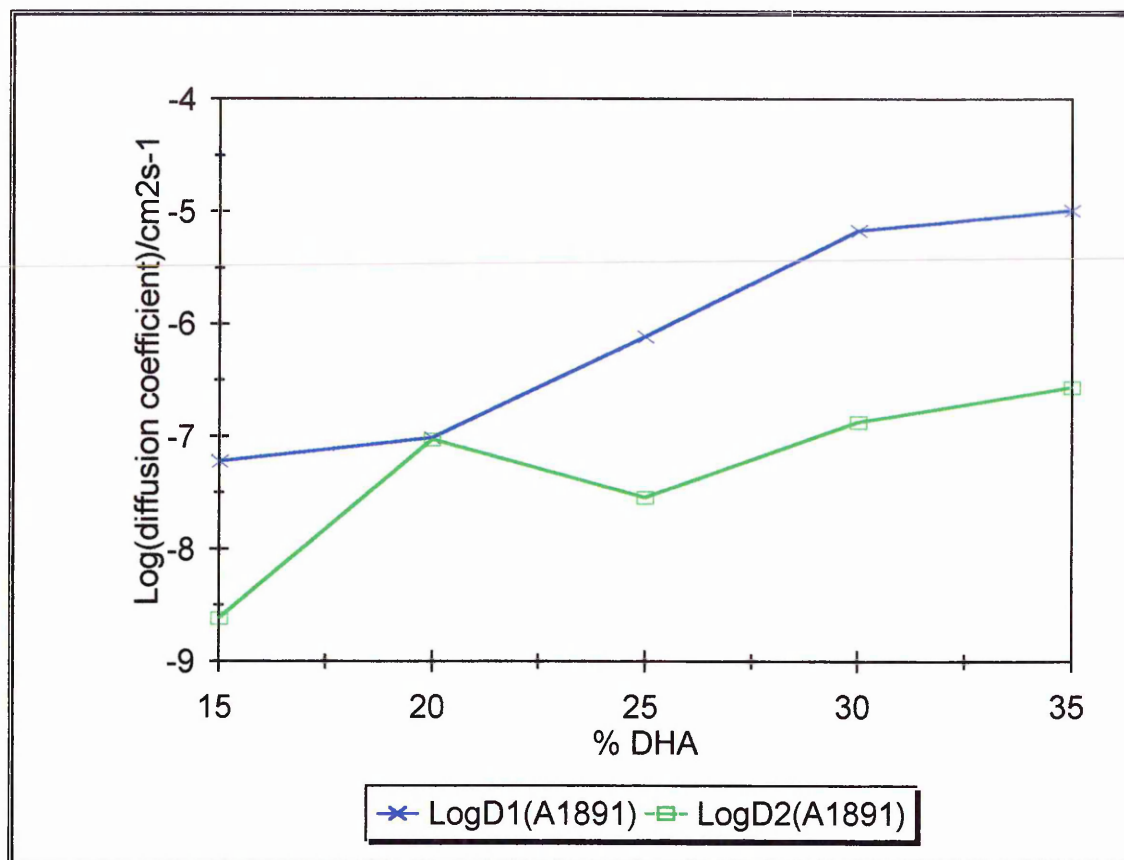


Figure 3.29 : The logarithm of the diffusion coefficients obtained from dual mode sorption fitting of A1891 diffusion vs. percentage plasticiser in the PVC film A1891

Figure 3.29 shows that in the case of A1891 diffusion, a similar trend was seen in the diffusion coefficients as was seen in the case of Y9669 diffusion. Both D_1 and D_2 increased overall with increasing plasticiser concentration. Like the Y9669 data, one point showed D_1 and D_2 with very similar values, but in this case it was the point at 25% DHA. Again it was suspected that this meant a poor fit to the dual mode sorption model. However, upon attempting to fit the data to the case I model, it was found that the data did not fit to the Fickian Case I model. The data was found to fit much better to the dual mode sorption model.. Again, the reason for the very similar diffusion coefficients is not known.

The results from the experiment where no fitting was possible (A1891 in 15% DHA plasticised PVC) are shown in Figure 3.30.

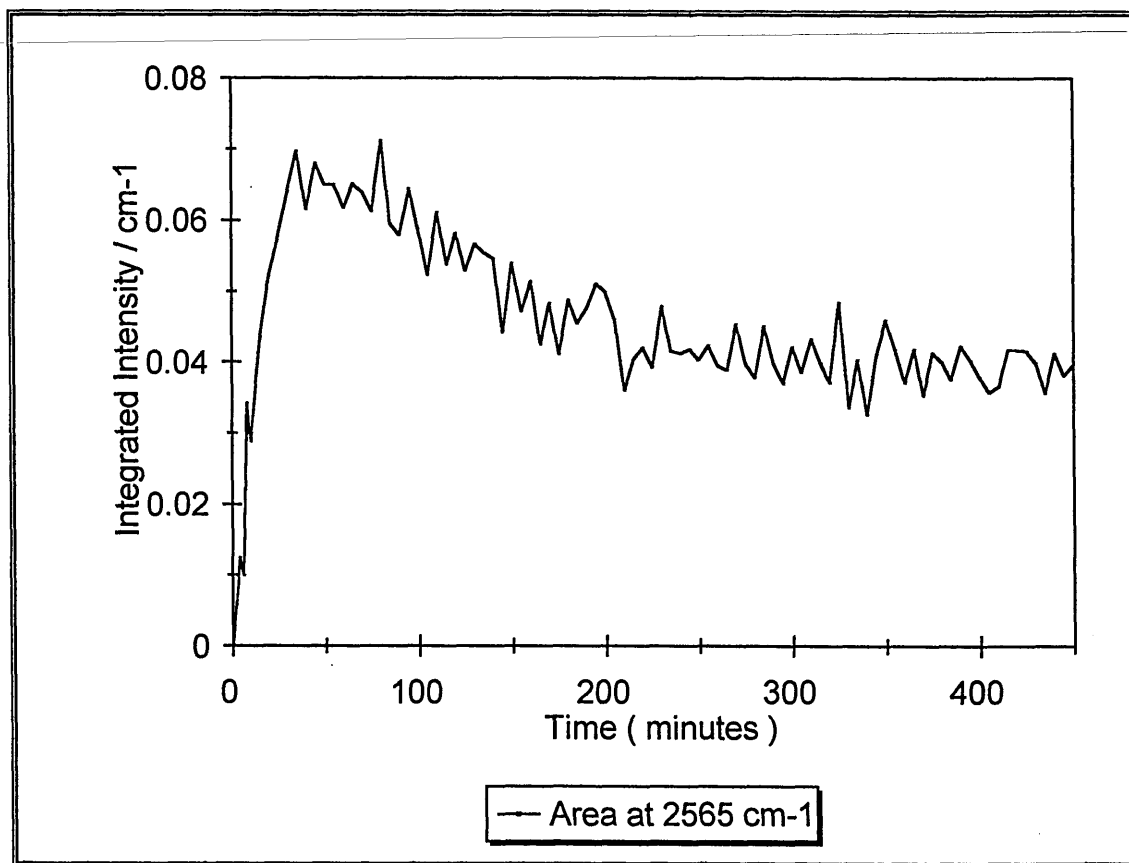


Figure 3.30 : The area of the $\nu(\text{SH})$ stretching band of A1891 (2565 cm^{-1}) vs. time for diffusion in 15% DHA plasticised PVC

Figure 3.30 shows that normal diffusion did not occur : the initial diffusion to the maximum intensity obtained occurred extremely quickly, and after this the intensity decreased, apparently reaching equilibrium at a lower intensity after about 300 minutes. It is not known why this occurred. The experiment was repeated twice and the same results observed each time. One possibility is that the initial increase was due to diffusion of the silane to the interface and that the subsequent decrease in intensity was due to swelling of

the PVC film. However, this seems unlikely, as it was seen in only this case; if swelling due to the presence of the silane were to blame, then it would be expected that it would occur in more than just this one experiment. Another possibility is that the behaviour was due to the microstructure of the film. This would explain why the effect occurred for one plasticiser concentration, but not why it did not occur for the other silanes. It may be that in the case of this particular plasticiser concentration, cracks or pinholes occurred in the polymer film, allowing fast initial diffusion to the surface of the ATR crystal, followed by diffusion into the bulk of the PVC film. This hypothesis is also very uncertain, however, as it does not explain why the effect was only seen with the silane A1891.

3.3.4 : Silane overlayers - PVC plasticised with polymeric plasticiser

In order to determine the effect of type of plasticiser on diffusion, it was decided to study the diffusion of silanes in PVC plasticised with a polymeric plasticiser. It is well known that in polymeric materials containing plasticiser, plasticiser migration can occur^{20,11}. This can occur as a result of weathering, swelling, temperature changes, or simply as a function of time. It was shown that upon allowing silanes to diffuse into PVC containing a monomeric plasticiser, a decrease in the plasticiser band intensities was observed. It was thought that this may have been due to the plasticiser migration out of the bulk of the film towards the outer surface of the film. Another possibility is that the PVC film swells when the silane diffuses into it. Because the volume sampled by the evanescent field is fixed (assuming no change in refractive index of the film), this would result in a net decrease in the concentration of plasticiser (and PVC) in the evanescent field.

Therefore the intensity of plasticiser and PVC bands in the spectra would decrease at the same time as the intensity of the silane bands are increasing. One way to distinguish between the two possibilities would be determine whether both PVC and plasticiser bands decrease in intensity. Unfortunately, the only PVC bands available in the spectral window of silicon are the $\nu(\text{CH})$ stretching modes around 2800 - 2950 cm^{-1} . These bands are overlapped by the $\nu(\text{CH})$ modes of both the plasticiser and the silane. This makes definitively interpretation of the spectra in this region very difficult.

One method used commercially in order to reduce or stop the migration of plasticiser is the use of oligomeric plasticiser²¹. It is well known that the tendency of chemically similar materials to undergo diffusion in polymeric films varies inversely with their molecular weights^{10,22}. This is due to the larger size of high molecular weight materials, and in the case of polymeric materials, the tendency to form entanglements with the matrix material. It was decided to perform similar experiments as described in section 3.2.2 but with Diolpate 7170 replacing DHA. These two materials are almost identical chemically (see section 3.1), and so any differences would be due to the difference in molecular weight.

Experiments were performed identically to those described in the last section, with Diolpate 7170 replacing DHA. The results obtained from the diffusion of Y9669 in PVC plasticised with 40% Diolpate 7170 are shown in Figure 3.31. The thickness of the PVC film was 7 μm .

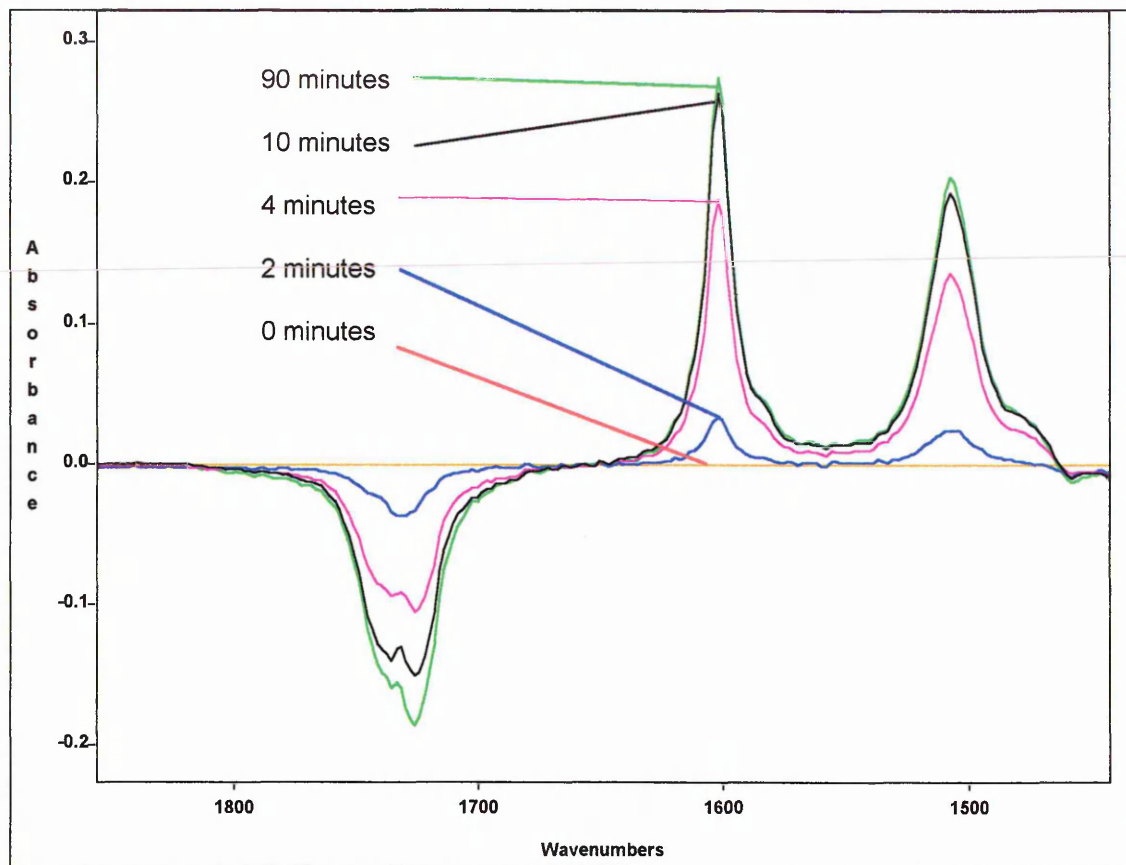


Figure 3.31 : The results of Y9669 diffusion in 40% Diolpate 7170 plasticised PVC

The integrated intensity of the 1602 cm^{-1} band of the Y9669 band in Figure 3.31, along with the dual mode sorption fitting obtained is shown in Figure 3.32.

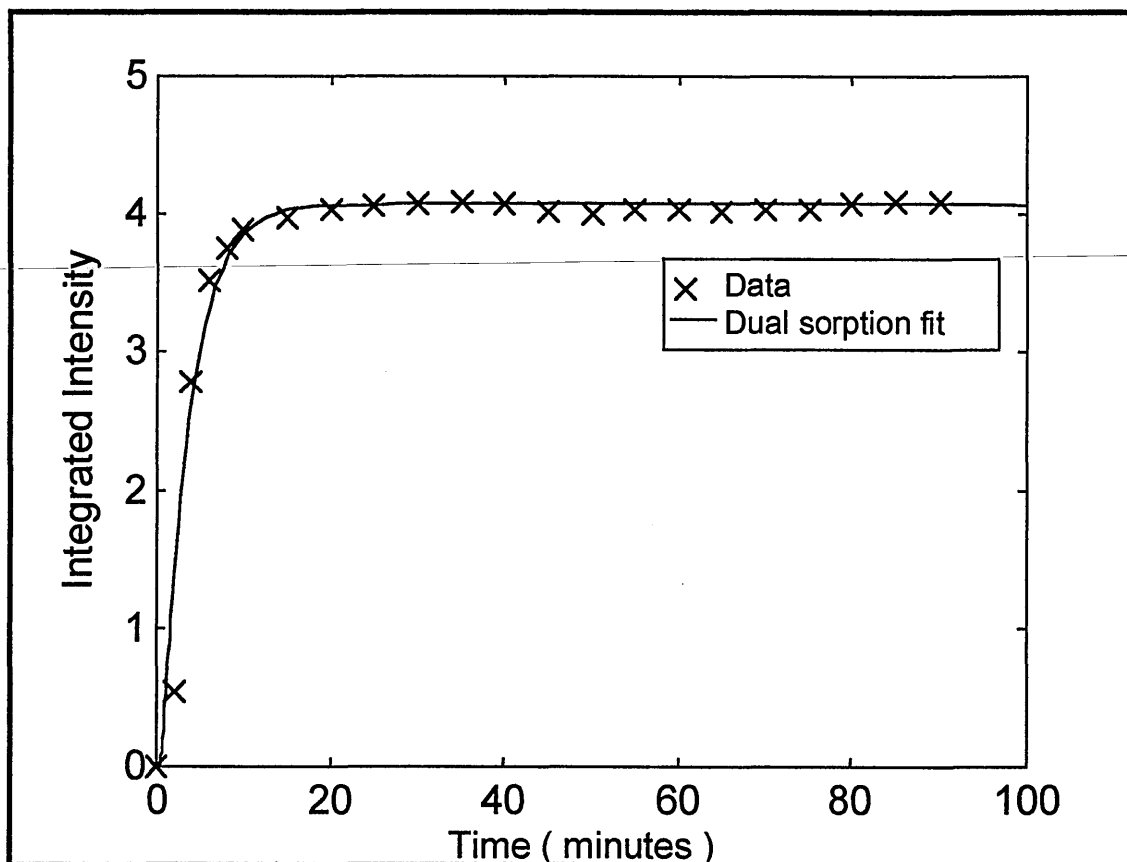


Figure 3.32 : The results of fitting data from Y9669 diffusion in 40% Diolpate 7170 plasticised PVC to the dual mode sorption model

It can be seen from Figure 3.31 and Figure 3.32 that the silane did diffuse through the film plasticised with Diolpate 7170. Figure 3.32 also shows that the silane diffusion fitted well to dual mode sorption kinetics. The data was again found not to fit the Fickian case I diffusion model. It can also be seen that despite the polymeric nature of the plasticiser, the carbonyl stretching mode (at 1726 cm^{-1}) still decreased as the silane diffused into the film. This implies that the reason for this decrease was not diffusion of the silane to the surface of the PVC film, but swelling of the PVC film due to the uptake of silane. Figure 3.33 shows the area of the 1726 cm^{-1} band of Diolpate 7170 versus time for the diffusion of Y9669 in 40% Diolpate 7170 plasticised PVC.

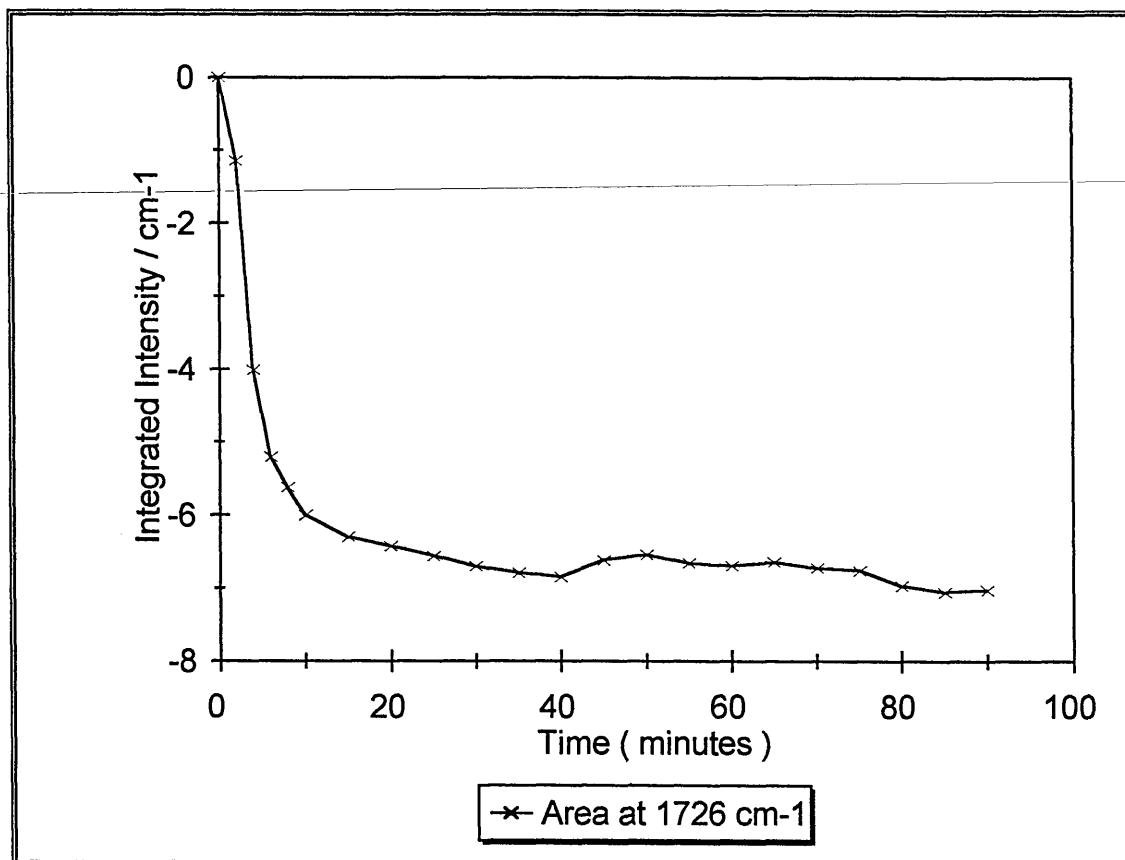


Figure 3.33 : Area of 1726 in 40% Diolpate 7170 PVC

Comparison of Figure 3.33 with Figure 3.32 shows that the decrease in intensity of the plasticiser band was somewhat slower than the increase in intensity of the silane bands. The difference in kinetics is not very great. It is believed that this proves the plasticiser did not diffuse away from the ATR crystal interface, because the large change in molecular weight of the plasticiser upon using Diolpate 7170 (which has six times the molecular weight of DHA) would have meant that the diffusion of the plasticiser would have been much slower than the diffusion of the silane if this were the case. In order to assess diffusion in Diolpate 7170 plasticised PVC more fully, experiments were performed with

all three silanes, using the limits of the plasticiser concentrations that gave results when using DHA (i.e. 40% plasticiser and 20% plasticiser). The results of dual mode sorption fitting to the data obtained are shown in Table 3.5.

% Diolpate 7170	Y9669	A1110	A1891
40	$D_1 = 4.59 \times 10^{-6}$ $D_2 = 1.62 \times 10^{-6}$ $X_1 = 0.53$	$D_1 = 1.07 \times 10^{-6}$ $D_2 = 8.80 \times 10^{-7}$ $X_1 = 0.96$	$D_1 = 1.04 \times 10^{-5}$ $D_2 = 2.76 \times 10^{-7}$ $X_1 = 0.69$
20	$D_1 = 2.36 \times 10^{-8}$ $D_2 = 3.59 \times 10^{-9}$ $X_1 = 0.86$	$D_1 = 3.74 \times 10^{-7}$ $D_2 = 1.99 \times 10^{-8}$ $X_1 = 0.40$	$D_1 = 2.84 \times 10^{-8}$ $D_2 = 2.67 \times 10^{-9}$ $X_1 = 0.95$

Table 3.5 : Diffusion coefficients obtained from fitting the data from silane diffusion in Diolpate 7170 plasticised PVC to the dual mode sorption diffusion model.

Table 3.5 shows that like the results with DHA as a plasticiser (Table 3.3), increasing the concentration of Diolpate 7170 greatly increases the diffusion coefficients resulting from the fitting procedure. It was again found that no data fitted the case I diffusion model, indicating that the mechanism of diffusion is independent of plasticiser molecular weight.

The Y9669 results show that the diffusion coefficients obtained for Diolpate 7170 plasticised PVC were similar to those for DHA plasticised material. Again, this showed that diffusion was independent of the molecular weight of the plasticiser, as well as that the two plasticisers have the same effect, when used in the same concentrations.

In the case of A1110, although the trends are the same for monomeric and polymeric plasticisers, there is somewhat more disparity between the values of the coefficients obtained. However, no overall trend can be discerned in the differences

between the values obtained. These differences all amounted to less than an order of magnitude, and it is believed that they were due to experimental errors.

The results for A1891 showed very close agreement between diffusion coefficients obtained using DHA and Diolpate 7170. At first glance, it seemed surprising that the results were so reproducible for A1891, considering the poor signal to noise obtained for the band used to generate the data (see Figure 3.20). The main difference between this silane and the others is that A1110 and Y9669 contain an amine group. The catalytic effect this has on the hydrolysis has been described in the literature^{7,8}. It seems likely that, despite the care taken to avoid exposure of the silanes to atmospheric water, some small amount of water inevitably came into contact with the silanes before the experiments were performed. If this were the case then one might expect the two amino silanes to undergo more hydrolysis than the mercaptosilane. If this did occur, and as suggested in section 3.2.1, the hydrolysed silanes diffused more slowly than unhydrolysed silanes, then the unrepeatability in the aminosilane results is likely to be have been due to slight differences in the level of hydrolysis or condensation of the amino silanes used. In contrast, the resistance to hydrolysis of the mercaptosilane meant that the material used was identical in each experiment, even if some exposure to water had occurred.

3.4 : DSC analysis of plasticised PVC films

The glass transition temperature (T_g) of a polymer is the temperature at which a major sub-melting chain motion starts to occur²³. This has the effect of radically changing

the mechanical properties of the polymer; it is said to go from the glassy to the rubbery state. Several lesser transitions may also exist, known collectively as sub-T_g transitions, but these are not considered here. In the pure PVC supplied by the Aldrich chemical company, the T_g is quoted as 80 °C. The glass transition is an effect which can occur over quite a broad temperature range. This means that the effect of the glass transition may be observed at considerably lower temperatures than the measured T_g, and as a consequence the T_g can be difficult to measure. Often the measured T_g will depend upon the technique used to measure it, and the way in which the technique is applied. Specifically, if a temperature – scanning technique is used, the rate at which the temperature is raised (or lowered) can change the measured T_g considerably.

Because above or near the T_g of a polymer, the polymer chains show increased motion, it was expected that the T would affect the diffusion seen. Therefore, it was decided to measure the T_g of the PVC films as cast. It was decided to use Differential Scanning Calorimetry (DSC) to measure the T_gs. Several alternative techniques exist to measure T_gs, notably Dynamic Mechanical Thermal Analysis (DMTA). However, most require a sample several mm. thick. Production of a sample this thick was not possible by casting, without severe degradation or poor solvent removal. As it was desirable to measure the films produced in the same way as those used in the diffusion experiments, it was decided to use DSC, which only requires a few milligrams of material.

DSC is a relatively simple technique. The sample in a metal sample pan, and an empty sample pan as a reference are placed in a closed sample holder, and directly

connected to individual resistive heaters. A desired temperature ramp rate is programmed into the controller, which then adjusts the flow of energy to the heaters so that the same temperature is maintained in both sample and reference pans. The extra energy supplied to the sample pan, therefore, shows the energy absorbed by the sample in changing its temperature. The output from the technique shows the energy flow to the sample versus the temperature. Any exothermic or endothermic process occurring in the sample give rise to a change in slope of this plot. In practice, the Tg of a polymer is measured as a 'step' in the plot.

DSC results were obtained at Pilkington plc using a DuPont 910 DSC cell coupled to a TA2100 controller. The DSC cell was calibrated for temperature using standard indium metal. A ramp heat rate of 10 °C per minutes was used from -100 to +100 °C. A sample plot is shown in Figure 3.34. This is the result from the 20% DHA plasticised sample.

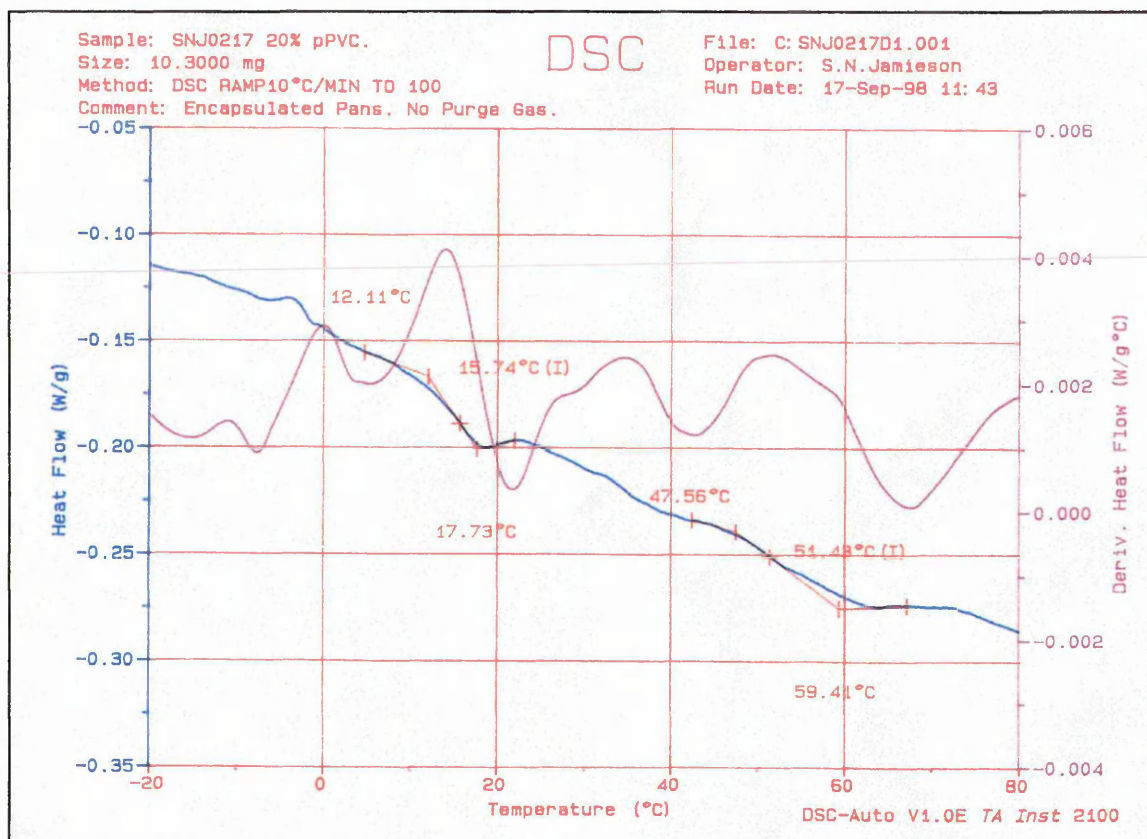


Figure 3.34 : Typical DSC output plot. The sample was 20% DHA plasticised PVC

The results of the Tg measurements are tabulated in Table 3.6.

Percentage Plasticiser	Inflection Tg (°C)
20	16
25	-1
30	-16
35	-19

Table 3.6 : The results of Tg measurements by DSC

Unfortunately, it was not possible to obtain Tg results for the 15 and 40 % DHA samples. However, the trend in Tg with plasticiser content is quite well known²⁴, and is shown by Figure 3.35 reproduced from reference 25.

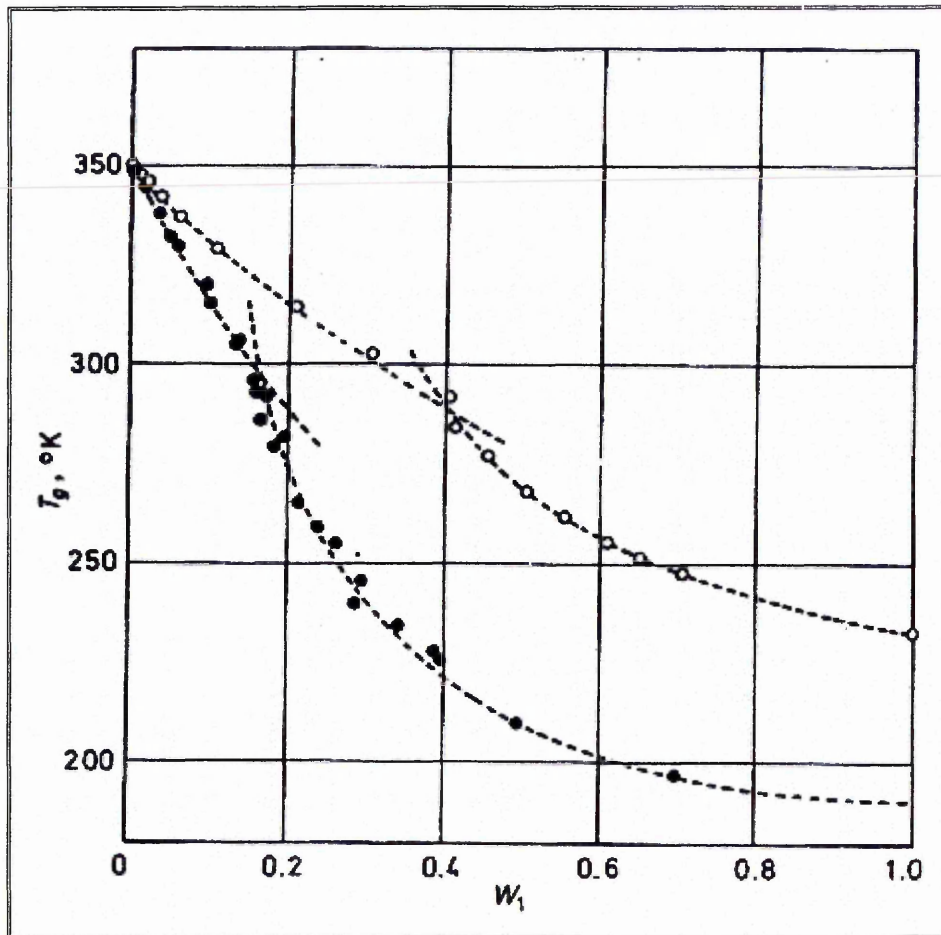


Figure 3.35 : The dependence of T_g of PVC upon plasticiser concentration (W_1). Open circles represent dicyclohexylphthalate, filled circles represent dibutylphthalate²⁵.

The measured values of the glass transition temperatures are plotted versus the percentage of plasticiser in the films in figure 3.36.

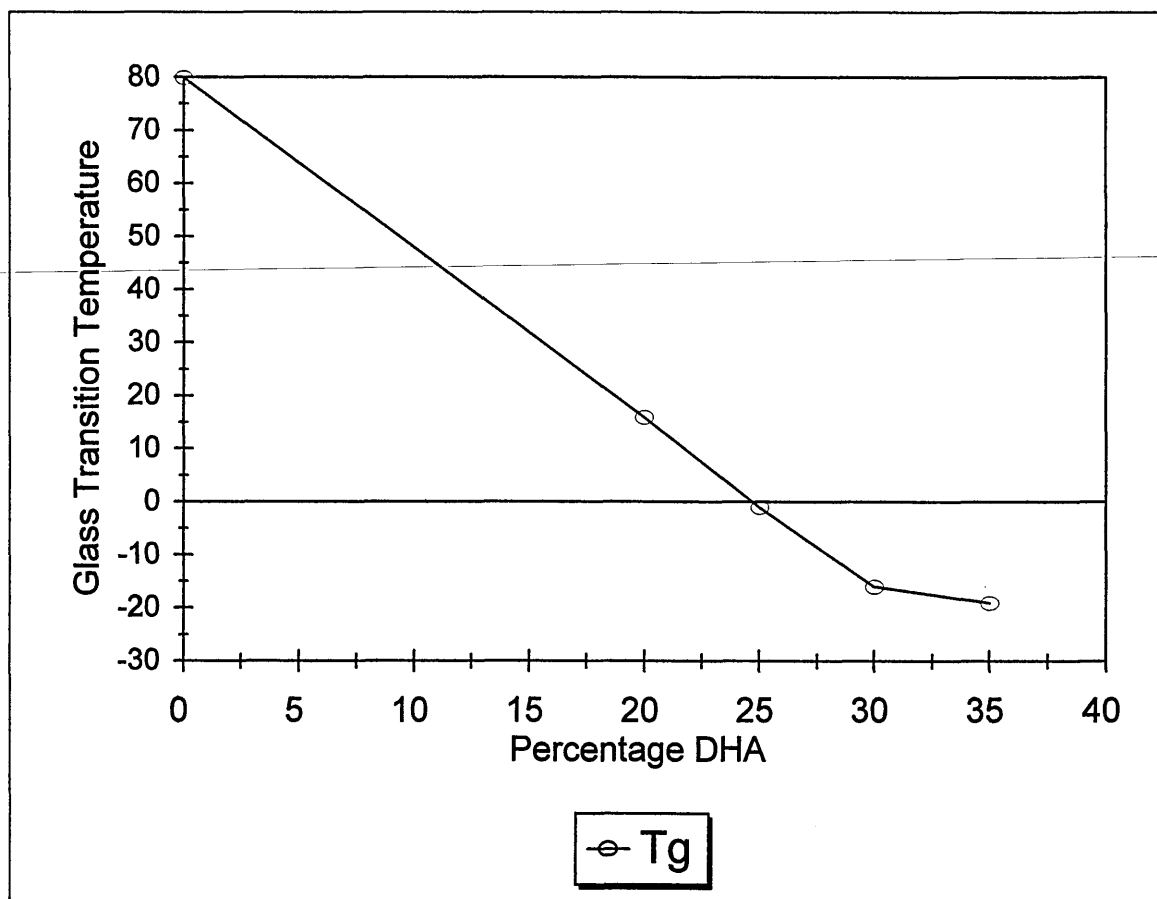


Figure 3.36 : Glass Transition temperature of plasticised PVC films measured by DSC vs. percentage of plasticiser

It can be seen from Figure 3.36 that the overall trend in the results as measured follows fairly closely the literature trend (Figure 3.35), in that initially a linear relation is seen, but the slope decreases at higher concentrations of plasticiser. With knowledge of the trend that occurs in the data from the literature, and the measured values, it is also possible to estimate the values for those samples which could not be measured. These have been estimated as : 25 °C for 40 % plasticised PVC, and 25 °C for 15% plasticised PVC. Using these values, the diffusion coefficients from fitting to the dual mode sorption model have been plotted versus Tg in figures 3.37, 3.38 and 3.39.

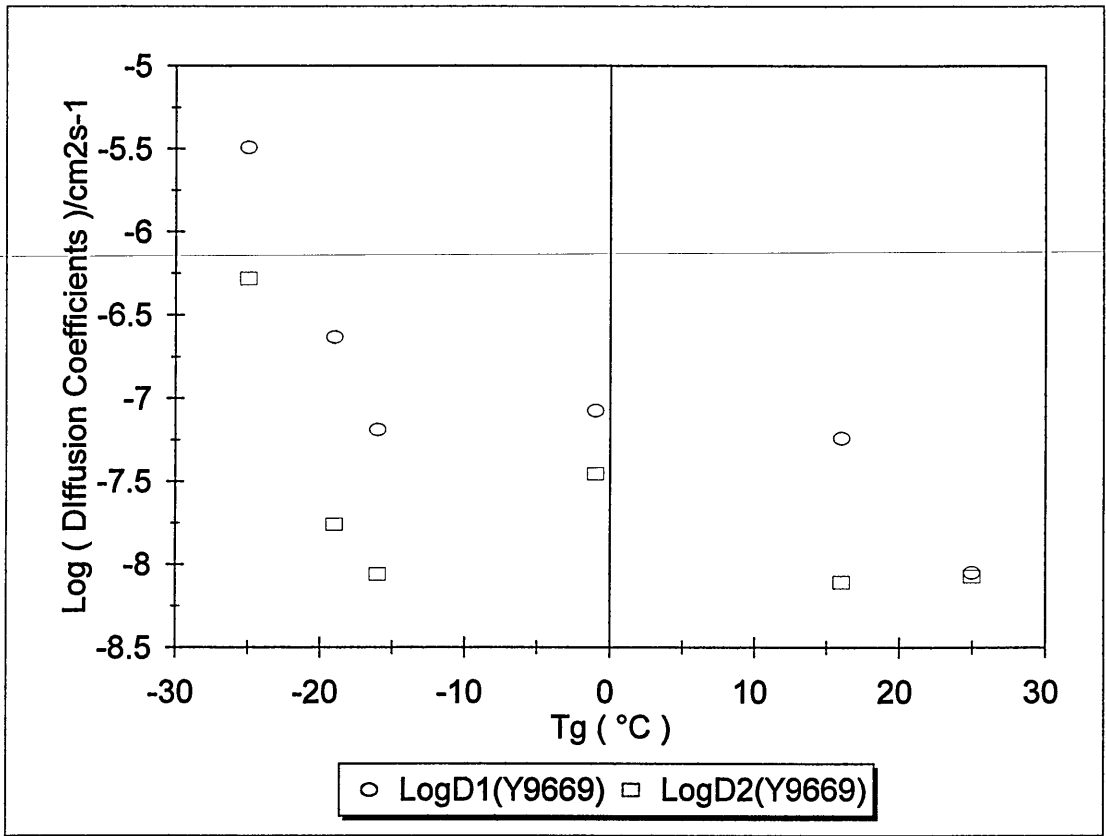


Figure 3.37 : Diffusion Coefficients from dual mode sorption fitting for Y9669 diffusion in plasticised PVC vs. Tg of the PVC

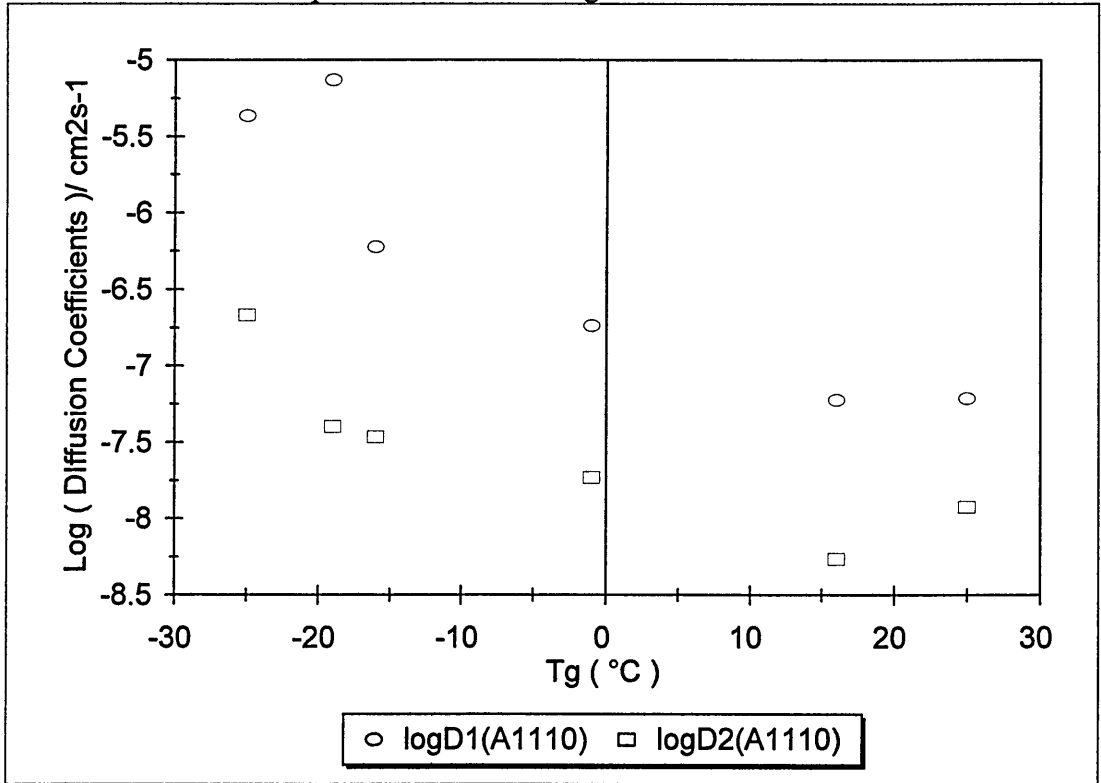


Figure 3.38 : Diffusion coefficients from dual mode sorption fitting for A1110 diffusion in plasticised PVC vs. Tg of the PVC

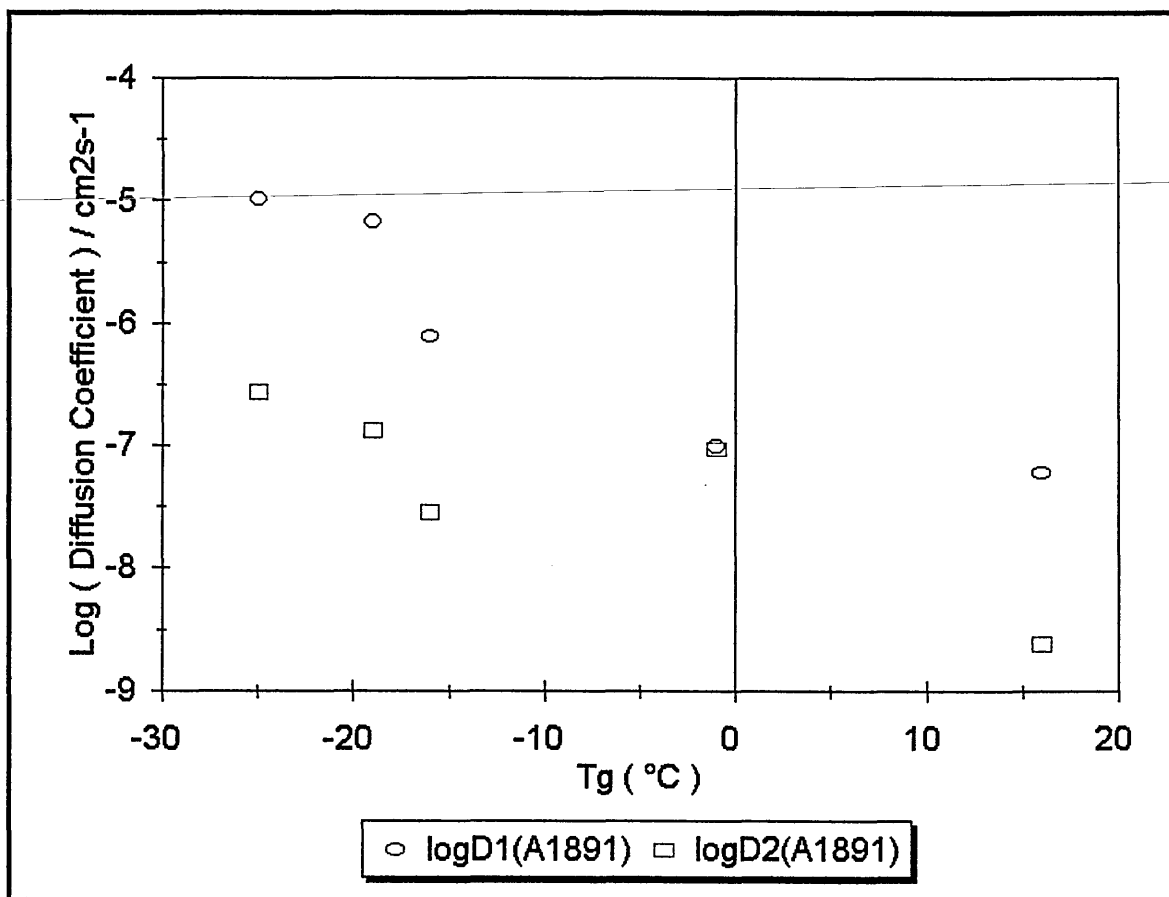


Figure 3.39 : Diffusion coefficients from dual mode sorption fitting for A1891 diffusion in plasticised PVC vs. Tg of the PVC

Figures 3.37, 3.38 and 3.39 show that for each of the silanes, as the Tg of a PVC film was reduced from 25 to -25 °C, the diffusion coefficients of the silane in the film increased by approximately 3 orders of magnitude.

3.5 : Silane overlayers - hydrolysed silanes

In order to determine whether hydrolysis affects diffusion, as was implied by previous results described in this chapter, and what the effect of hydrolysis on diffusion is,

it was decided to perform some diffusion measurements with pre-hydrolysed silanes. However, it was decided not to use the standard acidified IPA / H₂O solution as was described in section 3.2. This was because it is known that alcohols and water diffuse into polymers²⁶ including PVC^{27,28}. These materials may plasticise the polymer²⁹, and thus change the diffusion of silanes in the material, as well as complicating the spectral analysis. Therefore, it was decided to hydrolyse the silanes by exposure to atmospheric water, thus avoiding the problem of the hydrolysing solvent affecting the results. This did not alleviate the problem altogether, because the hydrolysis products (methanol or ethanol) would have been present in small concentrations in the diffusant material.

In order to determine the level of hydrolysis achieved, transmission infrared spectroscopy was used. The silane was sprayed onto a KBr plate, and allowed to interact with atmospheric water, while infrared spectra were obtained at regular intervals. The first experiment was performed with Y9669. The region of the spectra obtained showing the Si-O-Si stretching bands and the band at 992 cm⁻¹ is shown in Figure 3.40. This band was assumed to be equivalent to the Si-O-Et band used by Hoh *et al.*⁹ as an indication of hydrolysis, i.e. it is assigned to the Si-O-Me stretching mode of Y9669.

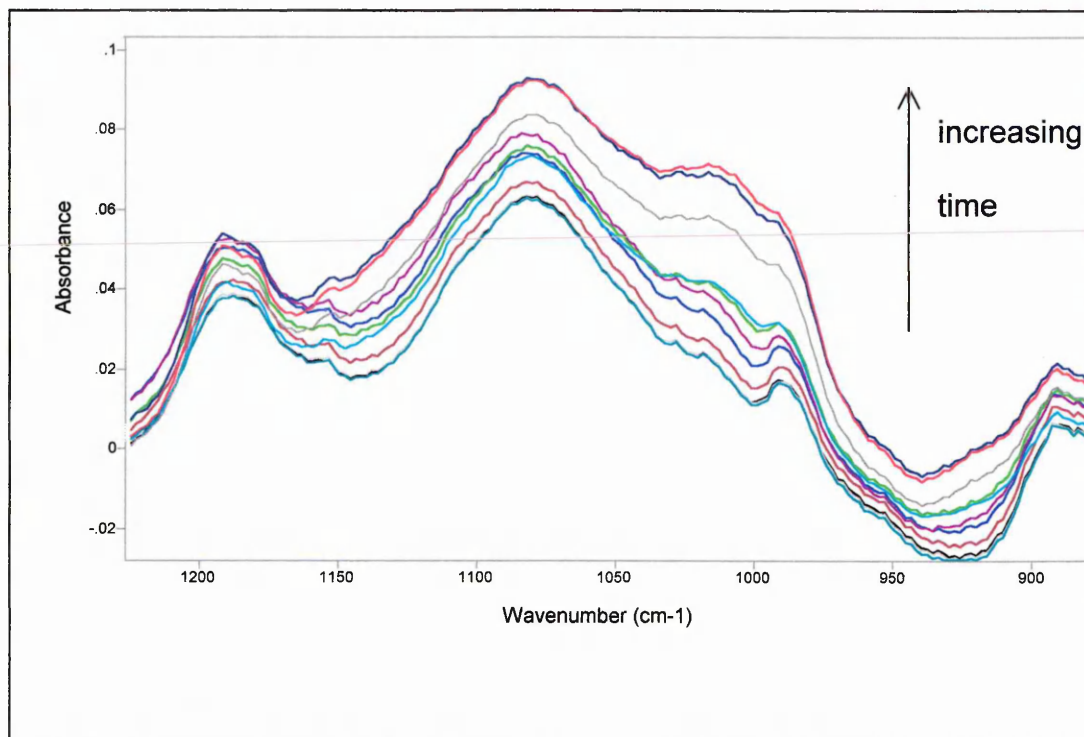


Figure 3.40 : The Si-O stretching region of spectra obtained in transmission of Y9669 undergoing hydrolysis with atmospheric water

It can be seen from

Figure 3.40 that the band at 992 cm^{-1} decreases in intensity with increasing time. This shows loss of Si-O-Me groups, i.e. hydrolysis of the Y9669. There is also a shoulder to the 1080 peak, at about 1020 cm^{-1} which increases in intensity. This may be due to the condensation of Y9669, as observed by McKnight *et. al.*³⁰ at 1038 cm^{-1} for the silane CSS (see section 1.2.2). In order to determine how the Si-O-Me stretching mode decreases with time, the spectra were analysed with a standard curve-fitting procedure, and the integrated intensity of the curve fitted to the 992 cm^{-1} plotted against experiment time. This is shown

in Figure 3.41.

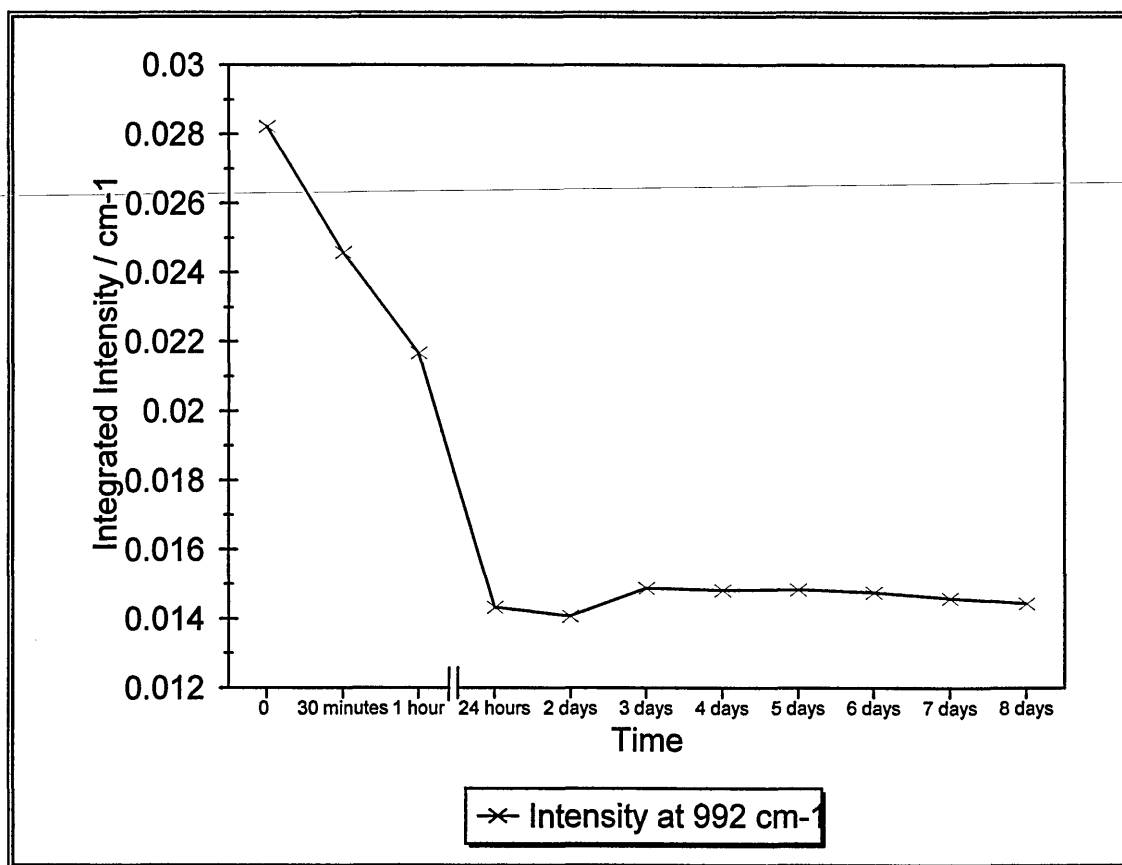


Figure 3.41 : The curve fitted intensity of the 992 cm⁻¹ band of Y9669 undergoing hydrolysis with atmospheric water

Figure 3.41 shows that hydrolysis is rapid in the first 2 hours, but that after 24 hours no further hydrolysis occurs. It is clear from Figure 3.41 that at this stage, and even up to 8 days of exposure, hydrolysis is not complete, the intensity of the Si-O-Me band remaining at about half of its original intensity. The diffusion of Y9669 which had been exposed to atmospheric water for 24 hours was investigated. The experiment was similar to those described in section 3.2.1. An unplasticised PVC film was cast from DMF solution. The thickness was 7 μm . After application of the pre-hydrolysed silane, spectra were taken after subsequent exposures to 70 °C of five minutes duration. The intensity of the 1602 cm⁻¹

band of the Y9669 is plotted versus time at 70 °C in Figure 3.42. For comparison, the data from unhydrolysed Y9669 is also included, and the spectra are intensity normalised.

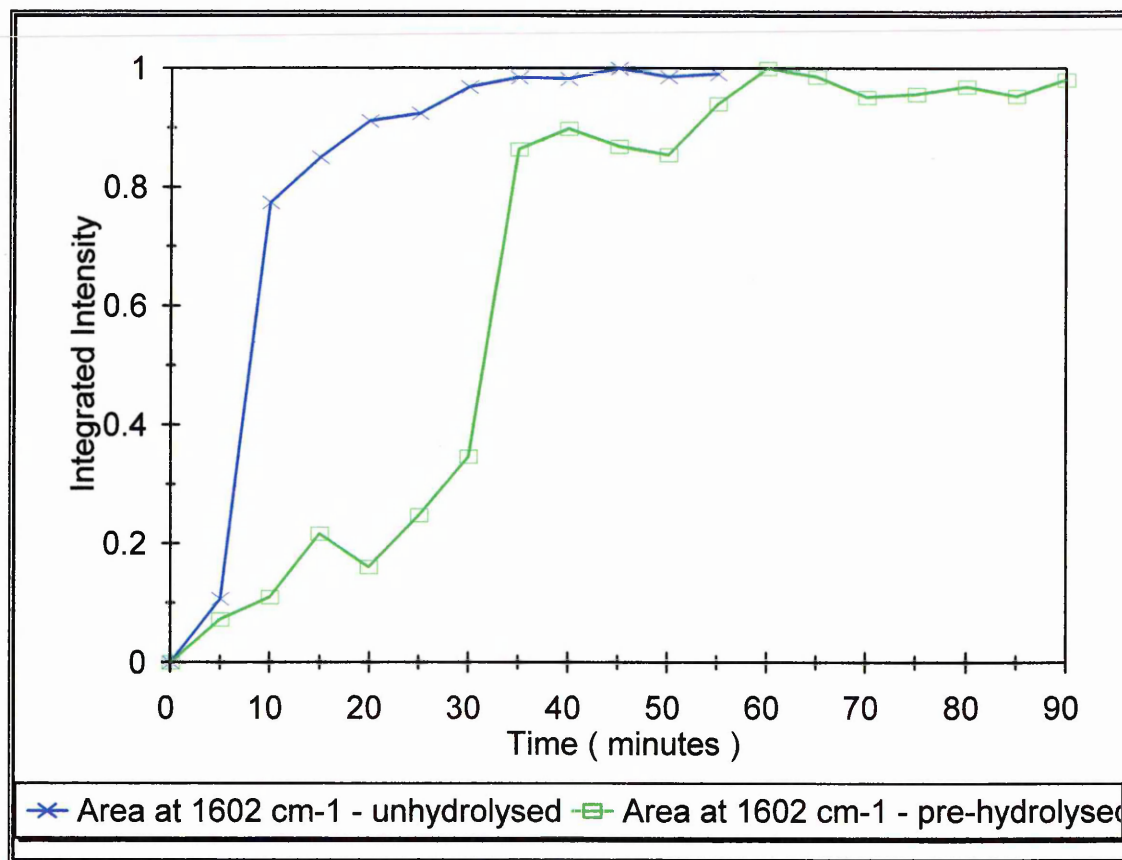


Figure 3.42 : The area of the 1602 cm⁻¹ band of hydrolysed and unhydrolysed Y9669 vs. time for diffusion in PVC at 70 °C

It is clearly shown by Figure 3.42 that Y9669 exposed to atmospheric water for 24 hours diffuses considerably slower than a fresh sample of Y9669. Therefore, it has been proven that hydrolysed Y9669 diffuses through unplasticised PVC at 70 °C more slowly than un-hydrolysed Y9669.

The hydrolysis of A1110 was studied in the same way; the material was sprayed onto a KBr plate, allowed to react with atmospheric humidity and analysed in the infrared spectrometer. The spectra in the Si-O stretching region are shown in Figure 3.43.

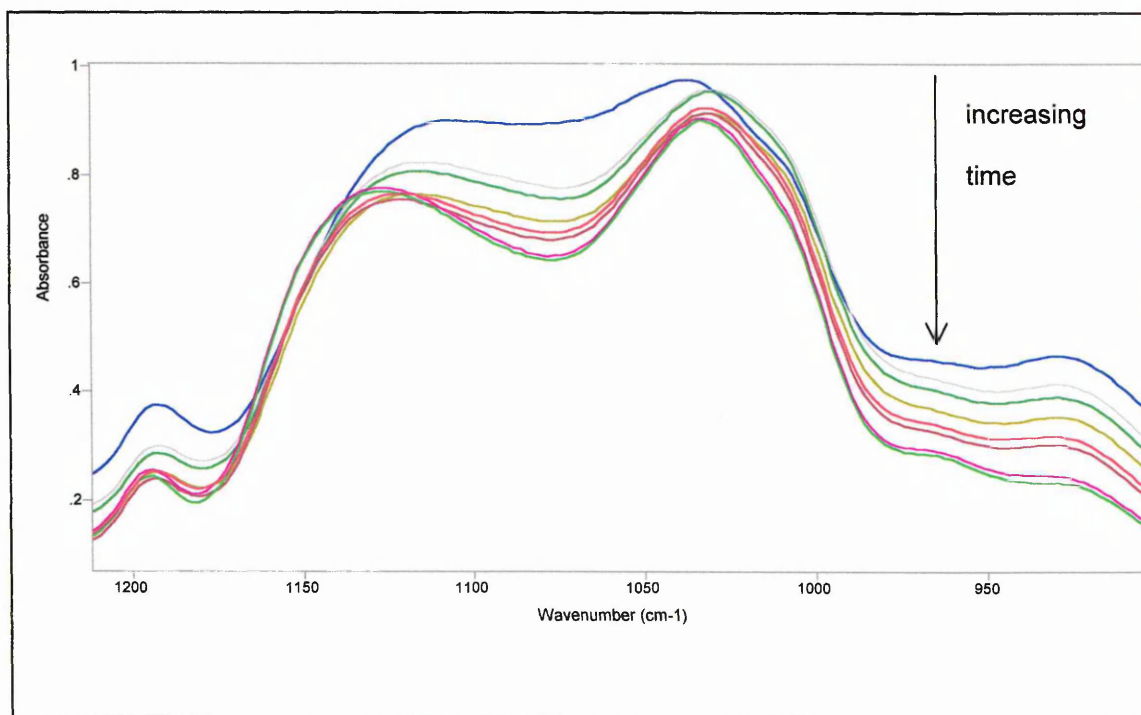


Figure 3.43 : The Si-O stretching region of spectra obtained in transmission of A1110 undergoing hydrolysis with atmospheric water

Figure 3.43 shows that the band at 930 cm^{-1} decreased in intensity with time of exposure to atmospheric water. Figure 3.43 also shows that the two Si-O-Si bands at 1037 and 1106 cm^{-1} broaden and move apart, with most change occurring before the second spectrum was taken (i.e. during the first 30 minutes). Ishida *et al.*³¹ found that in polyaminosiloxane undergoing a total cure, the two neighbouring bands at 1108 and 1045 cm^{-1} sharpened and moved apart slightly. Therefore this effect in Figure 3.43 is presumed to be due to condensation of the silane. The band at 930 cm^{-1} was curve fitted and the intensity is plotted in Figure 3.44 *versus* time of exposure.

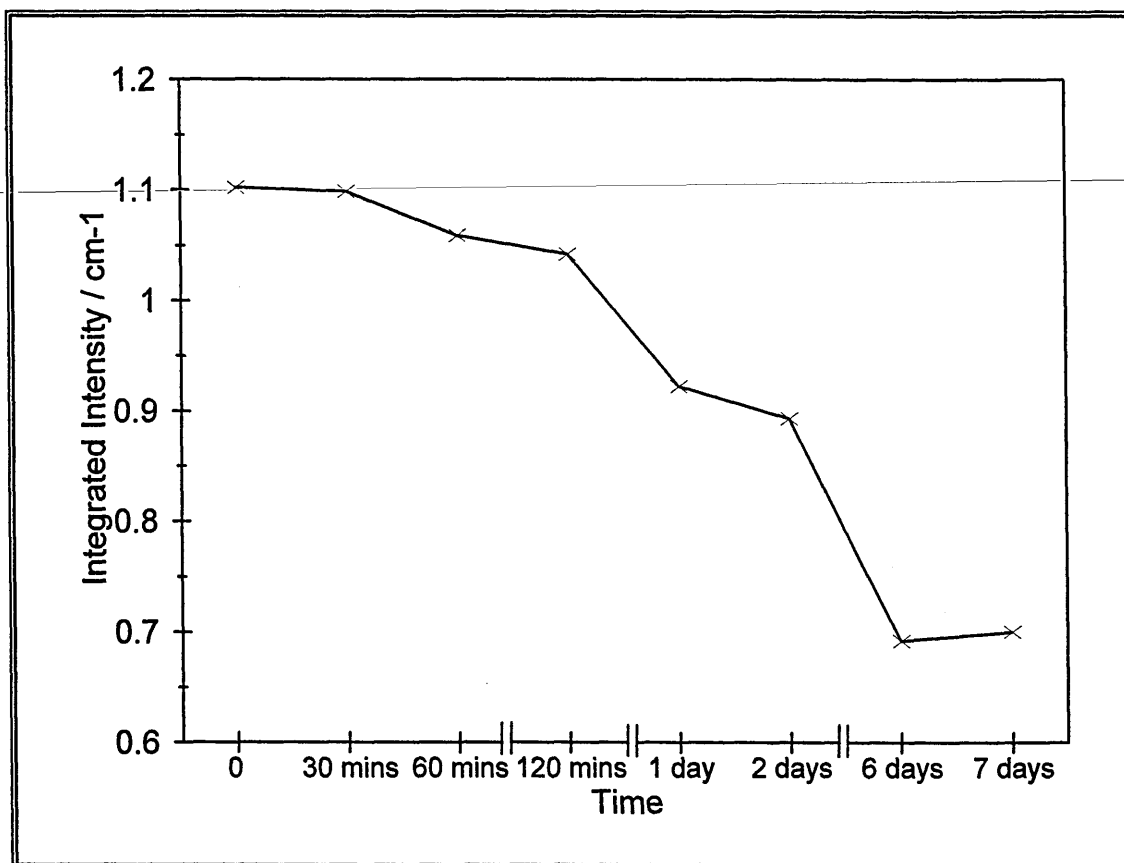


Figure 3.44 : The curve fitted intensity of the 930 cm⁻¹ band of A1110 undergoing hydrolysis with atmospheric water

Figure 3.44 shows that A1110 undergoes rapid hydrolysis over the first day of exposure, and then slower hydrolysis over the following week. Comparison of the amount by which the intensity of the Si-O-Me peaks decrease in intensity shows that Y9669 undergoes more hydrolysis over a week than A1110, but examination of the Si-O-Si stretching modes in the spectra suggests that A1110 undergoes more condensation. A diffusion experiment, equivalent to the Y9669 experiment described above was carried out using A1110 also. However, as with unhydrolysed A1110, no diffusion was observed for A1110 exposed to air for 24 hours. This is hardly surprising, as the spectra indicate that by

this stage the A1110 had undergone considerable condensation, making it less likely to show diffusion.

The same set of experiments were also carried out with A1891. However, it was noticed that the spectra decreased rapidly in intensity after the first spectrum was taken. This is shown in Figure 3.45, in which the first three spectra are shown. The absolute intensity of the 958 cm^{-1} band of the A1891 is plotted *versus* time in Figure 3.46.

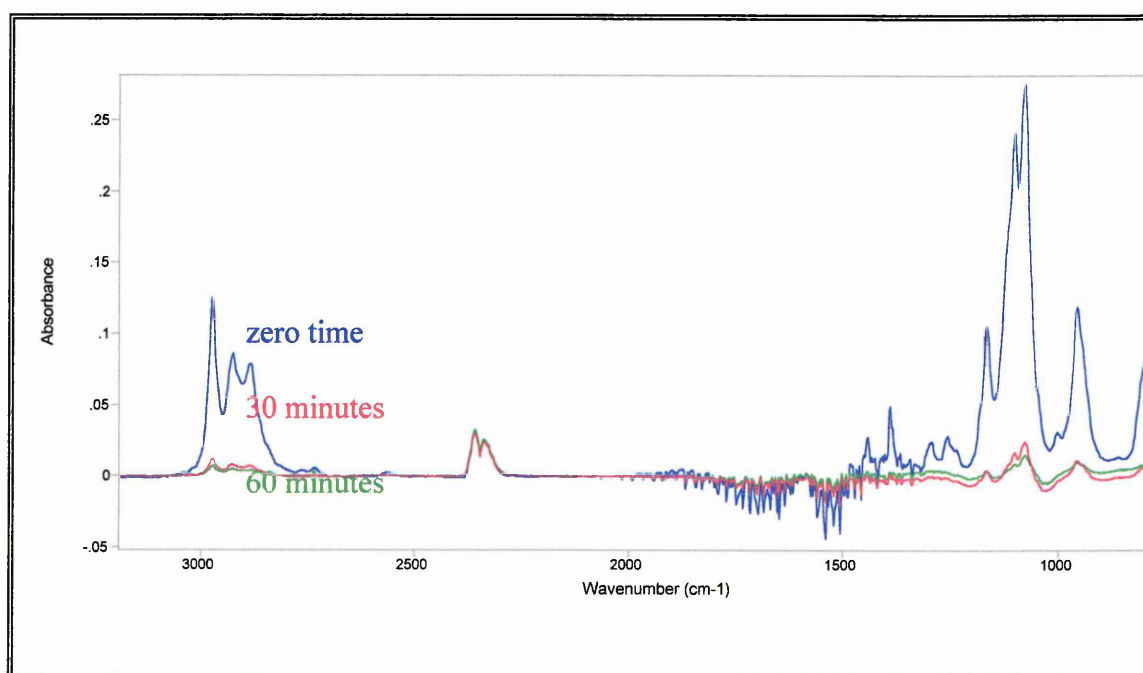


Figure 3.45 : The first 3 spectra of A1891 undergoing air hydrolysis

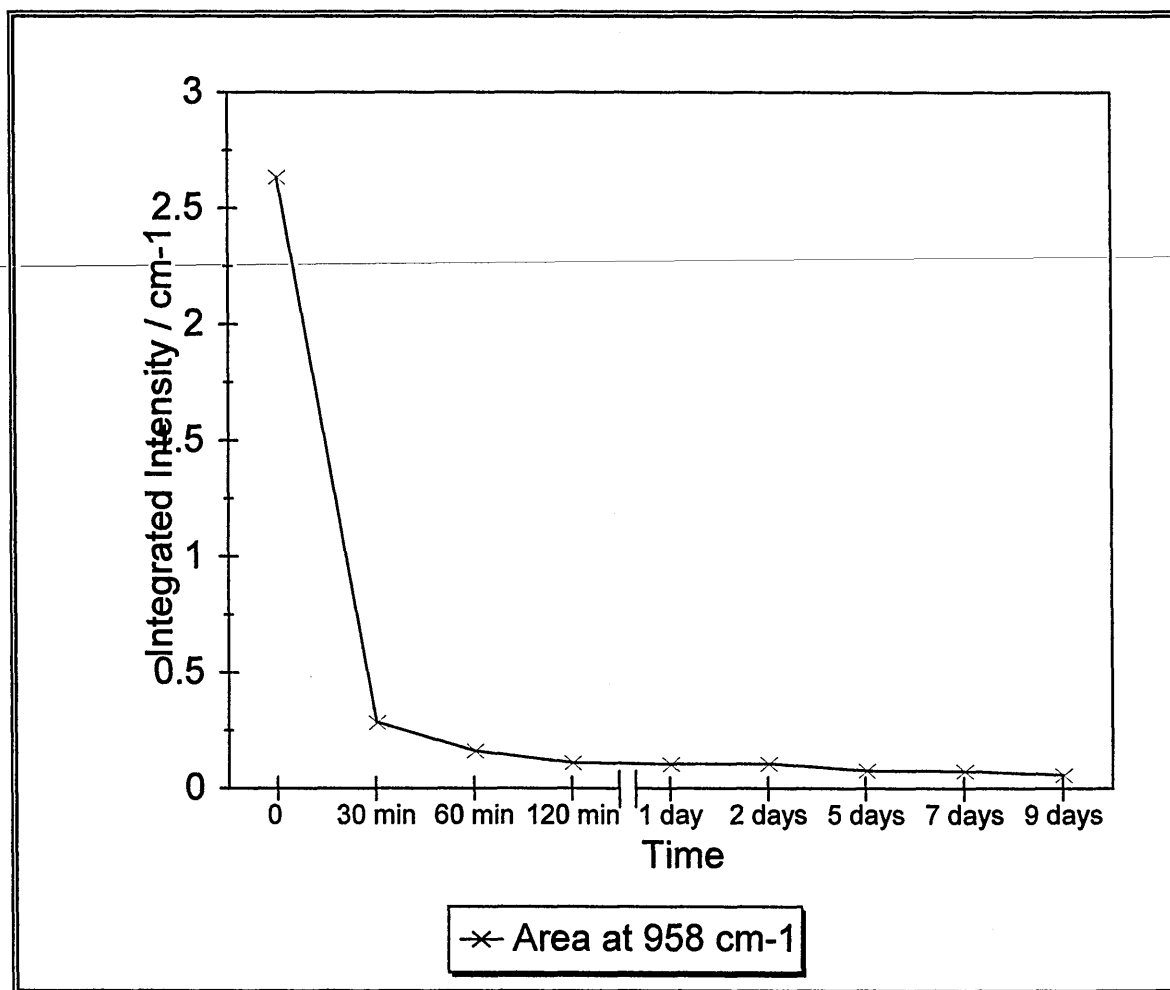


Figure 3.46 : The absolute intensity of the 958 cm⁻¹ band of A1891 undergoing air hydrolysis vs. time

Inspection of the sample showed that the A1891 film had run off the KBr plate. The experiment was repeated, keeping the time for which the sample was vertical (which is necessary to obtain the spectra) to a minimum, but the same effect occurred. It was not known why this effect was only seen with the A1891, but it may be that this silane was less viscous than the other two. To enable quantitative analysis of the hydrolysis, the integrated intensity of the 958 cm⁻¹ band of A1891 (assigned to Si-O-Et) stretching) was ratioed against the integrated intensity of the CH stretching region (i.e. 2780 to 3000 cm⁻¹). This region was chosen due to the lack of interference from water vapour or CO₂ bands, and the

high intensities seen. It was assumed that the intensities of these bands were totally insensitive to hydrolysis. The ratio of these two measurements is plotted versus time in Figure 3.47. For comparison, the absolute intensity of the 958 cm^{-1} band is plotted in Figure 3.46.

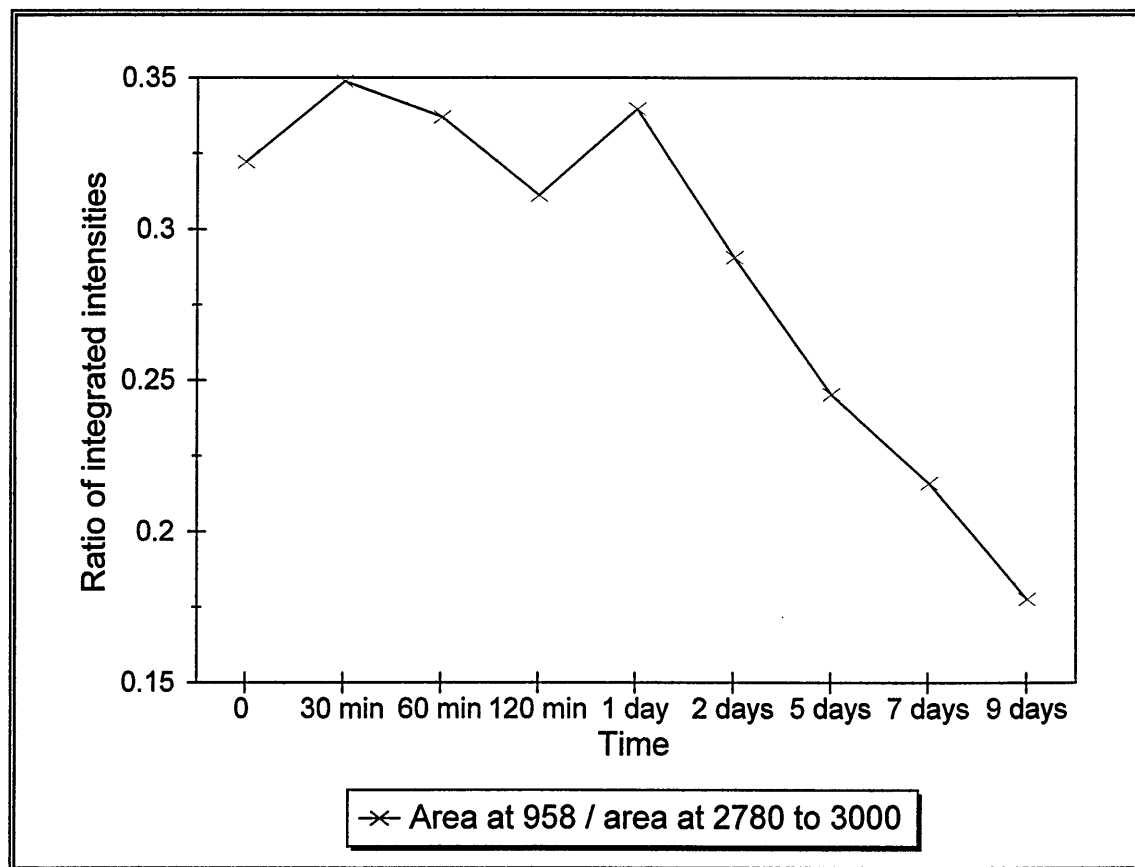


Figure 3.47 : The ratio of the integrated intensity of the 956 cm^{-1} band of A1891 undergoing hydrolysis with the integrated intensity in the C-H stretching region

Figure 3.47 shows that over the first 24 hours of exposure, little if any hydrolysis occurred. After this however, the hydrolysis occurred quite rapidly, and appeared to be still occurring after 9 days exposure. A diffusion experiment was also performed using A1891 that had been hydrolysed by exposure to air for 24 hours. The PVC film was $10\text{ }\mu\text{m}$. thick.

The results are plotted alongside those obtained for unhydrolysed A1891 in Figure 3.48.

Both sets of data have been intensity normalised.

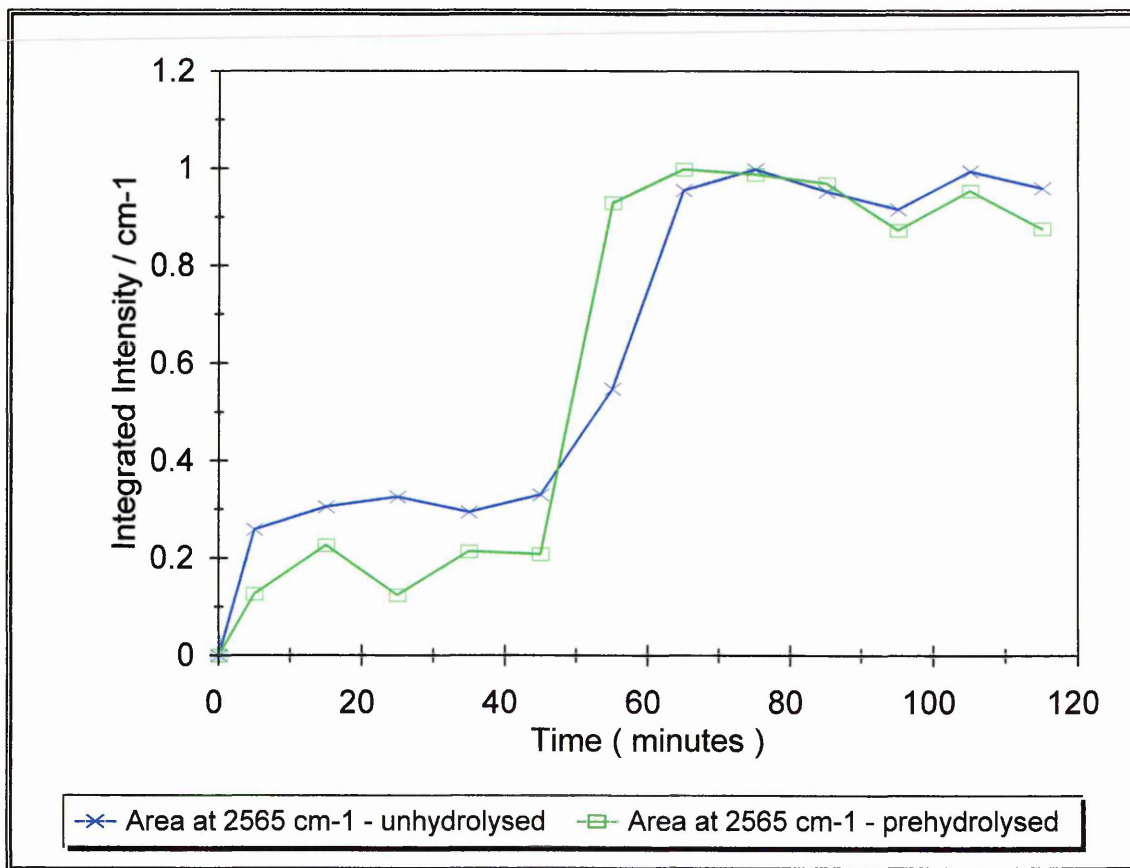


Figure 3.48 : The area of the $\nu(\text{SH})$ stretching band of hydrolysed and unhydrolysed A1891 vs. time fro diffusion in unplasticised PVC at 70 °C

Figure 3.48 shows that the diffusion of A1891 which had been exposed to air for 24 hours was very similar to that shown by unhydrolysed A1891. It appears that the diffusion may have been slightly slower in the case of the prehydrolysed silane, but the difference is very small compared to that observed in the case of Y9669, which had undergone much more hydrolysis in 24 hours of exposure to the atmospheric humidity. Overall, the results presented in this section strongly agree with the hypothesis that the hydrolysis of a silane slows the diffusion of the silane through unplasticised PVC films at 70 °C.

References

- 1 Hong, S. U., Barbari, T. A. and Sloan. J. M, Journal of Polymer Science part B - Polymer Physics, Vol. 36, No. 2, p. 337-(1998)
- 2 Sammon, C., Everall, N. and Yarwood, J., Macromolecular Symposia Vol. 119, p. 189 (1997)
- 3 Schlotter, N. E. and Furlan, P. Y., Vibrational Spectroscopy Vol. 3, p. 147 (1992)
- 4 Fieldson, G. T. and Barbari, T. A., Polymer Vol. 34, p. 1146 (1993)
- 5 Hair, M. L., Advances in Chemistry Series Vol. 234, p. 161 (1994)
- 6 Banga, R., PhD. thesis, Sheffield Hallam University (1995)
- 7 Blum, F. D., Meesiri, W., Kong, H.-S, and Gambogi, J. E., Journal of Adhesion Science and Technology Vol. 5, No. 6 (1991)
- 8 Morrall, S. W. and Leyden, S. E., in D.E. Leyden (Ed.), Proceedings of the Conference on Silanes, Surfaces. and Interfaces, Gordon and Breach (1985)
- 9 Hoh, K.-P., Ishida, H. and Koenig, J. L., Polymer Composites Vol. 9, No. 2 (1988)
- 10 Rogers, C. E. in Polymer Permeability, Ed. by Comyn, J., Chapman and Hall, London, p.56 (1985)
- 11 Sommer, W., in Plastics additives, Ed. by Gachter, R. and Muller, H., Hanser Publisher, Munich,(1985)
- 12 Beckmann, R. et. al., United States Patent No. 4,277,538 (1981)
- 13 Purvis, M. B. et. al., International Patent No. WO 95/19261 (1995)
- 14 Diffusion in Polymers, Ed. by Crank, J. and Park, G. S., Academic Press, London (1968)
- 15 Sammon, C., PhD. thesis, Sheffield Hallam University (1997)

- 16 Sammon, C., Everall, N. and Yarwood, J., *Macromolecular Symposia* Vol. 119, p. 189 (1997)
- 17 Pereira, M. R., PhD. thesis, University of Durham, (1994)
- 18 Vieth, W. R. and Sladek, K. J., *Journal of Colloid Science* Vol. 20, p. 1014 (1965)
- 19 Vieth, W. R. and Amini, M. A., in *permeability of Plastic Films and Coatings to Gases, Vapors and Liquids*, Ed. by Hopfenberg, H. B., Plenum Press, New York, p. 49 (1974)
- 20 Van Ooij, W. J., in *Industrial Adhesion Problems*, Ed. by Brewis, D. M., p. 89, Orbital Press, Oxford (1985)
- 21 Sommer, W., in *Plastics additives*, Ed. by Gachter, R. and Muller, H., p. 254, Hanser Publisher, Munich,(1985)
- 22 Hajatdoost, S., Olsthoorn, M. and Yarwood, J., *Applied Spectroscopy* Vol. 51, No. 12, p.1784 (1997)
- 23 Billmeyer, F. W., *Textbook of Polymer Science*, p. 321, 3rd. Edition, Wiley, New York (1984)
- 24 Plazek, D. J. and Ngai, K. L., in *Physical Properties of Polymers Handbook*, p. 139, Ed. By Mark, J. E., AIP Press, New York (1996)
- 25 Pezzin, G., Omacini, A. and Zilio-Grandi, F., *Chimica Industria (Milan)*, Vol. 50, p.309 (1968)
- 26 Yasuda, H. and Stannett, V., *Journal of Polymer Science Part B: Polymer Physics* Vol. 33, p. 2263 (1995)
- 27 Okuno, H., Renzeo, K. and Uragami, T., *Journal of Membrane Science* Vol. 103, p.31 (1995)

- 28 Shailaja, D. and Yaseen, M., Polymer International Vol. 32, p. 247 (1993)
- 29 Langevin, D., Grenet, J. and Saiter, J. M., European Polymer Journal Vol. 30, p.30 (1994)
-
- 30 McKnight, S. H. and Gillespie, J. W., Journal of Applied Polymer Science Vol. 64, part 10, p. 1971 (1997)
- 31 Ishida, H., Chiang, C.-H. and Koenig, J. L., Polymer Vol. 23, p. 251 (1982)

Chapter 4 : Raman depth profile studies of organosilane diffusion

In order to show that diffusion of organosilanes occurs in PVC films, and to determine the distribution of the silanes in the PVC films before, during and after diffusion, Raman depth profiling experiments have been carried out. As described in chapter 1, other workers have used different techniques to obtain depth - resolved information about silanes in polymeric films¹⁻⁴. However, the advantages of Raman confocal microscopy are that it can provide information on the micrometer scale⁵, and that depth profiles can be obtained *in situ*^{6,5}, allowing the collection of depth - resolved information without the need for sputtering of the sample, or sectioning.

4.1 : Experimental

In order to obtain information of relevance to the glass / silane / PVC system, it was decided to investigate a model laminate. The first material considered for use as a substrate for the laminates was polished quartz. It was found that the use of quartz gave rise to a broad curved background absorption. This meant not only that the peaks from the deposited materials were harder to see, especially those of low intensity, but also that removal of the curved baseline was required before analysis. A much better substrate was found to be polished silicon wafers. This material led to a flat baseline in the spectra collected. Silicon does have bands in the Raman, however, most notably a sharp band at 520 cm^{-1} assigned to the Si-Si stretching mode and its overtone band at 980 cm^{-1} . As these

bands did not interfere with any of the peaks of interest of the other materials, it was decided to use silicon as a substrate. An advantage of the presence of the bands due to silicon was that the 520 cm^{-1} band was found to be a very good indicator of the position of the surface of the silicon wafer. This helped to confirm that the depth profiles were calibrated correctly in the z - direction (i.e. the optical axis). The use of silicon as a substrate also meant that the resulting laminates were almost identical to those used in the infrared experiments, the only difference being that most of the laminates used in the Raman contained PVC films considerably thicker than those used in the infrared experiments(approximately $20\text{ }\mu\text{m}$. vs. $10\text{ }\mu\text{m}$. for the laminates used in the infrared experiments). Although silicon has a different structure to glass, the surface properties are very similar as the surface of oxidised silicon and glass both consist of SiO_2 and SiOH groups^{7,8}.

4.1.1 : Materials

Most of the materials used for the Raman experiments were exactly the same as described in section 3.1.1, but no plasticiser was incorporated into any of the PVC films. The silicon wafers were treated in the same way to clean them, but extra care was taken when diamond polishing, as the long experiment times and long heating treatments often led to increased silane bonding to the silicon surfaces. When cover slips were used they were very thin ($<100\text{ }\mu\text{m}$.) glass slides provided by Pilkington plc. These were available in a variety of thicknesses in the range 20 to $100\text{ }\mu\text{m}$. The $20\text{ }\mu\text{m}$. slides were extremely

fragile, but it was found that the thinner slides scattered less light, resulting in less signal loss when used. Therefore, 20 μm . cover slips were used for the depth profiling experiments described here.

4.1.2 : Spectroscopic measurements

All Raman spectroscopic measurements were made with a Renishaw Ramascope model 2000. The excitation source was a Helium-Neon (HeNe) gas laser emitting at 632.8 nm. This system is described in section 2.2.4. Only the grating optical path was used. The system can be operated in 'static' grating mode, giving a range of approximately 500 cm^{-1} , or in 'extended' mode, by rotating the grating as scanning progresses, which allows a range of approximately 250 cm^{-1} to 5000 cm^{-1} . The static mode is not only somewhat more accurate, but spectral acquisition is considerably faster if only a limited spectral range is of interest. When measuring depth profiles, it was found that measurement of one band of the silane was adequate, so it was decided to use the static grating mode. To obtain reference spectra, the extended mode was used in the range 400 to 4000 cm^{-1} . To obtain depth profiles, the instrument was fitted with an electronic microscope stage attachment from Prior Instruments Inc., allowing movement in x, y and z planes with 1 μm . accuracy.

When measuring depth profiles, it was necessary to know the confocal response of the instrument accurately; that is, how effectively the instrument rejected light from outside of the focal plane, and hence what the depth resolution was. It was considered desirable to

have 2 μm . or less confocality as measured by the FWHH criterion described in section 2.2.5. In order to ensure that this was the case, the 100X objective was used and the instrument set up in confocal mode by setting the entrance slit to 15 μm . width, and using only a 5 pixel height response on the CCD. Before each experiment a confocal test was carried out. This involved measuring the response from a silicon surface as the focus of the laser was moved away in 1 μm . steps, as described in section 2.2.5. For solid samples, reference spectra were obtained using the 50X objective. For liquid samples, the materials were placed in a quartz cuvette and the 20X ULWD objective was used.

4.1.3 : Spectra of materials

The Raman spectrum of the pure silanes are shown in shown in Figure 4.1 (Y9669), Figure 4.2, (A1110) and Figure 4.3 (A1891). The spectra were obtained from pure liquid silanes in a quartz cuvette. The silanes were handled in a nitrogen atmosphere to ensure that it remained un-hydrolysed. The 20X ULWD objective was used.

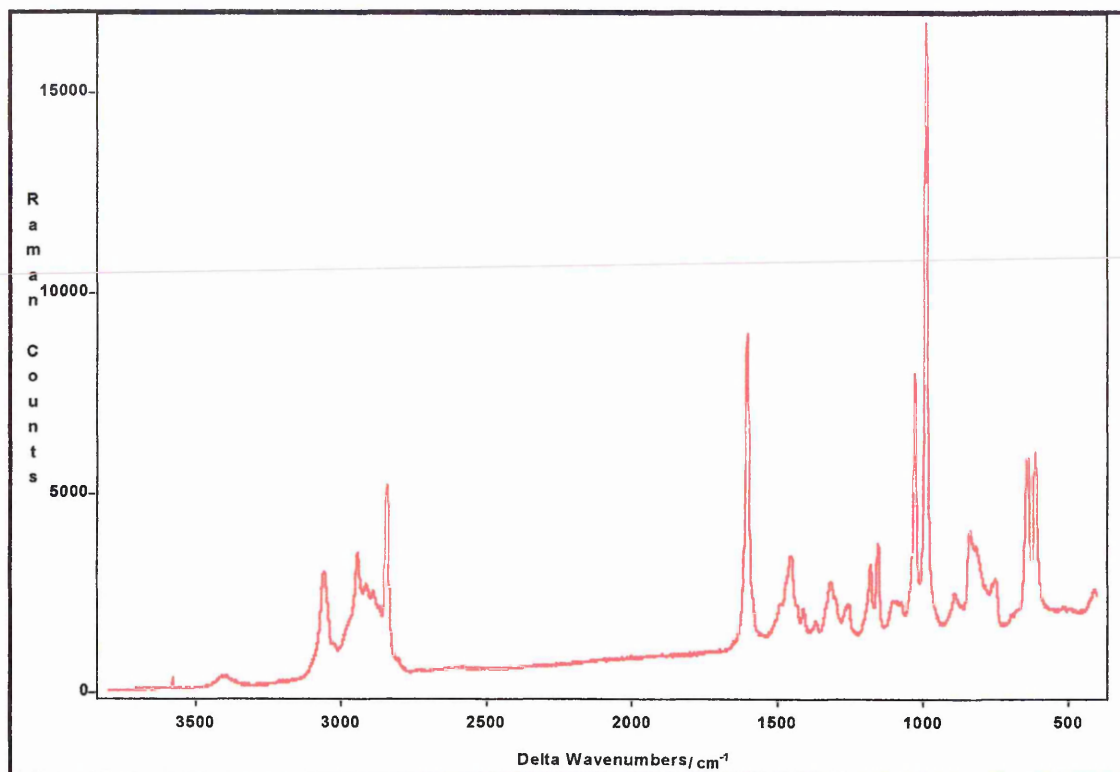


Figure 4.1 : The Raman spectrum of pure Y9669 (unhydrolysed)

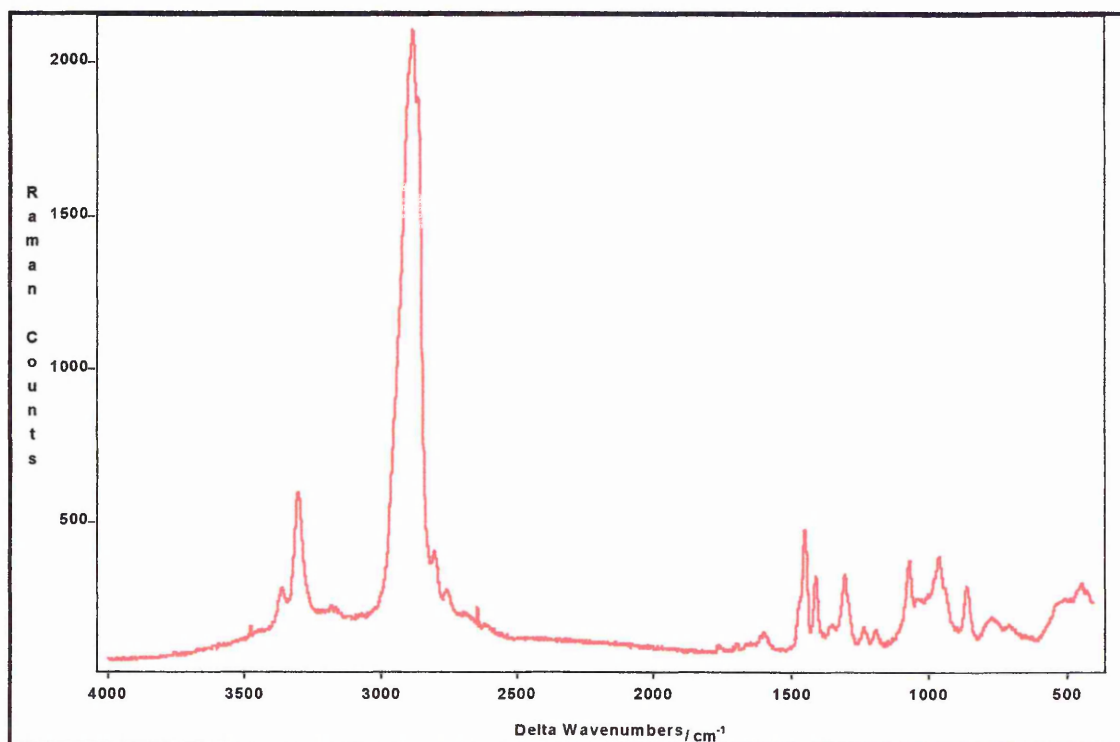


Figure 4.2 : The Raman spectrum of pure A1110 (unhydrolysed)

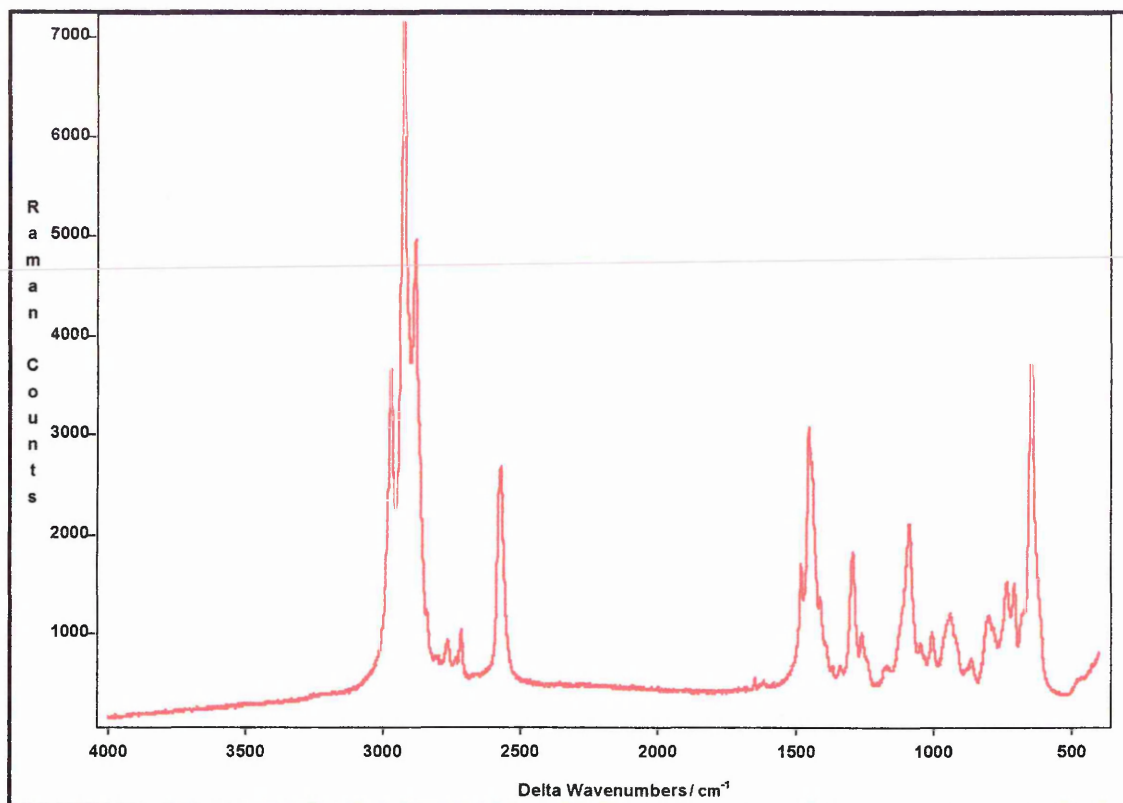


Figure 4.3 : The Raman spectrum of pure A1891 (unhydrolysed)

The same bands were used in the Raman depth profiling work as in the infrared diffusion work. It can be seen from comparison of Figure 4.3 with Figure 3.5 that the $\nu(\text{SH})$ stretching band is much more intense in the Raman than in the infrared. Again, it was not possible to assign the band at approximately 1600 cm^{-1} in the Y9669 spectrum to a single vibration, rather it is the sum of the $\nu(\text{C-C})$ ring stretching and $\delta(\text{NH})$ banding bands. It is therefore referred to simply as the 1600 cm^{-1} band.

Figure 4.4 shows the Raman spectrum of pure PVC powder. For comparison, Figure 4.5 shows the Raman spectrum of degraded PVC, obtained by heating the same PVC at $100 \text{ }^\circ\text{C}$ for 4 hours. It can clearly be seen that the spectra are very different.

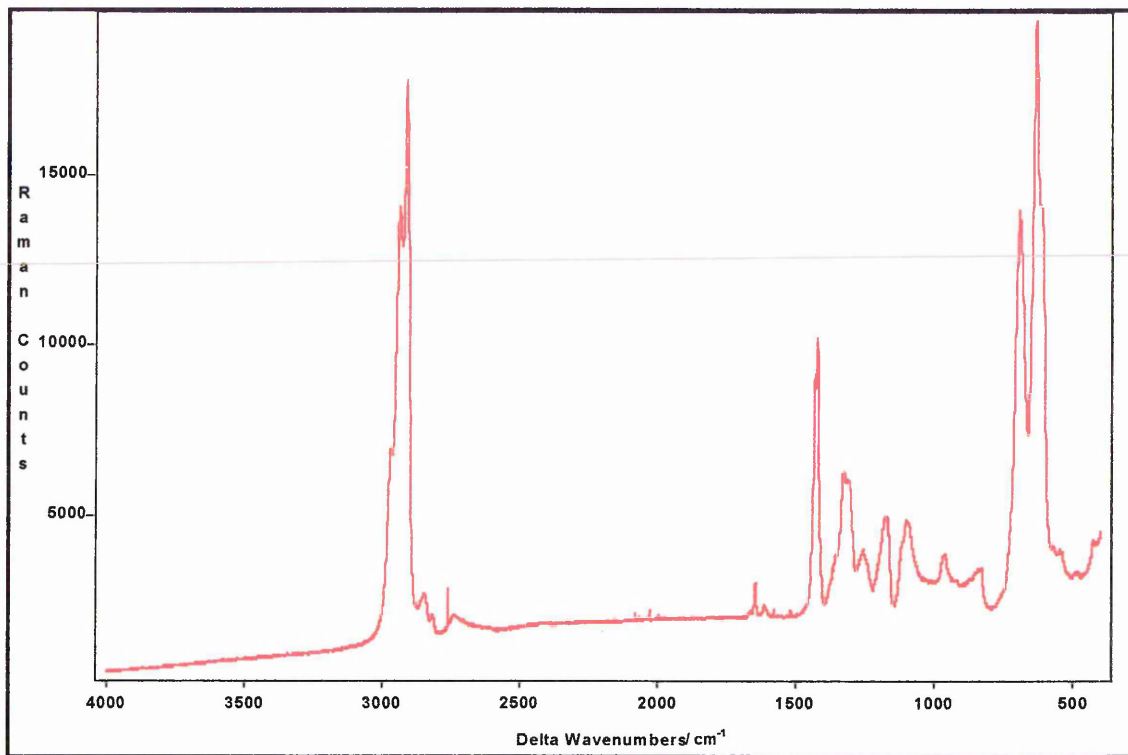


Figure 4.4 : The Raman spectrum of PVC obtained from pure PVC powder

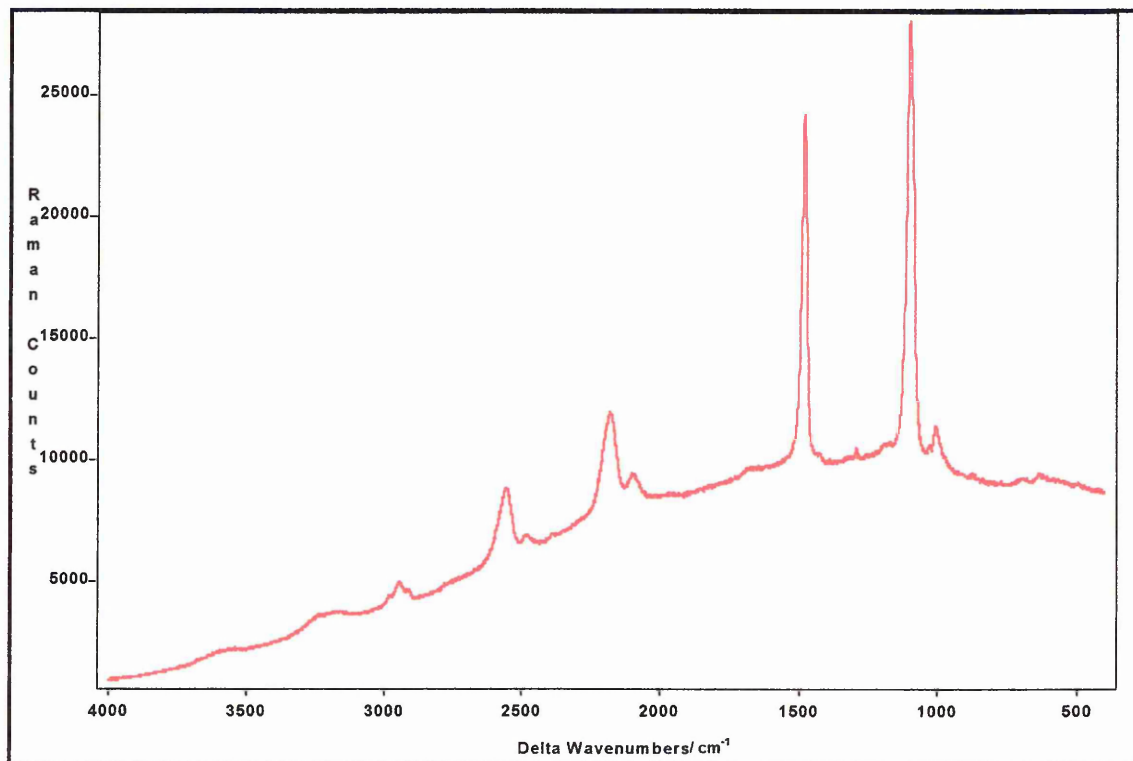


Figure 4.5 : The resonance Raman spectrum of degraded PVC film

When PVC is thermally degraded, the main reaction is homolytic loss of HCl resulting in polyene sequences along the polymer backbone. This is shown in Figure 4.6.

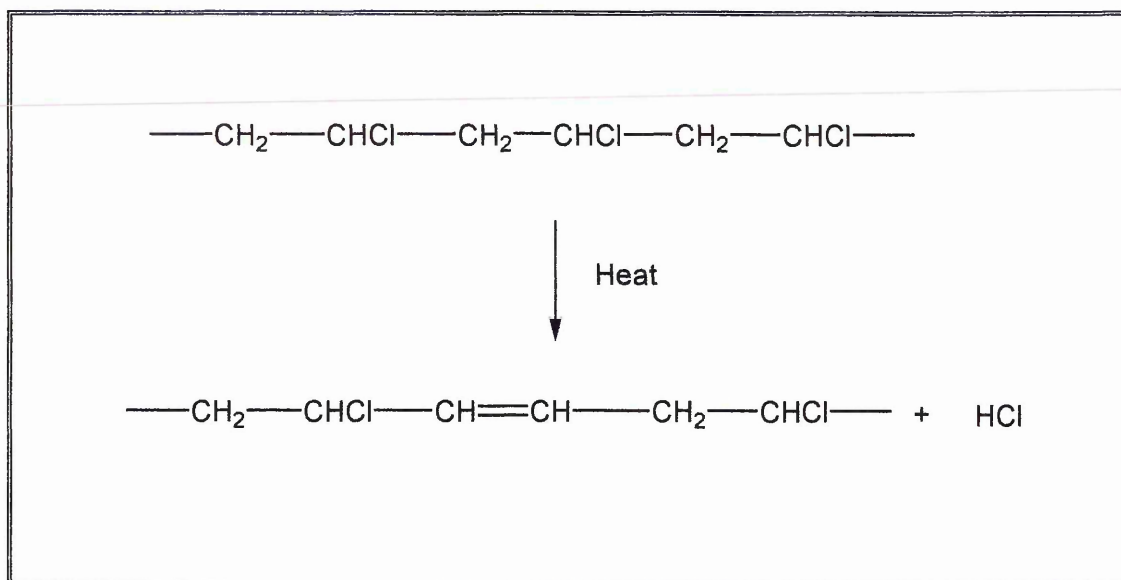


Figure 4.6 : The thermal degradation of PVC

The bands at 2560 cm^{-1} , 2186 cm^{-1} and the very intense bands at 1485 cm^{-1} and 1098 cm^{-1} in Figure 4.5 are resonance Raman bands, arising from the excitation wavelength coinciding with visible absorption wavelength of the polyene sequences in the degraded PVC. As these bands are extremely intense, they provide a very sensitive way of checking for degradation^{9,10}. Figure 4.7 shows the Raman spectrum of a PVC film cast from DMF and dried for 14 hours at 65°C . The spectrum can be seen to be essentially identical to Figure 4.4. The differences present are the bands at 520 cm^{-1} and 980 cm^{-1} from the silicon substrate. None of the resonance bands from degraded PVC are present. This proves that the as-cast films were not degraded by the drying process. Since the same procedure was used to prepare films for the infrared experiments, the films used for the infrared

experiments were also free of degradation. The film also shows that the solvent DMF had been completely removed as no carbonyl stretching band is present at 1675 cm^{-1} .

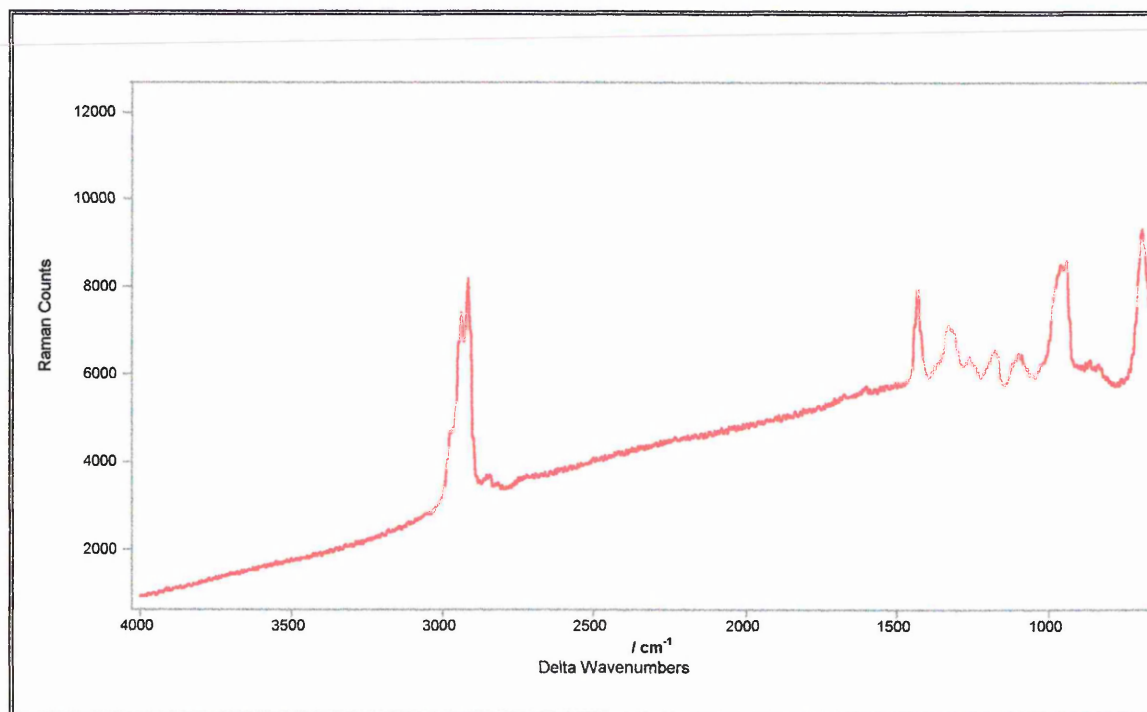


Figure 4.7 : The Raman spectrum of an as-cast PVC film on a silicon substrate

4.2 : Silane underlayer experiments

In the first experiments, silane was cast directly onto the silicon substrate. The silanes were pre hydrolysed in a 9:1 (v/v) IPA / H₂O solution, which was acidified with 3% (v/v) acetic acid to act as a hydrolysis catalyst. The silane film was heated to remove the solvent, and then PVC was cast onto the silane layer, and dried to remove solvent. In the first experiment, the laminate was then immediately examined to assess whether silane diffusion through the PVC film had occurred during the casting or drying process. The

silane used was Y9669 and the laminate was determined by Talysurf surface profiling to be approximately 50 μm . thick. In order to measure the depth profile, the laser was focused 10 μm . below the surface of the substrate, and the stage programmed to move 50 μm . up, in steps of 1 μm . A static spectrum centred at 1600 cm^{-1} was measured at each step.

A typical spectrum (from a depth of 5 μm . into the laminate) is shown in Figure 4.8.

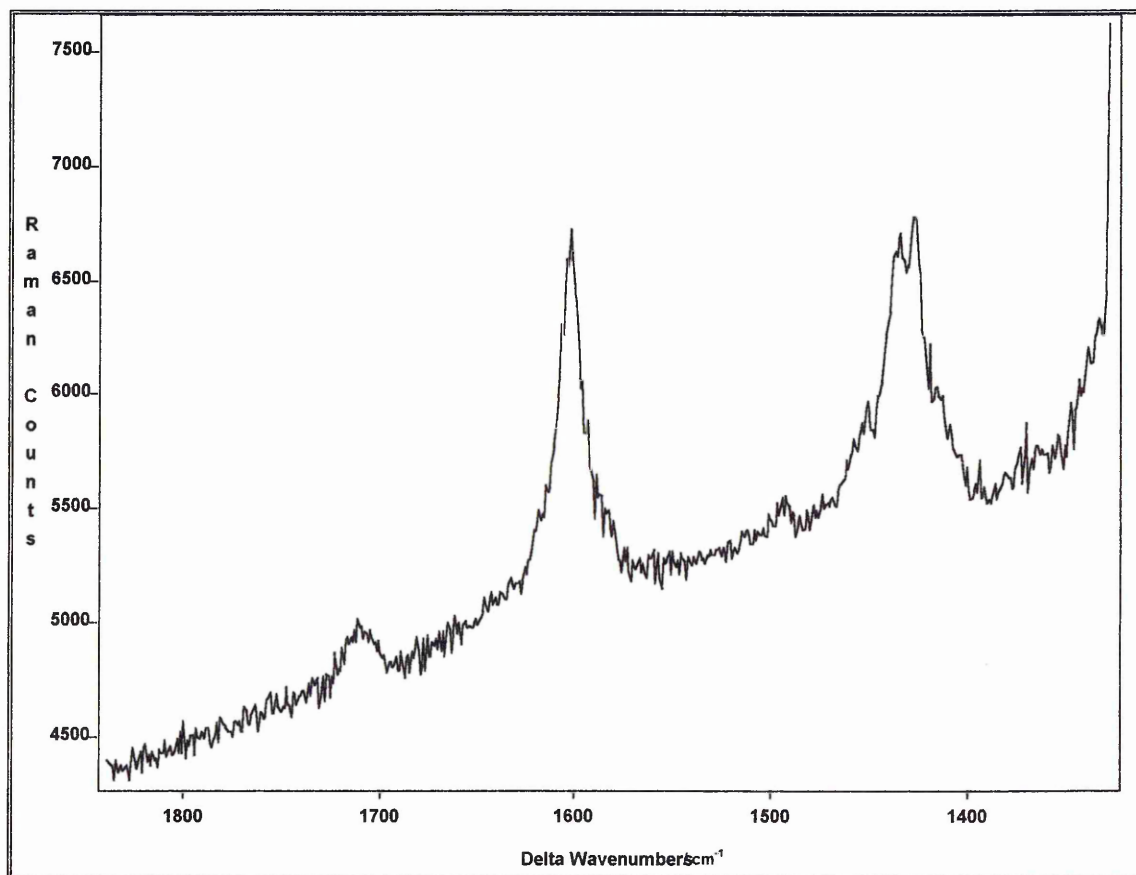


Figure 4.8 : The Raman spectrum from the first depth profiling experiment. Spectrum was taken 10 μm . above the substrate surface

Figure 4.8 shows the presence of both PVC (by the doublet at about 1430 cm^{-1}) and Y9669 (by the $\delta(\text{NH}_2)$ bending band at 1600 cm^{-1}). There is also a small peak at 1709 cm^{-1} . It is believed that this is the carbonyl stretching band of the solvent, DMF. Clearly, in this case, solvent removal was not completely effective. It was believed that this was due to the thickness of the film used. Therefore, in subsequent experiments, thinner PVC films were used.

In order to show the depth profiles graphically, the data were analysed by curve fitting. Simple Lorentzian bands were fitted to the data to obtain the area of the silane and PVC bands. The area of the bands have been plotted *versus* the distance the focus of the laser had moved in Figure 4.9. The bands displayed are the 1600 cm^{-1} band of Y9669 and the $\delta(\text{CH}_2)$ doublet of PVC.

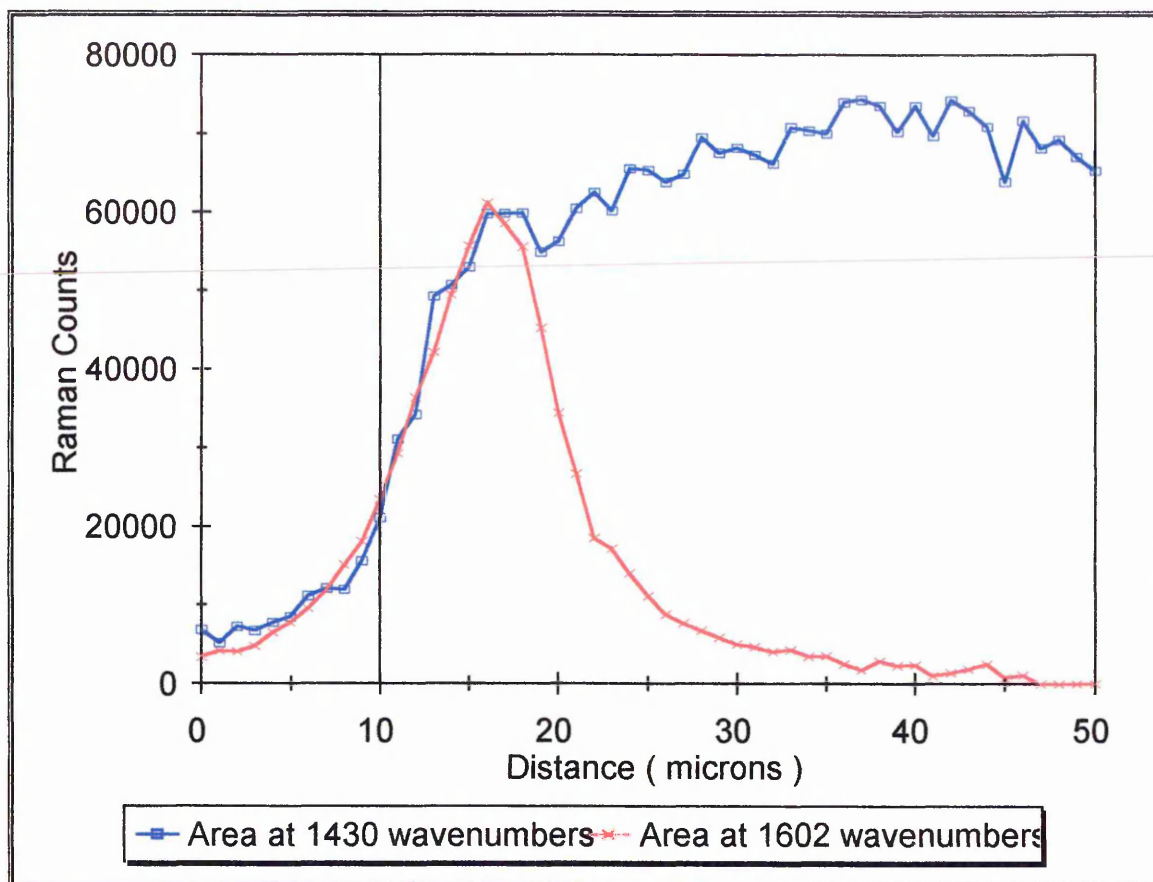


Figure 4.9 : Depth profile of a laminate consisting of silicon, hydrolysed Y9669 and PVC. The dashed line shows the position of the silicon interface

Figure 4.8 clearly shows that most of the Y9669 remained at the interface with the silicon wafer. Although some intensity of the Y9669 band was detected as far away as 30 μm . from the interface, it is thought that this was due to the confocal profile of the experiment, rather than due to a small amount of diffusion.

This experiment was repeated several times with thinner films so that the entire laminate could be depth - profiled. However, the same result was found each time : the Y9669 stayed near the silicon interface, and did not appear to have diffused significantly into the PVC film. Therefore, it was decided to anneal the laminate, to see if diffusion of

the silane could be thermally induced. A typical spectrum is shown in Figure 4.10. It can be seen from Figure 4.10 that there is no carbonyl stretching band at 1735 cm^{-1} . This shows that the use of a thinner PVC film allowed full removal of the solvent, DMF.

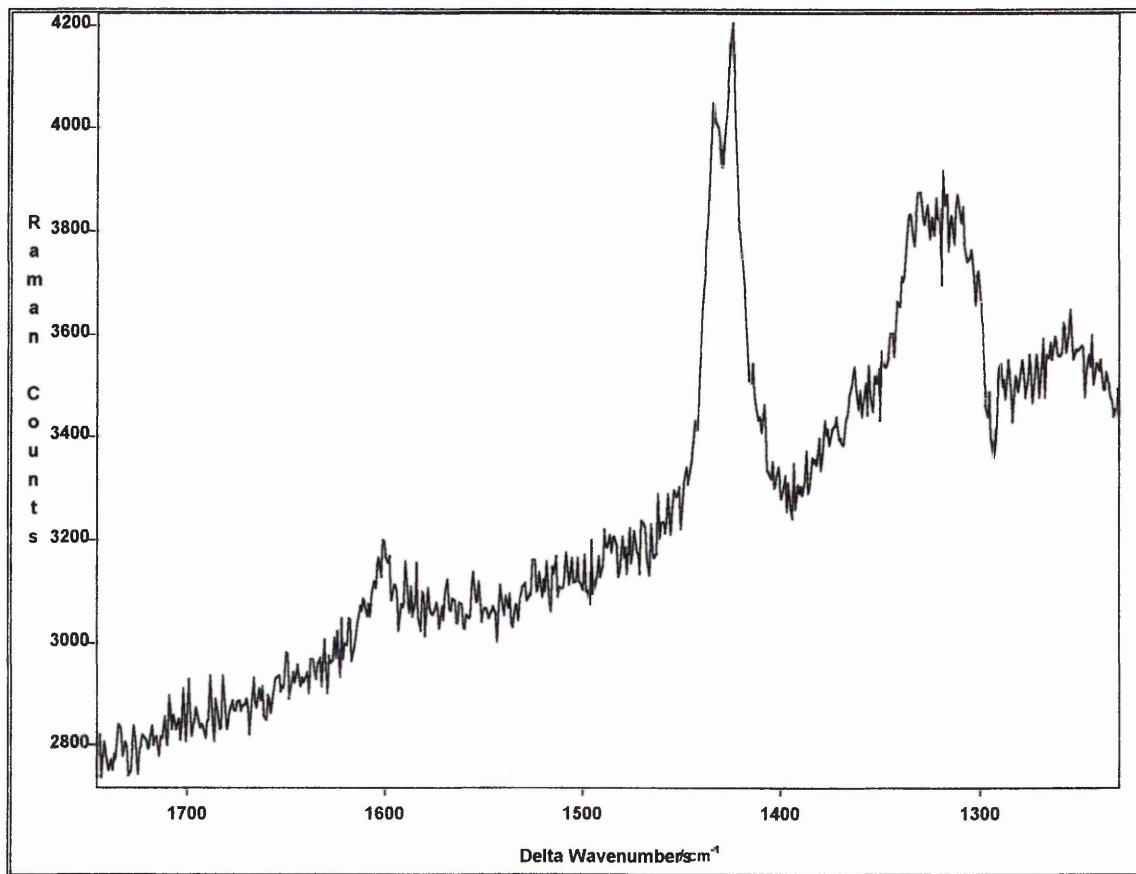


Figure 4.10 : Raman spectrum from multiple - anneal depth profiling experiment.

Before any annealing was carried out, a depth profile was obtained to measure the starting position of the silane. The laminate was then annealed by placing in an oven at 70°C for successive periods of 2.5 hours, 3.5 hours and 4 hours. A depth profile was obtained after each treatment. Thus, the total annealing time was 10 hours at 70°C . The curve-fitted band areas of the Y9669 1600 cm^{-1} band are shown in Figure 4.11. The laminate was determined to be $15\text{ }\mu\text{m}$. thick by Talysurf profiling.

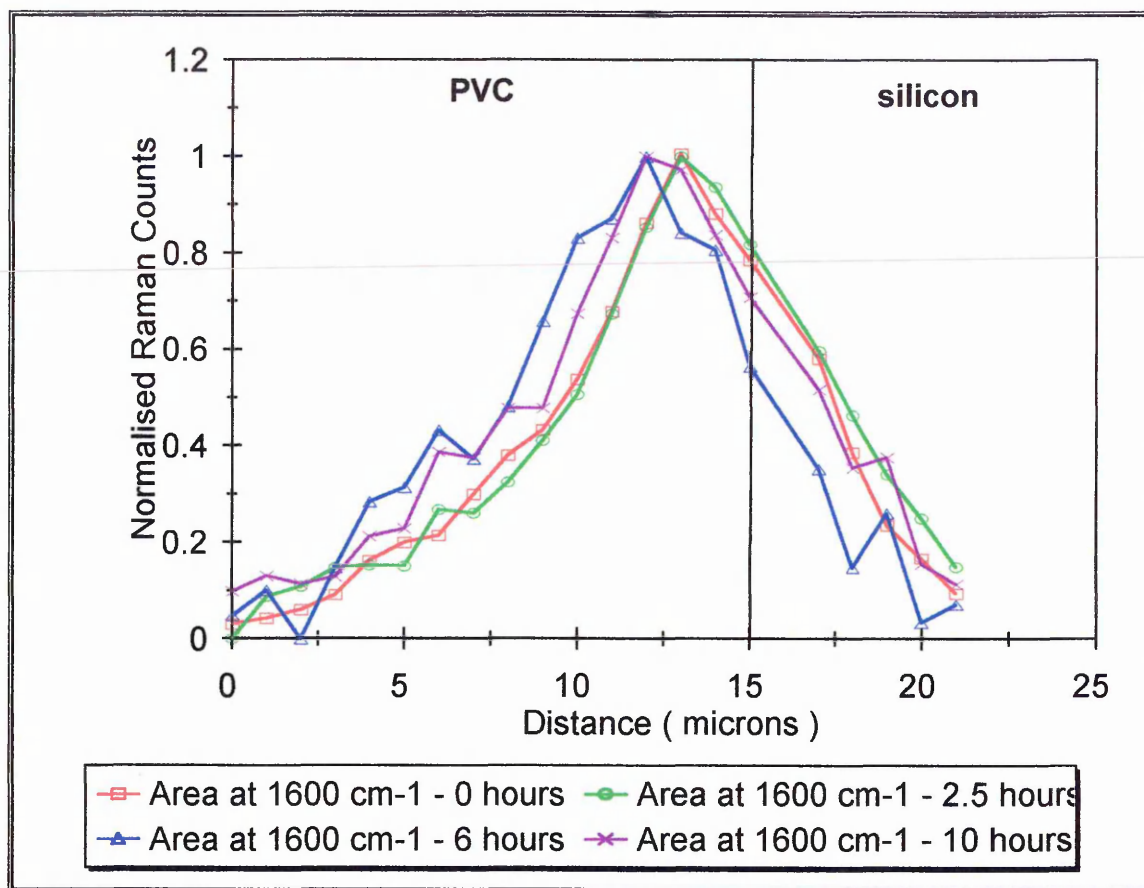


Figure 4.11 : The area of the 1600 cm⁻¹ band of Y9669 plotted *versus* distance for depth profiles of a silicon / Y9669 / PVC laminate. Times refer to annealing time at 70°C. The vertical line shows the position of the silicon interface.

It can be seen from Figure 4.11 that the Y9669 did not diffuse significantly into the PVC upon annealing at 70 °C. Close examination shows that the depth profiles after 2.5 hours annealing appear to be shifted about 1 μm. into the PVC. However, the measured depth resolution of the experiment was 2 μm. Therefore, the shift in the Y9669 intensity position was not significantly large enough to show diffusion.

4.3 : Silane overlayer experiments

The experiments using silane underlayers showed no significant diffusion of the silane into the PVC film. However, in those experiments the silane had been pre-hydrolysed, cast from solution and dried to remove solvent. This treatment is likely to have resulted in a condensed siloxane film^{4,11-13}. Therefore, it was decided to attempt to assess the distribution of unhydrolysed silane in PVC films. It was decided to use the silane overlayer configuration, as this would allow controlled formation of the PVC film, followed by application of the silane, which could then be monitored in its diffusion through the PVC film. Unfortunately, there is a practical problem with this experiment. The working distance of the 100X objective, which is necessary for confocal analysis is only 1.3 mm. This makes it difficult to use this objective to study a wet laminate without risking contamination of the objective with liquid. As the silanes studied are well known to have a strong affinity for glass surfaces¹⁴⁻¹⁶, it was considered that risking contamination of the objective in this way was to be avoided.

In the first experiment carried out in the silane overlayer configuration, the PVC film was cast from DMF and dried at 65°C for 14 hours. The Y9669 was then brushed onto the surface. In order to avoid any liquid silane remaining on the surface of the PVC film, the laminate was heated to induce diffusion. The PVC film with the silane layer on top was placed in the oven at 70 °C for 5 hours. A depth profile was then obtained at room temperature. The spectra showed no sign of the presence of DMF. The area of 1600 cm⁻¹ bending band of Y9669 is plotted *versus* time in Figure 4.12.

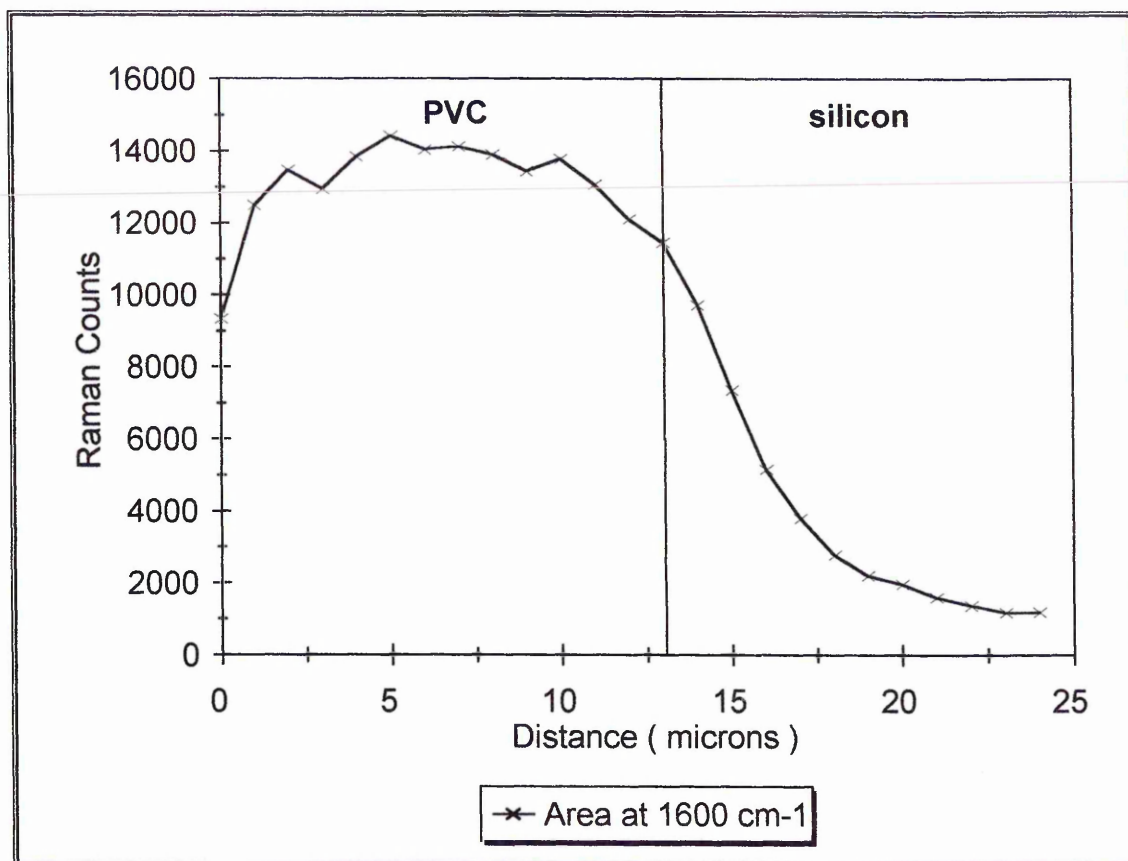


Figure 4.12 : The area of the 1600 cm^{-1} band of Y9669 versus distance for Y9669 brushed onto PVC and heated at 70°C for 5 hours

It can be seen that, unlike the case of the silane underlayer experiments, diffusion through the PVC film did occur in the first silane overlayer experiment. The Y9669 appears to be present throughout the thickness of the $15\ \mu\text{m}$. PVC film. At first glance, it appears that most silane is concentrated in the 5 to 10 μm . deep region, with less at the interfaces. However, it must be remembered that the depth profile is not a true concentration profile. Rather, it is the convolution of a concentration profile with the confocal response of the instrument, i.e. the confocal curve shown in figure 2.13. Because the confocal response is symmetrical, intensity at a point inside the film is contributed from

the focal plane and both above and below the focal plane, but at either the top or bottom interfaces, intensity is only contributed from out of the focal plane in one direction. Therefore the effect of the convolution will be to cause lower intensities at the interfaces, and higher intensities in the centre of the film, as well as to decrease the resolution of the experiment.

The main problem with experiment performed above was the possible contamination of the microscope objective with the silane. This meant that the depth profiles could only be measured after diffusion had occurred. It was decided to investigate the use of a protective cover slip. This would eliminate the possibility of contamination of the objective, as well as allowing the collection of depth profiles as soon as silane had been applied. Unfortunately, it was found that any glass cover slip significantly scattered light, leading to a loss of signal intensity, and hence to lower S / N. As can be seen from Figure 4.8 and Figure 4.10, the signal to noise was already quite low, due to the use of the confocal configuration. However, the very thin (20 μm .) cover slips provided by Pilkington plc. were found to reduce the signal loss considerably.

In the first experiment carried out in this way, a 21 μm . PVC film was cast on the silicon substrate. After solvent removal, Y9669 was brushed on the upper surface of the PVC film, then a 20 μm . cover slip placed over the silane. A depth profile was then obtained of the resulting laminate by focusing the laser 3 μm . above the PVC film, and obtaining 30 spectra at 1 μm . intervals into the PVC film. After this measurement, the laminate was placed in the oven at 70 °C for 1 hour. Another depth profile was then

obtained, in the same way as the first (at room temperature). After this measurement, the laminate was again placed in the oven for a further hour, and then another depth profile obtained, again in the same way. The resulting depth profiles are shown in Figure 4.13.

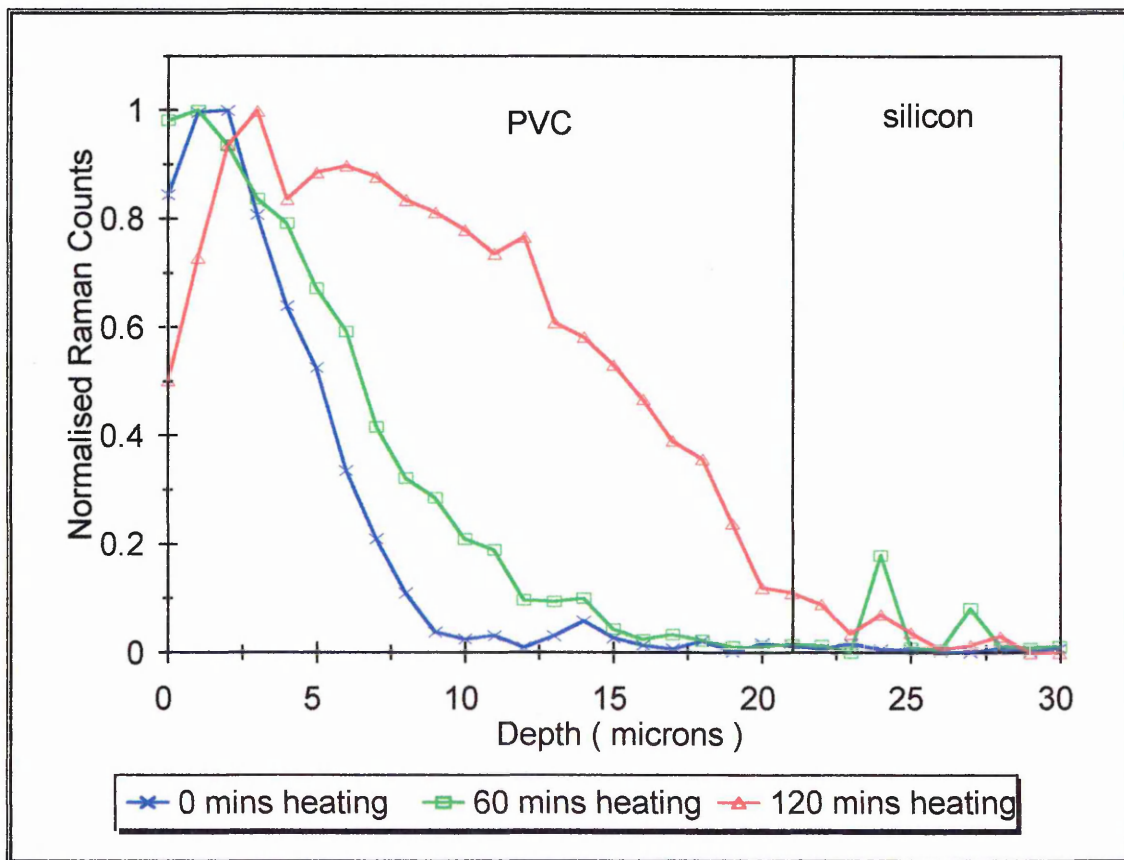


Figure 4.13 : The area of the 1600 cm^{-1} band of Y9669 vs. distance into a PVC film. The times refer to time spent at 70°C . The vertical line shows the position of the silicon interface.

Figure 4.13 shows that the Y9669 stayed mostly at the upper surface of the before heating. After heating for an hour, the Y9669 was mostly still at the upper surface, but more of the silane had diffused into the PVC. After 2 hours heating, the Y9669 has diffused considerably more through the PVC film. It appeared that even after 2 hours heating at 70°C , the Y9669 had not fully diffused through the film to the silicon interface.

This is somewhat surprising compared to the infrared results (see section 3. 2) which show that Y9669 had reached equilibrium in a 10 μm . PVC film after a cumulative heating time of 30 minutes. However, despite the fact that the laminates were quite similar, they were treated quite differently. The different heating regimes used in the different experiments may explain why the diffusion behaviour seemed quite different. As was discussed in chapter 3, the hydrolysis of the silane was found to considerably affect the diffusion characteristics. The treatment of the laminates in the oven for an hour may have accelerated the hydrolysis as compared to the 5 minute treatments used in the infrared experiments¹⁷. However, upon comparing the results obtained when using pre-hydrolysed Y9669 (i.e. Figure 4.11 in the last section) with those obtained using un-hydrolysed Y9669 (i.e. Figure 4.13 in this section), it can clearly be seen that the un-hydrolysed, un-condensed material diffused much further, even with less heating.

In order to assess the effect of silane chemistry on the distribution in PVC films, it was decided to perform a set of experiments using all three silanes, under the same conditions. In order that the results could be compared to those from the infrared experiments which had also been carried out for all three silanes, it was decided to use similar conditions. Unfortunately, it was not possible to make measurements in exactly the same way as the infrared measurements (i.e. a measurement after 5 minutes at 70 °C, then another 5 minutes treatment, and so on), as the depth profiles took at least 300 minutes to collect each. The time scale chosen was one depth profile before any heating, followed by 15 minutes heating, followed by another depth profile, followed by a further 45 minutes heating, and then a final depth profile. According to the infrared results, these

measurements should show no diffusion, intermediate diffusion, and equilibrium distribution respectively (at least in the case of Y9669 and A1891, see chapter 3). It is important to note, however, the spatial differences in the ATR-FTIR and Raman depth profiles experiments : The ATR - FTIR yielded information only from the few μm . near the silicon interface, whereas the depth profiles contained information from throughout the laminate, although the spatial and temporal resolution was lower.

The first experiment carried out in this way used Y9669 as the silane. The PVC film was 25 μm . thick, and contained no DMF. In the previous experiment it was noted that the depth profile did not cover a great enough distance to measure all of the Raman intensity from the silane. Therefore a longer profile was measured. The results are shown in Figure 4.14.

Figure 4.14 shows that before heating, no silane had diffused into the PVC film at all. The fact that the silane intensity curve is approximately symmetrical shows that this must be the case. The peak is very slightly broader towards the PVC, but by no more than the depth resolution of the experiment. Clearly, as the PVC film was 25 μm . thick, all of the film had been profiled in this experiment. After 15 minutes heating, the silane appeared to have diffused quite far into the film. This is in contrast to the last experiment described which showed little diffusion after an hour at 70 °C. After a further 45 minutes, the silane diffused further into the film, and considerable intensity could be detected even at the silicon interface.

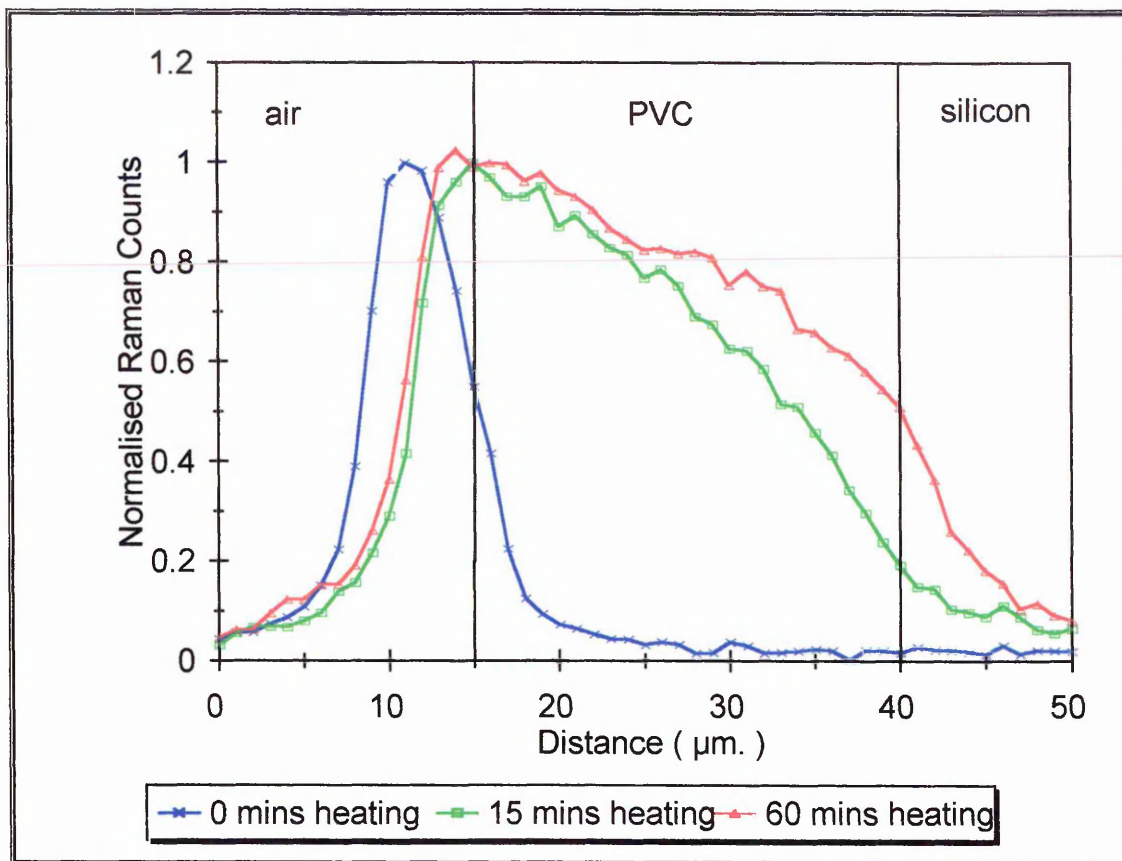


Figure 4.14 : The area of the 1600 cm^{-1} band of Y9669 plotted vs. distance for Y9669 diffusion in unplasticised PVC. Heating was carried out at $70\text{ }^{\circ}\text{C}$. The vertical lines show the positions of the interfaces

Due to the similar time-scales used, it is possible to compare the results from this experiment with those seen in the equivalent ATR - FTIR experiment. The intensity in the depth profile at the position of the silicon interface should be approximately equivalent to the ATR - FTIR intensity, assuming the same processes are occurring. Like the ATR - FTIR results, before heating, no intensity in this region was seen at all. After 15 minutes heating, an intermediate level of silane intensity was seen, and then much more was seen after 60 minutes. Although in the case of the ATR - FTIR results, a larger relative intensity was seen after 15 minutes, this may be due to the use of a thinner film, allowing the silane to diffuse to the interface in a shorter time.

The same experiment was then performed using A1110 as the silane. The film used was 24 μm . thick, and again there was no DMF present. The results are shown in Figure 4.15.

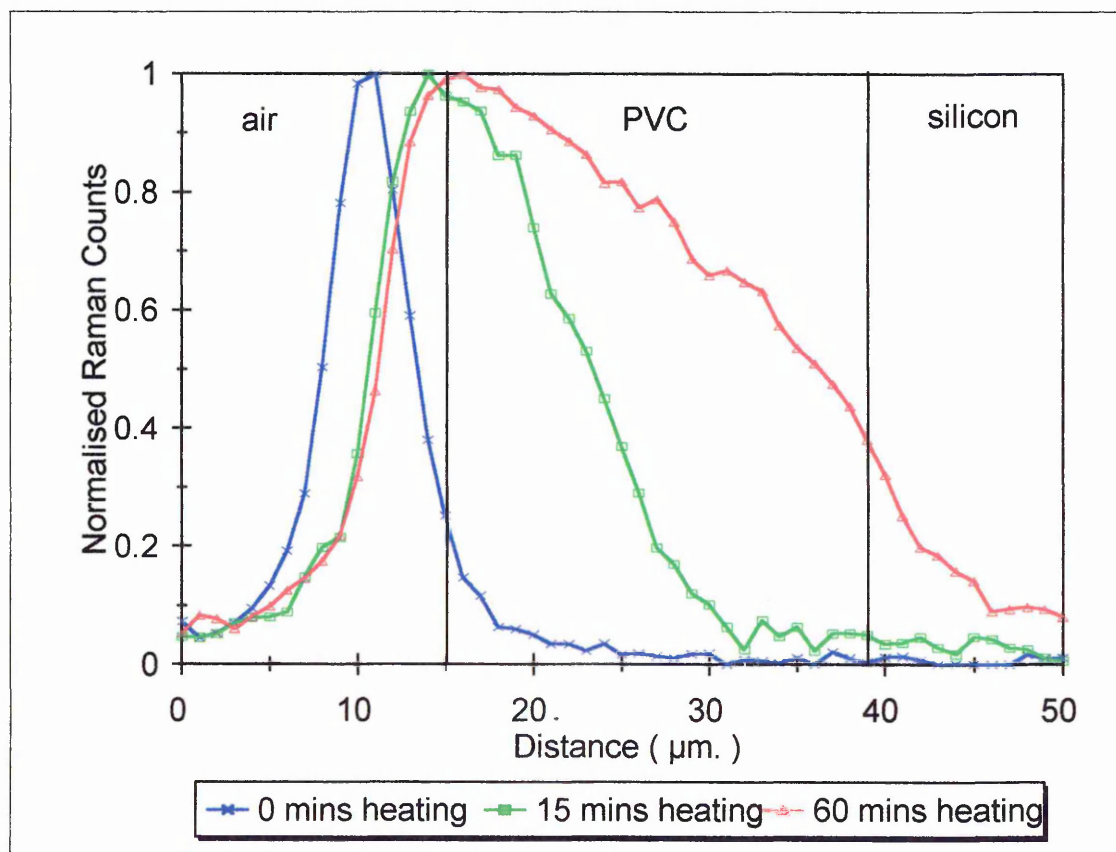


Figure 4.15 : The area of the NH bending mode of A1110 plotted vs. distance for A1110 diffusion in uPVC. Heating was carried out at 70 °C. The vertical lines show the positions of the interfaces.

Figure 4.15 shows that before heating, no diffusion of the A1110 through the PVC film occurred, and no intensity from the A1110 was detected at the silicon interface.. After 15 minutes heating, the silane had begun to diffuse through the PVC film. A small intensity from the silane could be detected at the silicon interface at this time. This small

intensity was probably only due to the 'tail' of the confocal response of the instrument, implying that the silane had only reached part of the way into the PVC film at this stage. After 60 minutes, however, a significant signal from the silane was detected at the silicon interface, showing that diffusion throughout the film had occurred.

These results contrast very strongly with those found in the ATR - FTIR experiments. In those experiments, no diffusion at all was observed in unplasticised PVC when heated at 70 °C. However, from the Raman depth profile results one would have expected to have seen a large intensity from the silane at the ATR crystal interface after one hour of heating at 70 °C. It is believed that the difference in the results was seen because the heating regimes were different, as in the ATR - FTIR experiments, the laminate was heated for only 10 minutes at a time. However, the diffusion does appear to be slower than that observed in the case of Y9669.

The experiment was also carried out using A1891 as the silane. The PVC film was 20 µm. thick, and no bands from DMF were seen in the spectra. The results are shown in Figure 4.16.

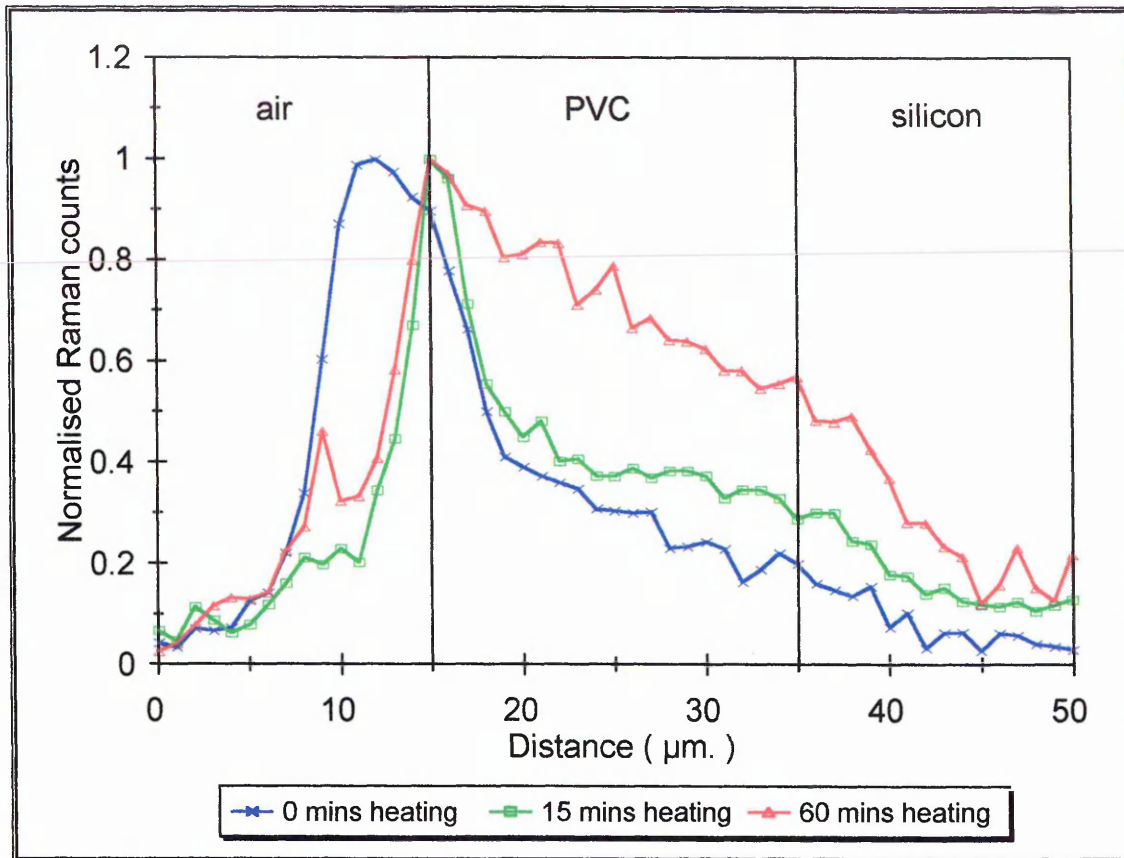


Figure 4.16 : The area of the SH stretching band of A1891 plotted vs. distance for A1891 diffusion in uPVC. Heating was carried out at 70 °C. The vertical lines show the positions of the interfaces.

Figure 4.16 shows that before the laminate was heated, most of the silane was at the upper surface of the laminate, but that some of the material had already diffused into the PVC film. After 15 minutes heating, some of the silane could be seen to remain at the upper surface of the PVC, but less than before the heating, and more silane was present through the bulk of the film. After a total of 60 minutes heating, the silane appeared much more evenly distributed through the PVC film. It is only the last profile (which it is assumed shows the equilibrium distribution of silane) which looks similar to the profiles obtained for the other silanes. The first two profiles look very different to those obtained for the other silanes. This implies that diffusion occurs differently for the A1891 material.

Comparing this data with that obtained for A1891 in unplasticised PVC by ATR - FTIR, it is interesting to note that in both cases, diffusion appears to be a two - step process : firstly a small amount of silane diffuses through the PVC followed by the bulk of the silane at a later stage. It cannot be proven using these techniques that the diffusion follows a different mechanism to that of the aminosilanes, but the agreement between the two techniques suggests that this is the case.

4.4 : Fourier Deconvolution of Depth Profiles

The Raman depth profiles obtained and presented in the previous section were a convolution of the real concentration profile of the silane in the PVC matrix with the instrumental response to that concentration profile. Therefore, if the instrumental response is known, it is theoretically possible to deconvolve the instrumental response from the measured depth profile to obtain the true concentration profile. In the case of the Raman depth profiles, the incomplete rejection of light scattered from regions out of the focal plane causes an instrumental response which prevents one from obtaining a true concentration profile. Therefore it was decided to attempt to deconvolve the confocal response of the instrument from the measured depth profiles. This is possible because the two functions which are convolved in real space are multiplied in Fourier space. That is,

$$FT(A * B) = FT(A) \times FT(B) \quad (4.1)$$

where FT is the Fourier transform procedure

* is the convolution process

A and B are the two functions.

Therefore, to obtain the concentration profile, we must perform a Fourier transform on the depth profile and the confocal response function, divide two functions thus obtained, and then perform an inverse Fourier transform to give the deconvolved depth profile. It was not possible to perform the deconvolution process on the measured data, as there were too few data points, and thus a large amount of uncertainty would result. The process has instead been carried out by fitting curves to the depth profiles obtained. These curves were then used to generate large number of data points which model the data obtained as depth profiles. Elsewhere¹⁸, the instrumental response used for deconvolution has been the response to a silicon surface in air, as shown in chapter 2. This is shown in Figure 4.17 along with an exponential function fitted to the data.

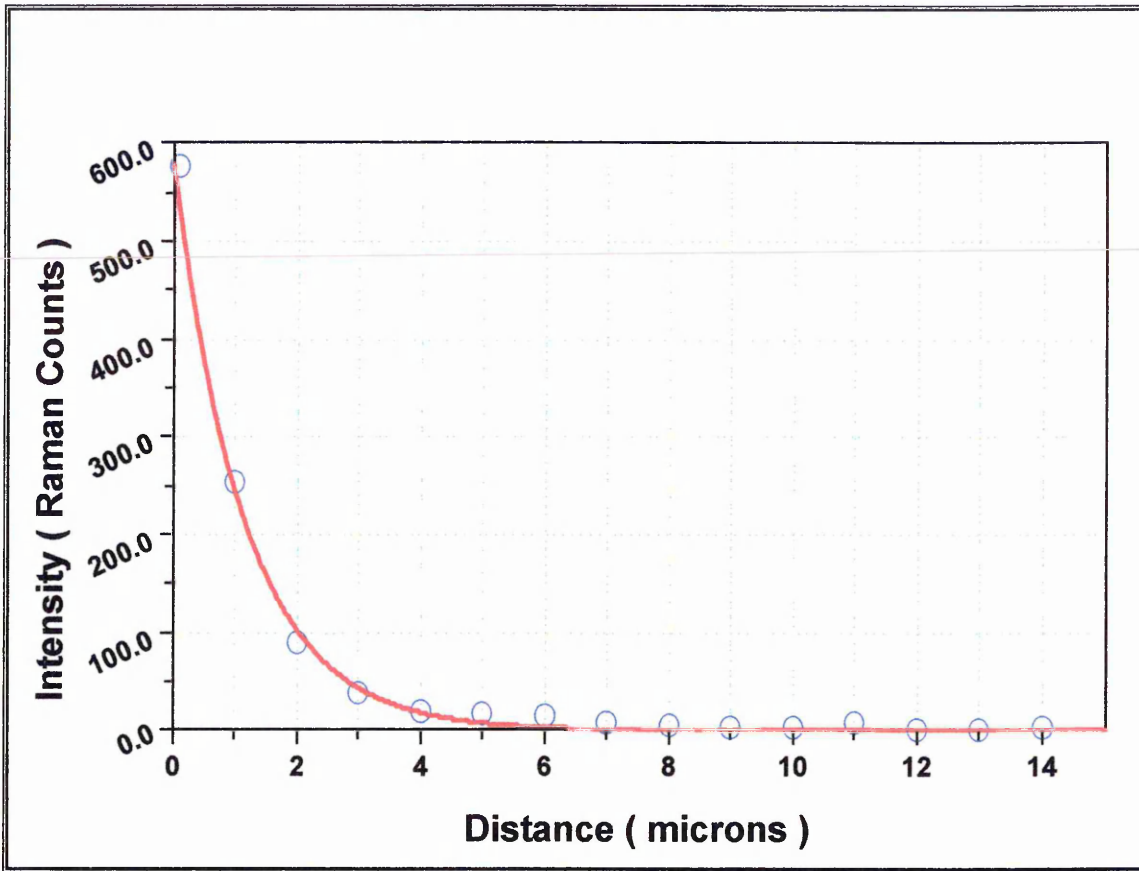


Figure 4.17 : The confocal response of the microscope in air (circles), and an exponential function fitted to the data (line)

The exponential fit to this data could be deconvolved from the curves fitted to the depth profiles, to give a deconvolved depth profile. However, the response of the microscope when performing a depth profile in a polymer film is not described well by this data. The reason for this is refraction of the laser light as it passes across the discontinuity in refractive indices at the air - polymer interface. This is described by Snell's law :

$$n_1 \sin\theta_1 = n_2 \sin\theta_2 \quad (4.2)$$

where n_1 is the refractive index of medium 1

n_2 is the refractive index of medium 2

θ_1 is the incident angle

and θ_2 is the refracted angle.

The effect of the refraction is shown schematically in Figure 4.18.

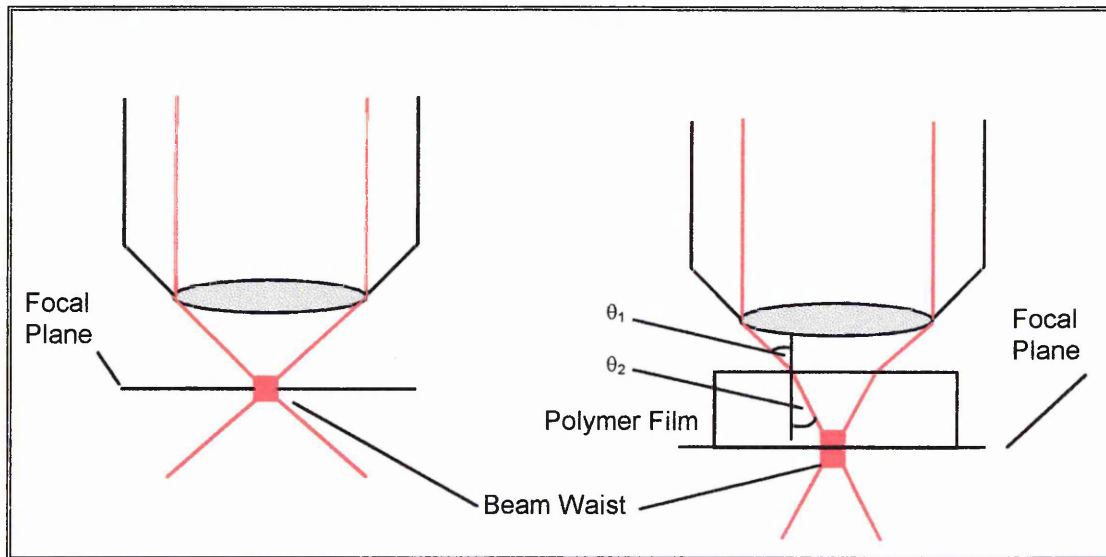


Figure 4.18 : Schematic of effect of focusing through a polymer film

It can be seen from Figure 4.18 that the effect of the refraction when focusing through a polymer film is twofold. Firstly, the focus of the laser is deeper into the film than expected. This would have no effect (to a first approximation) on the measurements described in the previous section, as all the distances quoted were relative to the sample. The second effect is that as the beam converges at the focal point at a lower angle of incidence, the effective NA of the experiment is lower when focusing through a transparent layer. This has the effect of creating a larger beam waist, and thus the depth resolution is reduced. Therefore in the experiments reported in the last section, and previously⁶, the

confocal response was not as shown in Figure 4.17. In order to determine the experimental response when focusing through layer of PVC, a second confocal profile was measured. This was done by casting a 20 μm . PVC film onto a silicon crystal, and measuring the confocal response under the PVC film. The results are shown in Figure 4.19.

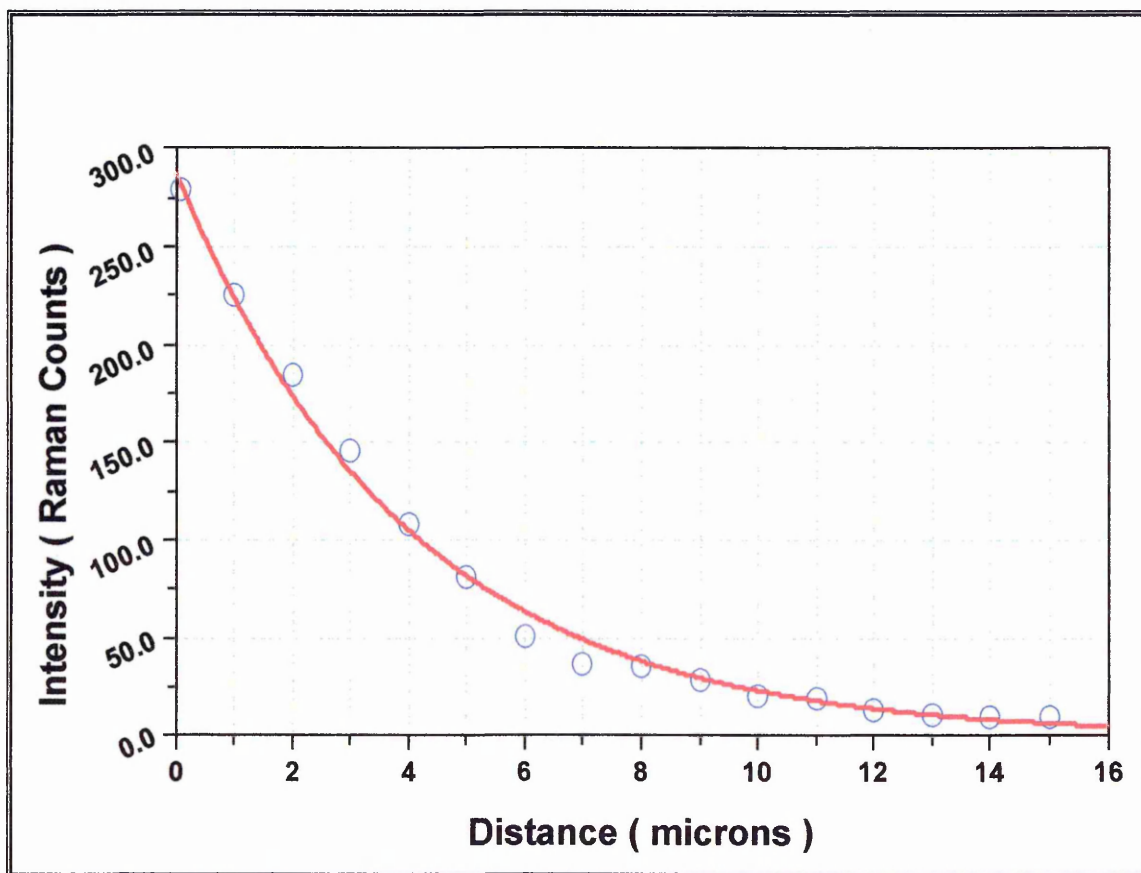


Figure 4.19 : The confocal response of the microscope under a 20 μm . PVC film (circles), and an exponential fitting of the data (line).

It can be clearly seen that the confocal response under a polymer film is very different to that in air. The spatial resolution achieved, measured by the full width at half height criterion described in section 2 is 5 μm ., as opposed to 2 μm . without the PVC film present. Because the refractive indices of all organic polymers are very similar, it may be

assumed that these results apply to other work^{18,6} carried out in polymer systems, where it was assumed that the confocal response was the same as that measured in air.

In order to deconvolve the data obtained, a program was written in the Matlab proprietary numeric computation and visualisation package. This package was chosen due to the ability to perform the analysis and plot the results within the same package. The program is shown below. The Matlab package does not use line numbers, so they have been added for ease of reference.

```
1   a = input('Input Gaussian curve parameter a : ');
2   b = input('Input Gaussian curve parameter b : ');
3   c = input('Input Gaussian curve parameter c : ');
4   w = input('Input Exponential parameter a : ');
5   count = 1;
6   for i=0:(30/2047):30
7       ga(count)=a*(exp(-(i-b)^2/(2*c^2)));
8       ax(count)=i;
9       ex(count)=exp(-w*i);
10      count=count+1;
11  end
12  ftga = fft(ga);
13  ftex = fft(ex);
14  ftresult = ftga./ftex;
```

```

15  result = ifft(ftresult);
16  realresult = real(ftresult);
17  realresult = realresult/max(max(realresult));
18  plot(ax,ga,'r')
19  hold on
20  plot(ax,ex,'b')
21  plot(ax,conl,'w')
22  hold off
23  xlabel ('Depth( $\mu\text{m.}$ )')
24  title ('Deconvolution Results')
25  legend ('Data','Exponential','Deconvolution')
26  ylabel ('Intensity')
27  set (gca,'ylim',[0 1.5])
28  s = input('Input filename for result data : ','s');
29  file = [s '.txt'];
30  eval(['save ' file ' realresult -ascii']);

```

The operation of the program is as follows. The first four lines accept inputted parameters of the curves which have been fitted to the experimental data. The program expects an exponential function for the instrument response and a Gaussian function for the data. The program then generates 2048 data points using these functions. Lines 12 and 13 perform the Fourier transforms of the data. Line 14 then divides the Fourier transform of the data by the Fourier transform of the experimental response. The dividend is then

inverse Fourier transformed to give the result (line 15), the imaginary part of which is discarded(line 16). Although the program is used with normalised data, the deconvolution often changes the intensity scale, therefore line 17 normalises the data in the y axis. The remainder of the program simply plots the two original functions, and the result of the deconvolution. Finally the program saves the deconvoluted data. An example of the output of the program is given in Figure 4.20. The data used was the first depth profile of Y9669 in unplasticised PVC (i.e. the blue curve in Figure 4.13), and the exponential is modelled on the response from silicon in air.

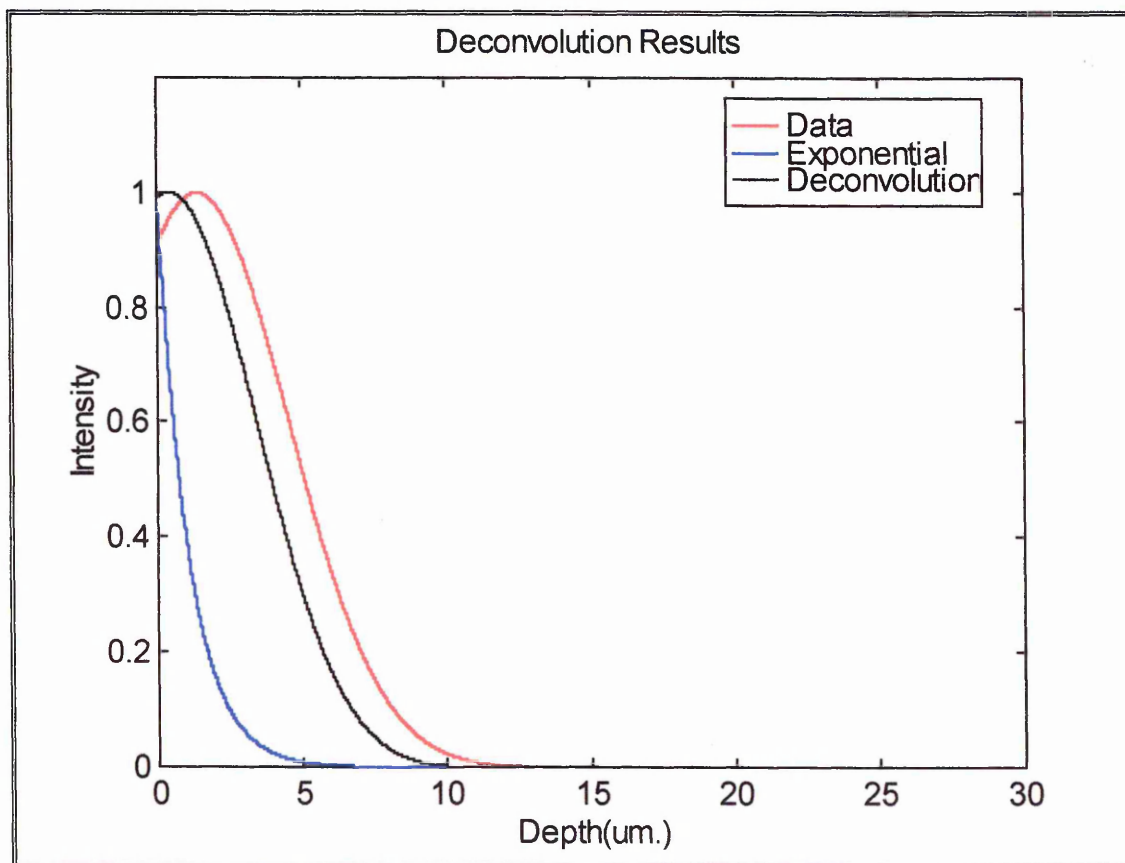


Figure 4.20 : Deconvolution results from the first Y9669 diffusion experiment. The confocal response modelled was that of silicon in air.

Figure 4.20 shows that after deconvolution of the modelled confocal response, the modelled depth profiles shifted to a lower depth. This indicates that the measured (i.e. convolved) profile made the silane appear to have diffused further into the PVC film than was actually the case. As shown by the comparison of Figure 4.17 and Figure 4.19, the confocal profile was considerably different when measured in a PVC film. Therefore, it was decided to model the confocal profile under PVC and perform the deconvolution process on the same depth profile to see what difference this made. The results using the exponential function fitted to the data measured under PVC are shown in Figure 4.21.

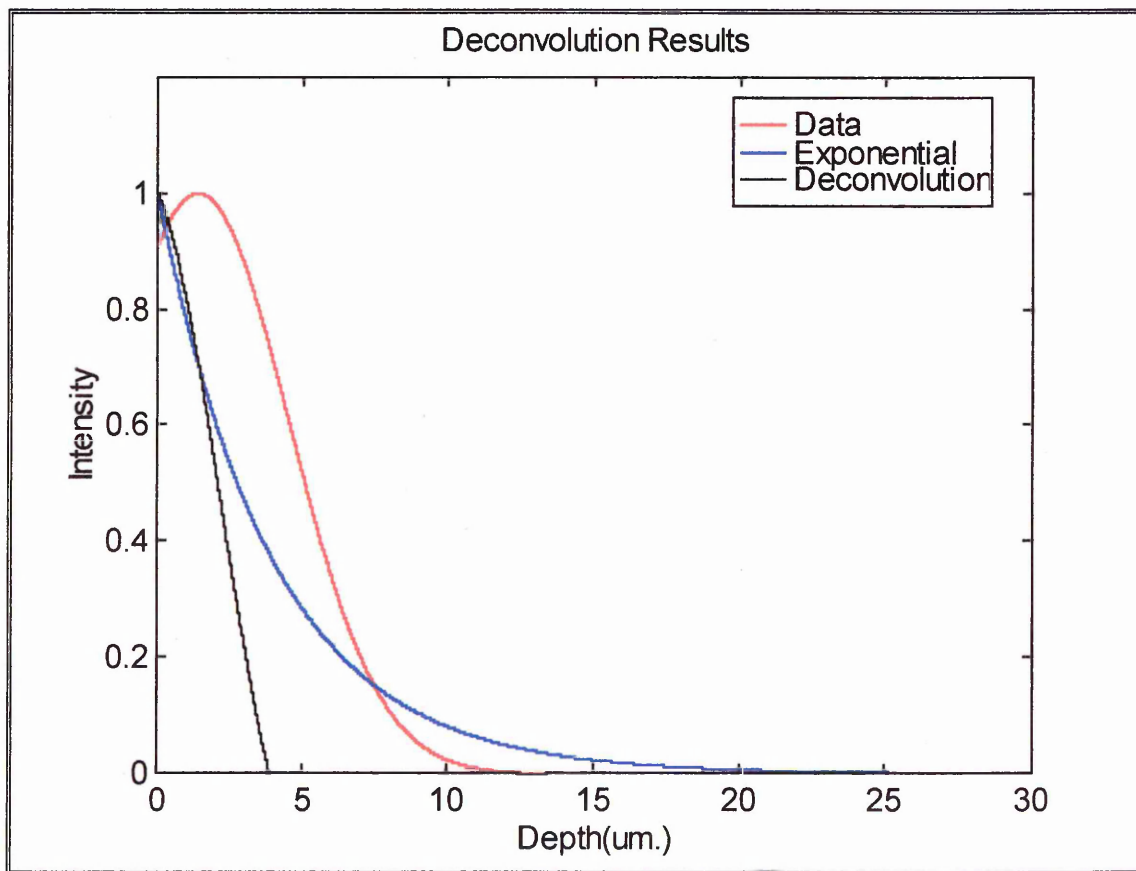


Figure 4.21 : Deconvolution of the data from the first Y9669 experiment. The confocal response used was that of silicon under a PVC film.

Comparison of Figure 4.21 with Figure 4.20 shows that the use of the confocal response measured under a PVC film made a large difference to the deconvolution results. Therefore, it was decided to use this response when performing the deconvolutions. All the ~~deconvolution results shown henceforth were obtained using the confocal response of~~ silicon under a PVC film. It should be noted that strictly speaking, the effect of the presence of the silane in the PVC film on the confocal response should also be modelled to give a true measure of the convolution process. However, this is an extremely complex process, as the silane moves in time through the film during the experiment, and is beyond the scope of this work.

The deconvolution results of all the depth profiles obtained in the first experiment (i.e. the results shown in Figure 4.13), using Y9669 in unplasticised PVC, and heating at 70°C for one and then two hours, are shown in Figure 4.22. All of the depth profiles were fitted to Gaussian curves for deconvolution.

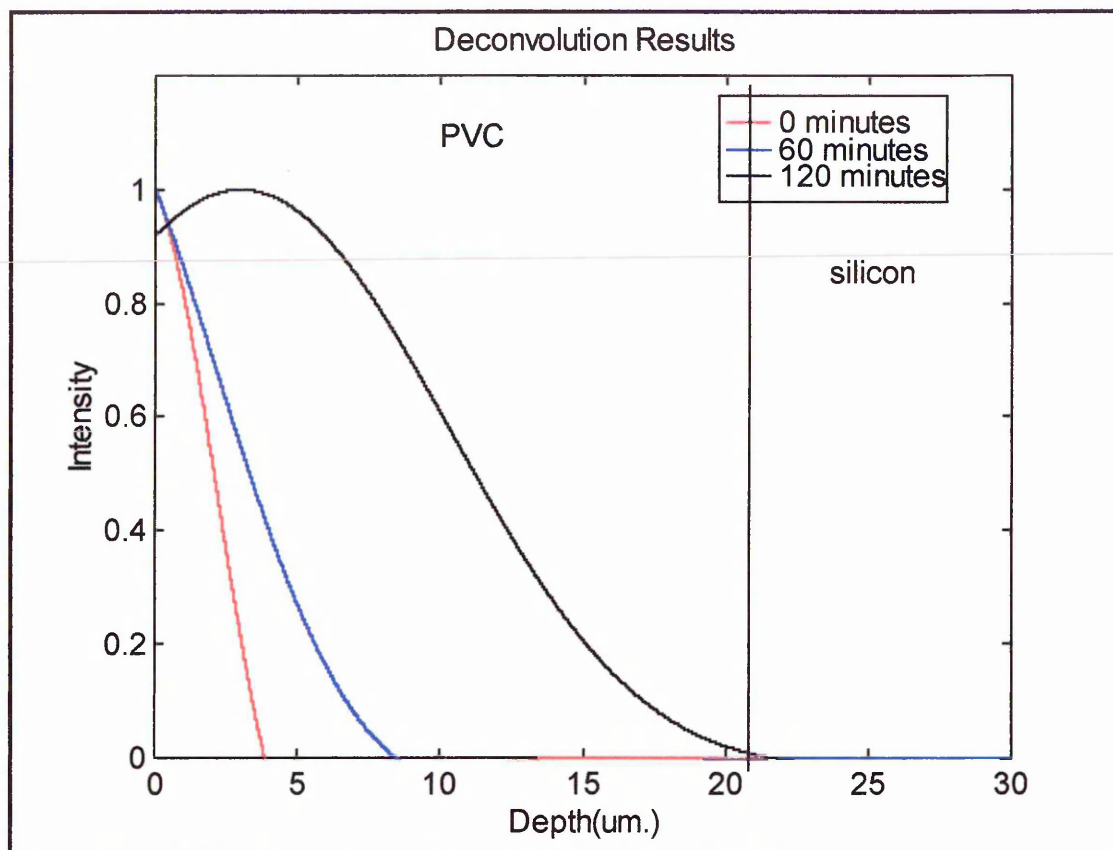


Figure 4.22 : The deconvolution results for Y9669 diffusion in unplasticised PVC heated hourly

Figure 4.22 shows that all of the depth profiles appeared to show less diffusion into the PVC film when the confocal response of the instrument was deconvoluted from the data. This makes sense, as the lower resolution of the convolved data would have the effect of broadening the concentration profile, making it possible to detect the silane even where none was present.

The results of performing the same deconvolution process on the results from the second Y9669 experiment, where the film was heated for 0, 15 and 60 minutes at 70 °C are shown in Figure 4.23.

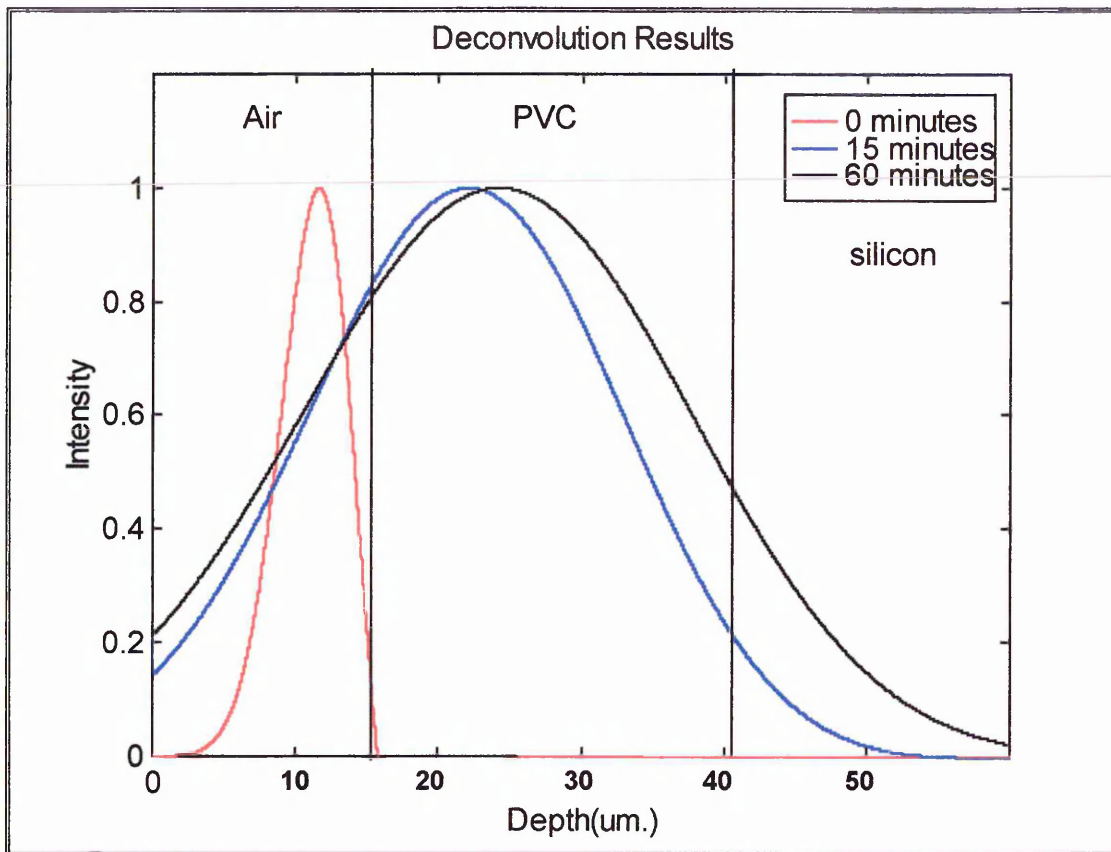


Figure 4.23 : The deconvolution results for Y9669 diffusion in unplasticised PVC heated for 0, 15 and 60 minutes at 70°C

Comparison of Figure 4.23 with Figure 4.14 shows that upon deconvolution of these results, the width of the depth profiles narrow somewhat, showing that the broadening effects of the confocal response have again been removed. This is especially true of the results of the first depth profile, before any diffusion which shows a sharp boundary at the silane / PVC interface. However, in the case of the 15 and 60 minutes heating profiles, the Gaussian curves do not fit the depth profiles well on the low depth side. This is because the depth profiles are asymmetrical. The effect of this is that the deconvolved curves are

broader compared to the depth profiles in the low depth region. Unfortunately, a simple function which modelled this part of the curves well was not found.

The results of performing the same deconvolution process on the results from the experiment using A1110 in unplasticised PVC where the film was heated for 0, 15 and 60 minutes at 70 °C are shown in Figure 4.24.

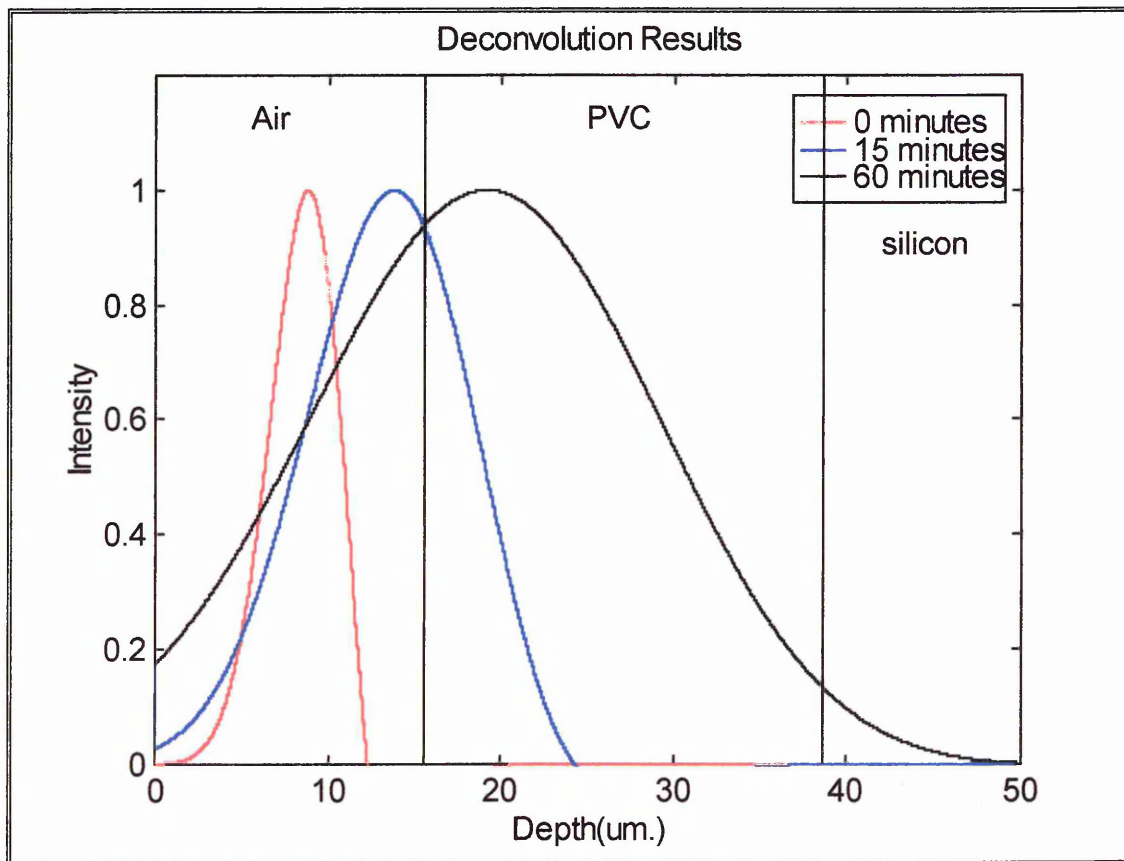


Figure 4.24 : The deconvolution results for A1110 diffusion in unplasticised PVC after 0, 15 and 60 minutes heating at 70°C

Comparison of Figure 4.24 with Figure 4.14 shows that upon deconvolution of these results, the width of the depth profiles again narrowed somewhat, showing that the

broadening effects of the confocal response have again been removed. This is especially true of the results of the first depth profile, before any diffusion which shows a sharp boundary at the silane / PVC interface. It can be seen that at the low depth side, the final depth profile has actually been broadened. This is because in this case, the depth profile does not fit well to a Gaussian model, as it is asymmetric, having a much sharper boundary at the low depth side. However, a simple function which modelled this aspect of the shape was not found.

In the case of the A1891 depth profiles, Figure 4.16 clearly shows that the data did not show a Gaussian distribution. The depth profiles, especially those at 0 and 15 minutes heating show a large concentration of silane at low depths (i.e. at the surface of the PVC film), and a smaller amount through the bulk of the film. A model which was found to fit this distribution was a rational function. This can be expressed as

$$Y = \frac{a + bx}{1 + cx + dx^2} \quad (4.3)$$

An example of the fitting of this model to the data from an A1891 depth profile is shown in Figure 4.25.

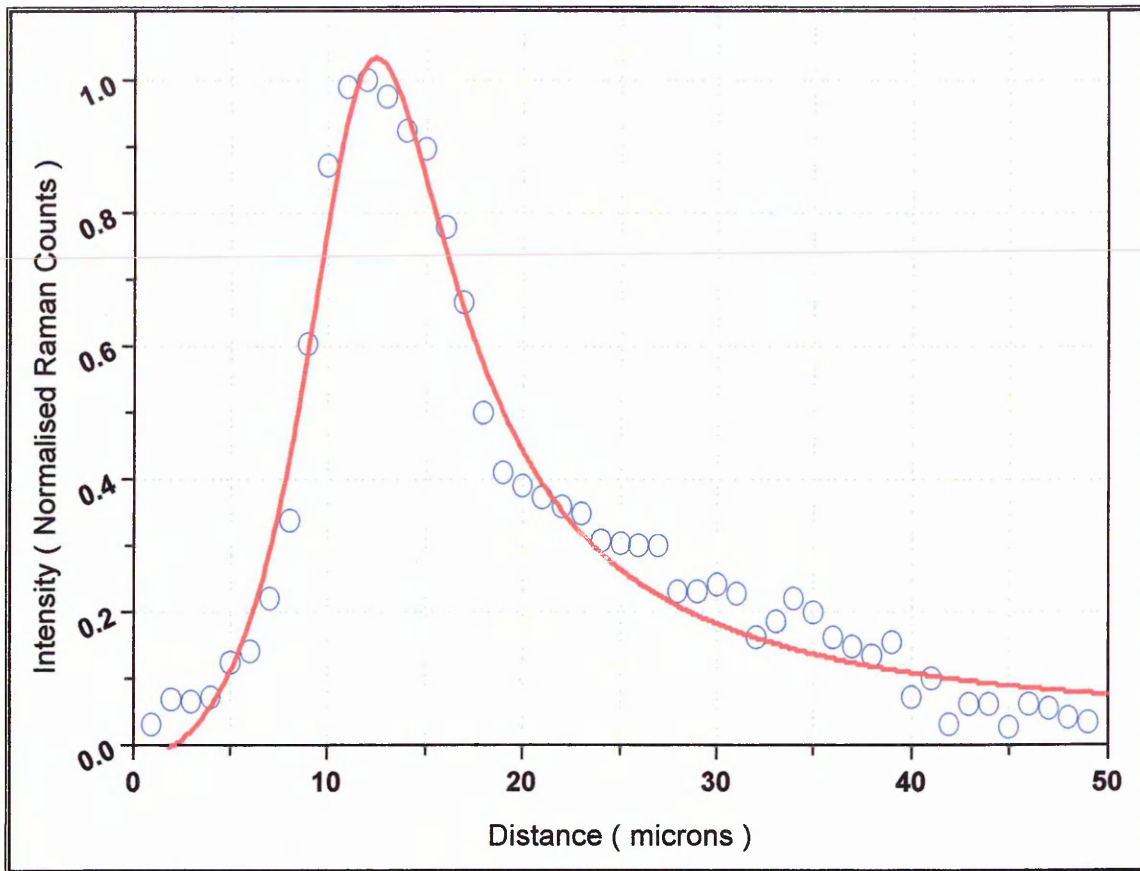


Figure 4.25 : Fitting of a rational function to the data from the first A1891 depth profiling experiment.

An example of the results of the deconvolution of this rational function is shown in Figure 4.26.

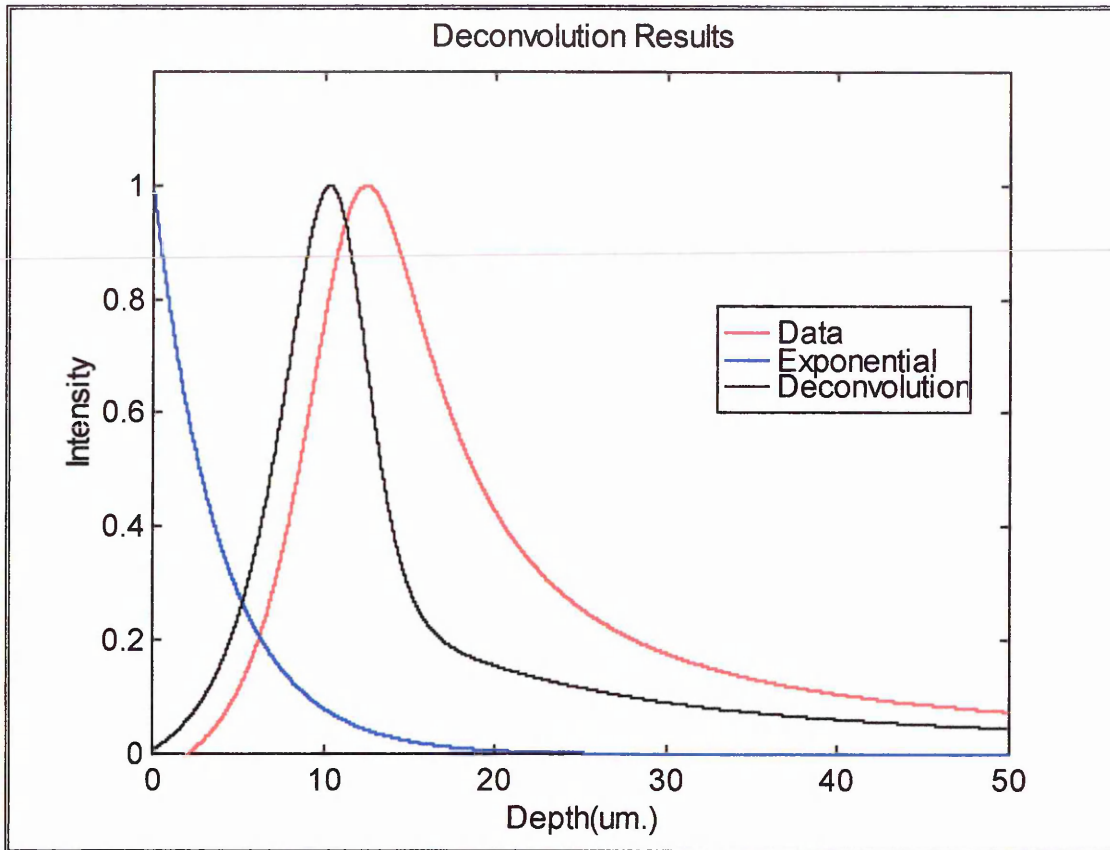


Figure 4.26 : Results of deconvolution of rational function fitted to the first depth profile of A1891.

Figure 4.26 shows that upon deconvolution, the rational function shifts to lower depth, and the lobe at about 10 - 15 μm. depth narrows considerably. The results of the deconvolution of all the depth profiles of A1891 are shown in Figure 4.27.

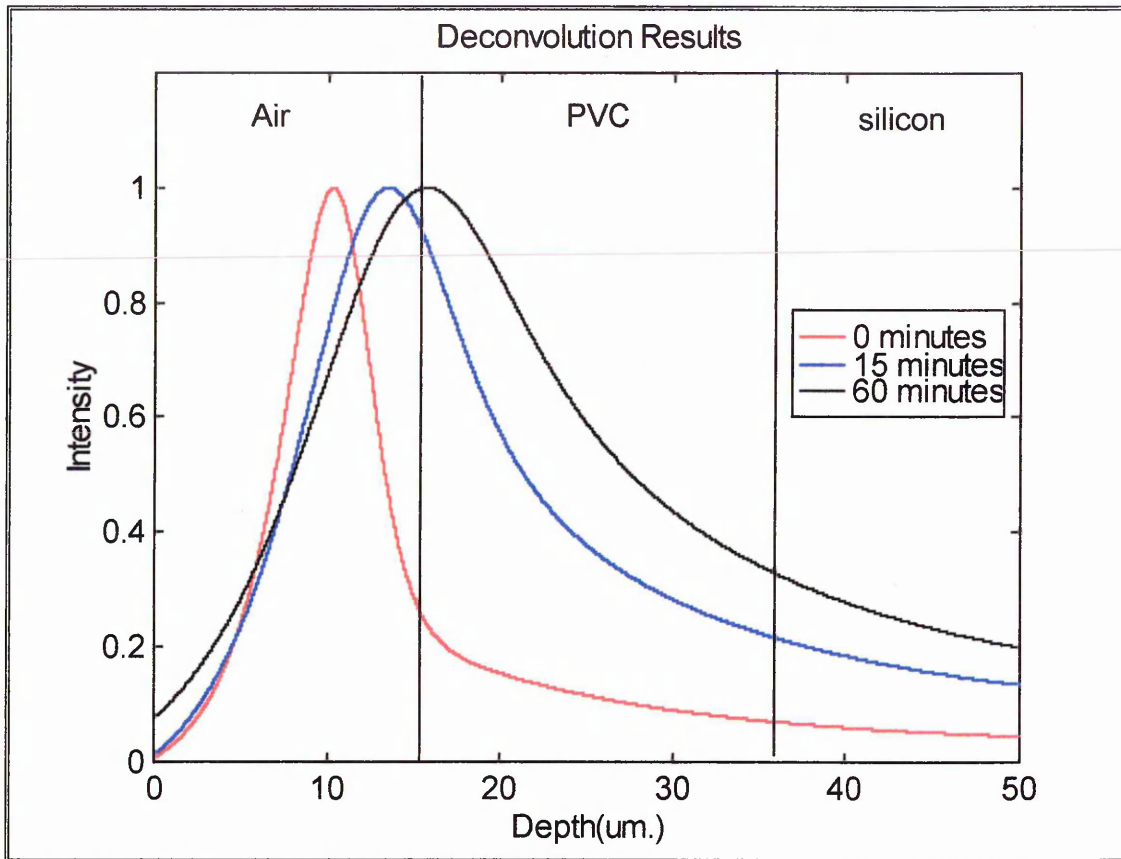


Figure 4.27 : The deconvolution results for A1891 diffusion in unplasticised PVC heated for 0, 15 and 60 minutes at 70°C

Figure 4.27 shows that in the case of the first depth profile, a much narrower concentration of material at the PVC surface is seen than in the raw data. The other depth profiles also show most of the silane remaining at the surface of the PVC film. In the case of the A1891 results, the deconvolution process was clearly unsatisfactory. The deconvolved curves show silane remaining present throughout the depth profile, i.e. even into the region where the silicon crystal was. This is because a simple function could not be found to adequately fit the distribution of the silane seen in the depth profiles. It is believed that the best way of getting a function to approximate the shapes seen in Figure 4.16, would be to combine several functions together, e.g. a sharp Gaussian curve at the

PVC interface, and a broader, less intense one throughout the remainder of the PVC film.

However, this is beyond the scope of this project, which aimed only to show that the

principle of Fourier deconvolution may be used to take account of the broadening process

caused by the instrumental response of the microscope. This has been well demonstrated

in this chapter.

References

- 1 Sung, N. H., Kaul, A., Chin, I. and Sung, C. S. P., *Polymer Engineering and Science* 22, No. 10, p. 637 (1982.)
- 2 Stein, J., Valenty, S. J., Smith, G. A., Brezniak, D. V. and Prutzman, L. C., *Macromolecules* Vol. 19 (1986)
- 3 Chaudhury, M. K., Gentle, T.M. and Plueddemann, E. P., *Journal of Adhesion Science and Technology* Vol. 1, No. 1 (1987)
- 4 Dibenedetto, A. T. and Scola, D. A., *Journal of Colloid and Interface Science* Vol. 64, No. 3 (1978)
- 5 Tabaksblat, R., Meier, R. J. and Kip, B. J., *Applied Spectroscopy* Vol. 46, No. 1, p.60 (1992)
- 6 Hajatdoost, S., Olsthoorn, M. and Yarwood, J., *Applied Spectroscopy* Vol. 51, No. 12, p. 1784 (1997)
- 7 Hair, M. L., *Advances in Chemistry Series* Vol. 234, p. 161 (1994)
- 8 Angst, D. L. and Simmons, G. W., *Langmuir* Vol. 7, P. 2236 (1991)
- 9 Ellahi, S., Hester, R. E. and Williams, K. P. J., *Spectrochimica Acta Part A - Molecular and Biomolecular Spectroscopy* Vol. 51, No. 4, p. 549 (1995)
- 10 Owen, E. D., Shah, M. and Twigg, M. V., *Polymer Degradation and Stability* Vol. 51, No. 2, p. 151 (1996)
- 11 Ishida, H., Chiang, C.-H. and Koenig, J. L., *Polymer* Vol. 23, p.251 (1982)
- 12 Boerio, F. J., Armogan, L. and Cheng, S. Y., *Journal of Colloid and Interface Science* Vol. 97, No. 2, p. 308 (1984)
- 13 Hoh, K.-P., Ishida, H. and Koenig, J. L., *Polymer Composites* Vol. 9, No. 2 (1988)

- 14 Opila, R.L., LeGrange, J. D. , Markham, J. L. , Heyer G. and Schroeder, C., M.,
Journal of Adhesion Science and Technology Vol. 11, No. 1, p. 1 (1997)
- 15 ~~Chiang, C.-H., Ishida, H. and Koenig, J. L., Journal of Colloid and Interface
Science, Vol. 74, No. 2, p.396 (1980)~~
- 16 Johansson, O. K., Stark, F. O., Vogel, G. E. and Fleischmann, R. M., Journal of
Composite Materials Vol. 1, p. 278 (1967)
- 17 Kurth, D. G. and Bein, T., Langmuir Vol. 11, No. 2, p.578 (1995)
- 18 C. Sammon, PhD. Thesis, Sheffield Hallam University (1997)

Chapter 5 : Raman studies of organosilane hydrolysis

It was shown in the previous sections that the hydrolysis or condensation state of the silanes had a significant effect on the diffusion properties of the silanes in PVC films. However, the rates of these reactions was not well known. The hydrolysis of various silanes has been studied by a number of techniques previously. These include Raman spectroscopy^{1,2}, NMR^{3,4}, and infrared spectroscopy⁵⁻¹¹. The aminosilane A1110 and the mercaptosilane A1891 are two of the most widely studied, and some of these studies have investigated the hydrolysis of these silanes^{3,7}. However, the hydrolysis of Y9669 has not been studied at all in the literature found. Therefore, in order to obtain comparable results, it was decided to examine the hydrolysis and condensation of all three silanes in order to be in a better position to interpret the diffusion data reported in chapters 3 and 6.

5.1 : Experimental

The hydrolysis measurements were carried out using Raman spectroscopy. This technique was chosen because previous work^{1,2} had identified bands common to many organosilanes which were indicative of the progress of hydrolysis. Hydrolysis was initiated as described in chapter 2, by mixing the silanes with an acidified IPA / H₂O solution. The solution was then sealed in a quartz cuvette and placed under the microscope, and spectra taken at regular intervals.

5.1.1 : Materials

The materials used were as described in chapter 3. The hydrolysis solution contained a 9:1 IPA / H₂O mixture. The solution was then acidified by the addition of 3% (v/v) acetic acid. All of the hydrolysis solutions contained 25% silane (v/v). All experiments were carried out at room temperature (25 ± 1 °C).

5.1.2 : Spectroscopic Measurements

Spectroscopic measurements were carried out with a Renishaw Ramascope system 2000 as described in chapter 2. The instrument was used in normal (i.e. non - confocal) mode. The 20X ULWD objective was used to allow focusing through the wall of the quartz cuvette. In order that a large number of Raman bands could be analysed, extended spectra were taken, generally in the range 500 to 1700 cm^{-1} .

5.1.3 : Spectra of Materials

The Raman spectra of the unhydrolysed silanes were presented in chapter 4. In order that the bands of the other materials in the hydrolysis solutions were not erroneously identified as silane bands, the spectra of IPA, water and acetic acid were taken. The Raman spectra of IPA, acetic acid and water are shown in Figure 5.1 to 5.3 . The spectra were all taken in a quartz cuvette using the 20X ULWD objective.

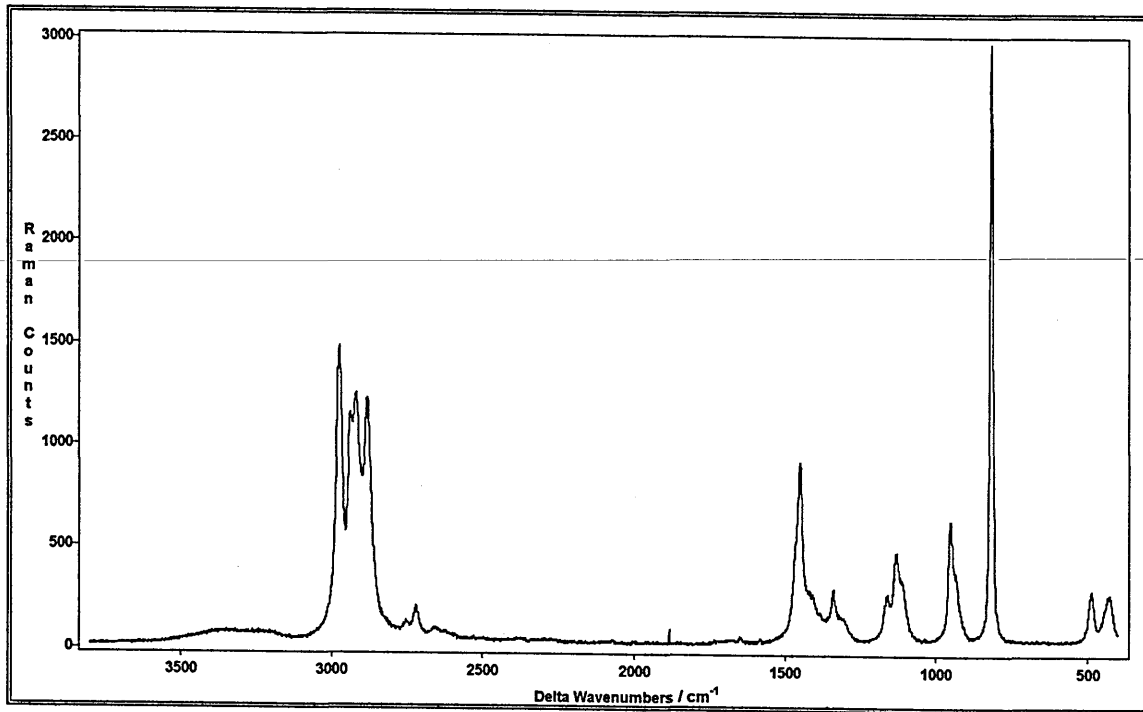


Figure 5.1 : The Raman spectrum of iso propyl alcohol (IPA)

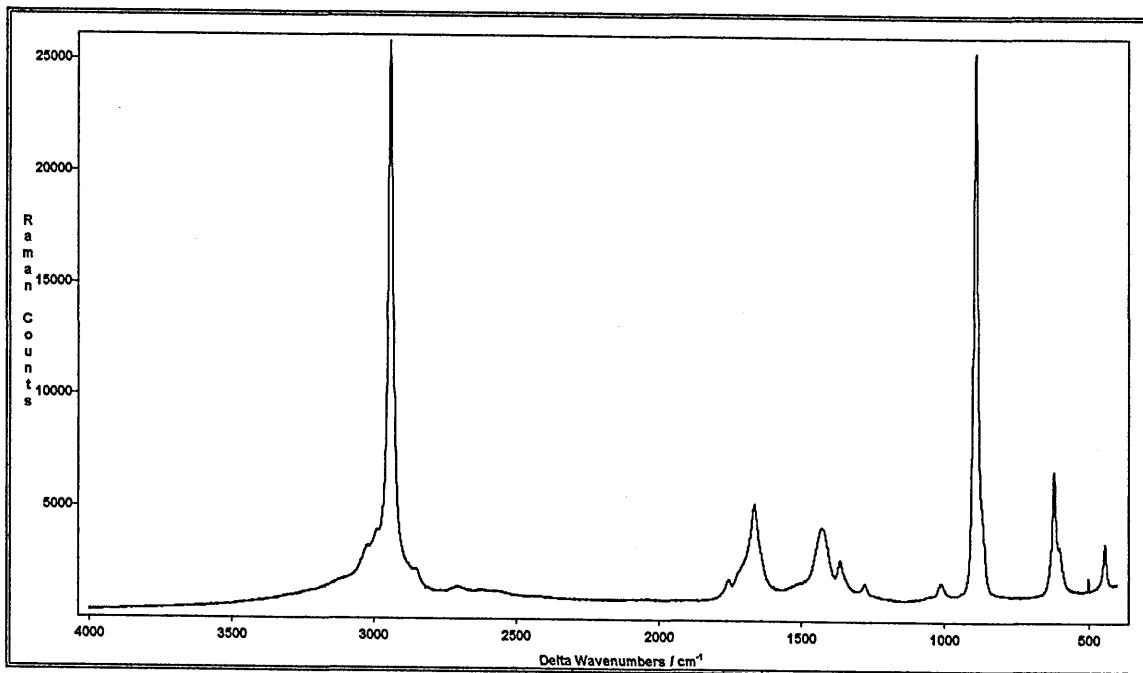


Figure 5.2 : The Raman spectrum of acetic acid

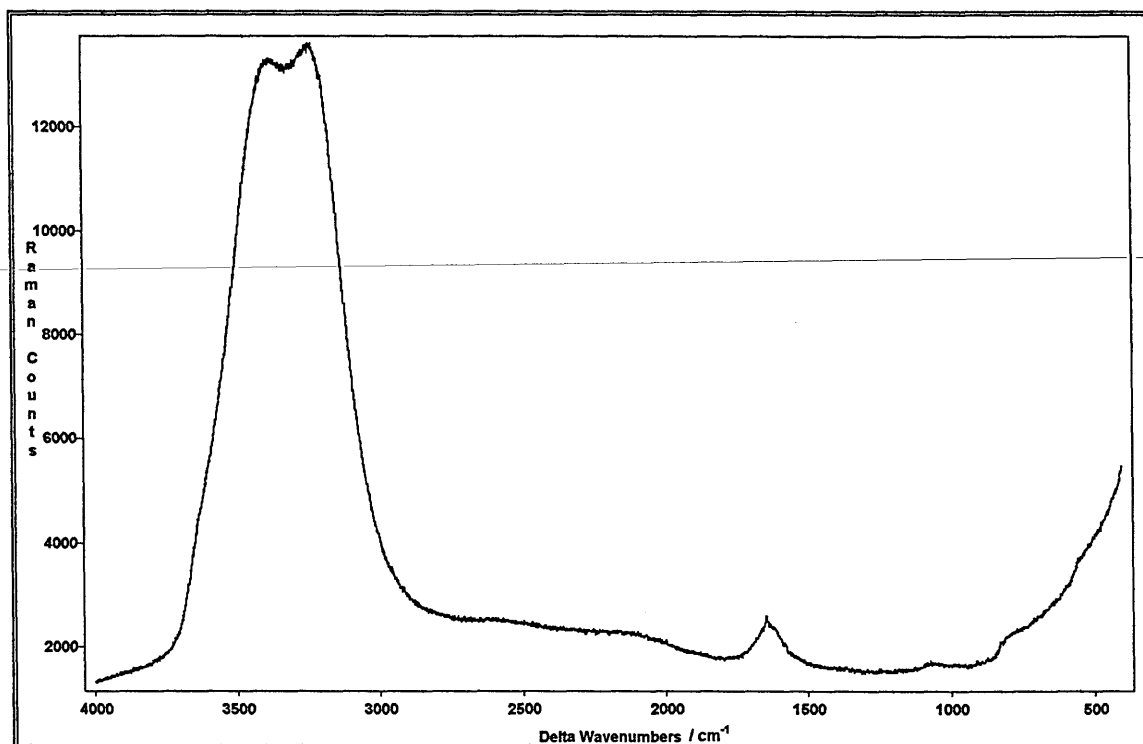


Figure 5.3 : The Raman spectrum of water

Figure 5.4 shows the Raman spectrum of the hydrolysis solution, consisting of a 9 to 1 (v/v) mixture of IPA and water, acidified by 3% added acetic acid. The spectrum was taken in a quartz cuvette using the 20 X ULWD objective. Comparison of the spectra shown shows that the spectrum of the hydrolysis solution is for practical purposes the same as that of IPA.

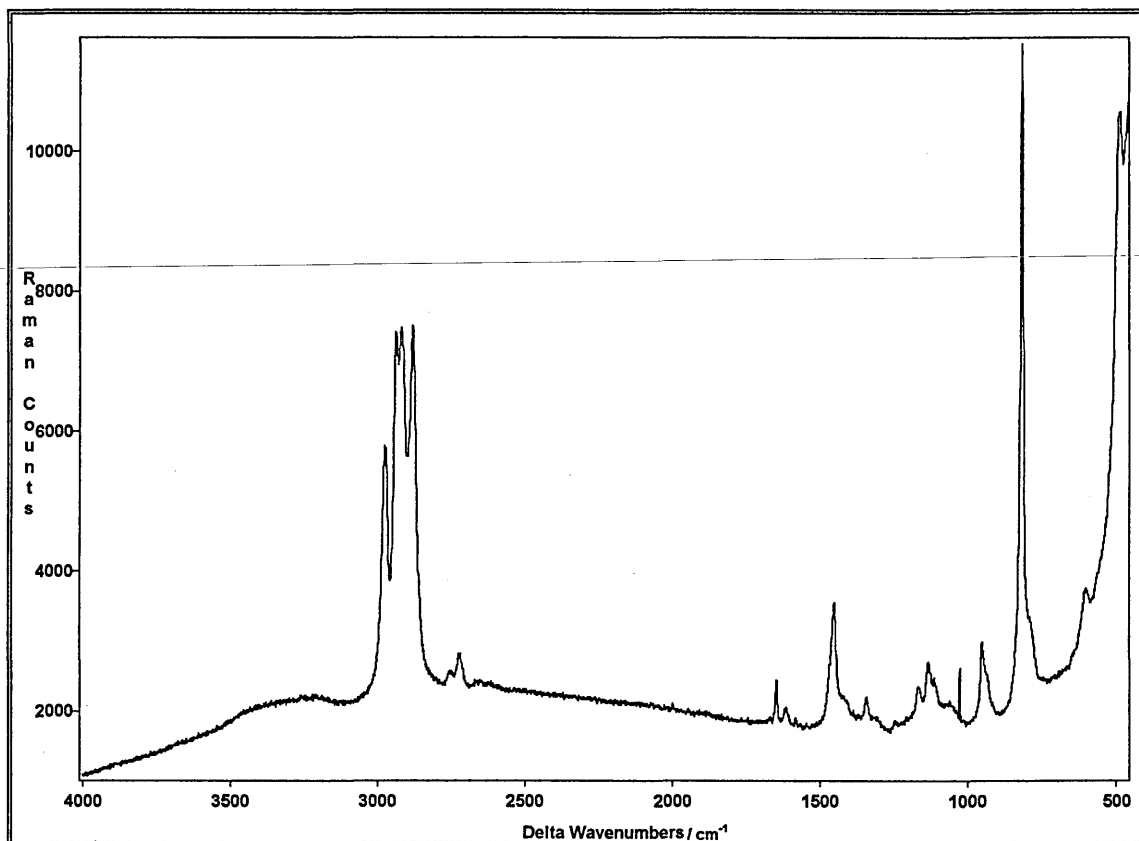


Figure 5.4 : The Raman spectrum of the hydrolysis solution (9:1 IPA / H₂O with 3% added acetic acid)

5.2 : Y9669 Hydrolysis Results

The Raman spectrum of , [3-(phenylamino)propyl]trimethoxysilane (Y9669, see figure 1.1) was taken every 30 minutes, in the range 250 to 1650 cm⁻¹ immediately after the Y9669 had been added to the hydrolysis solution and agitated. The spectra were taken until a total time of 24 hours had elapsed. The first and last spectra are shown in Figure 5.5. The spectra have been offset in the y-axis to make it easier to distinguish between them.

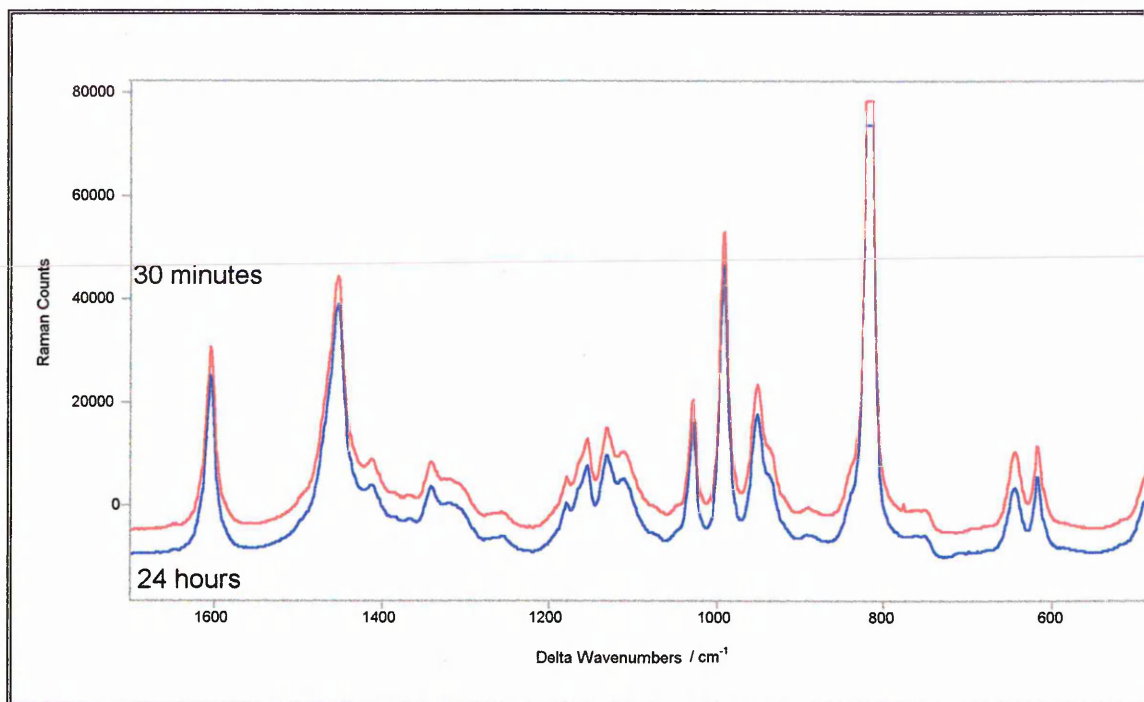


Figure 5.5 : The spectra of Y9669 in a 25% aqueous alcohol solution after 30 minutes and 24 hours. The spectra have been offset in the y-axis.

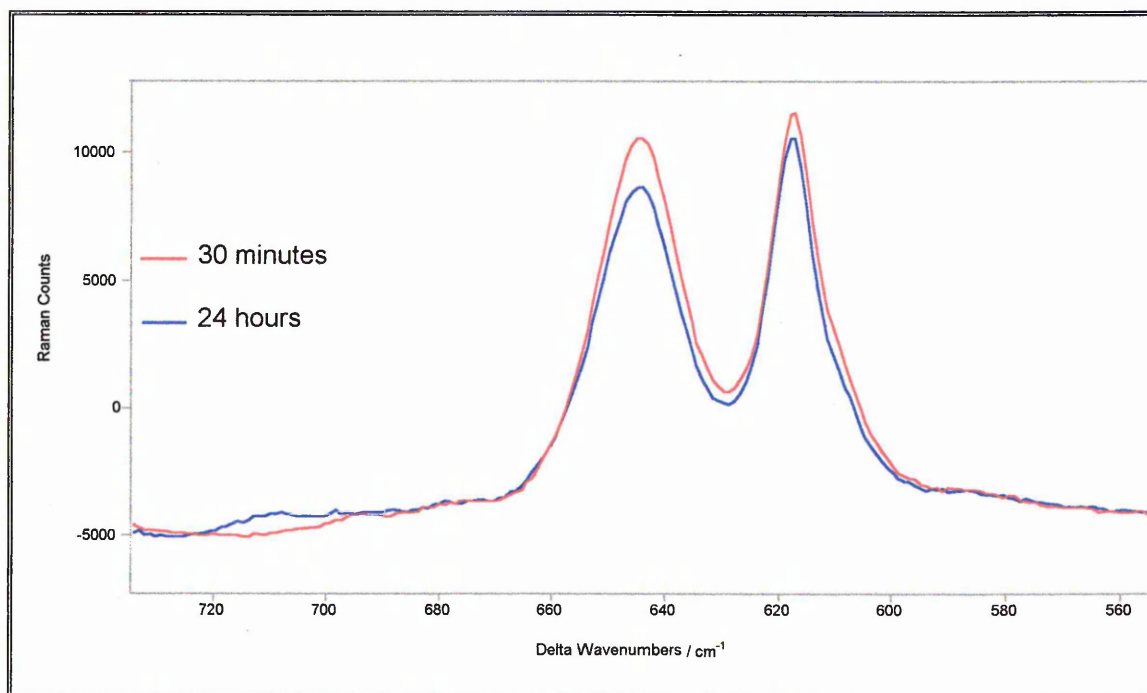


Figure 5.6 : The spectra of Y9669 after 30 minutes and 24 hours. The spectra are shown on the same y-axis

Figure 5.5 shows that the spectra changed very little over the experimental time of 24 hours. The spectral region of 540 to 740 cm^{-1} has been blown up and is shown in Figure 5.6. In this case, the spectra are shown on exactly the same scale.

Figure 5.6 shows that the two bands at 617 and 645 cm^{-1} both decreased in intensity during the course of the experiment, and that a small band at about 710 cm^{-1} appeared. Ishida et. al. assigned bands at 640 cm^{-1} and 612 cm^{-1} to Si-O-C stretching modes of unhydrolysed A1110². As Y9669 differs from A1110 only in having a phenyl ring attached to the amine group (see figure 1.1), we have assigned the 617 cm^{-1} and 645 cm^{-1} bands in Y9669 to Si-O-C stretching. The integrated intensity of these bands are plotted versus time in Figure 5.7 and Figure 5.8.

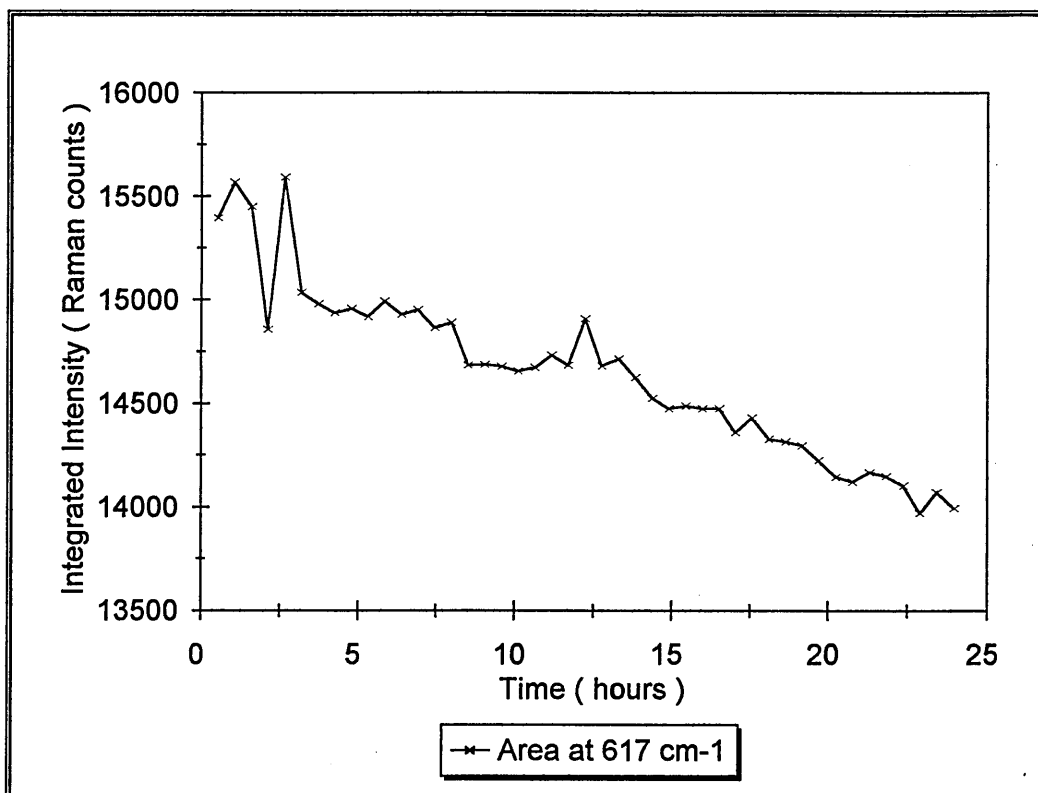


Figure 5.7 : The integrated intensity of the 617 cm^{-1} band of Y9669 plotted vs. time in the hydrolysis solution

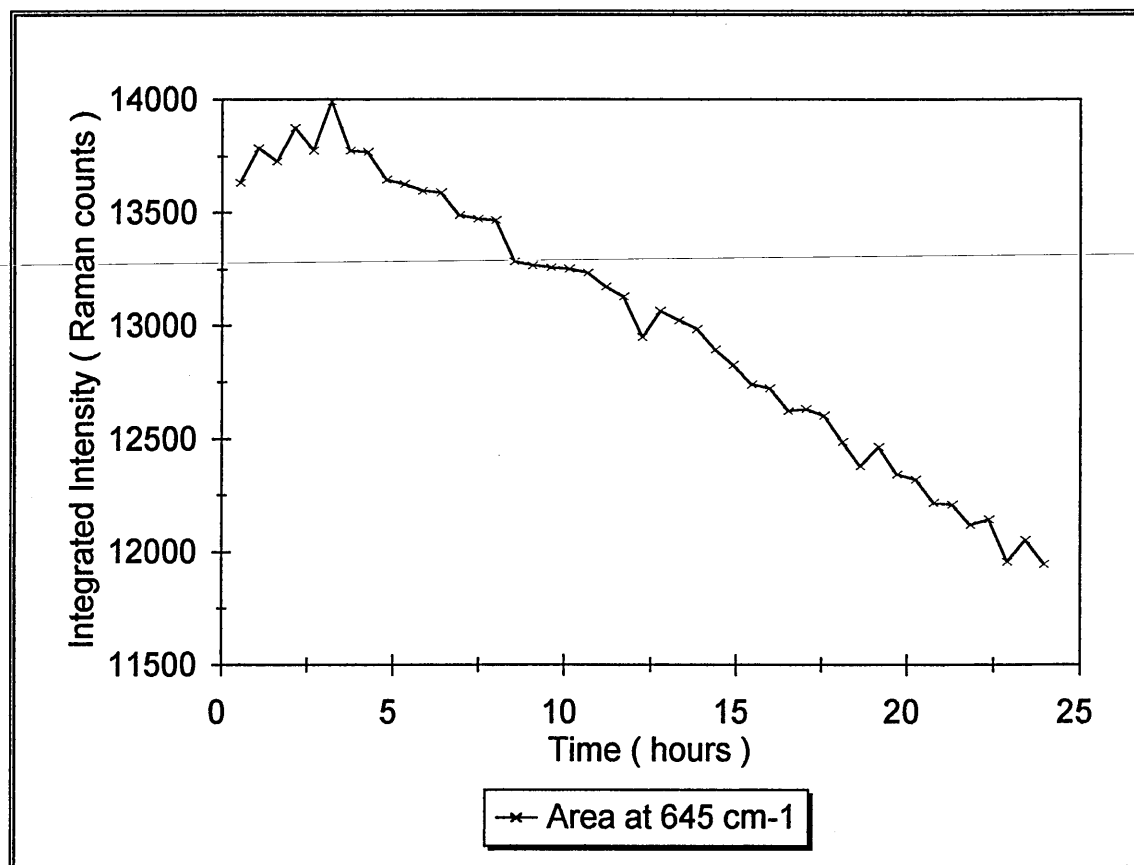


Figure 5.8: The integrated intensity of the 645 cm^{-1} band of Y9669 plotted vs. time in the hydrolysis solution

Figures 5.7 and 5.8 show that the intensities of the two bands assigned to Si-O-C stretching decreased throughout the experimental duration (24 hours). This showed that hydrolysis was occurring over this period of time, but also that hydrolysis was not complete after 24 hours. Both plots, but especially figure 5.8 showed an initial ‘induction period’ in which no decrease in Si-O-C stretching intensity occurred. This showed that the silane was initially stable to hydrolysis in solution for the duration of this induction period, which lasted approximately 4 hours.

The integrated intensity of the 710 cm^{-1} band of Y9669 which appeared during hydrolysis is plotted *versus* time in figure 5.9.

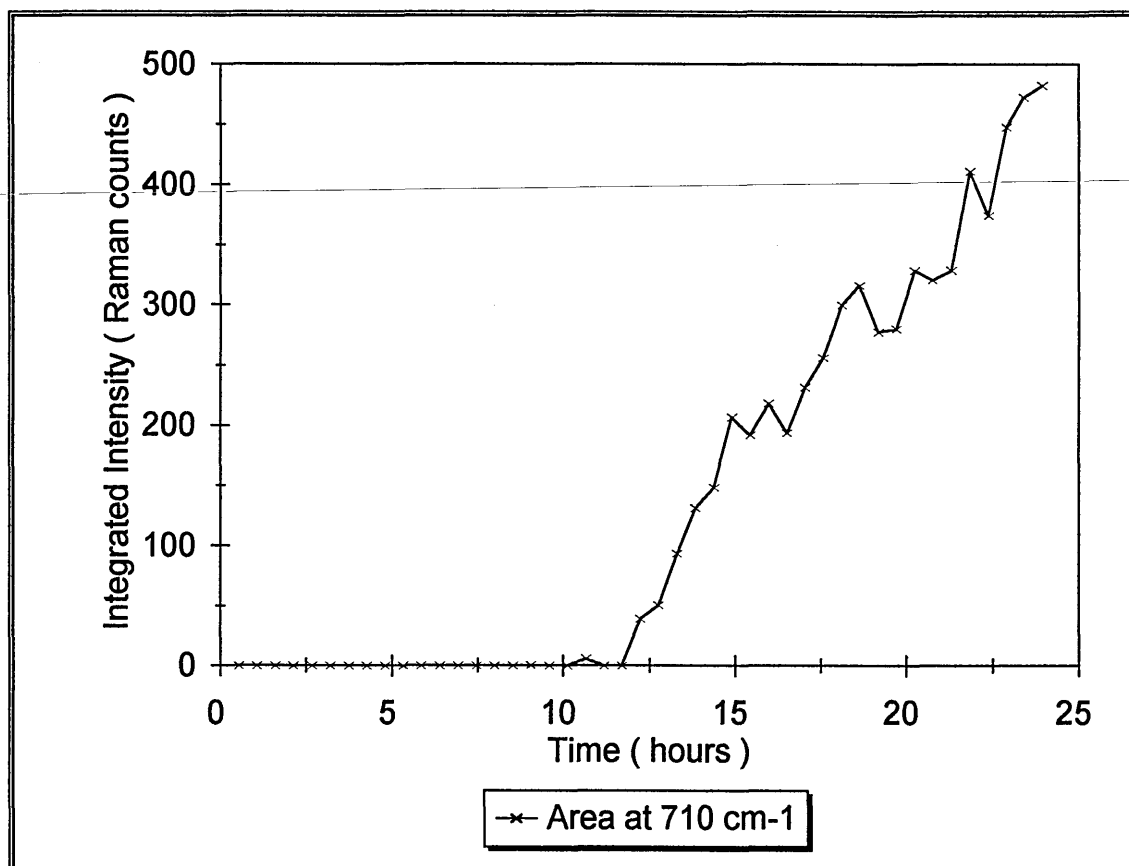


Figure 5.9 : The integrated intensity of the 710 cm^{-1} band of Y9669 plotted vs. time in the hydrolysis solution

Figure 5.9 shows that the band at 710 cm^{-1} appeared after a total hydrolysis time of 10 to 12 hours. Shih and Koenig¹ assigned a band at 710 cm^{-1} in methacryl silane to Si-O stretching in triply hydrolysed silane. Therefore we have assigned the band in Y9669 at 710 cm^{-1} to Si-O stretching of the triply hydrolysed silane. The combination of the decrease of the bands due to unhydrolysed silane (figure 5.7 and figure 5.8) and the increase of the band due to triply hydrolysed silane shows that the hydrolysis occurs over a time-scale of several tens of hours, the first silane molecules becoming totally hydrolysed only after 10 hours in the hydrolysis solution.

It is noteworthy that bands due to intermediate products, i.e. singly or doubly hydrolysed Y9669, were not seen. This implies that hydrolysis of the completely unhydrolysed silanes was slow compared with hydrolysis of the intermediate products to give the triply hydrolysed form of Y9669. This agrees with the suggestion made by Riegel et. al.¹² that the singly and doubly hydrolysed silanes are very reactive towards hydrolysis compared to the unhydrolysed material.

5.3 : A1110 Hydrolysis Results

In order to assess the hydrolysis of [3-(amino)propyl]trimethoxysilane (A1110, see figure 1.1), a 25 % solution was made up as described above, rapidly mixed, and then placed under the microscope. The extended Raman spectrum of the A1110 was taken every 10 minutes, in the range 350 to 1700 cm^{-1} . The spectra were taken until a total time of 24 hours had elapsed. The first and last spectra are shown in Figure 5.10.

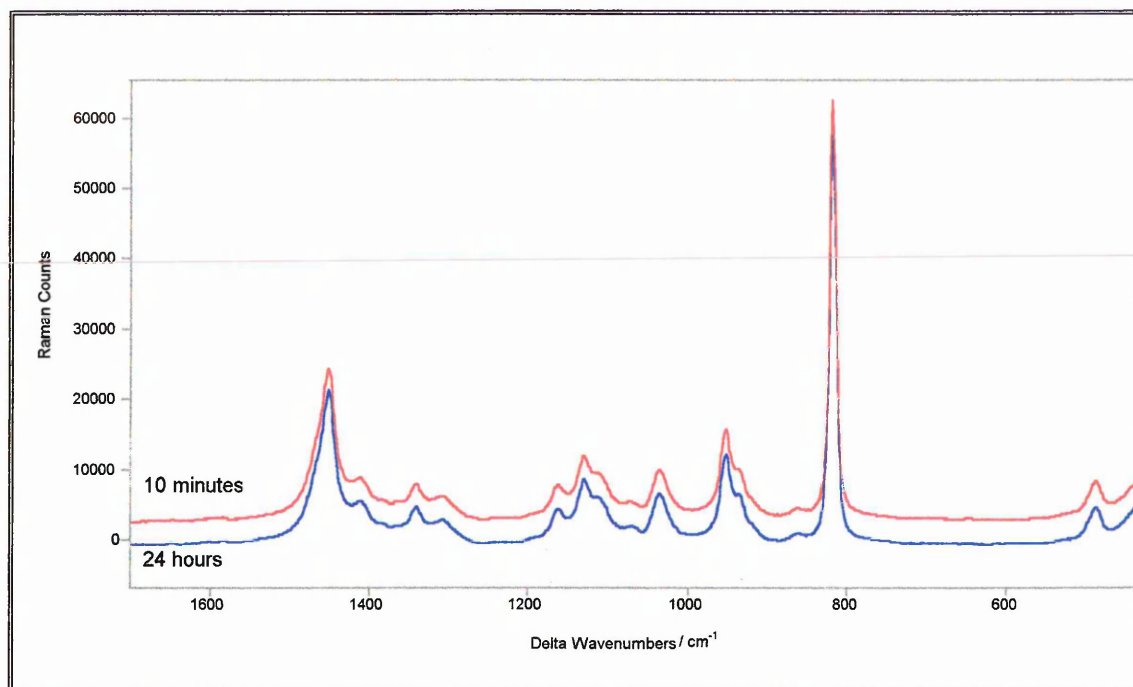


Figure 5.10 : The spectra of A1110 in a 25% aqueous alcohol solution after 10 minutes and 24 hours. The spectra have been offset in the Y-axis.

Figure 5.10 shows that the spectra of A1110 in the hydrolysis solution after 10 minutes and 24 hours were identical. One possible interpretation is that in acidic aqueous alcohol solution, no hydrolysis occurs, at least between 10 minutes and 24 hours after mixing. However, it can also be seen that the two bands assigned by Ishida to Si-O-C stretching at 612 cm^{-1} at 640 cm^{-1} are not present. This indicates that hydrolysis had already occurred in the first spectrum. If hydrolysis had occurred followed by condensation, then bands appearing and increasing in intensity due to the condensation products would have been seen. However, no increasing bands were seen, suggesting that condensation did not occur in this experiment. This agrees with the results found by Plueddemann¹³ who found that, in the case of 3-aminosilanes in aqueous solutions, hydrolysis occurred very quickly, but that the silane was then extremely stable to condensation. Morrall and Leyden found that A1100 (the ethoxy analogue of A1110)

hydrolysed and condensed in studies of neat silane exposed to atmospheric water, but that only hydrolysis (no condensation) occurred when A1100 was studied in solution, over the time-scale of the experiment (also 24 hours).

It is thought that the initial rapid hydrolysis is caused by the catalysis of the reaction by the amine group of A1110^{3,13}. The hydrolysed silanes are then stabilised due to an intramolecular hydrogen-bonded ring structure¹⁴. Plueddemann proposed two possible ring structures of the 3-aminosilanes showing this behaviour, which are reproduced in figure 1.8. Comparison of this figure with figure 1.1 suggests an explanation for A1110 showing this behaviour while Y9669 does not. Both structures in figure 1.8 rely on the silane being able to form an internal ring, allowing the Si-O and N-H bonds coming close to each other. This would be considerably less likely with the very large and rigid phenyl ring attached to the amine group. Therefore it is believed that it is this steric effect which prevents Y9669 showing the same hydrolysis and condensation behaviour as A1110.

5.4 : A1891 Hydrolysis Results

In order to assess the hydrolysis of [3-(mercapto)propyl]triethoxysilane (A1891, see figure 1.1), a 25 % solution was made up as described above, rapidly mixed, and then placed under the microscope. The extended Raman spectrum of the A1891 was taken every 10 minutes, in the range 450 to 1100 cm^{-1} . The spectra were taken until a total time of 20 hours had elapsed. The first and last spectra are shown in Figure 5.11, including a blown-up spectrum of the 600 to 700 cm^{-1} region.

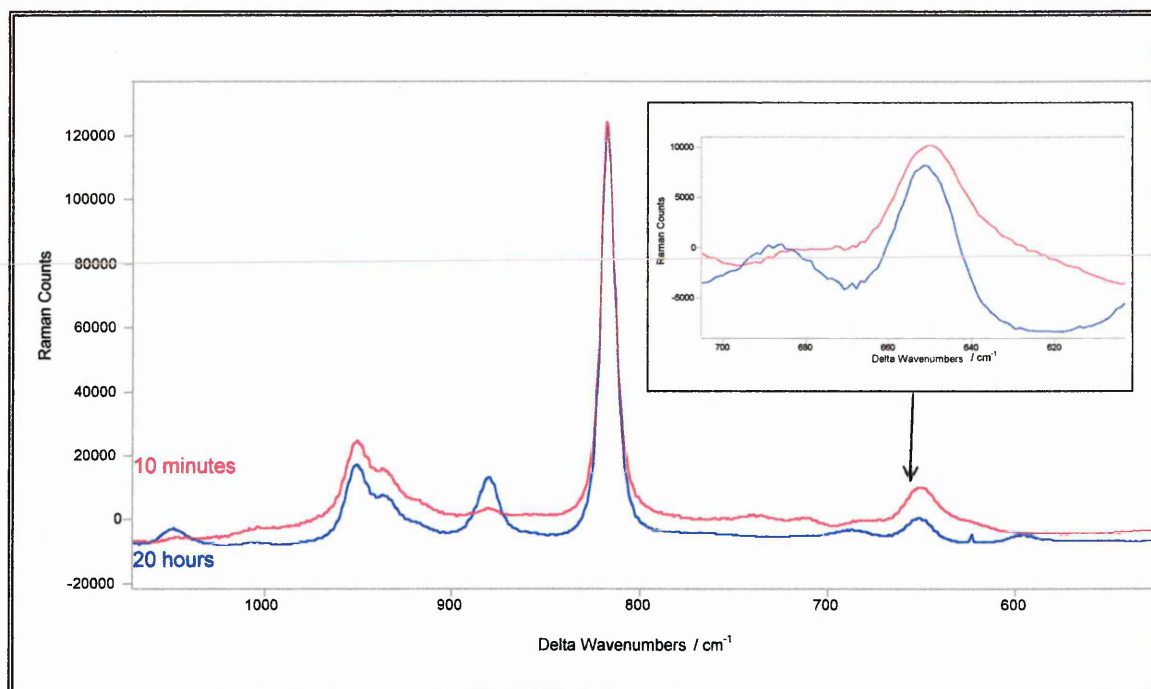


Figure 5.11 : The spectra of A1891 in 25% aqueous alcohol solution after 10 minutes and 20 hours

Figure 5.11 shows that unlike in the case of A1110, considerable changes occur in the spectrum of A1891 in the hydrolysis solution between 10 minutes and 20 hours after mixing. Ishida has assigned a band at 639 cm^{-1} of [3-(mercapto)propyl]triethoxysilane(i.e. A189, the methoxy analogue of A1891) to Si-O-C stretching of the unhydrolysed material. In other organosilanes, this band increases in frequency by 10 to 15 cm^{-1} on changing from the methoxy to the ethoxy form. Therefore, we have assigned the band in A1891 at 650 cm^{-1} to the Si-O-C stretching mode of the unhydrolysed material. It can be seen from Figure 5.11 that this band decreases in intensity over the reaction time, indicating that hydrolysis occurs. In order to show in more detail how this band changes over time, the integrated intensity of the band was obtained by using a curve-fitting routine. The integrated intensity of the band versus experiment time is plotted in Figure 5.12.

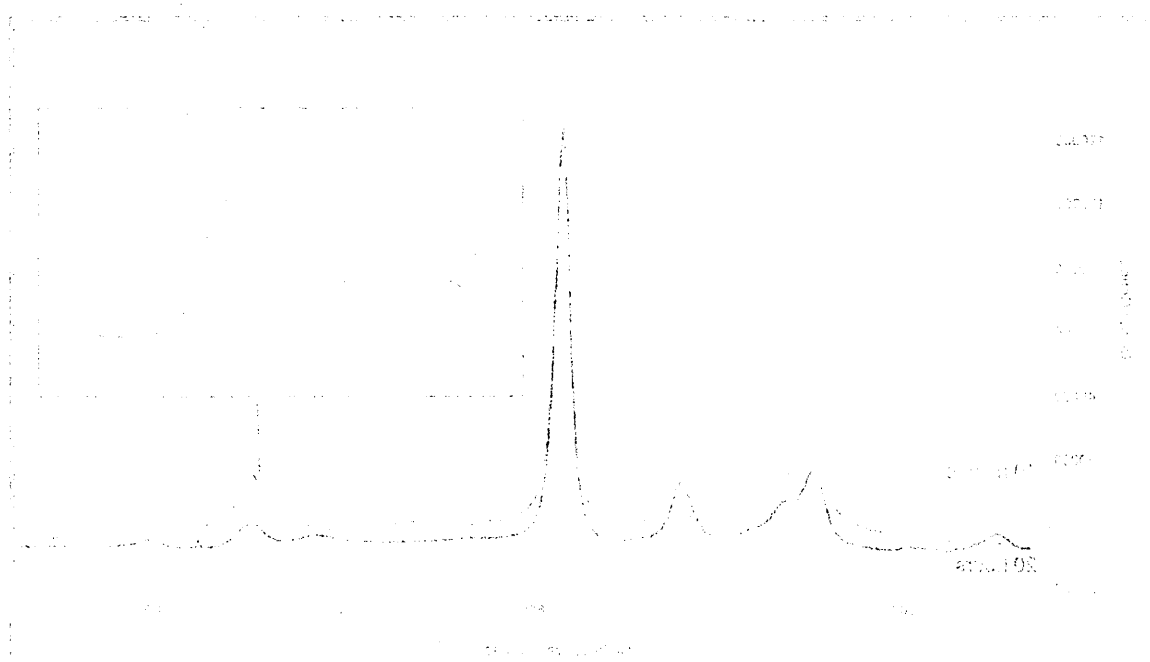


Figure 1. ¹³C NMR spectrum of the poly(2-vinylpyridine) (P2VP) sample. The spectrum shows a broad peak at approximately 170 ppm, which is characteristic of the carbonyl group in the polymer backbone. The x-axis represents the chemical shift in ppm, ranging from 0 to 200. The y-axis represents the intensity of the signal.

The ¹³C NMR spectrum of the poly(2-vinylpyridine) (P2VP) sample shows a broad peak at approximately 170 ppm, which is characteristic of the carbonyl group in the polymer backbone. The x-axis represents the chemical shift in ppm, ranging from 0 to 200. The y-axis represents the intensity of the signal. Other significant peaks are observed at approximately 155, 135, 115, and 75 ppm, corresponding to different carbon environments in the polymer chain. A small peak is labeled '201.08' at the far right of the spectrum.

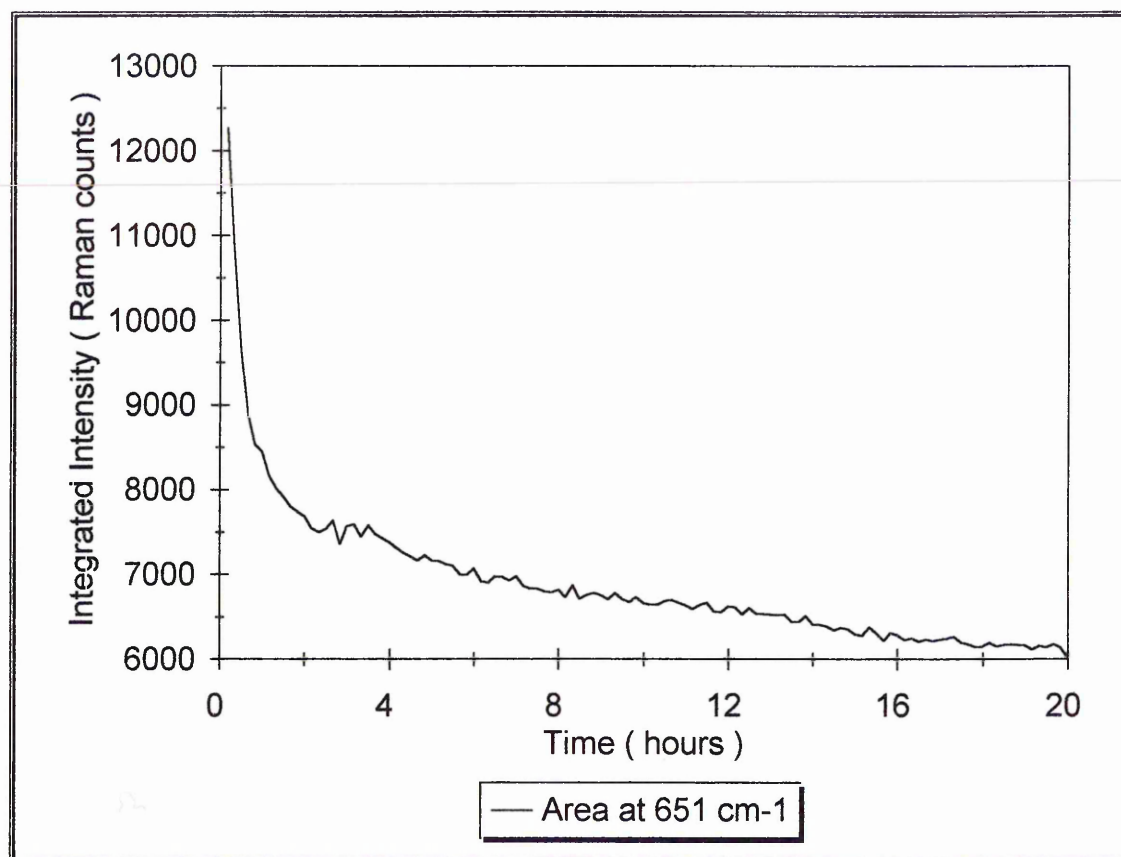


Figure 5.12 : The intensity of the 651 cm^{-1} band of A1891 vs. time in aqueous alcohol solution

Figure 5.12 shows that the intensity of the Si-O-C stretching band decreased very rapidly at first, and more slowly after about 2 hours. However, the band did not reach a true equilibrium, but continued to decrease in intensity throughout the time of the experiment. This showed that a large number of the available ethoxy groups were hydrolysed quickly, and hydrolysis then slowed, but continued at a steady rate. It is also worth noting that even after 20 hours, half of the initial intensity of the Si-O-C stretching band still remains, indicating that a large number of ethoxy groups remain unhydrolysed.

Figure 5.11 also shows a band at about 683 cm^{-1} which increased in intensity from the first to the last spectra. A band at 672 cm^{-1} was assigned by Shih and Koenig¹ to triply hydrolysed silane in vinyl silane, and it was assumed here that the band at 683 cm^{-1} in A1891 could be assigned to triply hydrolysed A1891. The intensity of this band versus time in the solution is shown in Figure 5.13.

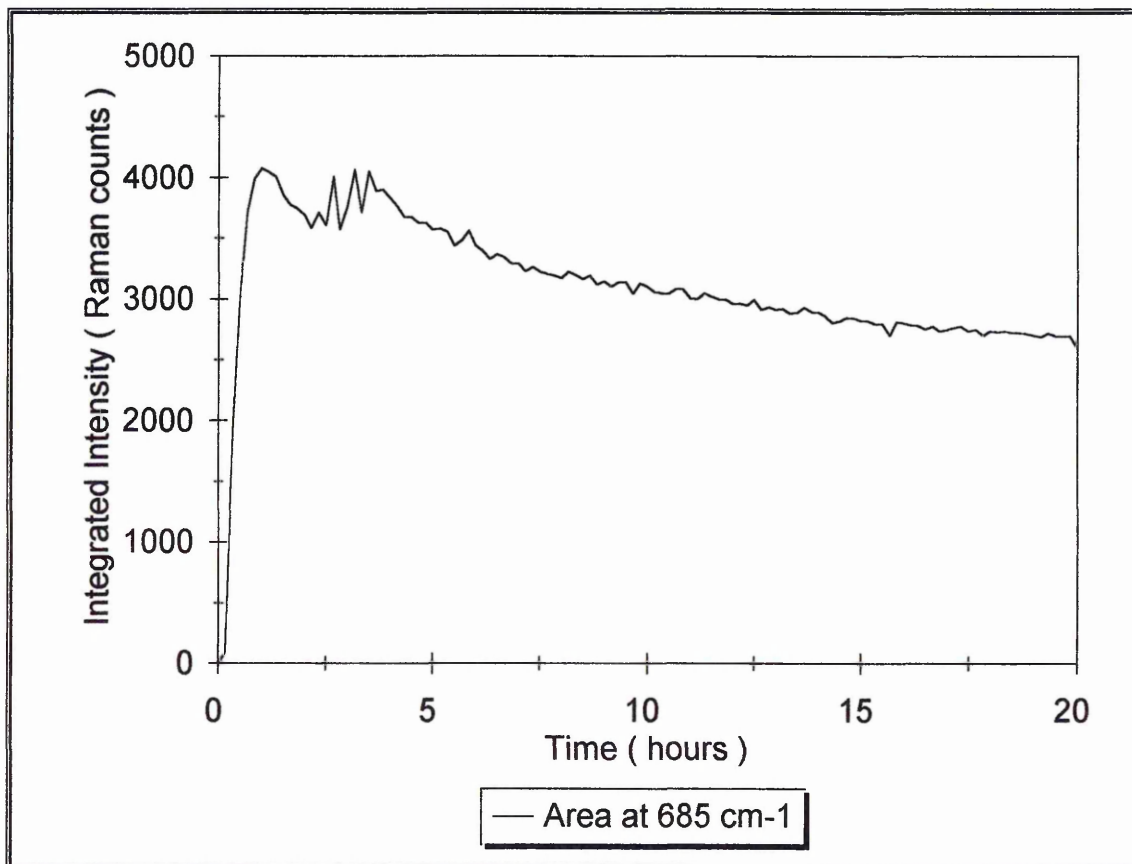


Figure 5.13 : The intensity of the 685 cm^{-1} band of A1891 vs. time in aqueous alcohol solution

Figure 5.13 shows that the 685 cm^{-1} band of A1891 initially increased quickly after mixing in the hydrolysis solution, and then decreased slowly in intensity throughout the experiment. This is consistent with the assignment of this band to triply hydrolysed silane, which would be expected to start with zero intensity and increase in intensity as hydrolysis

progresses. The decrease in intensity must have been due to condensation of the trisilanols formed.

It is interesting to compare the results obtained in the case of A1891 with those found for Y9669. In both cases a band assigned to Si-O stretching of triply hydrolysed silane was observed to appear in the course of the experiment. However, in the case of A1891, it increased in intensity very rapidly and then decreased slowly, and in the case of Y9669 it appeared only after 10 hours, and did not reach a maximum over the timescale of the experiment. Similarly, the decrease in intensity of the bands assigned to Si-O-C stretching in unhydrolysed silanes occurred much more quickly in the case of A1891 than in Y9669. This is somewhat surprising, as from the literature it might be expected that the amino silane would hydrolyse much more quickly. However, the experiments described here were carried out in the presence of acid catalyst. It would appear that, with an external catalyst, the mercaptosilane may hydrolyse faster than the amino silane Y9669.

It can be seen from Figure 5.11 that two other bands at 880 cm^{-1} and at 1048 cm^{-1} appeared during the experiment. The integrated intensities of these bands are plotted versus time in Figure 5.14 and Figure 5.15.

It is interesting to compare the results obtained in the case of A1891 with those found for Y9669. In both cases a band assigned to Si-O stretching of triply hydrolysed silane was observed to appear in the course of the experiment. However, in the case of A1891, it increased in intensity very rapidly and then decreased slowly, and in the case of Y9669 it appeared only after 10 hours, and did not reach a maximum over the timescale of the experiment. Similarly, the decrease in intensity of the bands assigned to Si-O-C stretching in unhydrolysed silanes occurred much more quickly in the case of A1891 than in Y9669. This is somewhat surprising, as from the literature it might be expected that the amino silane would hydrolyse much more quickly. However, the experiments described here were carried out in the presence of acid catalyst. It would appear that, with an external catalyst, the mercaptosilane may hydrolyse faster than the amino silane Y9669.

It can be seen from Figure 5.11 that two other bands at 880 cm^{-1} and at 1048 cm^{-1} appeared during the experiment. The integrated intensities of these bands are plotted versus time in Figure 5.14 and Figure 5.15.

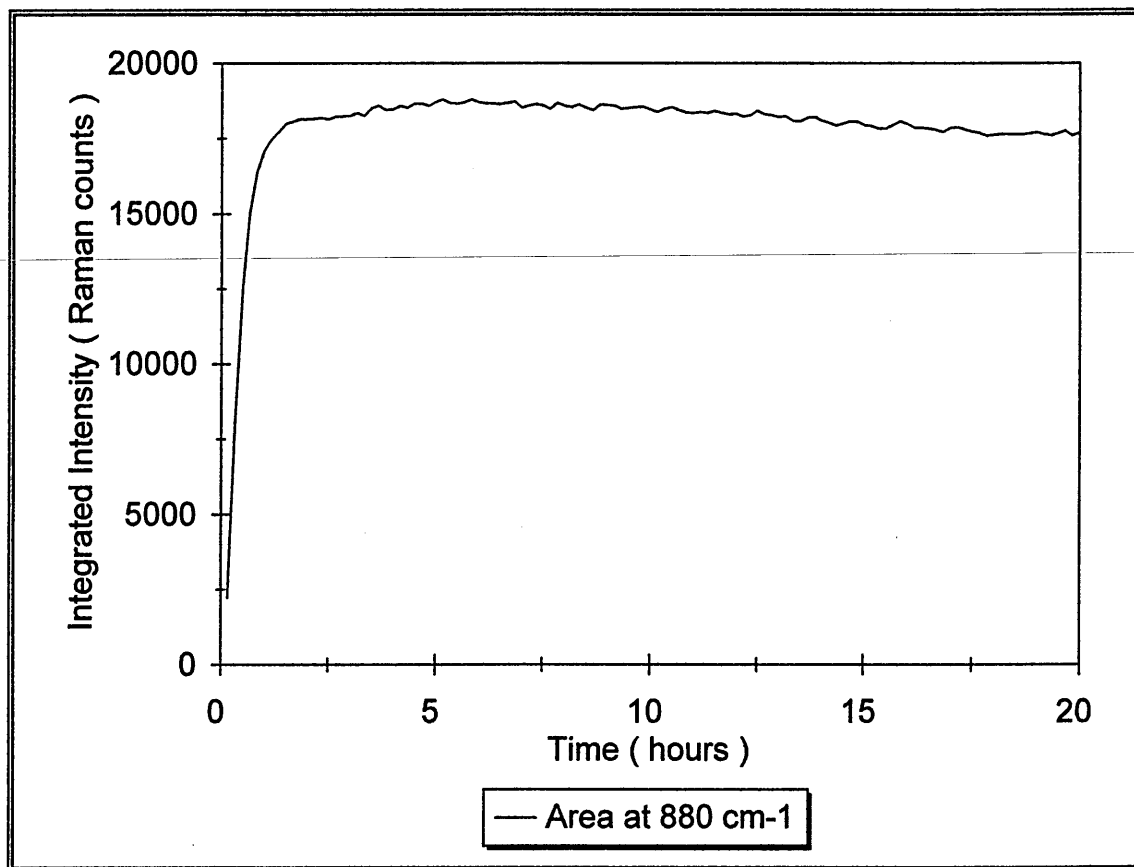


Figure 5.14 : The integrated intensity of the 880 cm^{-1} band of ethanol vs. time of A1891 hydrolysis

Figure 5.14 and figure 5.15 show that both the 880 cm^{-1} and 1048 cm^{-1} bands show the same kinetics, increasing rapidly in intensity, and then reaching equilibrium after about 2 hours. Clearly both bands arise from a product of hydrolysis. One of the major products of hydrolysis of A1891 is ethanol.. The spectrum of ethanol is shown in Figure 5.16.

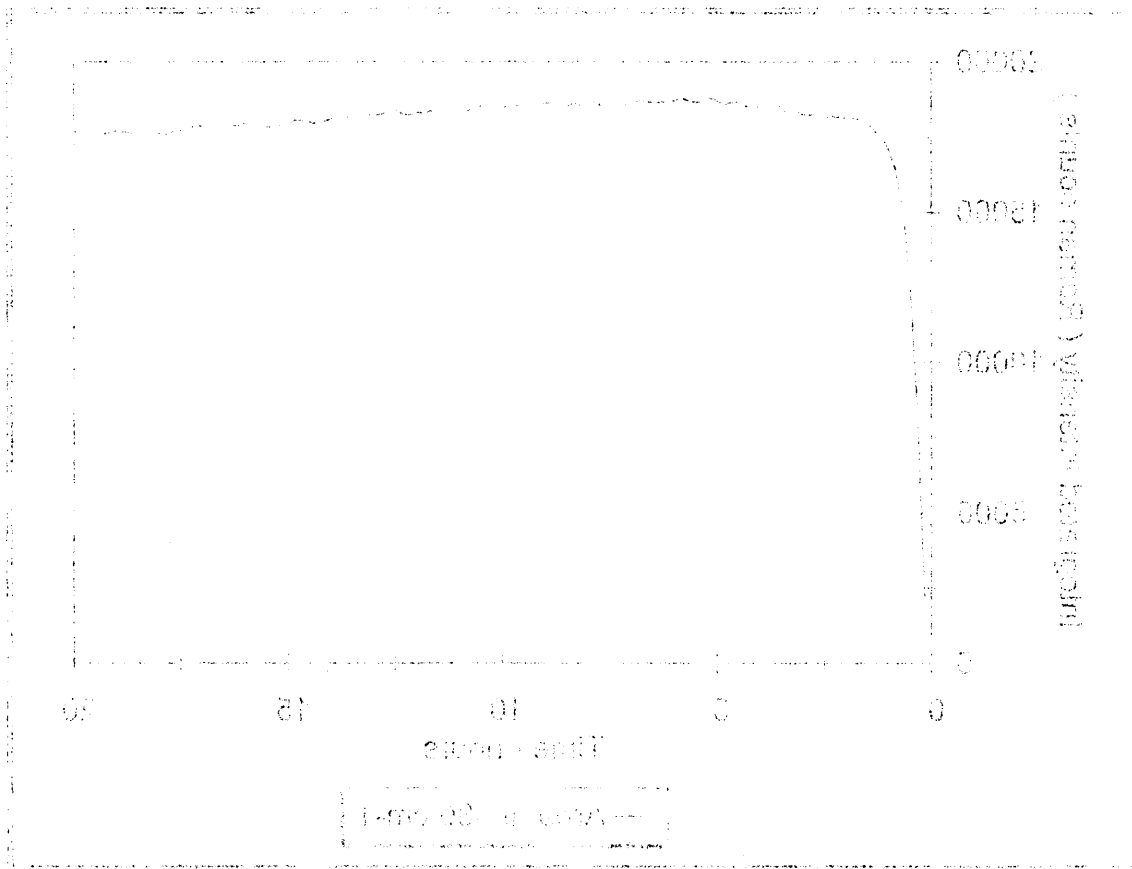


Figure 2.14: The measured weight percentage of a substance over time at 20°C. The weight percentage is 100% at 0 hours.

The weight percentage of a substance over time at 20°C is shown in Figure 2.14. The weight percentage is 100% at 0 hours and remains constant until about 18 hours. After 18 hours, the weight percentage decreases rapidly, reaching 0% at 24 hours. The weight percentage is 100% at 0 hours and 0% at 24 hours.

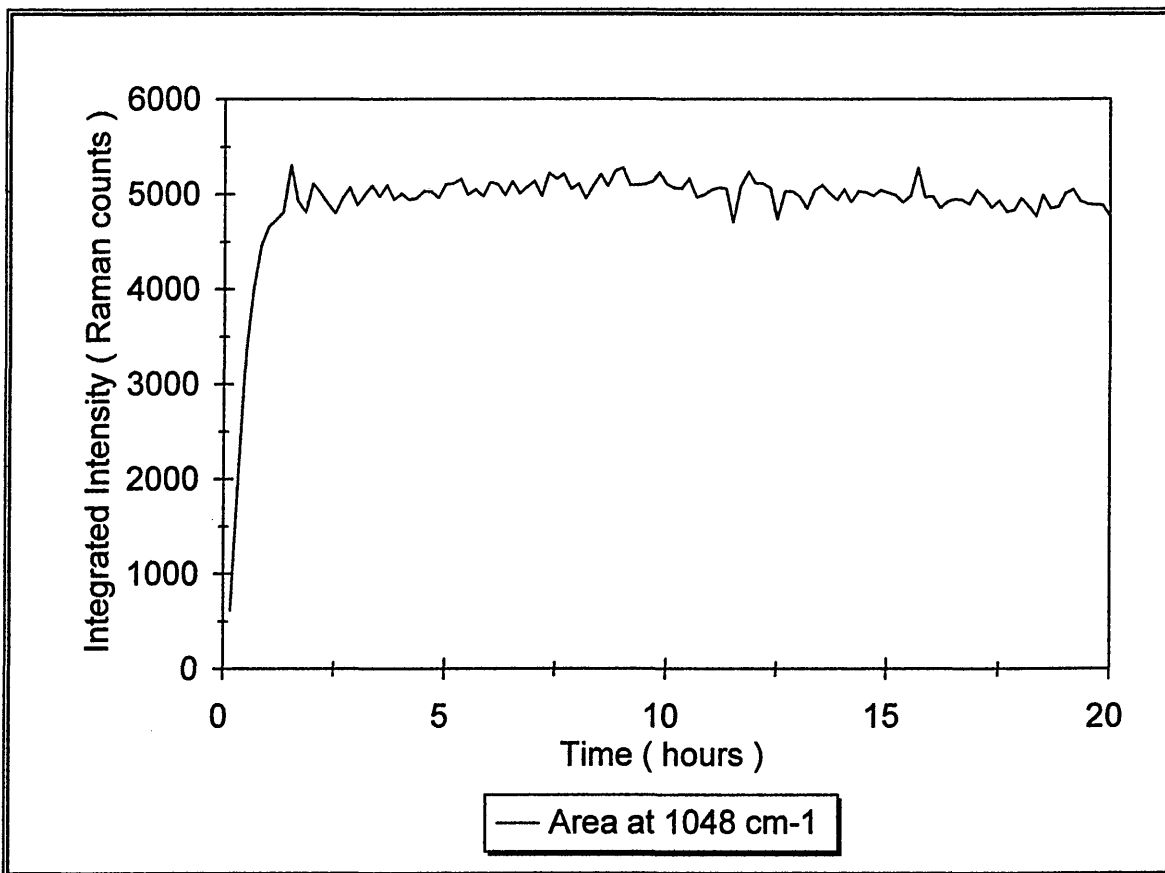


Figure 5.15 : The integrated intensity of the 1048 cm^{-1} band of ethanol vs. time of A1891 hydrolysis

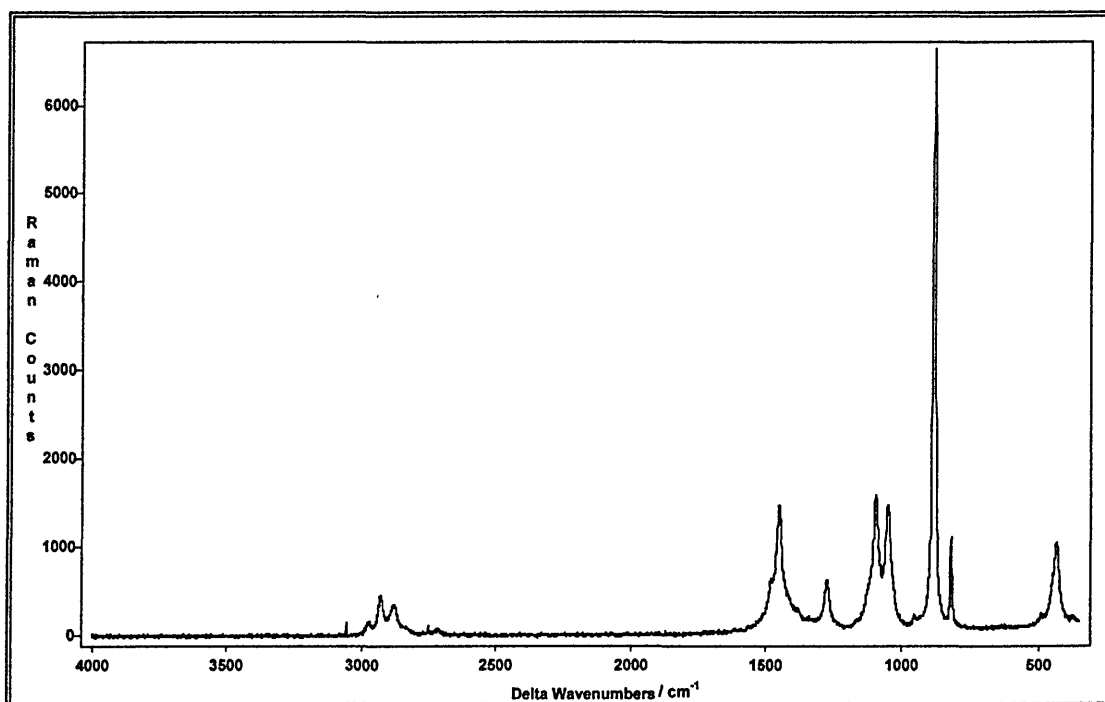


Figure 5.16 : The Raman spectrum of ethanol

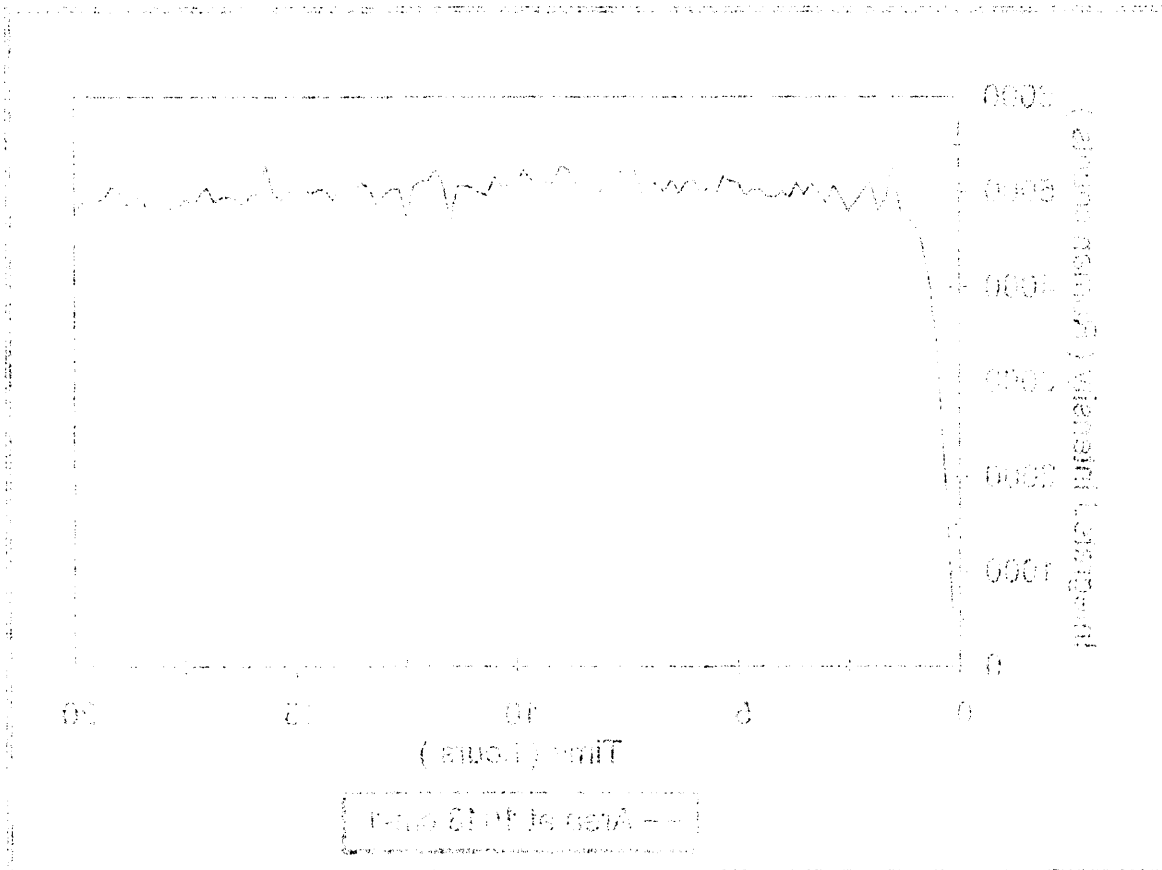


Рис. 1. Зависимость относительной концентрации мономера от относительной концентрации инициатора при $k_p \text{[M]}_0 \text{[I]}_0 t = 0.0002$.

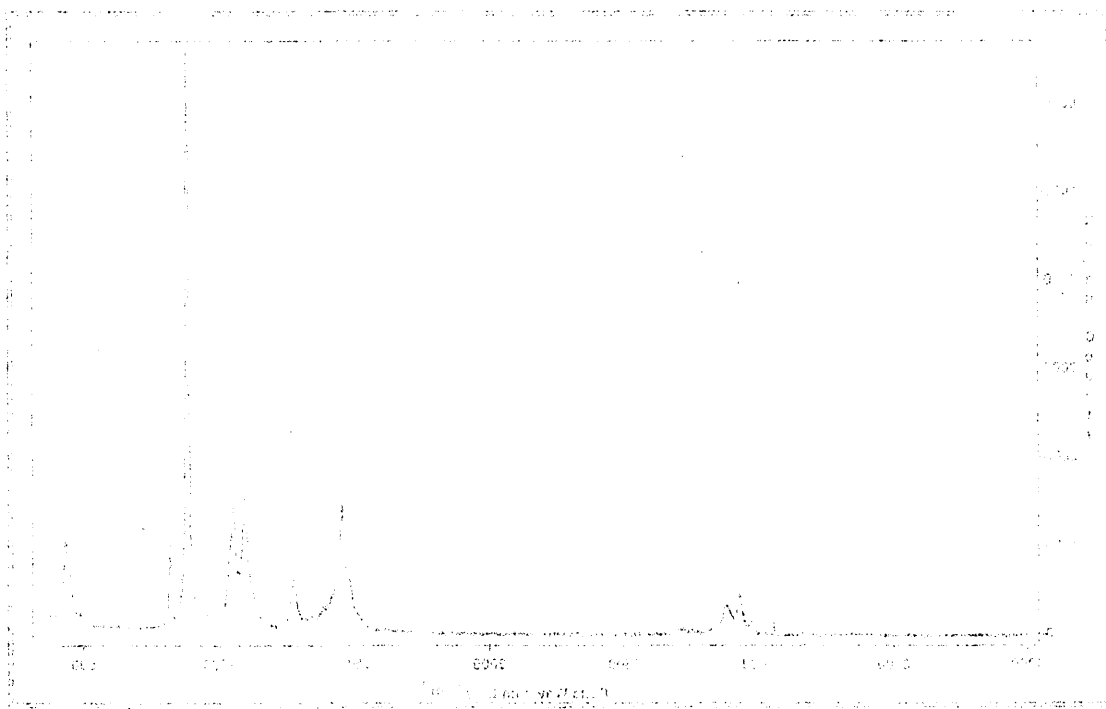


Рис. 2. Зависимость относительной концентрации мономера от относительной концентрации инициатора при $k_p \text{[M]}_0 \text{[I]}_0 t = 0.0002$.

Figure 5.16 shows that ethanol has a strong band at 880 cm^{-1} and a weaker band at 1048 cm^{-1} . These bands are assigned to the $\nu(\text{CO})$ stretching mode and $\nu(\text{CCO})$ stretching modes of ethanol, respectively. This ethanol is a product of hydrolysis of A1891, and the increase in intensity of this band is an alternative method of measuring hydrolysis. It is interesting to compare the shape of figure 5.12 with figures 5.14 and 5.15. One would expect, that if the ethanol is a product of the hydrolysis of A1891, that the two curves would show exactly the opposite trends. To a certain extent, this is true, as figure 5.12 shows a rapid decrease in intensity up to 2 hours time, and the ethanol bands show a rapid increase up to this time. However, the band due to unhydrolysed A1891 continues to decrease in intensity after this time, whereas the ethanol bands do not increase further, and decrease in intensity very slightly towards the end of the experiment. The ethanol produced must be going on to react further. It is not known what this reaction is, although it could be reaction with the acid catalyst which is present. However, this observation acts as a reminder that the system studied rapidly becomes very complex as hydrolysis progresses.

It is believed that one of the processes that may occur when lamination is carried out industrially using silane coupling agents is hydrolysis of the silane coupling agent by water present in the PVC interlayer. Furthermore, it is believed that this process may be vitally important to the success of the lamination process. In order to determine what parameters may be important for this process, several attempts were made to follow the process in model laminates, as were used in chapters 3 and 4. The strategy used was as follows. PVC films, cast onto silicon crystals, were exposed to known humidities to change the level of water present in the PVC. The laminates were then analysed by focusing the Raman

Figure 1.10 shows the effect of the addition of a small amount of a weak base to a solution of a weak acid. The pH of the solution increases from 3.75 to 4.75. The addition of a weak base to a solution of a weak acid results in a solution that is more basic. This is because the weak base reacts with the weak acid to form a weak conjugate base and a weak conjugate acid. The weak conjugate base is a stronger base than the weak acid, and the weak conjugate acid is a weaker acid than the weak acid. The overall effect is that the solution becomes more basic. The pH of the solution increases from 3.75 to 4.75. This is because the weak base reacts with the weak acid to form a weak conjugate base and a weak conjugate acid. The weak conjugate base is a stronger base than the weak acid, and the weak conjugate acid is a weaker acid than the weak acid. The overall effect is that the solution becomes more basic. The pH of the solution increases from 3.75 to 4.75.

It is important to note that the pH of the solution does not change if the weak base is added to a solution of a strong acid. This is because the strong acid is a much stronger acid than the weak acid, and the weak base is a much weaker base than the strong acid. The overall effect is that the solution remains acidic. The pH of the solution does not change if the weak base is added to a solution of a strong acid. This is because the strong acid is a much stronger acid than the weak acid, and the weak base is a much weaker base than the strong acid. The overall effect is that the solution remains acidic. The pH of the solution does not change if the weak base is added to a solution of a strong acid.

microscope at a fixed position in the PVC film, and spectra were continuously taken. The aim was to monitor the intensities of the Raman bands sensitive to hydrolysis and condensation as described in this chapter for *ex situ* experiments.

However, the *in situ* experiments were found to be complicated by several problems. Firstly, the change in intensity of the 'marker' bands due to hydrolysis was overlaid with changes in intensity due to diffusion of the silanes through the PVC. This was not considered an insurmountable obstacle since, in principle, the diffusion could be taken into account by measuring the hydrolysis band intensity as a ratio versus a band of the silane which was not sensitive to hydrolysis. Secondly, PVC has two extremely intense Raman bands at 635 and 614 cm^{-1} which overlap the SiOC stretching bands of the silanes (which were to be used for hydrolysis measurements). Attempts were made to separate the contributions of the bands from the two materials, but as the silane was present in lower concentrations than the PVC, and the bands were weaker, this was found to be very difficult. It was decided that this method was not a viable one for following the hydrolysis of silanes *in situ*. However, it was decided that it may be possible to follow the *in situ* hydrolysis indirectly by measuring the effect it had on the diffusion properties of the silanes. It was shown in chapter 3 that prehydrolysed silanes were observed to undergo slower diffusion to unhydrolysed silanes. Therefore it was decided to follow the diffusion in films with different water contents, to see if *in situ* hydrolysis would occur, and affect the diffusion properties.

As described in chapter 1, various authors^{3,5,15,16} have attempted to use simple kinetics in order to follow the hydrolysis of silanes in solution. However, as discussed by

Leyden and Atwater⁵, simple first and second order kinetics are not applicable to such complex systems. However, as various authors had reported pseudo-first and pseudo-second order kinetics^{3,5,16}, the logarithmic intensities and reciprocal intensities of the bands were plotted against time (i.e. first and second order plots), in order to see whether such kinetics were being seen in the results shown above. In none of these cases were straight line relationships seen. Therefore the hydrolysis of none of these silanes showed first or second order kinetics under the conditions seen here. Considering the work of Atwater and Leyden, this is not surprising, as it was shown that even in the case of a silane with a single hydrolysable group, second order kinetics were seen. Clearly, much more complex hydrolysis kinetics were seen here.

References

- 1 Shih, P. T. K. and Koenig, J. L., *Materials Science and Engineering* Vol. 20, p. 137 (1975)
- 2 Ishida, H., Chiang, C.-H. and Koenig, J. L., *Polymer* Vol. 23, p. 251 (1982)
- 3 Blum, F. D., Meesiri, W., Kang, H.-J. and Gambogi, J. E., *Journal of Adhesion Science and Technology* Vol. 5, No. 6 (1991)
- 4 Plueddemann, E. P., Ed. *Interfaces in Polymer Matrix Composites*, Academic Press, New York, (1974)
- 5 Leyden, D. E. and Atwater, J. B., *Journal of Adhesion Science and Technology* Vol. 5, No. 10, p.815 (1991)
- 6 Trens, P., Denoyel, R., and Rouquerol, J., *Langmuir* Vol. 11, No. 2, p. 551 (1995)
- 7 Morrall, S. W. and Leyden, D. E. in *Silanes, Surfaces and Interfaces*, Ed. by Leyden, D. E., Gordon and Breach (1985)
- 8 Boerio, F. J., Armogan, L. and Cheng, S. Y., *Journal of Colloid and Interface Science* Vol. 73, No. 2 (1980)
- 9 Kurth, D. G. and Bein, T., *Langmuir* Vol. 11, No. 2, p.579 (1995)
- 10 Miller, J. D., and Ishida, H. in *Chemically Modified Surfaces*, Ed. by Leyden, D. E., Gordon and Breach (1986)
- 11 Hoh, K.-P., Ishida, H. and Koenig, J. L., *Polymer Composites* Vol. 9, No. 2 (1988)
- 12 Riegel, B., Blittersdorf, S., Kiefer, W., Hofacker, S., Müller, M. and Schottner, G., *Journal of Non-Crystalline Solids* Vol. 226, p. 76 (1998)
- 13 Plueddemann, E. P., in *Chemically Modified Surfaces*, Ed. by Leyden, D. E., Gordon and Breach (1986)

- 14 Plueddemann, E. P., Silane Coupling Agents, Plenum Press, New York, (1991)
- 15 Pohl, E. R and Osterholz, F. D., in Molecular Characterisation of Composite Interfaces, Ed. by Ishida, H. and Kumar, G., p. 157, Plenum Press, New York (1985)
- 16 Savard, S., Blanchard, L. P., Leonare, J. and Prud'homme, R. E., Polymer Composites Vol. 5, p. 242 (1984)

Chapter 6 : Studies of organosilane diffusion in humidity - controlled films

In order to determine whether the presence of water in PVC films could affect the diffusion properties of silanes in the films, experiments were carried out using films that had been exposed to known humidities. It was thought that the silane might hydrolyse whilst undergoing diffusion, and this would change the diffusion properties. It was shown in chapter 3 that prehydrolysed silanes showed different diffusion properties to fresh, unhydrolysed silanes. The diffusion of the silanes in humidity - controlled films was studied by both ATR - FTIR spectroscopy and Raman microscopy.

6.1 : Experimental

6.1.1 : Materials

The silane used for the experiments was , [3-(phenylamino)propyl]trimethoxysilane (Y9669, see figure 1.1). This was chosen firstly because it was shown in chapter 3 that Y9669 diffusion was highly sensitive to prehydrolysis, at least in the case of heat - induced diffusion through unplasticised PVC. Secondly, Y9669 was chosen because the strong band at about 1600 cm^{-1} in both the infrared and Raman spectra (figures 3.5 and 4.1) and results in high spectral signal to noise ratio. The material has been described and the spectra shown in chapters 3 and 4. The material was handled in an inert nitrogen environment (in a glove bag) to prevent hydrolysis before the start of the experiment.

In the Raman experiments, films approximately 24 μm . thick were cast from DMF, as described in chapter 4. In the infrared experiments, films approximately 10 μm . thick were cast from DMF as described in chapter 3. In both cases the PVC contained 15% (w/w) DHA. This level of plasticiser was chosen to allow the diffusion to be followed at room temperature, but to make the diffusion sufficiently slow to allow the diffusion to be followed by Raman microscopy (which requires fairly long spectral acquisition times). The amount of water in the PVC was controlled by exposing the film to the vapour of saturated aqueous salt solutions. In one series of experiments, the film was exposed to the vapour of a saturated potassium carbonate solution ($\text{K}_2\text{CO}_3(\text{aq})$), which produces a relative humidity of 44% at 25 $^\circ\text{C}^1$. In the second set of experiments the films were exposed to the vapour of a saturated ammonium chloride solution ($\text{NH}_4\text{Cl}(\text{aq})$) which produces a relative humidity of 80% at 25 $^\circ\text{C}^1$. The films were exposed to the vapour by placing them alongside a beaker of the salt solution in a sealed desiccator jar. The films were left in the desiccator for 48 hours. It is well known that water vapour diffuses into PVC films^{2,3}, so it was assumed that this treatment would result in PVC films containing different concentrations of water. Another set of experiments used films which had not been exposed to controlled humidity; these films were therefore the same as the 15% DHA films used in the work described in previous chapters.

6.1.2 : Spectroscopic measurements

In the Raman experiments, the laminates were placed under the microscope as soon as the Y9669 had been applied and then the microscope was focused a distance of 6 μm .

above the interface between the PVC and the silicon substrate. Thus, silane diffusion into the film could be monitored as a function of time by measuring the increase in intensity of the silane bands. This experiment was therefore analogous to the ATR-FTIR experiments, and should show similar results. In this respect, it would have been preferable for the laser to have been focused at the silicon interface, but this was found to lead to very low signal, so the focus was moved into the film to increase the signal to noise ratio obtained, and thus decrease the spectral acquisition time required. Static spectra were obtained, centred at 1600 cm^{-1} . Spectra were obtained every 10 or 20 minutes. After the experiment had finished, a depth profile of the laminate was measured, as described in chapter 4. All Raman measurements used a $20\text{ }\mu\text{m}$. glass cover slip to prevent contamination of the microscope objective by the silane.

The infrared experiments were carried out in the same way as described in chapter 3. Y9669 was brushed onto the upper surface of the treated films, and the laminates then placed in the FTIR spectrometer. Spectra were measured every 5 minutes, co-adding 520 scans. The experiment continued for a total time of 6 hours.

6.2 : Raman analysis of Y9669 diffusion in PVC exposed to atmospheric conditions

In the first experiment, a film which was not exposed to known humidity was used. The results of the diffusion measurement using the Raman microscope are shown in Figure 6.1. Spectra were obtained every 5 minutes, for a total time of 9 hours. The results show

the integrated intensity (obtained by curve fitting) of the 1600 cm^{-1} band of Y9669 versus time.

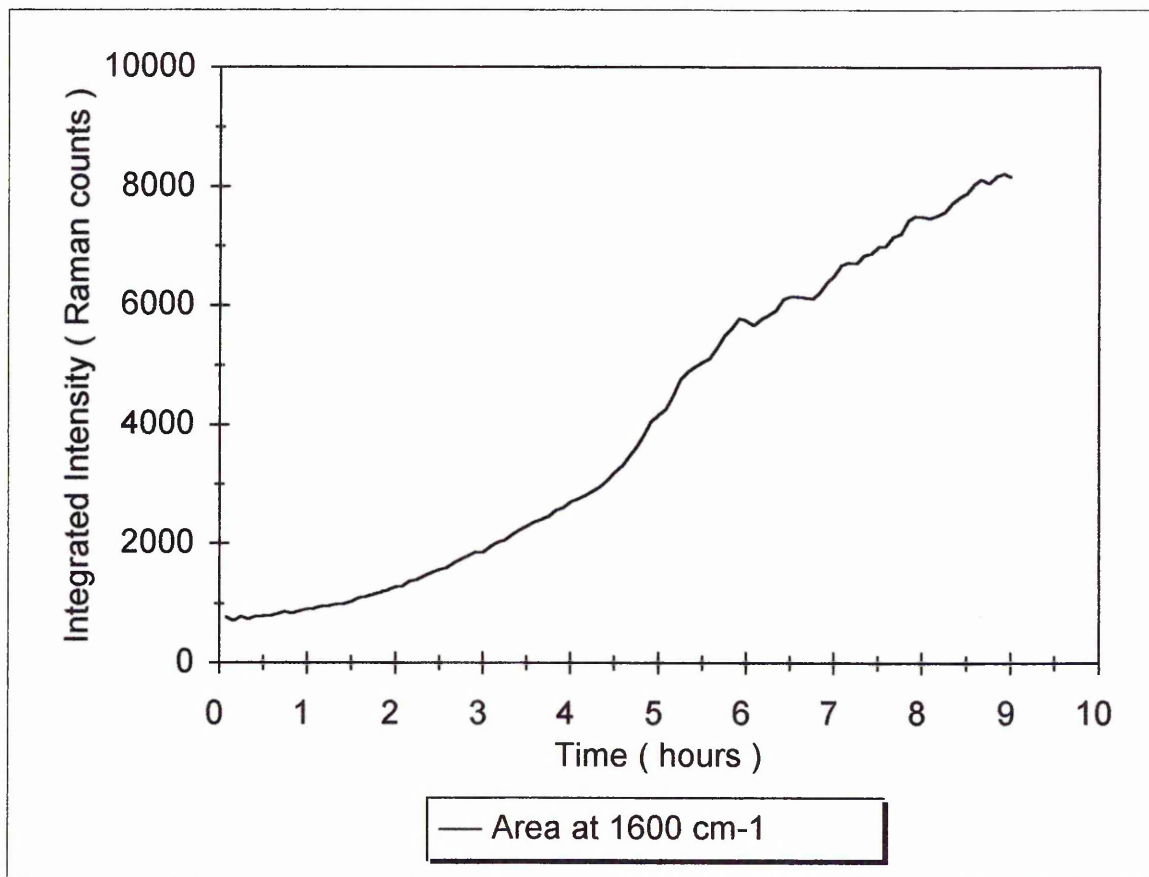


Figure 6.1 : The integrated intensity of the 1600 cm^{-1} Raman band of Y9669 vs. time $6\mu\text{m}$. above the interface. The film was exposed to normal atmospheric conditions

Figure 6.1 shows that the intensity of the silane band at the position $6\mu\text{m}$. above the bottom of the PVC film increased slowly at first, and then more rapidly. After 9 hours the intensity was still increasing, but the rate of increase appears to be just starting to decrease towards the very end of the experiment. It is supposed that an equilibrium was reached shortly after the end of the experiment. After this experiment, the microscope was set up in confocal mode and a depth profile was measured of the laminate in the same XY position

as the measurement described above. The depth profile was not obtained immediately after the measurements described above, but approximately 15 hours later. It is therefore assumed that the depth profile represents the equilibrium distribution of Y9669 in the PVC. The depth profile is shown in Figure 6.2.

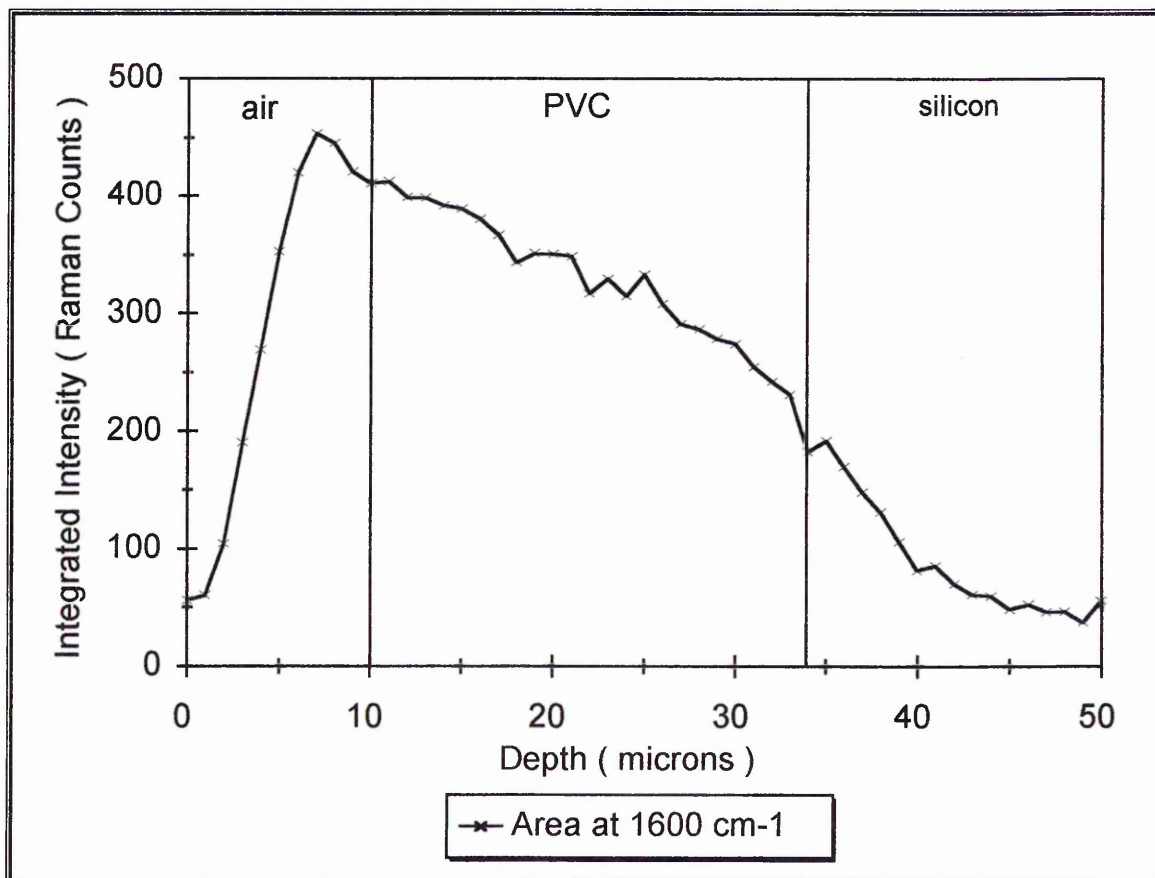


Figure 6.2 : The integrated intensity of the 1600 cm^{-1} Raman band of Y9669 vs. distance after diffusion was complete. The PVC was exposed to atmospheric conditions.

Figure 6.2 shows that the Y9669 had diffused throughout the film after 15 hours after the end of the kinetic experiment. The distribution of the silane is similar to that shown in chapter 4 in unplasticised PVC after annealing. There appears to be a small excess of silane at the upper surface of the PVC, which may indicate that not all of the Y9669 had diffused into the film.

6.2.1 : Infrared analysis of Y9669 diffusion in PVC exposed to atmospheric conditions

The infrared experiments described in this chapter were carried out in the same way as those described in chapter 3. The only difference was the humidity exposure of the PVC films. Therefore, in the case of the film exposed to atmospheric conditions (that is, no specific treatment) the experiment was exactly the same as one from chapter 3, namely Y9669 diffusion in PVC containing 15% DHA. Therefore, performing this experiment again provided a check on the consistency of the results. The integrated intensity of the 1602 cm^{-1} band of Y9669 has been plotted *versus* time in Figure 6.3. Figure 6.3 also shows the dual mode sorption fitting obtained.

Figure 6.3 shows that very similar results were obtained as when the experiments described in chapter 3 were carried out. The data fits quite well to the dual mode sorption model. The data was not found to show Fickian Case I diffusion kinetics. In Table 6.1 the diffusion coefficients from the equivalent experiments in chapter 3 are compared with the diffusion coefficients obtained from the above fitting.

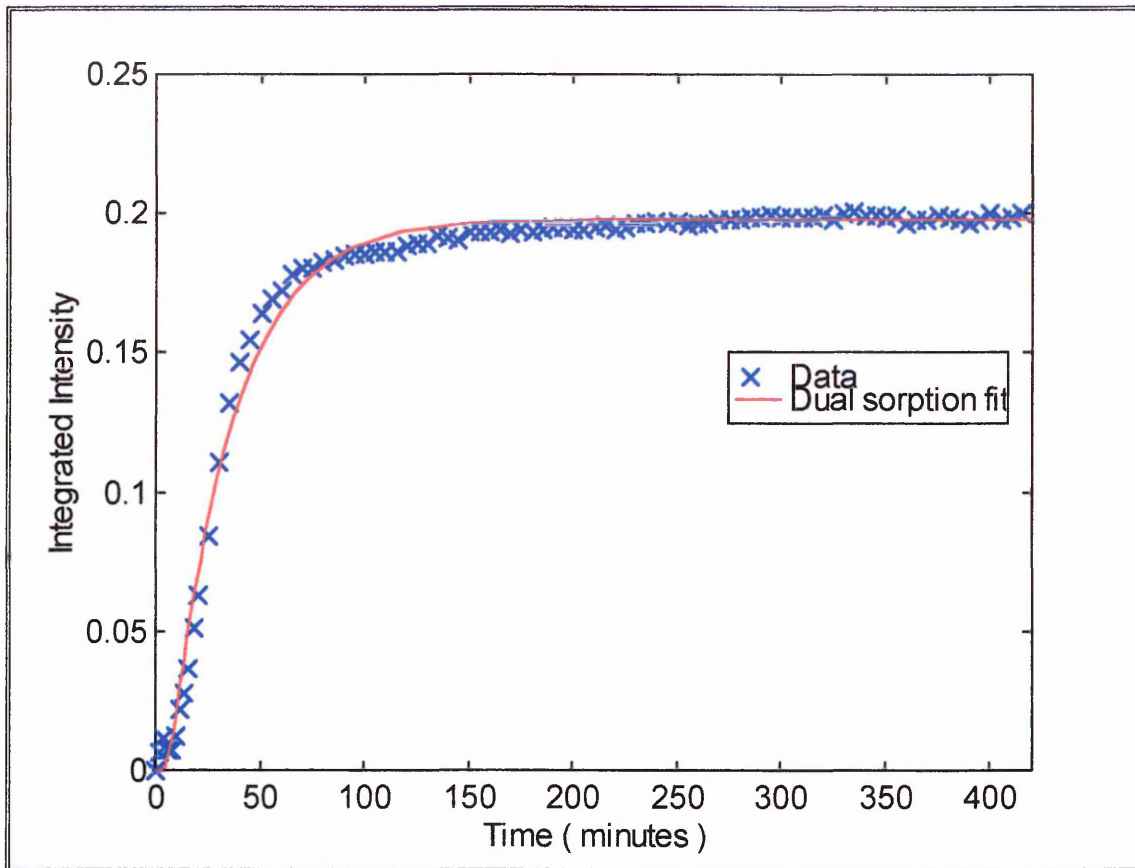


Figure 6.3 : The integrated Intensity of the 1600 cm^{-1} infrared band of Y9669 vs. time. The film was exposed to atmospheric conditions

Average result from Chapter 3	Result in Chapter 6
$D_1 = 8.96 \times 10^{-9}$	$D_1 = 9.92 \times 10^{-9}$
$D_2 = 8.55 \times 10^{-9}$	$D_2 = 4.62 \times 10^{-9}$
$X_1 = 0.69$	$X_1 = 0.51$

Table 6.1 : Comparison of results from chapter 3 and chapter 6

Table 6.1 clearly shows that the experiments yielded very similar results. These results will be discussed further later in reference to the results obtained when the films were humidity-controlled.

6.3 : Raman analysis of Y9669 diffusion in PVC exposed to $K_2CO_3(aq)$ vapour

In the second experiment, the 15% DHA plasticised PVC film was exposed to the vapour of K_2CO_3 for 48 hours before the experiment was carried out. This atmosphere had a relative humidity of 44 %. The film was 24 μm . thick. The spectra were taken every 10 minutes, and the total length of the experiment was 18 hours. The results of the kinetic Raman experiment are shown in Figure 6.4

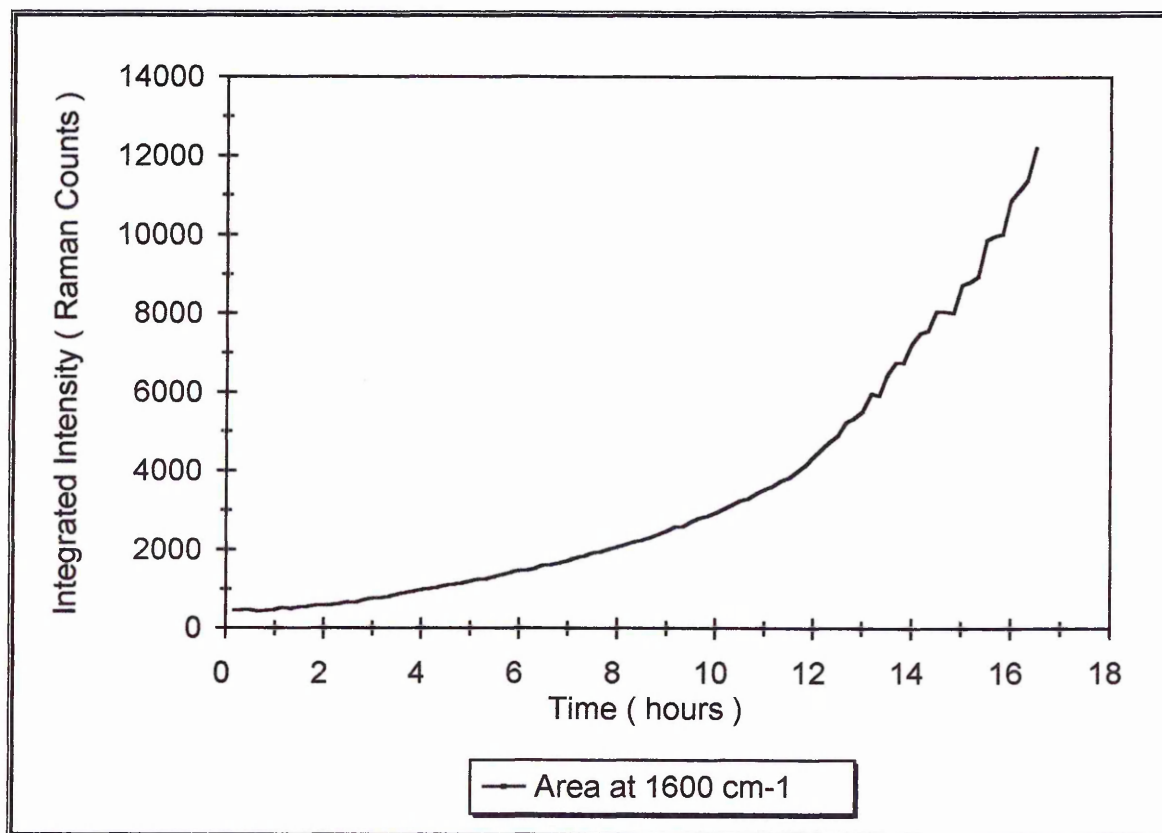


Figure 6.4 : The integrated intensity of the 1600 cm^{-1} Raman band of Y9669 vs. time. The film had been exposed to K_2CO_3 (Relative Humidity of 50%).

Figure 6.4 shows that the intensity of the 1602 cm^{-1} band of Y9669 initially increased slowly and then more quickly up to 16.5 hours after the start of the experiment. After this time, the spectra became so intense that the detector was saturated. This was initially surprising, but observation of the film after the end of the experiment showed a brown patch at the focal point of the laser, indicating that thermal degradation had occurred. This was presumably due to burning by the laser. This had not occurred in the depth profiling experiments described previously, as the focus of the laser was periodically moved (usually at least every 20 minutes). Clearly, with the use of the microscope in non-confocal mode, the intensity of the laser is such that the heat generated cannot be dissipated quickly enough, and degradation occurs. The depth profile could not be measured due to this degradation, as the intensity of the spectrum saturated the detector again. The effect of the degradation on the spectra was to cause a broad fluorescence background to appear, as shown in figure 4.5. The signal to noise ratio of the spectra was also reduced. This meant that although the curve fitted intensity of the silane bands was not affected by the degradation, eventually the baseline became so high that the peaks saturated the detector. This is shown in Figure 6.5, which shows one of the spectra of the degraded film.

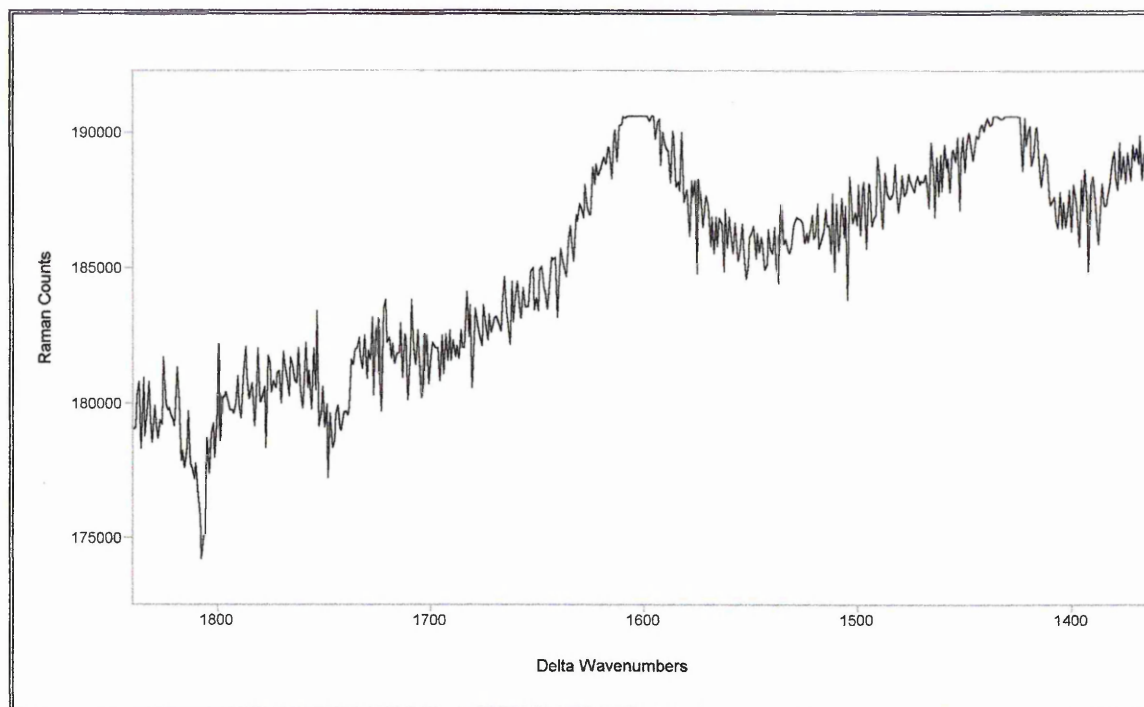


Figure 6.5 : Raman spectrum from kinetic study of Y9669 diffusion in $K_2CO_3(aq)$ treated film, showing poor S/N and saturation of detector.

Despite the premature end of the experiment, comparison of Figure 6.2 with Figure 6.1 shows that the diffusion was taking place much more slowly in the case of the film which had been exposed to the vapour of the solution of K_2CO_3 . This is presumably because water in the PVC film caused the silane to undergo hydrolysis in situ, possibly leading to condensation to siloxane oligomers, and slowing diffusion.

6.3.1 : Infrared analysis of Y9669 diffusion in PVC exposed to $K_2CO_3(aq)$ vapour

The infrared analysis of the film exposed to $K_2CO_3(aq)$ vapour was carried out in the same way as that exposed to atmospheric conditions. The film was 10 μm . thick. The

integrated intensity of the 1600 cm^{-1} band of Y9669 is shown in Figure 6.6. The plot also shows the dual mode sorption fit obtained.

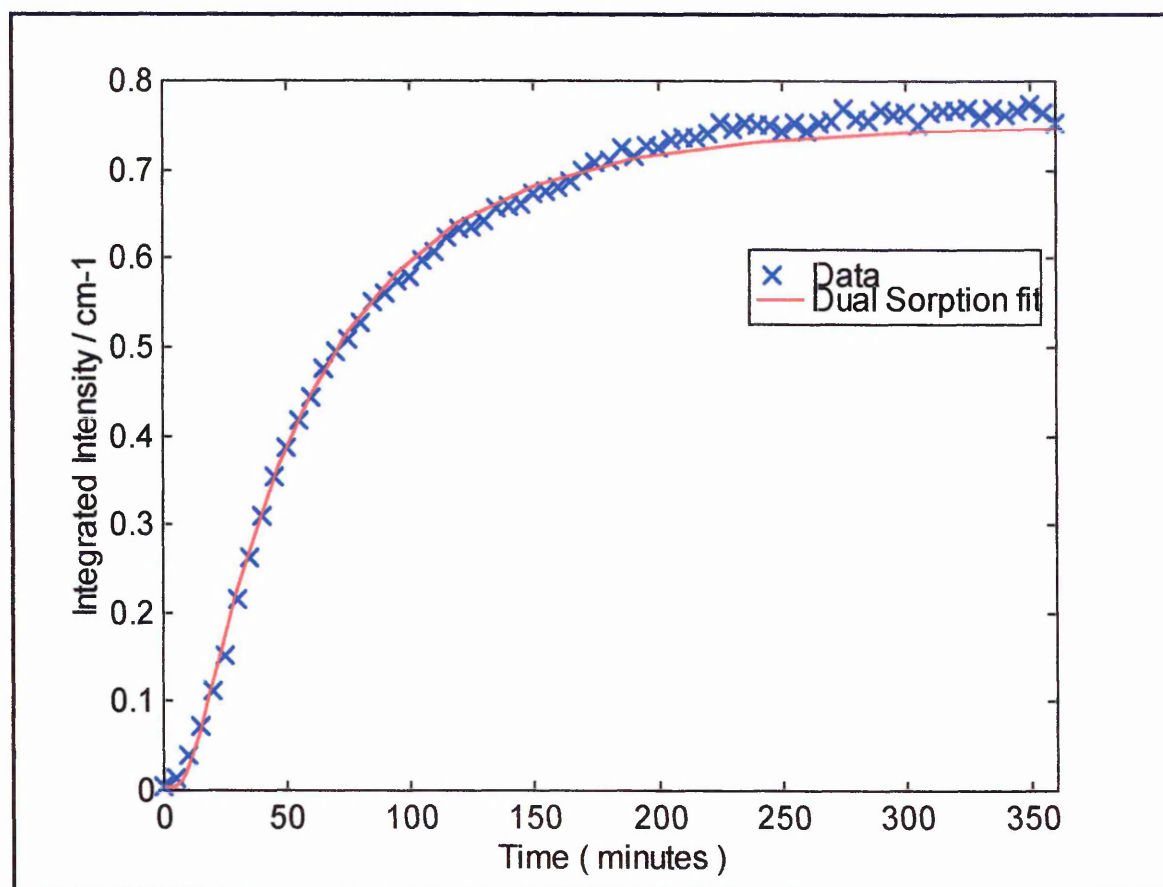


Figure 6.6 : The integrated intensity of the 1600 cm^{-1} infrared band of Y9669 vs. time. The film had been exposed to $\text{K}_2\text{CO}_3(\text{aq})$ (relative humidity 50%).

6.4 : Raman analysis of Y9669 diffusion in PVC exposed to $\text{NH}_4\text{Cl}(\text{aq})$ vapour

In the third experiment, the $24\ \mu\text{m}$. 15% DHA plasticised PVC film was exposed to the vapour of NH_4Cl for 48 hours before the experiment was carried out. This atmosphere had a relative humidity of 80 %. It was decided that it was desirable to measure the intensity of the band for longer than was possible in the previous experiment (

16.5 hours), as the diffusion had not reached equilibrium. Therefore the intensity of the laser was reduced to half of its maximum power by use of the laser attenuation filter wheel on the Ramascope. To compensate, longer scans were used. The results of the kinetic Raman experiment are shown in Figure 6.7. The spectra were taken every 20 minutes, and the total length of the experiment was 36 hours.

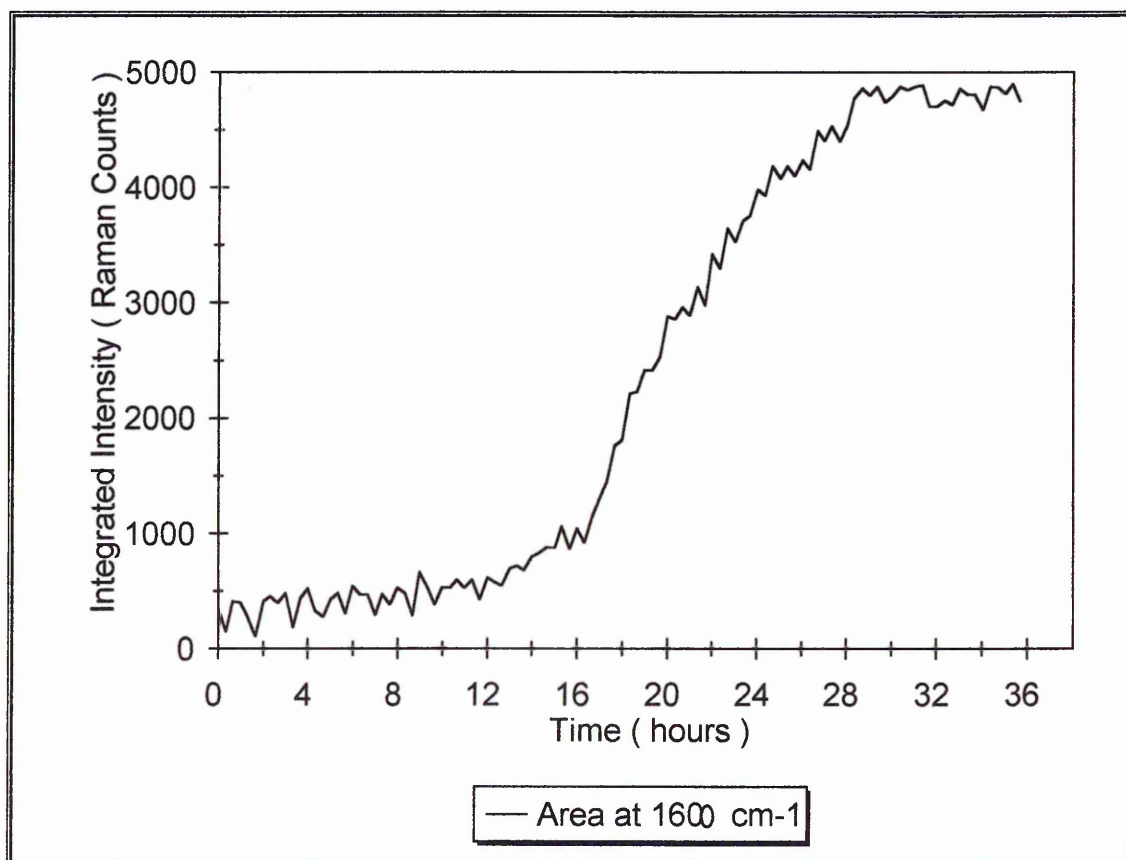


Figure 6.7 : The integrated intensity of the 1600 cm^{-1} Raman band of Y9669 vs. time. The film had been exposed to NH_4Cl (Relative Humidity of 90 %)

After the kinetic Raman experiment was complete, a Raman depth profile of the laminate was obtained, The plot of the integrated intensity of the 1600 cm^{-1} band of Y9669 *versus* distance is shown in figure 6.8.

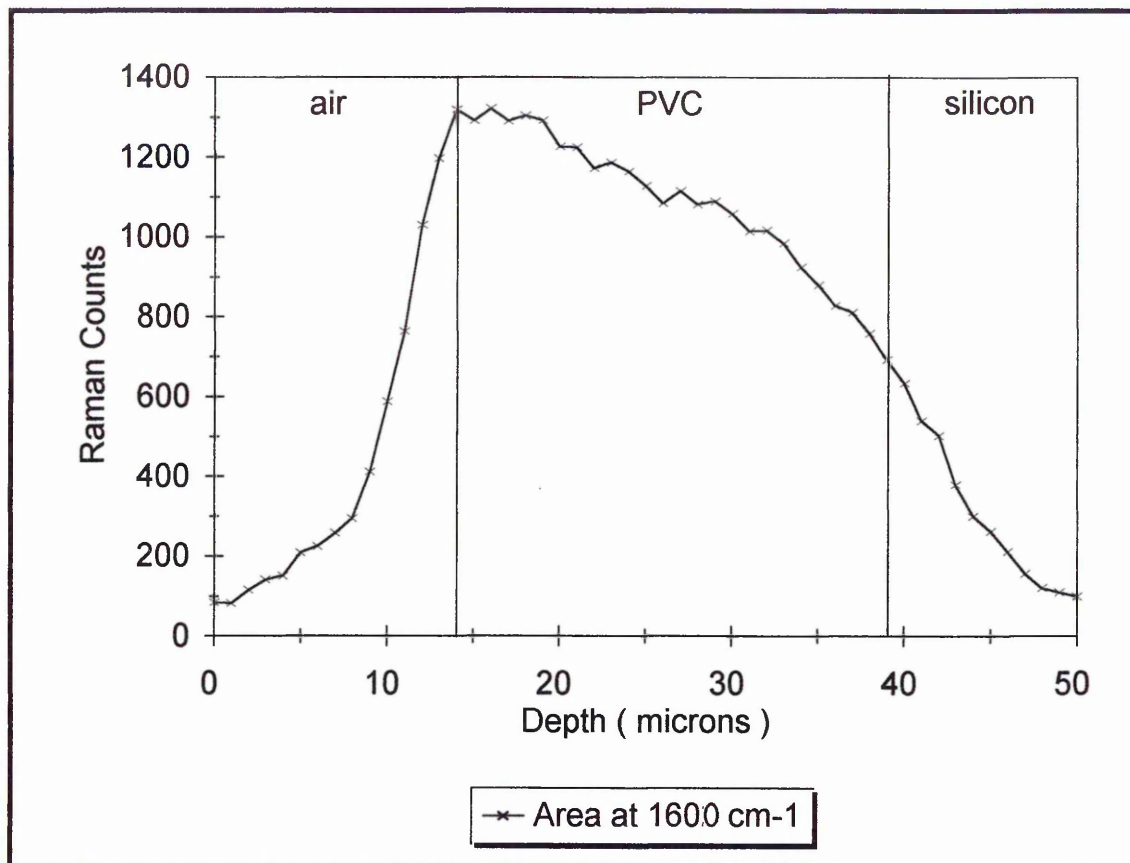


Figure 6.8 : The integrated intensity of the 1600 cm^{-1} band of Y9669 *versus* distance after diffusion into a film exposed to $\text{NH}_4\text{Cl}(\text{aq})$ vapour (relative humidity of 90 %)

Figure 6.7 shows that initially, the intensity of the 1600 cm^{-1} band of the Y9669 increased very slowly if at all. The increase in intensity then became faster, and eventually slowed and equilibrium appears to have been reached after about 28 hours. Clearly, reducing the laser power was successful in stopping degradation. It is assumed that the laser power was low enough so that almost all of the heat from the laser could be conducted away, as there was no sign of degradation in the film at all. Clearly, the diffusion seen in Figure 6.7 is slower than that in Figure 6.1, indicating that the presence of water in the film does slow diffusion of Y9669 through the film. Presumably this was due to hydrolysis of the silane *in situ*. As the diffusion was not observed to equilibrium in the

second experiment (Figure 6.4), comparison of the kinetics with those in the third experiment is not simple, but it would appear that the higher level of humidity that the film was exposed to in the later experiment slowed diffusion more than the lower level. It is interesting to note that the literature indicates that water may act as a plasticiser for PVC⁴, which may lead us to expect faster diffusion with higher level of water in the film. However, it appears that the effect of the water on silane condensation has more effect upon the diffusion rate than plasticising the PVC.

In order to provide some quantitative information on the change in diffusion properties upon treating the film with humidity control, the increase in intensity of the Y9669 band in the Raman kinetic analysis has been measured over a fixed time period for all three results. In order to do this, the integrated intensities of the band at 1600 cm^{-1} after 20 minutes, and 9 hours have been ratioed. The results are shown in Table 6.2 which show how much more intensity was detected by the microscope after 9 hours than in the first spectrum. For example, for the film treated by atmospheric conditions, the intensity was increased by approximately 11 times after 9 hours compared to its initial value.

Conditions	1600 cm ⁻¹ band area after 9 hours / initial area
Atmospheric Conditions	10.6
K ₂ CO ₃ (aq)	5.4
NH ₄ Cl(aq)	1.2

Table 6.2 : The increase in intensity of the 1600 cm⁻¹ Raman band of Y9669 after 9 hours for all three film treatments

Table 6.2 shows that compared to the initial intensities, the film treated at 50% relative humidity showed twice as much increase in Y9669 intensity as the treatment at atmospheric conditions, and the film treated at 80% relative humidity showed ten times as much increase. Clearly, humidity - controlled treatment of the films can dramatically change the diffusion kinetics of silanes in the films. It should be noted, however, that the response of the system to increased diffusion is not linear. This is because of the non-linear confocal profile of the instrument response. A small increase in the diffusion rate would therefore give rise to a greater relative increase in this ratio, so these results are not directly proportional to diffusion rates, and cannot be compared directly to diffusion coefficients.

Figure 6.8 shows that after diffusion the Y9669 was present throughout the PVC film. The depth profile looks very similar to that shown in Figure 6.2, but without the small excess of silane at the surface of the film, indicating that all of the silane diffused into the film. Due to the relatively non-reproducible nature of the application method of

the silane (It was brushed onto the PVC film by hand), it is possible that the surface excess was due to more silane having been applied to the film in the earlier experiment. That is, if more silane than can be absorbed by the film is applied, some appears to stay on the surface, leading to the small bump in silane intensity seen in Figure 6.2.

6.4.1 : Infrared analysis of Y9669 diffusion in PVC exposed to $\text{NH}_4\text{Cl}(\text{aq})$ vapour

The infrared analysis of the 10 μm . PVC film that had been exposed to $\text{NH}_3\text{Cl}(\text{aq})$ vapour was carried out as described for the previous films. The integrated intensity of the 1600 cm^{-1} band of Y9669 is plotted versus time in Figure 6.9.

Figure 6.9 shows that there was quite a long (ca. 20 minutes) induction period in the experiment during which little, if any, increase in the intensity from the Y9669 occurred. The intensity then increased and eventually slowed its increase in a sigmoidal fashion. However, it can be seen that unlike the two previous experiments, the equilibrium was not reached during the 6 hour experiment. This was presumably due to in situ hydrolysis and possibly condensation to an oligomeric siloxane. The fact that the infrared intensity did not reach equilibrium, although it did in the case of the 50% relative humidity, showed that increased water in the PVC film led to increased hydrolysis of the silane as it diffused through the film.

Figure 6.9 also shows that the data did not fit very well to the dual mode sorption model. This is presumably related to the presence of the induction period seen in this experiment. This was not observed in any of the other Y9669 experiments using plasticised PVC. However, it is interesting to note that a similar effect was observed when Y9669 was prehydrolysed, and diffusion through unplasticised PVC was induced by annealing (section 3.4, figure 3.35).

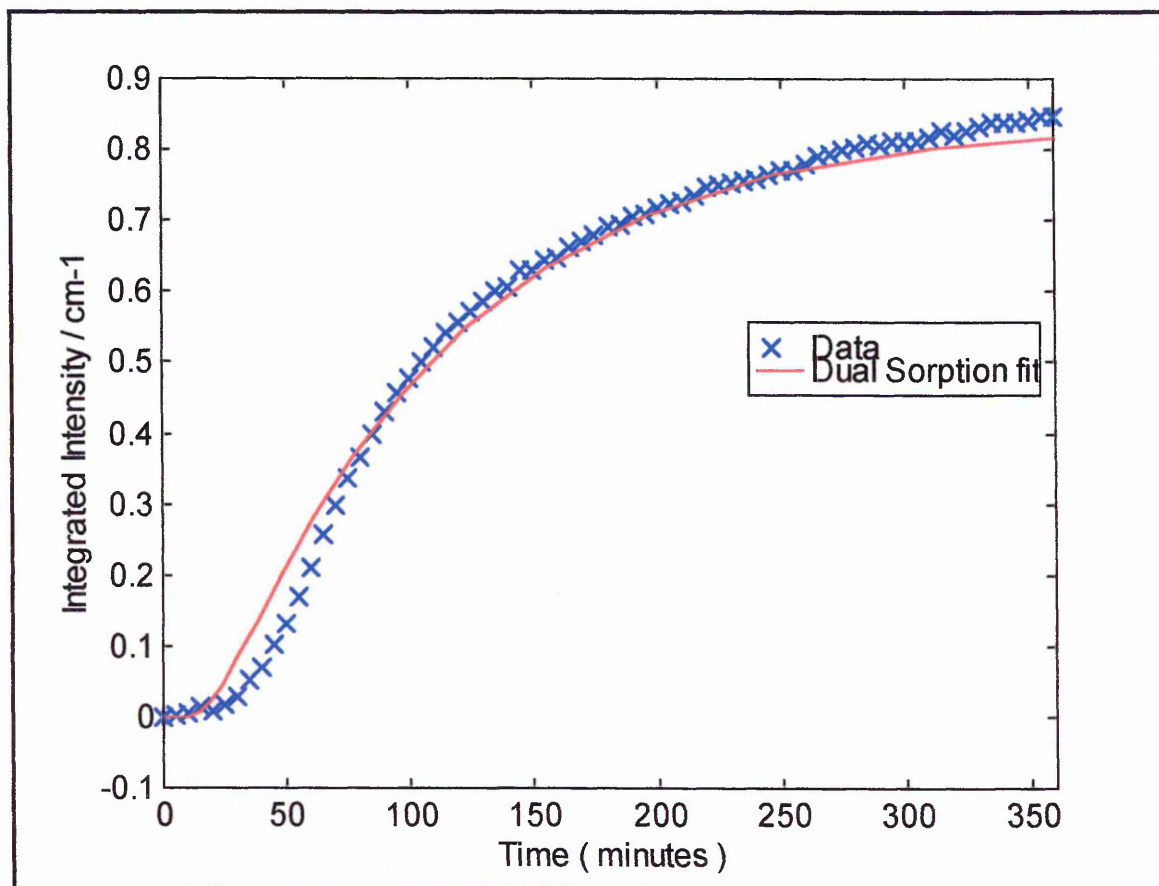


Figure 6.9 : The integrated intensity of the 1600 cm^{-1} infrared band of Y9669 vs. time. The film had been exposed to $\text{NH}_4\text{Cl}(\text{aq})$ vapour (relative humidity 80%)

It is believed that this shows that when Y9669 diffuses through a film containing a significant amount of water, the kinetics of diffusion are different because the silane undergoes simultaneous hydrolysis and diffusion. Although the dual mode sorption model does not fit very well to the data from the last experiment, the diffusion coefficients obtained from the fitting are believed to still give an approximate idea of the relative kinetics of the diffusion in the three films. Table 6.3 shows the diffusion coefficients obtained from the fitting of infrared data of diffusion in films exposed to atmospheric conditions, $K_2CO_3(aq)$ water vapour, and to $NH_4Cl(aq)$ water vapour.

	Atmospheric Conditions	$K_2CO_3(aq)$	$NH_4Cl(aq)$
D_1	9.92×10^{-9}	9.12×10^{-9}	4.31×10^{-9}
D_2	4.62×10^{-9}	4.25×10^{-9}	2.93×10^{-9}
X_1	0.51	0.77	0.90

Table 6.3 : The diffusion coefficients obtained from dual mode sorption fitting of the infrared data from all three film exposures.

Table 6.1 shows that the values of the two diffusion coefficients were almost identical in the case of the film treated by exposure to atmospheric conditions, and that exposed to $K_2CO_3(aq)$ vapour, which has a relative humidity of 50%. This is perhaps not surprising, as the humidity in the laboratory may have been expected to be close to 50%. The value of X_1 is somewhat smaller in the case of the film exposed to atmospheric conditions, however. This may explain the more 'flattened' shape of the first diffusion profile, as the slower diffusion process (D_2) dominated the behaviour more. In the case of

the film exposed to $\text{NH}_4\text{Cl}(\text{aq})$, both diffusion coefficients are smaller than found for the other two cases. Despite the poor fitting of the kinetics to the dual mode sorption model, this is believed to show the effect of hydrolysis of the silane in situ, causing slower diffusion.

There was a noticeable difference in the trend in the results found in the ATR-FTIR and Raman results. In both cases, diffusion in films exposed to 80% relative humidity was slower than that in films exposed to atmospheric humidity. However, in the Raman results, diffusion in films exposed to 44% relative humidity was slower than in films exposed to atmospheric humidity, but in the infrared results, the diffusion rates were very similar. Firstly, it should be stated that the atmospheric humidity was very variable, as the experiments were all carried out on different days. However, there is one possible explanation for the difference between the infrared and Raman results. In the case of the Raman experiments, the laminate was taped to a microscope slide at the edges to make sample handling simpler. Also, the laminate was covered by a glass slide after application of the silane. It is thought that if the humidity treatment had caused raised water levels in the PVC film compared to the untreated film, then these factors might mean that the film used in the Raman experiments retained this water for longer. This would have the effect of making the Raman experiments seem to show more hydrolysis, i.e. slower diffusion of the silane.

References

- 1 Feast, R. C, and Astle, M. J., Ed., Handbook of Chemistry and Physics, 61st. edition, CRC Press, Florida (1981)
- 2 Okuno, H., Renzeo, K. and Uragami, T., Journal of Membrane Science Vol. 103, p.31 (1995)
- 3 Shailaja, D. and Yaseen, M., Polymer International Vol. 32, p. 247 (1993)
- 4 Langevin, D., Grenet, J. and Saiter, J. M., European Polymer Journal Vol. 30, p.30 (1994)

Chapter 7 : Conclusions

All of the work described in this thesis involved the investigation of the diffusion and reactions of the three organosilanes Y9669, A1110 and A1891. Therefore the results of the different chapters are all of relevance to each other. In this chapter, the conclusions from chapters 3, 4, 5 and 6 will be discussed, and then the interrelation of the results from different chapters will be discussed. After this, the overall conclusions of the work will be drawn. Finally, some suggestions for future work will be made.

7.1 : ATR-FTIR analysis of the kinetics of diffusion

In chapter 3, the diffusion of all three silanes in a variety of PVC films was measured using micro ATR-FTIR spectroscopy. Initial experiments used the silane underlayer configuration used by Banga¹. These experiments showed no diffusion of the silanes into the PVC film. We believe that this was due to the condensation of the silane underlayer during solvent removal.

The experiments using the silane overlayer configuration were able to detect diffusion. It was found that alternately annealing the laminate at 70 °C and taking a spectrum at room temperature led to an increase in the intensity of bands from the Y9669 until equilibrium was reached. This showed that diffusion had occurred. However, exposure of the silane to atmospheric humidity before the experiment was observed to slow

this diffusion. In the same experiment using A1110, no diffusion at all was detected. In the same experiment using A1891, diffusion was observed, but an 'induction period' was observed at the start of the experiment in which little diffusion occurred. It was thought that the annealing of the PVC at 70 °C might have allowed diffusion because near the Tg of the PVC (which was 80 °C), the PVC chains were more mobile.

This hypothesis was tested by plasticising the PVC to lower its' Tg. In plasticised PVC, diffusion was observed at room temperature. A series of experiments were carried out with plasticiser levels between 15 and 40% (v/v), using all three silanes. In all cases, diffusion of the silane through the PVC was observed. However, in the case of A1891 diffusion in 15% plasticised PVC, an anomalous diffusion profile was seen, in which the intensity of the silane band decreased after it had reached a maximum. In no cases did the data fit to Fickian case I diffusion kinetics. In all cases, except the anomalous one, a reasonable fit was obtained to the dual mode sorption model. The diffusion coefficients generated from the fitting process increased by 2 to 3 orders of magnitude (faster diffusion) as the plasticiser concentration was increased from 15 to 40%. It was found that the infrared bands due to the plasticiser decreased in intensity as the silane diffused into the PVC. Experiments using an oligomeric plasticiser showed very similar diffusion kinetics to those using a monomeric plasticiser with similar chemistry, at the same concentrations. The bands of the oligomeric plasticiser also showed the same decrease in intensity as the silane diffused into the film. It is believed that this showed that the uptake of silane swelled the PVC film, explaining the decrease in intensity of the plasticiser bands.

All three silanes were hydrolysed by exposure to atmospheric water. In all three cases, a band in the 900 to 1000 cm^{-1} region (assigned to Si-O-R stretching by Hoh *et. al.*²) was indicative of the progress of hydrolysis. Y9669 was found to hydrolyse the quickest, followed by A1110 and then A1891. Y9669 which had been hydrolysed in this way for 24 hours was shown to undergo slower diffusion through unplasticised PVC upon annealing than un-hydrolysed Y9669. A1110 showed no diffusion when either hydrolysed or unhydrolysed. A1891 which showed little hydrolysis over 24 hours showed very similar diffusion before and after the treatment.

7.2 : Raman depth profile analysis of diffusion

It was shown that it is possible to determine the location of the silane in a silane / PVC / silicon laminate using confocal Raman microscopy. Depth profiles of the PVC or the silicon may also be obtained in the same manner. Care must be taken when interpreting the depth profiles to take account of the confocal response of the microscope. However, unlike ATR-FTIR spectroscopy, Raman confocal microscopy is capable of showing what is happening throughout the PVC film.

Depth profiles were measured of the silane underlayer laminates. It was shown that even upon annealing the laminates for 10 hours, the silane did not diffuse away from the surface of the silicon crystal.

In the case of the silane overlayer laminates, the depth profiles showed the position of the silane in the laminate before, during and after diffusion induced by annealing. All three silanes underwent diffusion upon annealing the laminates at 70 °C. The depth profiles of Y9669 and A1110 showed very similar shapes. In the case of A1891, however, a differently shaped depth profile was observed before and during diffusion. In this case a large reservoir of the silane stayed on the outside of the PVC film, whilst a small amount of the silane diffused throughout the PVC film. When diffusion was complete, however, the depth profiles of all three silanes looked the same. It is not known why A1891 displayed this anomalous behaviour.

The confocal response of the microscope was measured by measuring the intensity of a silicon band in 1 μm . steps from the surface of the silicon. It was shown that due to the refraction of the laser as it crosses the air / PVC interface, the beam waist was stretched, which reduced the spatial resolution from 2 μm . to 6 μm . The effect of the convolution of the confocal response was removed from the depth profiles by a Fourier Transform technique. This reduced the distance over which the silane was detected in the measured depth profiles, i.e. the spatial resolution of the experiment was effectively increased.

7.3 : Raman hydrolysis measurements

In chapter 5, the hydrolysis of all three silanes in aqueous alcoholic solutions was investigated using Raman spectroscopy. The solution contained an acid catalyst. This solution was previously used by Banga to hydrolyse silanes¹.

In the case of Y9669 the decrease in intensity of bands equivalent to those assigned to SiOC stretching in A1110 by Ishida *et. al.*³ showed the loss of the unhydrolysed silane. After 10 hours the appearance of a band assigned to triply hydrolysed silanes⁴ showed that some silanes had undergone complete hydrolysis.

In the case of A1110, no change in the Raman spectra occurred over 24 hours. Correlation of the spectra with the literature showed that the A1110 had undergone extremely rapid hydrolysis, as shown by the lack of the bands assigned by Ishida *et. al.*, but was then stabilised in solution to condensation by an intermolecular hydrogen-bonded ring structure.

The spectra of the solution containing A1891 showed the greatest changes upon hydrolysis. The band assigned to SiOC stretching of unhydrolysed silanes decreased and a band assigned to triply hydrolysed A1891 increased rapidly, and then slowly decreased, showing that the hydrolysed A1891 was undergoing condensation. Bands due to the ethanol, which was a product of the hydrolysis could also be seen to appear in the spectrum. The increase in intensity of these bands initially showed similar kinetics to the loss of the unhydrolysed silane, but then the intensity of the ethanol bands decreased in intensity slightly.

7.4 : Diffusion in humidity- controlled films

In chapter 6, the effect of altering the water content of 15% plasticised films on the diffusion of Y9669 through the films was studied with both ATR-FTIR spectroscopy and Raman microscopy. Films exposed to two relative humidities of 44% and 80% as well as a film without controlled humidity were examined.

The Raman intensity near the bottom of the PVC film was monitored as a function of time. The Y9669 showed slower diffusion in the film exposed to 44% relative humidity than in the untreated film. The Y9669 showed even slower diffusion in the film exposed to 80% relative humidity. Depth profiles after diffusion were measured, and showed the same shape as the equilibrium depth profiles from chapter 4.

Infrared measurements made using PVC films treated in the same way showed that diffusion coefficients obtained from Y9669 diffusion in a film treated at 44% relative humidity were only slightly less than those obtained from diffusion in an untreated film. however, the coefficients from a film treated at 80 % relative humidity were considerably lower. Differences in sample handling may explain the disparity between the relative rates of diffusion in the infrared and Raman experiments.

7.5 : The interrelation of the results

Both the infrared and Raman depth profiling results showed that in the silane underlayer laminates, diffusion of Y9669 into the PVC layer did not occur. From the ATR-FTIR results alone, it would have been difficult to confirm this, as the expected change would have been to see a small change in the large intensity of the silane bands, especially as the sensitivity of the evanescent field of the ATR experiment rapidly decreases further into the PVC film. From the depth profiles measured, however (figure 4.11), it can clearly be seen that the silane layer does not interdiffuse into the PVC layer. From the hydrolysis measurements, it was shown that over 24 hours, Y9669 undergoes hydrolysis in solution, but no condensation was observed. However, in casting the prehydrolysed silane films for the silane underlayer experiments, the film of silane solution was heated at 80 °C in order to remove the IPA and water solvents. It might be expected that this would have the effect of accelerating condensation, especially as the product of condensation (i.e. water) was being continuously removed. Therefore it is believed that the silane films used in the silane underlayer experiments consisted of highly condensed siloxane polymers, explaining why no diffusion occurred.

In the silane overlayer experiments using unplasticised PVC, the results using Y9669 can be correlated by comparing the intensity at the same distance from the PVC surface (i.e. the silanes had diffused the same distance) at the corresponding times in the FTIR-ATR experiments and Raman depth profiling experiments. This can be done by comparing the measured ATR-FTIR intensity (as the experiment essentially measures the intensity at the silicon interface, the silane concentration measured was that of the silane which had diffused 10 μm .), with the intensity in a Raman depth profile at the point 10

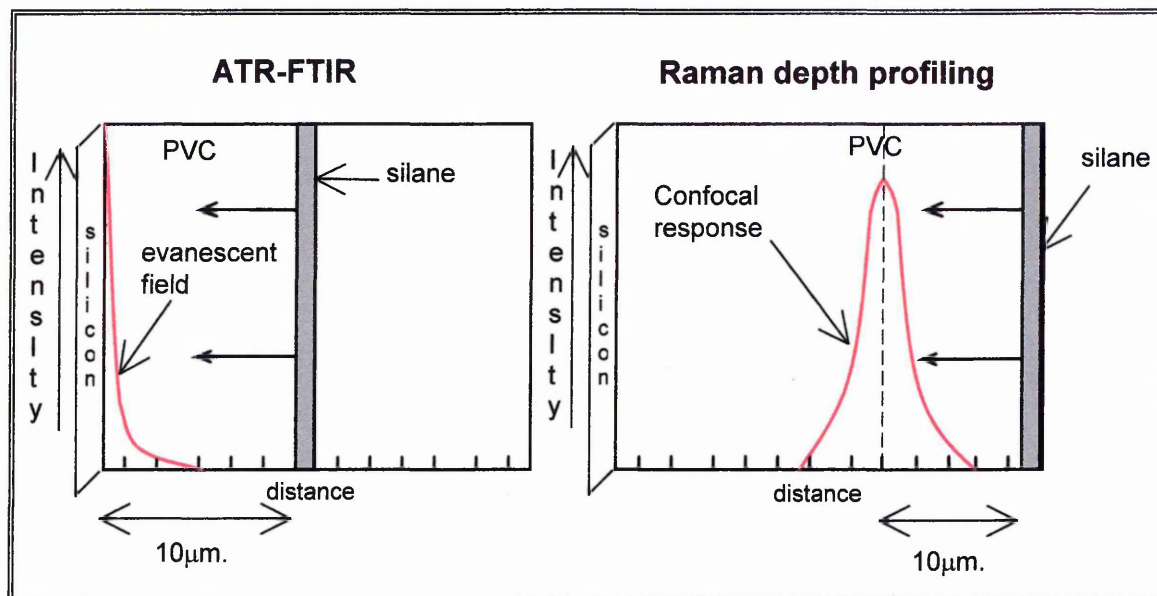


Figure 7.1 : Schematic diagram showing comparison of ATR measurements of diffusion and measurements taken from depth profiles (not to scale)

It can be seen from Figure 7.1 that the two experiments are somewhat similar in that in both cases there is a rapidly increasing response to the diffusing silane from the experiment as a distance of 10 μm. is approached. The experiments are different, however, in detail. In the Raman experiment, the silane diffuses past the measurement point, but does not in the ATR-FTIR experiment. This should not have a great effect if the silanes are distributed heterogeneously through the film at equilibrium. The quantitative effect of the intensity response with distance is also different in the two cases, as was shown in chapter 2. It is expected that the ATR-FTIR response falls off much more quickly than the Raman response (cf. figures 2.6 and 2.13).

In the case of Y9669, comparing figure 3.12 with figure 4.14, it can be seen that in both cases, before any heating, only a small intensity, if any, could be seen 10 μm. from the PVC surface. After 15 minutes, a large proportion (of the order of 90% of the equilibrium

intensity (the last value measured) was seen at this point. This data may be shown more clearly by plotting the normalised intensity at the same distance from the PVC surface, at the same times, for each silane. The infrared intensity of Y9669 and the Raman intensity of Y9669 10 μm . into the PVC film measured in this way are compared in Figure 7.2. Intensities have been normalised to their equilibrium values (which are taken as the last value measured)

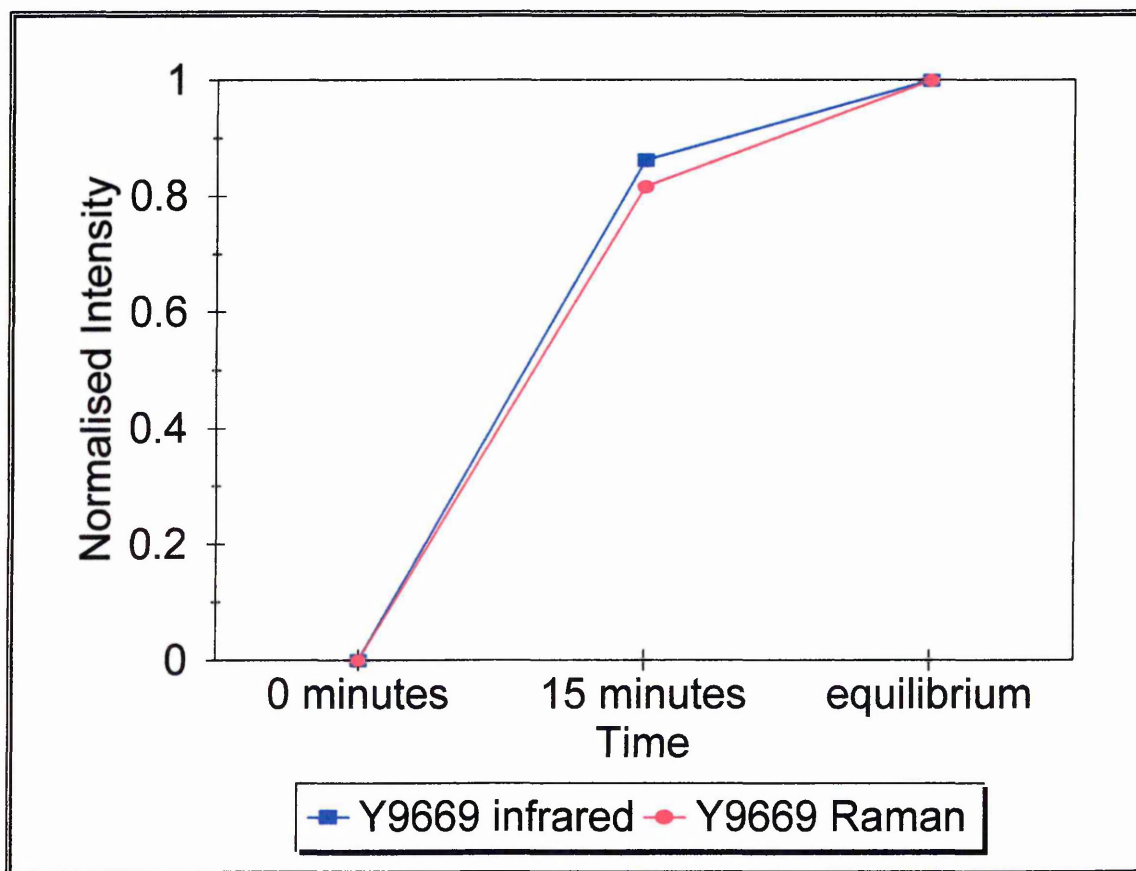


Figure 7.2 : Comparison of the infrared and Raman intensities of Y9669 from annealing experiments in unplasticised PVC

The infrared and Raman intensities for A1110 cannot be compared, as no diffusion was observed in the infrared experiment. However, the Raman values are plotted

in Figure 7.3 to allow comparison with the results from the other silanes. The intensities observed in the A1891 experiments are compared in Figure 7.3.

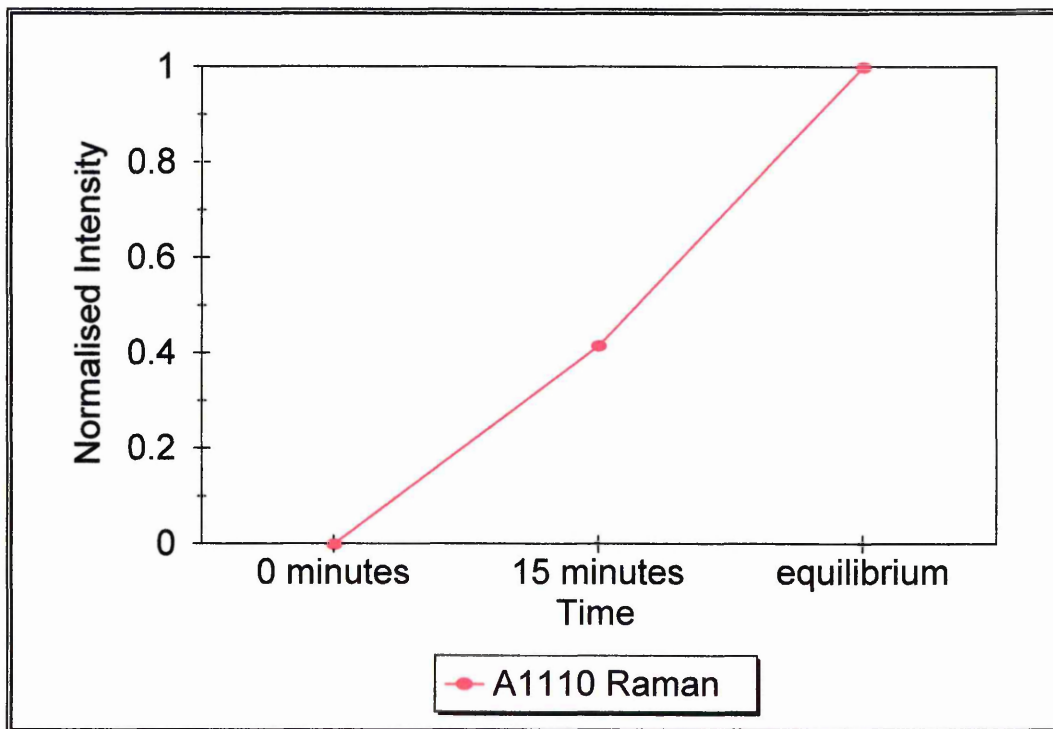


Figure 7.3 : Plot of the normalised Raman intensity of A1110 from annealing experiments in unplasticised PVC

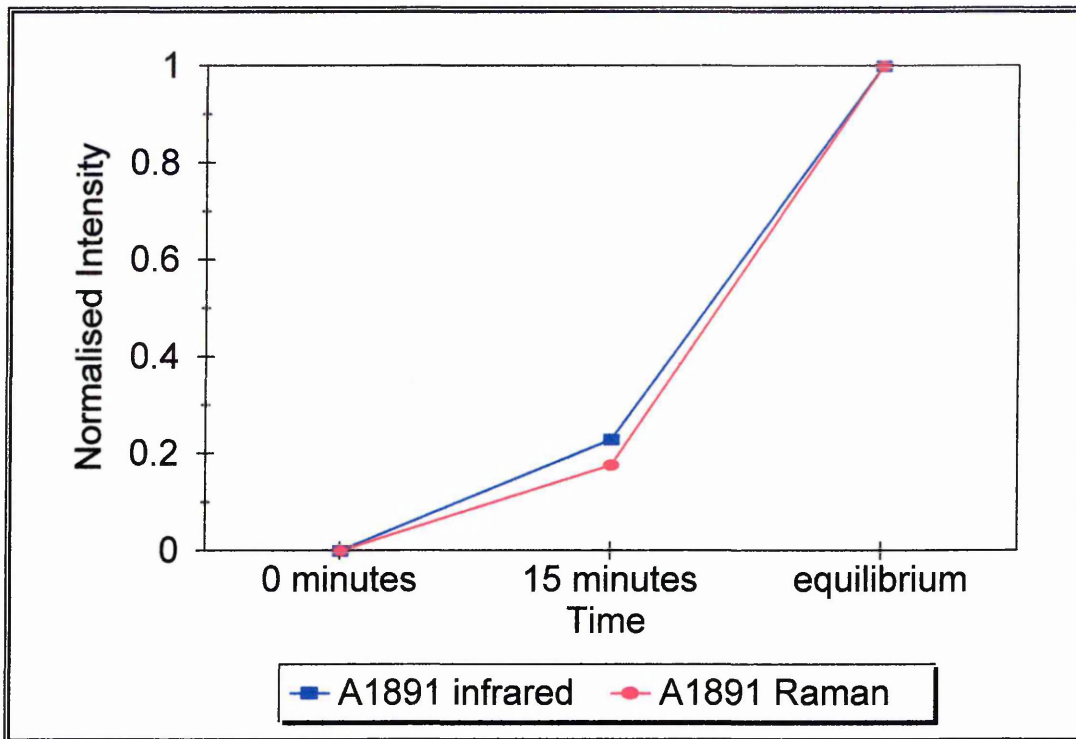


Figure 7.4 : Comparison of the infrared and Raman intensities of A1891 from annealing experiments in unplasticised PVC

The preceding three figures clearly show that the three silanes all show different behaviour when treated in the same way. However, figure 7.1 and figure 7.3 also show that it is possible to obtain the same information from both ATR-FTIR kinetic studies and confocal Raman microscopic depth profiles, and that the data show the same trends. This shows that in practice the response of the evanescent field in ATR-FTIR spectroscopy and the confocal profile in Raman confocal microscopy show very similar intensity - distance responses. We believe that this is the first time that data from the two techniques have been directly compared in this way. It is not clear why A1110 was not observed to undergo diffusion in the infrared experiment; especially in light that it showed very similar diffusion characteristics to Y9669 in the ATR-FTIR studies of diffusion in plasticised PVC, and in the Raman depth profile studies. The main difference which could affect the behaviour

between the two annealing experiments was the heat treatment of the laminate. It is possible that the repeated treatment of the laminate at 70 °C for 5 or 10 minutes intervals in the ATR-FTIR experiment caused the A1110 to undergo hydrolysis, preventing the diffusion, whereas the treatment for 15 and then another 45 minutes in the Raman experiment did not have this effect.

Comparison of the various data obtained on hydrolysis shows that the conditions under which hydrolysis took place were very important. When hydrolysis took place in aqueous solution, with an acid catalyst present (chapter 5), A1891 was shown to hydrolyse faster than Y9669. However, in ambient conditions, reacting with atmospheric water with no catalyst present (chapter 3), Y9669 was observed to undergo hydrolysis much faster than A1891. This is presumably because A1891 requires a catalyst to undergo rapid hydrolysis, whereas aminosilanes such as Y9669 are thought to be able to undergo self catalysis of the hydrolysis process⁵. In the case of A1110, it was observed that in aqueous solution, hydrolysis was extremely rapid, but no condensation was observed, whereas under ambient conditions hydrolysis was relatively slow, but subsequent condensation also occurred.

Comparison of the results from chapter 3 and chapter 6 also helps to explain what was observed. Because the data in chapter 3 had previously shown that prehydrolysed Y9669 showed slower diffusion than unhydrolysed Y9669, we could be confident in saying that the mechanism by which the presence of water in a PVC film slowed diffusion was that the water hydrolysed the silane *in situ*, leading to slower diffusion kinetics. The

similar depth profiles shown in chapters 4 and 6 also allow us to be confident in stating that these depth profiles represent an equilibrium distribution of silane throughout the PVC film, and that although hydrolysis slowed diffusion, the silane eventually reached the same distribution in the PVC film.

7.6 : Overall conclusions

The broadest conclusion that can be drawn from the work presented here is that the organosilane / PVC / silicon system is an extremely complicated one where the reactions of the silanes are critically dependent on many factors, including PVC film composition and humidity, silane type application method and pre-treatment, and laminate age and thermal history. However, some more specific conclusions are stated below.

All of the silanes investigated are capable of diffusion through PVC films. Diffusion through unplasticised PVC is very slow or non-existent at room temperature, but occurs readily near the glass transition temperature of the PVC. The diffusion occurs readily at room temperature in plasticised PVC and the diffusion is faster with higher plasticiser concentrations. The kinetics of diffusion may be modelled by a dual sorption model but do not show Fickian case I kinetics. The diffusion kinetics are also dependent on the hydrolysis state of the silane. Hydrolysed silanes diffuse slower through both plasticised and unplasticised PVC.

The hydrolysis kinetics of the silanes are highly dependent on silane functional group and the hydrolysis conditions employed. A1110 hydrolyses extremely quickly in aqueous solution but is then highly resistant to condensation to a polysiloxane. On the other hand, if allowed to react with ambient humidity it shows slower hydrolysis and readily condenses. Y9669 showed hydrolysis under both sets of conditions and also showed evidence of condensing to a polysiloxane under ambient conditions. A1891 showed extremely slow hydrolysis under ambient conditions, but very fast hydrolysis in aqueous solution, when a catalyst was present. There was no evidence of condensation in either case. It was also shown that it is possible for Y9669 to be hydrolysed by water present in the PVC film as it undergoes diffusion; as expected this reaction slows the diffusion of the silane through the PVC film.

Both ATR-FTIR spectroscopy and Raman microscopy were shown to be extremely suitable to the study of the reactions and diffusion of small molecules such as organosilanes outside and inside polymer laminates. More importantly, the two techniques yield complementary information about the system and used together gave a fuller understanding of the reactions occurring than either technique used separately. When the measurements made by the two techniques were comparable, it was shown that at least qualitatively the two techniques gave the same results.

The evidence shown here that silanes may undergo both diffusion and hydrolysis, and presumably condensation in PVC / silicon laminates helps to explain the mechanism of adhesion in industrial PVC / glass laminates. The fact that it has been shown that these

processes may occur *in situ* leads us to expect that the major process which contributes to adhesion is interdiffusion of the silane and PVC, and probably formation of an interpenetrating polymer network⁶, due to *in situ* condensation of the silanes by water present in the laminate. The process described as the chemical bonding theory⁵ may well occur, but it is expected that both processes are necessary for optimum adhesion.

7.7 : Future Work

It was observed that the behaviour of all three silanes was different. However the reasons for these differences remain unclear. Performing these experiments with a wider range of silanes; specifically silanes with a systematic variation of alkoxy group and functional group, would allow determination of the factors which determine and organosilanes behaviour.

The experiment described here used a very simple model of laminated safety glass. Now that the processes which occur in such systems and the methods which may measure them have been determined, application of similar methods to more realistic models should be carried out. For example, the use of more industrially relevant temperatures (e.g. 120 to 150 °C), thicker PVC films, and the inclusion of industrial PVC additives (e.g. heat stabilisers and processing aids) would provide information more relevant to the processes which occur during glass lamination.

The reason why the A1110 failed to show diffusion in the infrared annealing experiment was not clear. Several experiments could be performed to find out what was happening. Raman depth profiles of the laminate with 5 minutes annealing times would show whether the silane diffused at all. Alternatively, experiments involving applying the silane directly on to an ATR crystal, or alternately on a very thin PVC film (for example a few 100 nm.) could be performed. This would allow infrared spectroscopic determination of the hydrolysis state of the silane, using the same bands used in chapter 3. This might require the use of a different ATR crystal material, such as germanium, as silicon absorbs infrared around the 1000 cm^{-1} region. Carrying out the experiments using the other silanes as well would ensure that the differences between their behaviours could be determined.

The hydrolysis *in situ* was observed indirectly by the effect it had upon the diffusion characteristics of Y9669. The use of an alternate ATR crystal material would also allow the infrared spectroscopic determination of hydrolysis kinetics, and the factors which affect them, inside a PVC laminate.

The analysis of the diffusion mechanism is incomplete. Although the data fitted well to the dual sorption model, it was not checked whether the data fitted to the Fickian Case II diffusion model, or other diffusion models. This should be investigated.

References

- 1 Banga, R., PhD. thesis, Sheffield Hallam University (1995)
- 2 Hoh, K.-P., Ishida, H. and Koenig, J. L., Polymer Composites Vol. 9, No. 2 (1988)
- 3 Ishida, H., Chiang, C.-H. and Koenig, J. L., Polymer Vol. 23, p. 251 (1982)
- 4 Shih, P. T. K. and Koenig, J. L., Materials Science and Engineering Vol. 20, p. 137
 (1975)
- 5 Plueddemann, E. P., in Chemically Modified Surfaces, Ed. by Leyden, D. E.,
 Gordon and Breach (1986)
- 6 Plueddemann, E. P., Silane Coupling Agents, 2nd. edition, Plenum Press, New York
 (1990)

Conferences Attended

1. The 3rd Martin and Willis Prize Meeting, Glaxo, Ware, 16th October 1996, and the Infrared and Raman Discussion Group (IRDG) Meeting, Glaxo, Stevenage, 17th October 1996. Poster presented : 'ATR-FTIR study of the diffusion of organosilanes in PVC films'.
2. The 3rd. MAG AWARD for Young Microspectroscopists, Perkin Elmer, Seer Green, 30th April 1997. Talk presented : 'Study of the Diffusion of Silane Coupling Agents in PVC films using Raman Confocal Microscopy'.

Prize awarded - The 1997 Microspectroscopy Applications Group (MAG) Award for best oral presentation.
3. Polymer Surfaces and Interfaces III, University of Durham, 14th – 18th July 1997. Poster presented : 'Study of the diffusion of Silane Coupling Agents in PVC films using Raman Confocal Microscopy'.
4. 4. The 4th Martin and Willis Prize Meeting, University of Leeds, 31st. March 1998, and the 156th Meeting of the IRDG, 1st. April 1998, University of Leeds. Poster presented : 'Study of the diffusion of Silane Coupling Agents in PVC films using Raman Confocal Microscopy'.

Prize awarded - The 1998 Martin and Willis IRDG award for best poster presentation.
5. The 13th. European Symposium on Polymer Spectroscopy, Lancaster University, 20th – 23rd July 1998. Poster presented : 'Study of the diffusion of silane coupling agents in PVC films using Raman confocal microscopy and ATR-FTIR spectroscopy'.